PRODUCTION ROUTES TO TUNE CELLULOSE NANOCRYSTAL PROPERTIES AND THEIR PERFORMANCE AT HIGH TEMPERATURES

PRODUCTION ROUTES TO TUNE CELLULOSE NANOCRYSTAL PROPERTIES AND THEIR PERFORMANCE AT HIGH TEMPERATURES

BY ORIANA VANDERFLEET, B.ENG.

A Thesis submitted to the School of Graduate Studies in partial

fulfillment of the requirements for the degree Doctor of Philosophy

McMaster University

DOCTOR OF PHILOSOPHY   McMaster University

(Chemical Engineering)   Hamilton, Ontario

TITLE: Production routes to tune cellulose
                          nanocrystal properties and their
                          performance at high temperatures

AUTHOR: Oriana Vanderfleet
                          B. Eng., McMaster University

SUPERVISOR: Professor Emily D. Cranston

NUMBER OF PAGES: xviii, 244

Abstract

This thesis explores new and existing cellulose nanocrystal (CNC) production methods and evaluates their effects on CNC properties, with emphasis on their thermal performance. CNCs produced from industrial and lab-scale processes possess a wide range of surface chemistries, surface charge contents, as well as structural and morphological properties which affect their performance in CNC-based applications. Despite the broad range of available CNC properties, some challenges persist, particularly in the incorporation of CNCs into hydrophobic matrices, high brine liquid formulations, and high temperature applications. Herein, sulfated and carboxylated CNCs produced from large-scale processes were thoroughly characterized and key differences in their thermal performance and self-assembly and rheological behaviors were identified. Furthermore, an optimization study on phosphoric acid hydrolysis parameters and a novel surface modification method which deposits cellulose phosphate oligosaccharides onto CNC surfaces were proposed. The optimization study revealed that CNCs with high colloidal stability could not be produced with phosphoric acid alone; however, the weak acid hydrolysis allowed for precise control over CNC length. The deposition of oligosaccharides onto CNCs, however, resulted in highly colloidally stable CNCs possessing both phosphate and sulfate functional groups. Furthermore, this surface modification method altered CNC surface charge content, water interactions, and the viscosity of their aqueous suspensions. In these studies, however, changes in CNC thermal performance were difficult to elucidate.

As such, to further understand the effects of CNC properties on both their dried and aqueous form thermal performance, a systematic comparison of sulfated, phosphated, and carboxylated CNCs was performed. CNCs were produced with new acid blend hydrolyses (i.e., combining sulfuric and phosphoric acid) as well as existing organic acid hydrolyses and oxidation routes. The combined effects of surface chemistry and counterion profoundly affected the thermal performance of dried CNCs, whereby sulfated and carboxylated CNCs were less thermally stable with proton and sodium counterions, respectively. Additionally, dried CNCs with more surface charge groups, shorter cellulose chains, and higher specific surface areas were found to be less resistant to high temperatures. As such, the new CNCs produced with acid blends exhibited superior thermal performance in their dried form due to their lower charge contents and longer cellulose chains. In their aqueous suspension form, carboxylated CNCs far outperformed both sulfated and phosphated CNCs at high temperatures; their suspensions remained colloidally stable at temperatures up to 150°C for extended time periods. Overall, this thesis equips CNC users and researchers with knowledge and tools to expand the usage of CNCs in commercial applications, particularly those which require high temperatures such as melt-processed polymer composites and oil and gas extraction fluids.

Lay abstract

This thesis contributes to a broader effort in replacing non-renewable and emissions intensive materials with sustainable alternatives such as nanocellulose. Nanocelluloses are nanometer-sized (where one nanometer is one billionth of a meter) cellulose particles manufactured from wood, cotton, or other natural resources. Nanocelluloses are made within Canada on a tonne-per-day scale; this value-added wood product presents an opportunity to refresh the Canadian forest industry. While nanocelluloses have many potential applications, their usage is somewhat limited by their inability to resist heat. This thesis examines changes in nanocellulose properties at high temperatures and evaluates how nanocellulose production methods affect their particle properties and thermal performance. New production methods are explored that increase nanocellulose resistance to heat, alter their dimensions, and change their interactions with water. Overall, this work aims to expand the usage of nanocellulose in commercial products such as coatings, plastics, industrial fluids, food products, and cosmetics (to name a few) by helping researchers select the right kind of nanocellulose for their intended applications.

Acknowledgements

First, I would like to thank my supervisor, Emily. To say I learned a lot from you over the past five years would be an understatement. Thank you for challenging me, for providing me with endless opportunities to grow and explore avenues of interest, and for strengthening my research and communication skills. Pursuing a PhD is difficult yet having your support and knowing how deeply you value the success of your students has kept me going on numerous occasions.

I would also like to extend my thanks to all past and present members of the Cranston group. Thank you for endless hours spent training me on equipment, discussing research results, listening to practice talks, and teaching me the ins and outs of graduate school. Most importantly, thank you for being a distraction when I needed one, for making me laugh, and for creating a space where lasting friendships were built.

I would also like to thank the researchers with whom I collaborated to produce this thesis. Throughout my PhD, I spent time at McMaster University, Université Grenoble Alpes, and the University of British Columbia. At these institutions, I worked with many wonderful people who are co-authors in this thesis, including Gwendoline Delepierre, Dr. Elina Niinivaara, Behzad Zakani, Daniel Osorio, Dr. Michael Reid, Dr. Julien Bras, Dr. Laurent Heux, Francesco D'Acierno, Dr. Carl Michal, and Jaclyn Winitsky. I also had the chance to work with many fantastic researchers at Schlumberger (Dr. Jazmin Godoy-Vargas, Dr. Mohan K.R. Panga, and Dr. Valerie Lafitte), the McMaster Analytical X-Ray Diffraction Facility, the Xerox Research Centre of Canada, as well as Dr. Eero Kontturi (Aalto University) and Dr. Akira Isogai (University of Tokyo). To all my collaborators, thank you for sharing ideas, providing insightful discussion, and, in some cases, working with me in the lab. The quality and breadth of work in this thesis would not have been achieved without you and I am thankful for the time and energy you have dedicated to these research projects.

To my parents, Scott and Josée, my sister, Brigitte, and to all my extended family and friends: thank you for keeping me sane throughout this journey. Thank you for lending a listening ear in periods of frustration, for constantly reminding me what I can achieve, and for generously celebrating my milestones and achievements.

To my lab-partner extraordinaire Elli: I am so lucky to have spent my entire graduate degree alongside you. This is a rare occurrence in the transient world of academia and one I do not take for granted. Thank you for trouble-shooting experiments with me, for making me laugh every day, and for being a dear friend outside of the lab.

To my husband Blair: any thanks issued here will barely scratch the surface of my gratitude. I owe so much of my success to your patience, support, and encouragement. You believe in me when I doubt myself and you ground me when I am stressed. Thank you for being there at the end of every hard day, for embracing a cross-country move in the middle of our graduate degrees, and for building a life with me that is so worth living.

Table of contents

Table of figures

Table of tables

Abbreviations and symbols

Abbreviations

AFM	Atomic force microscopy
AGU	Anhydroglucose unit
BGB	Blue Goose Biorefineries
CNCs	Cellulose nanocrystals
CNFs	Cellulose nanofibrils
CNT	Chiral nematic tactoid
CP/MAS	Cross-polarization/magic angle spinning
DLS	Dynamic light scattering
DLVO	Derjaguin–Landau–Verwey–Overbeek
DMF	Dimethylformamide
DMSO	Dimethyl sulfoxide
DOE	Design of experiments
DP	Degree of polymerization
DP_w	Weight average degree of polymerization
DS	Degree of substitution
DTG	Derivative thermogravimetry
EDL	Electric double layer
GPC	Gel permeation chromatography
HMF	5-hydroxymethyl-2-furfural
ICP-OES	Inductively coupled plasma – optical emission spectrometry
LODP	Levelling-off degree of polymerization
MCC	Microcrystalline cellulose
NT	Nematic tactoid
PAH	Poly(allylamine hydrochloride)
PEG	Polyethylene glycol
POM	Polarized optical microscopy
PTFE	Polytetrafluoroethylene
QCM-D	Quartz crystal microbalance with dissipation
SAC	Strong acid cation
SEC	Size exclusion chromatography
TEM	Transmission electron microscopy
TEMPO	2,2,6,6-tetramethylpiperidine 1-oxyl
TGA	Thermogravimetric analysis
USDA	United States Department of Agriculture
XRD	X-ray diffraction

Symbols

Γ_{H2O}	Amount of bound surface water
Δf	Resonance frequency
ζ	Zeta
ρ	Density
χ_c	Crystallinity index
C	Sensitivity constant of QCM-D sensor
c*	Critical concentration for liquid crystal formation
$Đ$	Dispersity
M	Molecular weight
M_w	Weight-average molecular weight
n	Measurement harmonic for QCM-D
T_{max}	Temperature at the maximum degradation rate
T_{onset}	Onset of thermal degradation

Chapter 1

Introduction and objectives

_____

1.1 Introduction

Since the 19th century, the earth's average surface temperature has increased by nearly 1°C, a change which is attributed to increased greenhouse gas emissions.[1] To mitigate climate change, researchers are looking for new ways to reduce the greenhouse gas emissions associated with common products and processes. This is reflected in a shift from petrochemically-derived materials, which are emissions-intensive, towards biobased materials, which generally result in fewer emissions.[2] Biobased materials are derived from renewable resources such as plants, animals, fungi, or bacteria, and their supply can be replenished within a human time scale. This renewability, combined with a lower global warming potential, has motivated an exponential increase in biobased material research efforts over the past 20 years. Scientists are both incorporating biobased materials into existing products and formulations, as well as designing entirely new products made exclusively from biobased materials. One such innovation is the discovery of cellulose nanocrystals (CNCs), which are rod-shaped nanoparticles produced from wood pulp or other cellulose sources. In today's climate crisis, harvested wood products are exceptionally relevant as they present an opportunity for carbon storage.[3] As such, finding new opportunities to use CNCs and other wood-based materials can help countries achieve their current emission reduction targets.

CNCs were first produced by Nickerson and Habrle in 1947 by subjecting wood pulp to boiling sulfuric or hydrochloric acid.[4] This process was found to preferentially degrade the disordered regions within cellulose chains, while the ordered regions remained intact. The resulting nanoparticles were rod-shaped and highly crystalline. Additionally, those produced with sulfuric acid formed stable colloidal suspensions in water due to their anionic surface groups. While the discovery of CNCs deepened scientists' fundamental understanding of cellulose and its structure, it predated both the emergence of nanotechnology and widespread interest in replacing petrochemical products with biobased alternatives. As such, the efforts of Nickerson, Habrle, and other pioneers in the field were not pursued much further until decades later. In the 1990s, scientific interest in nanotechnology emerged as carbon nanotubes and buckyballs were discovered. Concurrently, CNCs gained interest as their liquid crystal properties[5,6] and their ability to act as reinforcing agents in polymer nanocomposites were reported.[7] Following this, CNCs continued to show promise in numerous applications, for example, as rheological modifiers

in aqueous formulations,[8] as interfacial stabilizers in emulsions and foams,[9,10] and as scaffolds for biomedical applications.[11] In 2011, extensive scale-up efforts came to fruition and CelluForce Inc. opened the first industrial CNC production facility, operating at a tonne-per-day capacity.[12] Since then, CNC research efforts and commercialization pathways have continued to gain momentum. This can be attributed to the widespread industrial production of CNCs, the renewability of their feedstock, and their numerous functional attributes.

Despite impressive research and scale-up efforts, some challenges exist in expanding the use of CNCs in commercial products. One such limitation is the behavior of CNCs at high temperatures. Freeze-dried CNCs begin to degrade around 160°C in their native form; however, this can be extended to nearly 300°C by performing a counterion exchange.[13] CNCs in suspension also undergo changes at high temperatures: significant desulfation occurs at temperatures as low as 70°C, eventually rendering CNCs colloidally unstable and causing them to aggregate and sediment.[14] Due to their unremarkable thermal performance, typical sulfated CNCs are not suitable for high temperature applications such as rheological modifiers in oil and gas extraction, as well as materials which require high processing temperatures, for example melt-processed polymer nanocomposites.

To overcome these limitations and successfully incorporate CNCs into a wider range of commercial products, researchers and industrial CNC producers have developed new production routes. By varying the cellulosic starting material as well as the nature of the production method and its processing parameters, CNCs with various morphological and chemical properties have been produced. The connection between specific CNC properties and thermal performance; however, has not been thoroughly investigated. Furthermore, post-production processing parameters including CNC concentration, counterion, and drying methods, can also influence thermal performance. As such, developing a thorough understanding of CNC thermal performance requires systematic studies in which all variables can be carefully assessed. This understanding is invaluable to the CNC community as it will enable researchers and industrial producers to target specific CNC properties when developing new production routes. Ultimately, CNCs capable of performing in high temperature applications can further reduce the usage of emissions intensive materials such as those derived from petrochemical resources.

1.2 Thesis objectives

While sulfated, wood-derived CNCs are suitable for many applications, some products and formulations may benefit from different CNC properties to maximise their performance. As such, expanding the usage of CNCs in commercial applications requires a wide range of available CNC properties. Additionally, the knowledge of how these properties impact the performance of CNC-based materials is essential. Equipped with a thorough understanding of CNC properties, researchers will be able to select appropriate CNC types for their intended products, as well as develop new production routes that target specific

CNC properties. This thesis aims to deepen the current understanding of CNC production routes, and their ability to tune CNC properties and performance, with a focus on high temperature applications. More specifically, this thesis will:

1. **Explore new and existing production methods and their influence on CNC properties**. This work thoroughly characterizes CNCs produced from industrial and lab-scale processes, revealing a wide range of surface chemistries, surface charge contents, as well as structural and morphological properties. Additionally, these studies aim to link CNC properties to performance to maximize their added value in solid materials and liquid-based formulations. This also prompts the investigation of new production routes that target CNCs with specific attributes, providing further opportunities to expand their application suite.

2. **Investigate the effects of CNC properties on thermal performance** by systematically comparing both freeze-dried CNC powders and aqueous CNC suspensions from new and existing production methods. This work evaluates the combined effects of surface chemistry and counterion, as well as the impact of cellulose degree of polymerization, on CNC thermal performance. The result is a guide to predictable CNC performance over a wide range of temperatures, which is relevant for both academic and industrial researchers.

1.3 Thesis outline
This thesis contains nine chapters and includes three peer-reviewed publications, three submitted manuscripts, and one manuscript in preparation for publication.

Chapter 1: Introduction and objectives
This chapter describes the motivation for the thesis and outlines its objectives.

Chapter 2: Background and literature review
This chapter provides an overview of the literature in topics related to the thesis and its objectives.

Chapter 3: Benchmarking cellulose nanocrystals part II: New industrially produced materials
This chapter presents a thorough and systematic study of CNCs from four industrial producers and benchmarks them against sulfated lab-made CNCs. The five CNC types were extensively characterized to determine the effects of each production route on CNC properties including surface charge density, dimensions, crystallinity, and the molecular weight distribution of cellulose chains. Additionally, the thermal performance, self-assembly behavior, water binding capacity, and rheological profile were determined for each CNC type. Overall, this chapter highlights both the subtle and significant differences between five CNC types and acts as a guide for both academic and commercial users

looking to optimize the performance of CNC-based products. This chapter has been submitted to *Langmuir*.

Chapter 4: *Optimization of cellulose nanocrystal length and surface charge density through phosphoric acid hydrolysis*

This chapter utilizes a design of experiments approach to evaluate the effects of phosphoric acid hydrolysis parameters on CNC properties. A statistical model was generated to predict CNC length based on hydrolysis time and temperature, as well as phosphoric acid concentration. General trends in colloidal stability and phosphate content were also reported, both of which increased with harsher hydrolysis conditions. Overall, this chapter provides insight into CNC production via phosphoric acid hydrolyses and presents optimized parameters to produce CNCs with greater colloidal stability and size uniformity. This chapter was published in *The Philosophical Transactions of the Royal Society A*.

Chapter 5: *Tuning physicochemical properties of cellulose nanocrystals through an in-situ surface modification method*

This chapter presents a novel method to tune cellulose nanocrystal properties through the in-situ deposition of oligosaccharides during CNC production. This easily scalable surface modification route alters the surface charge content, colloidal stability, surface chemistry, and rheological properties of CNCs. Furthermore, the extent and chemical functionality of the modification can be carefully controlled through the deposition parameters and by tuning the oligosaccharide properties, which are produced in a separate process. This chapter has been submitted to *Biomacromolecules*.

Chapter 6: *Insight into thermal stability of cellulose nanocrystals from new hydrolysis methods with acid blends*

This chapter provides insight into the dry thermal degradation of esterified cotton CNCs prepared from acid blends and heated with varying counterions. In acid form, CNC surface charge content was found to govern thermal performance, regardless of ester surface chemistry. Conversely, in sodium form, thermal performance was highly influenced by the cellulose degree of polymerization. Overall, this chapter elucidates the thermal behavior of esterified CNCs while also demonstrating new routes to tailor their thermal and colloidal stability. This chapter was published in *Cellulose*.

Chapter 7: *Effects of surface chemistry and counterion selection on the thermal behavior of carboxylated cellulose nanocrystals*

This chapter investigates the thermal degradation of carboxylated CNCs produced using new and existing methods and benchmarks the results against those of typical sulfated CNCs. Counterion selection, and subsequent interactions with CNC surface charge groups, were found to significantly impact CNC thermal performance. In contrast to their sulfated counterparts, carboxylated CNCs demonstrated superior thermal performance in acid form

compared to sodium form. Additionally, this chapter demonstrates that CNCs with higher surface charge contents and surface areas degrade at lower temperatures. This chapter is in preparation for publication.

Chapter 8: *Hydrothermal treatments of aqueous cellulose nanocrystal suspensions: Effects on structure and surface charge content*

This chapter examines the effects of high temperature and pressure treatments on CNC suspension properties and enables researchers to understand CNC thermal performance. Overall, CNCs underwent few morphological changes; however, their surface charge content was significantly decreased after heat treatment, which resulted in loss of colloidal stability and aggregation. Sulfated CNCs exhibited the most severe aggregation, while CNCs hydrolyzed with acid blends or subjected to oxidative treatments were less affected. As such, this chapter elucidates CNC suspension behavior after heat exposure and guides users to select CNCs with improved high temperature performance. This chapter has been submitted to *Cellulose*.

Chapter 9: *Conclusions and outlook*

This chapter emphasizes the major contributions to knowledge presented in this thesis and suggests future research directions in the field of cellulose nanocrystals and their applications.

1.4 Other contributions

Other published contributions to date (not included in this thesis):

Bushell, M., Meija, J., Chen, M., Batchelor, W., Browne, C., Cho, J.Y., Clifford, C.A., Al-Rekabi, Z., Vanderfleet, O.M., Cranston, E.D., Lawn, M., Coleman, V.A., Nyström, G., Arcari, M., Mezzenga, R., Chon Park, B., Shin, C., Ren, L., Bu, T., Saito, T., Kaku, Y., Wagner, R., and Johnston, L.J., Particle size distributions for cellulose nanocrystals measured by atomic force microscopy: an interlaboratory comparison. *Cellulose* (2021). https://doi.org/10.1007/s10570-020-03618-4

1.5 References

1. Lindsey, R. & Dahlman, L. Climate change: Global temperature. *Climate.gov* https://www.climate.gov/news-features/understanding-climate/climate-change-global-temperature (2020).

2. Weiss, M. *et al.* A Review of the Environmental Impacts of Biobased Materials. *J. Ind. Ecol.* **16**, (2012).

3. Johnston, C. M. T. & Radeloff, V. C. Global mitigation potential of carbon stored in harvested wood products. *Proc. Natl. Acad. Sci. U. S. A.* **116**, 14526–14531 (2019).

4. Nickerson, R. F. & Habrle, J. A. Cellulose intercrystalline structure. *Ind. Eng. Chem.* **39**, 1507–1512 (1947).

5. Revol, J.-F., Bradford, H., Giasson, J., Marchessault, R. H. & Gray, D. G. Helicoidal self-ordering of cellulose microfibrils in aqueous suspension. *Int. J. Biol. Macromol.* **14**, 170–172 (1992).

6. Revol, J.-F., Godbout, D. L. & Gray, D. G. Solidified liquid crystals of cellulose with optically variable properties. (1994).

7. Favier, V., Chanzy, H. & Cavaillé, J. Y. Polymer nanocomposites reinforced by cellulose whiskers. *Macromolecules* **28**, 6365–6367 (1995).

8. Li, M. C., Wu, Q., Song, K., Qing, Y. & Wu, Y. Cellulose nanoparticles as modifiers for rheology and fluid loss in bentonite water-based fluids. *ACS Appl. Mater. Interfaces* **7**, 5009–5016 (2015).

9. Kalashnikova, I., Bizot, H., Cathala, B. & Capron, I. New pickering emulsions stabilized by bacterial cellulose nanocrystals. *Langmuir* **27**, 7471–7479 (2011).

10. Hu, Z., Xu, R., Cranston, E. D. & Pelton, R. H. Stable Aqueous Foams from Cellulose Nanocrystals and Methyl Cellulose. *Biomacromolecules* **17**, 4095–4099 (2016).

11. Osorio, D. A. *et al.* Cross-linked cellulose nanocrystal aerogels as viable bone tissue scaffolds. *Acta Biomater.* **87**, 152–165 (2019).

12. Reid, M. S., Villalobos, M. & Cranston, E. D. Benchmarking cellulose nanocrystals: from the laboratory to industrial production. *Langmuir* **33**, 1583–1598 (2017).

13. Vanderfleet, O. M. *et al.* Insight into thermal stability of cellulose nanocrystals from new hydrolysis methods with acid blends. *Cellulose* **26**, 507–528 (2019).

14. Beck, S. & Bouchard, J. Auto-Catalyzed acidic desulfation of cellulose nanocrystals. *Nord. Pulp Pap. Res. J.* **29**, 6–14 (2014).

Chapter 2

Background and literature review
_____

This section provides an overview of cellulose nanocrystals (CNCs), their existing production routes, and their thermal performance. Challenges in expanding CNC usage, particularly at high temperatures, are highlighted. Furthermore, production routes to address these challenges, and their ability to do so on an industrial scale, are discussed. This section is based on a review article written by myself with input from my supervisor, Dr. Emily Cranston. Text and figures are reproduced or adapted with permission from Springer Nature Limited © 2020.

Vanderfleet, O.M.; Cranston, E.D., "Production routes to tailor cellulose nanocrystal performance", *Nature Reviews Materials* **2021**, 6, p. 124-144.https://doi.org/10.1038/s41578-020-00239-y

2.1 Cellulose nanocrystals

Cellulose nanocrystals (CNCs) were first produced in 1947 by researchers Nickerson and Habrle.[1] Cellulose was exposed to either sulfuric or hydrochloric acid at boiling temperatures, which was found to preferentially degrade less-ordered regions within the native cellulose structure. The remaining crystalline regions, referred to as cellulose micelles, and consisting of packed cellulose chains approximately 280 glucose units long, were further studied[2] and imaged[3] by Rånby et al. in 1949 and 1951, respectively. Following these studies, Mukherjee and Woods outlined the importance of acid concentration in CNC production and introduced the now commonly used 64 wt% sulfuric acid hydrolysis method.[4] Despite these early reports, there was a 40-year gap in research before scientific interest in CNCs was reignited in the 1990s; a timeline detailing research and development milestones is provided (Figure 2.1). As CNC research progressed, many terms were used to identify these cellulosic nanomaterials, including hydrocellulose; cellulose sols, monocrysals, micro(crystallites), microcrystals, (nano)whiskers, nanowires; and nanocrystalline cellulose. In 2017, standard terms and definitions were published, which concretized the term cellulose nanocrystals (CNCs).[5] Owing to their high specific Young's modulus,[6] ease of dispersion in polar solvents,[7] liquid crystal tendencies,[8] and non-toxicity,[9] CNCs have attracted great attention and have applications ranging from biomedical devices, water purification technologies, energy production and storage, food and cosmetic modifiers, to composite and construction materials. CNCs are now produced industrially in tonne-per-day quantities and as such, are suitable for high-volume, commercial applications.[10–12] The performance of CNCs in composite materials, in both liquid and solid forms, is heavily dependent on the methods used to produce them as well as the cellulosic source material.
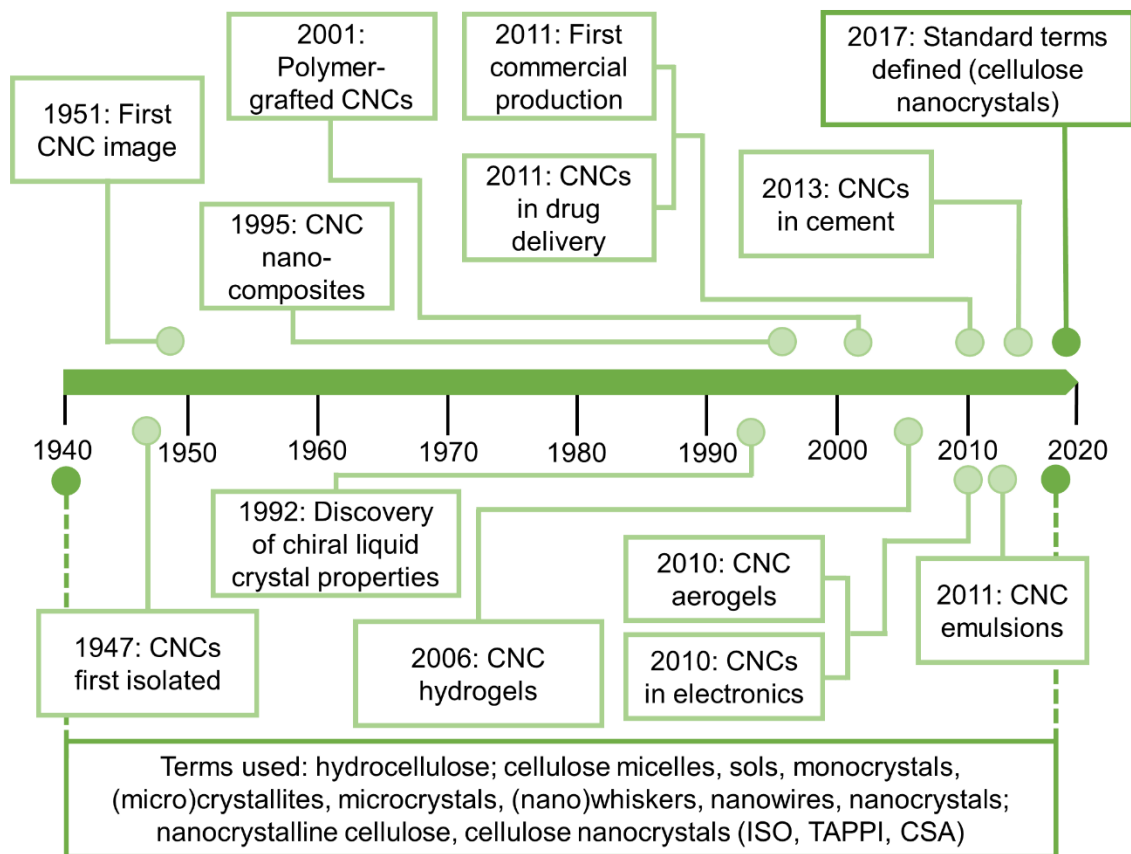
Figure 2.1. A timeline detailing CNC production,[1] imaging,[3] liquid crystalline properties,[8] nanocomposites,[13] polymer-grafting,[14] hydrogels,[15] aerogels,[16] electronics,[17] drug delivery,[18] emulsions,[19] cements,[20] industrial production as well as the standardization of CNC terminology.[5]

Most commonly, CNCs are produced by sulfuric acid hydrolysis whereby cellulose chains undergo two reactions: hydrolysis of glycosidic bonds and esterification of surface hydroxy groups.[21] The hydrolysis of glycosidic bonds, which occurs rapidly within the less-ordered regions of cellulose, decreases the length of cellulose chains until mostly crystalline regions remain. Simultaneously, a fraction of the surface hydroxy groups is esterified to form sulfate half-ester groups that are anionic under practical working solution conditions. (Note that CNCs produced from sulfuric acid hydrolysis are also called sulfated CNCs as a result of this surface esterification and are sometimes erroneously referred to as sulfonated CNCs which is incorrect, because it would require a carbon-sulfur bond, not a carbon-oxygen-sulfur bond, which has never been shown experimentally.) As a result of the two mechanisms occurring during acid hydrolysis, CNCs possess three crucial properties: colloidal stability in aqueous suspensions, nanoscale dimensions (with rod-like shape and high aspect ratio), and a high crystallinity index (Figures 2.2a, 2.2b, and 2.2c). The first property stems from electrostatic repulsion between neighboring CNCs and the latter two

properties result from the degradation of disordered regions in cellulose during hydrolysis. For many CNC applications, these target properties are essential.
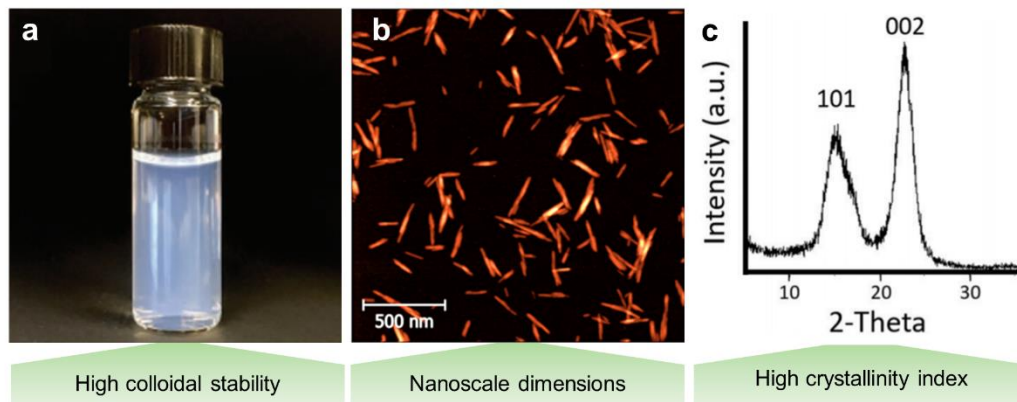
Figure 2.2. (a) A colloidally stable 1 wt% aqueous CNC dispersion. (b) An atomic force microscopy image showing the whisker-like shape of CNCs. (c) An X-ray diffraction pattern of highly crystalline CNCs in the native cellulose I crystal structure. Panels (a) and (c) are adapted from ref. 22, Royal Society of Chemistry. Panel (b) is adapted with permission from ref. 23, American Chemical Society.

The performance of CNCs can be roughly evaluated based on the three target properties: aqueous colloidal stability, size and crystallinity index (Figures 2.2a, 2.2b, and 2.2c). If particles are well-dispersed and resist aggregation and sedimentation in a liquid medium, they are deemed colloidally stable. For CNCs, this stability is governed by Derjaguin–Landau–Verwey–Overbeek (DLVO) theory (the balance of van der Waals attraction and electrostatic repulsion) or sometimes results from steric or electrosteric repulsion, for example, with hairy nanocelluloses.[24] High colloidal stability is essential to produce uniform dispersions with predictable and consistent performance. For example, material processing, viscosity and shelf-life are highly dependent on colloidal stability. Charged CNC colloidal stability can be inferred by measuring electrophoretic mobility and subsequently calculating zeta potential following Smoluchowski's theory or the recently reported, and more accurate, modified Oshima-Overbeek equation.[25] Absolute zeta potential values between 0 and 10 mV are categorized as highly unstable, 10 to 20 mV are relatively stable, 20 to 30 mV are moderately stable and magnitudes exceeding 30 mV are considered highly stable.[26] Colloidal stability can also be assessed using light transmission through a CNC suspension, or measuring apparent particle size by dynamic light scattering (DLS), over time, to determine if and when aggregation or sedimentation occurs.[22]

CNC dimensions and shape are also key properties that govern their performance: CNCs with nanoscale lengths and high aspect ratios are desirable. Nanoscale dimensions provide CNCs with high surface-area-to-volume ratios which means that adding a small amount to a material greatly affects its properties, and for a given mass, the smaller the nanoparticles, the larger the number of available sites for chemical reactions, and adsorption or release of other chemical moieties. Furthermore, high aspect ratios allow CNCs to self-assemble into

liquid crystalline phases, adopt robust mesh structures to stabilize interfaces, and form percolated networks, for example, in polymer nanocomposites.[8,27] CNC size is measured by microscopy techniques, primarily atomic force microscopy (AFM) and transmission electron microscopy (TEM), calculated from small angle neutron or X-ray scattering,[28,29] or inferred from light scattering, for example, DLS or laser light scattering.[22,30,31] While DLS is a straightforward measurement, its results are often reported as hydrodynamic radii, meaning the Stokes-Einstein equation relates translational diffusion coefficient to particle size under the assumption of hard, spherical particles.[26] Although modified Stokes-Einstein equations are available for cylindrical particles (and these report two dimensions: length and diameter),[26] they are seldom used in the analysis of CNC size. Furthermore, DLS measurements are heavily weighted by aggregates.[26] Microscopy is more accurate but time-consuming and is not immune to inaccuracies (such as tip broadening effects in AFM or staining issues in TEM).[32] Typically, CNCs have microscopy lengths of 100 – 200 nm and cross-sections of 5 – 20 nm, or apparent sizes <100 nm by DLS.[10]

The third property used to assess the performance of CNCs is their crystallinity index, which indicates the degree of order of the cellulose chains that make up the particles themselves and indicates the completeness of the reaction used in their production. Crystallinity of CNCs is primarily linked to mechanical properties but can also affect chemical reactivity and thermal stability. While CNCs are generally in the native cellulose I allomorph, variations in starting material or process can accidentally or purposely introduce cellulose II.[10,33,34] The crystallinity index of CNCs can be determined through a variety of techniques including Raman spectroscopy, NMR spectroscopy and X-ray diffraction (XRD),[35,36] although there is some controversy over which technique is most accurate. XRD is the most widely used technique and does not require calibration. Despite its widespread use, all crystallinity index values determined from XRD are not equal as a consequence of differences in sample preparation and curve fitting procedures. Several methods exist to translate X-ray diffractograms into a single crystallinity index (also called degree of crystallinity and given as a percentage). Nevertheless, because sample preparation and instrumentation make it difficult to compare between reported values,[37] comparisons are only approximate.

2.2 Cellulose nanocrystal production

Despite the prevalent use and widespread industrial production of sulfated CNCs from cotton and wood pulp, many alternate production routes have emerged. Importantly, they are all chemical isolation methods based on acid hydrolysis or oxidation, in contrast to the mechanical methods (sometimes combined with enzymatic or chemical pre-treatment) used to produce the longer, fibrillated, heterogeneous and less crystalline form of nanocellulose, namely cellulose nanofibrils (CNFs). Research efforts related to CNC production are often motivated by some of the challenges which limit the use of sulfated CNCs, such as their hydrophilic character,[38] their tendency to aggregate in high ionic strength environments,[29] and their lack of thermal stability.[39] Additionally, some efforts are focused on using low-value biomass sources,[40–42] improving the yield,[43–45] or reducing the environmental impact of CNC production routes.[46,47] To accomplish these goals, a variety of mineral[48,49] and organic acids,[47,50] as well as mixed acids,[39,51,52] have been used to produce CNCs.

Moreover, acid-free processes such as oxidation,[53,54] enzymatic hydrolyses,[55–57] and ionic liquid-mediated technologies[58–62] have been investigated. These new production routes, combined with the study of dozens of starting cellulose sources,[63] have resulted in CNCs with varying surface chemistry, surface charge density and morphology.

2.2.1 Production routes

The most well-studied and widely used protocol to produce CNCs uses concentrated sulfuric acid to hydrolyse and esterify cellulose (Figure 2.3a)[64] in under 2 hours with yields in the range of 20-75%. Sulfuric acid is a strong acid and the high concentration of protons attacks the glycosidic bonds faster in less-ordered regions of cellulose. As these bonds are broken, the cellulose chains become shorter and the average degree of polymerization decreases until the disordered regions have been fully degraded and the level-off degree of polymerization (LODP) is reached (Figure 2.3b).[1,65] If the hydrolysis reaction is allowed to continue, the degree of polymerization of the cellulose chains, and the CNC length, will continue to decrease but very slowly compared to the initial decrease. Generally, when the LODP is reached, the acid and cellulose slurry is quenched to terminate the reaction. At this stage, the sulfated CNCs can be easily centrifuged into a pellet because the high ionic strength of the quenched slurry screens electrostatic repulsion, and the acid is subsequently removed by centrifugation and dialysis. Lastly, the aqueous CNC suspension is sonicated with an ultrasonic probe (to unhinge the crystals) and filtered (to remove any unhydrolyzed cellulose or impurities). The common lab-scale process to produce CNCs (Figure 2.3c) has similarities to industrial-scale production, such as acid concentration, time, temperature and mixing; however, the quenching, purification, neutralization, and drying steps have required optimization for larger scale production. The resulting CNCs are highly crystalline nanoparticles with deprotonated sulfate half-ester surface groups which meet all three target properties discussed in the previous section.
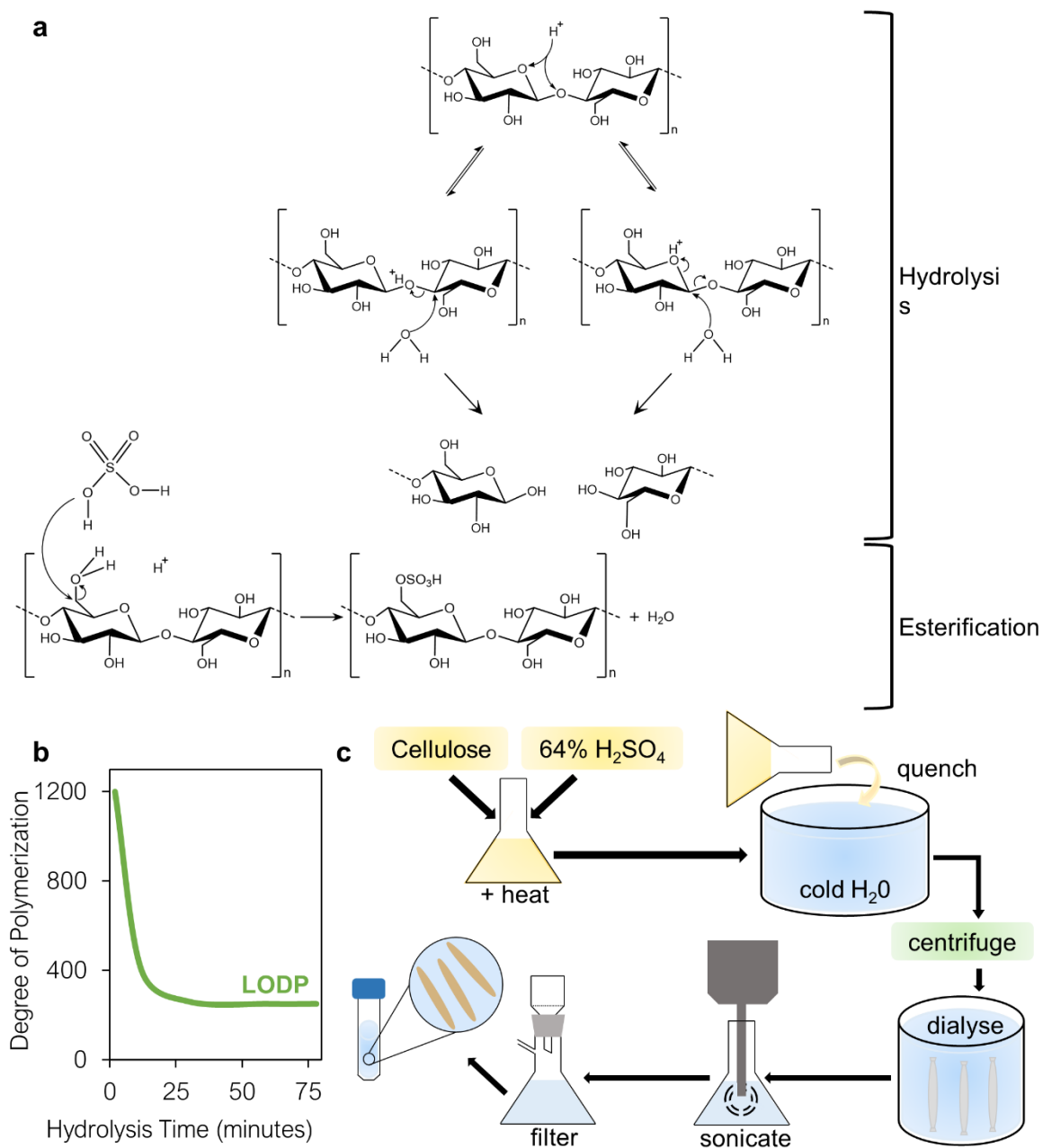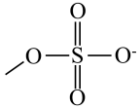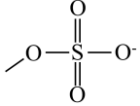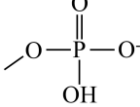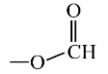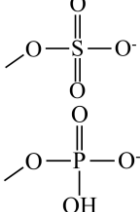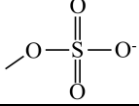
Figure 2.3. (a) Mechanism for hydrolysis and esterification of cellulose subjected to concentrated sulfuric acid. (b) A schematic showing the leveling off degree of polymerization (LODP) of cellulose chains during sulfuric acid hydrolysis. (c) A schematic of the laboratory-scale production of CNCs.

Despite the uniformity, reproducibility, high yield, stability, and predictable properties of CNCs made with sulfuric acid, many researchers have investigated alternative production routes. The viability of these methods can be assessed by evaluating the target properties of the resulting CNCs (Table 2.1). Additionally, the yield is assessed because a high yield
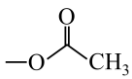
is a requirement for any economically feasible industrial process. Besides sulfuric acid, several other mineral acids have been used to produce CNCs. Hydrochloric, hydrobromic and phosphotungstic acid hydrolyses produce high yields of CNCs with high degrees of crystallinity.[43–45,49] The resulting CNCs, however, are uncharged and form large aggregates; this is undesirable for most applications as they lose the advantages of being nano-sized and cannot form uniform dispersions with consistent properties. Interestingly, if yield is of primary concern, gaseous HCl hydrolysis gives a 97% yield from cotton, attributed to swelling and crystallization of the disordered cellulose regions during the relatively slow process, which is a significant improvement over all industrially produced CNC yields.[43] The challenge is that the CNCs produced from HCl vapour hydrolysis need post modification (with (2,2,6,6-tetramethylpiperidin-1-yl)oxyl, that is, TEMPO-mediated oxidation, for example) to impart surface charge, colloidal stability and individualized nanoparticles. While CNCs produced with phosphoric acid, a weak acid, do possess phosphate half-ester groups,[48] the improvement in colloidal stability over uncharged CNCs from other mineral acid hydrolyses is small.[48,66] Although there is little functional difference, CNCs can be classified as either uncharged or unstable (Table 1), the latter of which have some surface charge groups but not enough to impart the targeted colloidal stability. As such, if a single mineral acid is to be used, CNCs with high colloidal stability, uniform nanoscale lengths and high crystallinities can only be produced using sulfuric acid.

Lately, interest has grown in using organic acids to produce CNCs with new surface functionalities. While CNCs can be made using these processes, the degree of crystallinity which can be achieved is generally lower than those made with mineral acids.[47,50,67–69] Furthermore, some organic acid hydrolyses sacrifice yield or colloidal stability. While CNCs made with oxalic or maleic acids are colloidally stable, their yields are low.[47] Conversely, CNCs produced with formic acid have higher yields, yet the resulting CNCs have low colloidal stability and form aggregates.[69]

Table 2.1 Cellulose nanocrystal production routes and resulting properties.

Production route	Reagents	CNC surface chemistry	Colloidal stability	Size (CNC length)	Crysta-llinity index	Yield	Ref.[a]
Mineral acids	Sulfuric acid	sulfate ester structure	Highly stable	Nano	70-93%	20-75%	[1,10,70,71]
	Sulfuric acid & ultra-sonication	sulfate ester structure	NR	Nano; some aggregates	77-81%	53-71%	[72]
	Phosphoric acid	phosphate ester structure	Unstable	Nano	81-97%	76-80%	[48,66]
	Hydrochloric acid (liquid)	Unmodified	Uncharged	Nano; very aggregated	86-88%	80-93%	[1,45,73]
	Hydrochloric acid (vapour)	Unmodified	Uncharged	Nano; very aggregated	58-64%	97%	[43]
	Hydrochloric acid hydrolysis of TEMPO-CNF	carboxylate structure	NR	Nano	78-80%	69-85%	[74]
	Hydrobromic acid	Unmodified	Uncharged	Nano; very aggregated	91%	70%	[49]
	Phosphotung-stic acid	Unmodified	Unstable	Nano & micro	80-85%	20-88%	[44,75]
Organic acids	Oxalic acid	carboxylate structure	Highly stable	Nano & micro	80-83%	1-25%	[47]
	Oxalic acid dihydrate & mechanical disintegration	carboxylate structure	NR	Nano; some aggregates	74-79%	84-99%	[50,67]
	Maleic acid	carboxylate structure	Highly stable	Nano; some aggregates	72-81%	1-13%	[47,68]
	Formic acid	formate ester structure	Unstable	Nano & micro; very aggregated	66-75%	70-78%	[69]
Acid blends	Phosphoric & sulfuric acids	sulfate and phosphate ester structures	Relatively stable	Nano	94-95%	NR	[39]
	Sulfuric & hydrochloric acids	sulfate ester structure	Highly stable	Nano; some aggregates	83%	NR	[76]

	Hydrochloric & citric acids		NR	Nano; some aggregates	78%	5-20%	[77]
	Hydrochloric & malonic acids		NR	Nano; some aggregates	75%	5-20%	[77]
	Hydrochloric & malic acids		NR	Nano; some aggregates	78%	3-20%	[77]
	Hydrochloric & acetic acids		NR	Nano; very aggregated	NR	15-35%	[78]
	Hydrochloric & butyric acids		NR	Nano; very aggregated	NR	22%	[78]
	Hydrochloric & 2-bromo-propionic acids		NR	Nano; some aggregates	78%	46%	[51]
	Hydrochloric & 3-mercapto-propionic acids		NR	Nano	81%	50%	[51]
	Hydrochloric & 4-pentenoic acids		NR	Nano	65%	48%	[51]
	Hydrochloric & 2-propynoic acids		NR	Nano	74%	62%	[51]
	Hydrochloric & nitric acids		Highly stable	Nano; some aggregates	73-82%	90-91%	[79]
Oxidizing agents	TEMPO-mediated oxidation & ultrasonication		Highly stable	Nano	60-80%	69-94%	[53]
	Sodium periodate		Sterically stabilized	Nano	NR*	50%	[41]
	Sodium periodate & sodium borohydride		Sterically stabilized	Nano	NR*	60-79%	[80]
	Ammonium persulfate		NR	Nano	64-91%	14-81%	[54]
	Hydrogen peroxide		Highly stable	Nano; some aggregates	NR	20-50%	[81]
Ionic liquids	1-butyl-3-methyl-imidazolium hydrogen sulfate		NR	Nano & micro; very aggregated	82-96%	NR	[59,82]
	1-ethyl-3-methyl-		Uncharged	Nano; very aggregated	73%	44%	[58]

	imidazolium acetate						
	Tetrabutyl-ammonium acetate	$-O$ $\overset{O}{\|}$ CH_3	Uncharged	Nano & micro; very aggregated	51%	NR	[60]
	Choline chloride and oxalic acid dihydrate, followed by mechanical disintegration (deep eutectic solvents)	$\overset{O}{\|}$ O^-	NR	Nano; very aggregated	66-71%	68-78%	[61]
	Choline chloride, oxalic acid dihydrate and *p*-toluenesulfonic acid (deep eutectic solvents)	$\overset{O}{\|}$ O^-	NR	Nano; very aggregated	57%	66%	[62]
Other	Subcritical water	Unmodified	Uncharged	Nano	79%	22%	[83]
	Sulfur dioxide and ethanol (AVAP®)	Unmodified	Uncharged	Nano; very aggregated	93%	24%	[84]

AVAP®, American Value Added Pulping; CNC, cellulose nanocrystal; CNF, cellulose nanofibrils; NR, not reported. 2,2,6,6-tetramethylpiperidin-1-yl)oxyl, TEMPO
[a]References cited point to pioneering work with a given production route or a study focused on process optimization.

To overcome some of the drawbacks of organic acids, weak acids, or mineral acids that do not impart surface charge, mixtures of acids have been used to produce CNCs. Most acid blends combine a strong mineral acid (hydrochloric or sulfuric acid) with an organic acid or a weak mineral acid because the kinetics of cellulose hydrolysis are largely governed by acid concentration, which is directly related to proton concentration.[64] When strong acids are used to produce cellulose nanocrystals, higher proton concentrations result in a rapid and uniform hydrolysis. If weak acids are used alone, equilibrium dictates that the acid groups are not fully dissociated, and sufficiently high proton concentrations cannot be achieved. Therefore, by combining multiple acids, highly crystalline nanoscale particles can be achieved owing to the strong acid contribution while surface chemistry can be tailored by the choice of the weaker acid. In some cases, two esterifying acids have been used. For example, blends of sulfuric and phosphoric acid produce CNCs with both sulfate and phosphate groups.[39] In most cases, however, hydrochloric acid is used in conjunction with organic acids and these production routes generally produce nanoscale CNCs with moderately high crystallinities. The colloidal stability of these acid blend-produced CNCs has not been thoroughly characterized, however, some samples, particularly those made with 3-mercaptopropionic, 4-pentenoic and 2-propynoic acids appear well dispersed when imaged by AFM.[51] Overall, the use of acid blends to produce CNCs which meet all target properties and have a variety of surface chemistries is a growing research area which promises to expand the use of CNCs in diverse applications.

Importantly, CNCs can be produced without acid; common methods to do so include oxidation reactions, enzymatic hydrolyses or production with ionic liquids or subcritical water. Of these methods, oxidation reactions yield some of the best results: CNCs are consistently colloidally stable, have nanoscale dimensions, and high crystallinities.[24,53,54] Furthermore, extremely high densities of surface carboxyl groups can be achieved, particularly in the case of TEMPO-oxidized CNCs and CNCs made with ammonium persulfate.[53,85] While TEMPO-oxidized CNCs can be obtained as a post-production surface modification on acid-hydrolyzed CNCs,[14,86,87] they can also be directly produced through extensive sonomechanical treatment of TEMPO-oxidized pulp or microcrystalline cellulose (MCC),[53] or through an acid hydrolysis of TEMPO-oxidized CNFs (Table 2.1).[74] Alternatively, sterically-stabilised CNCs can be produced by using sodium periodate as the oxidising agent; these CNCs have peeled or fibrillated cellulose surface chains with aldehyde (or converted hydroxy, carboxyl, or amine) groups.[24,80] Transition-metal-catalyzed oxidative routes and sulfur dioxide with ethanol (American Value Added Pulping (AVAP®) process)[84] have also been used to produce nanocellulose mixtures with a significant fraction of CNCs.[10,88] Both CNCs with carboxyl groups and aldehyde groups present opportunities for surface modification that cannot be achieved with sulfate groups, such as carbodiimide coupling and chemical crosslinking via hydrazone chemistry.[89]

Beyond oxidative methods, no other acid-free methods to produce CNCs have been successful at achieving all three target properties. CNCs produced with ionic liquids are generally uncharged or colloidally unstable and therefore form large aggregates.[58–60,82] Furthermore, they often have lower crystallinities than CNCs made with sulfuric acid.[58,60] CNCs have more recently been produced using deep eutectic solvents, which are a

subcategory of ionic liquids (for example, choline chloride combined with oxalic acid dihydrate),[61,62] and, although these solvents impart carboxyl groups onto the CNC surfaces, some aggregates are still present and the crystallinity indices are low (Table 2.1). Similarly, CNCs produced with subcritical water are uncharged, despite having high crystallinities.[46] Lastly, at this stage of research and development, CNCs produced with enzymatic hydrolyses do not meet any of the three target properties: they are colloidally unstable, nanoscale dimensions are not consistently achieved and they have low crystallinities.[55–57] These results outline the difficulty in producing high-performing CNCs via alternate production routes. It is unsurprising that sulfuric acid hydrolysis and oxidative methods are the most common processes reported in the literature and are the major focus of scale-up efforts.

2.2.2 Optimization of production routes

Many efforts have been made to optimize the production of cellulose nanocrystals, particularly from sulfuric acid. Although some optimization studies focus on varying one reaction parameter at a time, many have used response surface methodology , which generates mathematical models capable of determining optimal reaction conditions.[44,66,71,90,91] The effects of hydrolysis parameters such as reaction time (10 min to 18 h), temperature (26-80 ºC), acid concentration (16-68 wt.%) and acid to pulp ratio (0.5-1.5 g pulp mL^{-1} acid) on CNC surface charge density, size, crystallinity and yield have been evaluated.[70,71,91–97] Although maximizing CNC yield is often the focus of optimization studies, CNC performance is equally as important; ideal CNCs will have high colloidal stability in water (from high surface charge), nanoscale dimensions and high crystallinity while being produced from a high-yield process. In general, harsher hydrolyses (longer, hotter, or more concentrated acid) produce CNCs with smaller sizes and more surface charge groups. The yield and crystallinity, however, have a parabolic relationship with hydrolysis harshness. If the hydrolysis is not harsh enough, disordered regions will remain unhydrolyzed and only a few CNCs will be produced while the rest of the initial cellulose mass is recovered as solid residue. If the hydrolysis is too harsh, however, crystalline regions begin to degrade, thus reducing both yield and degree of crystallinity.[70,71,94–96]

Overall, the acid concentration is the dominant factor in determining CNC properties; the range of acid concentrations which can successfully produce CNC is narrow, and the frequently used concentration of 64 wt.% sulfuric acid is generally regarded as the optimal value (higher concentrations risk significant swelling and dissolution of cellulose).[4,10,70] The length of time and the temperature of the hydrolysis are also important factors; however, these can depend on the geometric setup and scale of the reaction. Similar optimization studies have also been performed on other production routes including hydrolyses with subcritical water,[98] phosphoric acid[48,66] and maleic acid.[90]

2.2.3 Sources of biomass

CNCs are most commonly produced from lignocellulosic sources such as wood pulp, grasses and cotton. In some regions, however, wood is scarce while other cellulose sources are more plentiful. As a result, CNCs have been successfully produced from agricultural waste products such as sugarcane bagasse, apple pomace, garlic straw, pineapple leaf and

tomato peel, to name a few.[42,99–102] For each new biomass source, a process must be developed to isolate the cellulose from other components such as hemicelluloses, lignin, inorganics and waxes. For wood pulp, cotton and most plants, the cellulosic fraction is quite high; however, for agricultural residue, the cellulose yield after purification is typically only 30-40% and can be as low as 13%.[41,102,103]

In general, CNCs from wood pulp and cotton sources are similar: they have lengths between 100 and 200 nm, which is owing to the LODP of the fibres themselves (cotton fibres and bleached sulfite pulps have LODP values of 200-250 and 200-280, respectively).[65] Despite their similarities, subtle differences in sizes (which are statistically insignificant) have been suggested: wood pulp CNCs appear slightly shorter.[104] This observation could explain why other properties like liquid crystalline self assembly, viscosity, diffusion coefficients and surface activity differ significantly.[104] Comparing CNCs from softwood (spruce) and hardwood (eucalyptus) pulps, however, has indicated that the target properties are extremely similar if produced following the same protocol.[93] Some plants, such as ramie and hemp, have more crystalline cellulose fibres to begin with and higher LODP values (ca. 300-350).[65,105] Theoretically, they should produce longer CNCs, however, inconsistent hydrolysis protocols between research groups make direct comparisons difficult. Noteworthy yields above 70% come from Miscanthus giganteus,[106] eucalyptus[70] and jute.[107] Although subtle differences exist among lignocellulosic starting materials, the effects of the hydrolysis conditions often prevail.[108]

CNC production, however, is not limited to lignocellulosic biomass. CNCs have also been produced from tunicates (where the cellulose is found in the mantle or tunic of these sea animals) and algae.[57] Additionally, bacterial cellulose can be produced from live cultures of gram-negative acetic acid bacteria (for example, Komagataeibacter xylinus, formerly known as Gluconacetobacter xylinus and Acetobacter xylinum) or purchased as nata de coco, which is an edible coconut gel.[57] These starting materials tend to produce longer CNCs and can reach lengths over 1 µm.[93] While CNCs from tunicates consistently have lengths in the micrometre range, CNCs from algae[109–112] and bacterial cellulose[113,114] can be closer in size to lignocellulosic CNCs, depending on the method used to produce them (Table 2.2). Although many uses would benefit from longer CNCs, using tunicate cellulose as a starting material is infeasible for most large-scale applications owing to cost and extensive pre-cleaning and separation procedures needed, as such, other routes to greatly enhance CNC aspect ratio would be welcomed. Overall, although some cellulose sources (particularly tunicates) produce CNCs with significantly different properties, many starting materials only offer subtle differences, which are even more difficult to compare when production routes differ as well.

2.2.4 Industrial production
Currently, CNCs are industrially produced by ten organizations (Table 2.2)[11,12,115] which have pilot, demonstration, or semi-industrial plant facilities with production capacities in the kilogram to tonne-per-day range (on a dry basis). CelluForce Inc. is the world's largest producer of CNCs (since 2011) with Alberta Pacific Forest Industries Inc., GranBio and Anomera Inc. following close behind and with the commissioning of new plants in

progress. The first European CNC plant will be built by MoRe Research, a joint effort between Melodea Ltd., Holmen AB, and RISE Research Institute of Sweden AB, in Örnsköldsvik, Sweden (further production capacity and timeline information is currently unavailable). Smaller pilot-scale facilities are primarily research organizations focused on process optimization (for consistency, purity, quality, and economics),[116] novel production routes, and the development of new purification techniques, drying methods and industrially feasible surface modification strategies. For example, process intensification was carried out by FPInnovations (the first organization to work on scale-up in collaboration with McGill University's Pulp & Paper Research Centre in the early 2000s, and then joined forces with Domtar Inc. to create CelluForce Inc.) and the Forest Products Laboratory of the United States Department of Agriculture (USDA). Although these organizations have provided CNCs for research and development, they do not sell products in large volumes. Formerly, the CNCs produced by the USDA's Forest Products Laboratory could be procured from the University of Maine's Process Development Centre,[117] but this is no longer the case: CNCs purchased from the University of Maine are now produced by CelluForce Inc.

Sulfuric acid hydrolysis remains the most common production route at the industrial scale – this process provides high quality sulfated CNCs that meet the property targets discussed above and are the primary CNC type that have been used in commercial application development.[10] The innovations that were needed to move to this tonne-per-day production capacity included handling and recycling strong acids at scale, new membrane filtration systems for purification, and spray drying of CNCs into a redispersible powder[118] for easier shipping and an extended shelf life. Recently, the first continuous H_2SO_4 hydrolysis process has been reported (replacing the batch process and using three-times less acid) by InnoTech Alberta in conjunction with Alberta Pacific Forest Industries Inc. (with engineering carried out by NORAM Engineering and Constructors Ltd.).[119] This continuous reactor process may offer significant savings in time, chemicals and energy costs.

Table 2.2. Current and planned industrial production of cellulose nanocrystals (CNCs).

Company	Location	Biomass source(s)	Production volume	CNC surface chemistry	Production route	Ref.[a]
Alberta-Pacific Forest Industries Inc.	Alberta, Canada	Hard or softwood kraft pulp and dissolving pulp	500 kg per day	Sulfated	Sulfuric acid hydrolysis (continuous process)	[119]
Anomera Inc.	Ontario, Canada	Softwood pulp	30 kg per day (current); 1 tonne per day (projected 2020)	Carboxylated	Dilute hydrogen peroxide oxidation	[81]
Blue Goose Biorefineries Inc.	Saskatchewan, Canada	Viscose grade dissolving pulp	10 kg per day	Carboxylated	Transition metal catalyzed oxidation	[120]
CelluForce Inc. (can also be procured from University of Maine)	Quebec, Canada	Bleached softwood kraft pulp	1 tonne per day (since 2012)	Sulfated	Sulfuric acid hydrolysis (batch process)	
Cellulose Lab	New Brunswick, Canada	Dissolving or commercial pulp, cotton, sisal, tunicate	10 kg per day	Sulfated (+ surface modifications)	Sulfuric acid hydrolysis (batch process)	
GranBio (formerly American Process Inc.)	Georgia, USA (Brazilian-owned)	Woodchips (eucalyptus), agricultural residues, energy crops	500 kg per day	Unmodified (+ grade containing lignin coating)	AVAP® patented process with ethanol and SO_2 (continuous process)	[84,121–124]
FPInnovations	Quebec, Canada	Bleached chemical wood pulp	1.5 kg per day	Sulfated or phosphated	Sulfuric or phosphoric acid hydrolysis (batch process)	
InnoTech Alberta	Alberta, Canada	Various bleached hard or softwood pulp	2 kg per day	Sulfated	Sulfuric acid hydrolysis (batch &	

					continuous process)	
Melodea Ltd.	Rehovot, Israel	Various bleached hard or softwood pulp	>10 tonnes per year (projected 2020)	Sulfated	Sulfuric acid hydrolysis (batch process)	
USDA Forest Products Laboratory	Wisconsin, USA	Dissolving pulp	10 kg per day	Sulfated	Sulfuric acid hydrolysis (batch process)	

AVAP®; American Value Added Pulping; USDA, United States Department of Agriculture.

[a]Where available, references are included for patents and journal articles describing the production route; the majority of the information was solicited for a TAPPI *International Conference on Nanotechnology for Renewable Materials* conference presentation (2019) (ref. 140) or was obtained from market reports (refs. 11 and 12).

The production of CNCs following oxidative routes is emerging as a highly scalable and cost-efficient process to make carboxylated CNCs (by Anomera Inc. and Blue Goose Biorefineries Inc.). These routes use dilute hydrogen peroxide[81] and transition-metal catalyzed oxidation,[120] respectively, and bear no resemblance to the ammonium persulfate oxidation method[54] patented by the National Research Council of Canada in 2011 and licenced by BioVision Inc., (turned Advanced Cellulosic Materials Inc.) which is no longer in operation. Another promising route to produce low-cost CNFs and CNCs is the GranBio AVAP® process which uses (recyclable) ethanol and SO_2 to remove hemicelluloses, lignin, resins and extractives while producing strong lignosulfonic acids which then hydrolyse disordered cellulose to isolate a high crystallinity end product.[84] The resulting CNCs (with unmodified cellulose surface chemistry) are combined with other products from the reaction (but can be size fractionated) and are either bleached or may have deposited lignin to decrease the nanoparticle surface hydrophilicity. Low operating and capital costs, combined with standard unit operations and readily available chemicals, represent a significant advantage.

The majority of commercial production routes claim (to varying extents) that they are feedstock agnostic, meaning the CNC product quality is not substantially biomass source dependent. The biomass is almost always heavily bleached prior to CNC production; as such, lignin and hemicelluloses are removed (unless they will add value, for example, with lignin increasing CNC hydrophobicity), making the exact cellulose source irrelevant. While softwood and hardwood pulps are common starting materials in industry, woodchips, bark, agricultural residues (corn cobs and stover, kenaf, and cane straw), energy crops (switchgrass, miscanthus, and bamboo) and purer celluloses, like dissolving pulp and cotton have also been demonstrated (with the latter two sources having been shown to be indistinguishable at the 2 kg-per-day production scale).[10] In most production processes, the degraded sugars can be fermented into biochemicals such as bioethanol and removed lignin can be burned for energy (as done during chemical pulping) offering other revenue streams.

Clearly, industrial production of CNCs is on the upswing and multiple suppliers are crucial for market growth. While information regarding the cost of CNCs is difficult to find and will change over time with process, scale, and feedstock refinement, researchers and companies are encouraged to assess the added value of CNCs in their product, the volume of CNCs required (as well as the total volume of the product) and the preferred quality (or grade) of CNCs to conclude whether their cost is reasonable. Different CNC grades are evolving; including premium grades (for food, medical, cosmetic, and personal care), and performance grades (for construction, industrial processing, and environmental remediation), and materials are commercially available in spray dried, freeze dried, and dispersion forms. Standardization efforts are underway to support turning this nanoscience into true nanotechnology.[5,125–131] While some people claim the hurdles for widespread multi-sector commercialization of CNCs stem from being stuck in a position of technology push rather than market pull, commercial products do exist and many more are close to deployment. Some companies have a focus application area, for example, Anomera Inc. in cosmetics, and Blue Goose Biorefineries in cement reinforcement, but for the most part, they overlap in exploring the potential of CNCs in the following applications: paints, inks,

varnish, and coatings; adhesives; oil and gas; food; health care, pharmaceutical and dental; cosmetics; consumer and specialty paper and board; pulp, paper and industrial processing; packaging, plastics and composites; rubbers and elastomers; components in electronics; absorbents and porous materials; textiles; cement and concrete; and water treatment.

2.2.5 Outlook on cellulose nanocrystal production
Despite their positive attributes and widespread industrial production, CNCs made with sulfuric acid still have limitations. One limitation is their performance at high temperatures; although CNC thermal stability is relatively high for an organic material, improving the thermal stability would benefit, for example, melt compounding with high melting temperature polymers, and a range of engineering fluids and separation processes. Another area where CNC performance is lacking is in environments of high ionic strength where electrostatic interactions are screened and van der Waals attraction dominates leading to aggregation and sedimentation of particles. Lastly, the use of CNCs in hydrophobic environments, for example as reinforcing agents in polymer nanocomposites, is limited by their hydrophilicity.

The potential to expand the use of CNCs and improve material behavior has motivated researchers to investigate alternative source materials and production routes, which may also increase yield and economics, and limit further physical and chemical CNC treatments down the line. In some cases, the new CNCs produced fail to achieve the basic target properties (e.g., well-dispersed, nano-whisker shaped particles with crystalline morphology); this simply demonstrates the magnitude of the challenge. In other cases, new production routes show promise; however, CNC users must know how to select the right CNCs for their desired applications. As such, a thorough understanding of the effects of production routes on CNC properties, and the subsequent effects of these properties on CNC performance, is required. Ultimately, this will accelerate the large-scale implementation of CNCs as materials for biomedical devices; reinforcing agents in nanocomposites; rheological modifiers; and interfacial stabilizers for emulsions, gels, and foams.

2.3 Cellulose nanocrystal thermal performance
2.3.1 Thermal performance of dried cellulose nanocrystals
The thermal stability of CNCs dictates their performance in formulations and materials that must be processed or used at high temperatures. Thermal stability refers to the onset of thermal degradation and is typically measured via thermogravimetric analysis, in which a dried cellulose sample is heated at a constant rate while its mass is monitored.[132] While CNCs are a novel class of nanomaterials, they are cellulose-based, and as such, their thermal degradation mechanisms are similar to those of native cellulose. Upon exposure to heat, cellulose first undergoes "activation"; in this stage, no weight loss occurs, however, the degree of polymerization of cellulose chains decreases to its levelling off degree of polymerization (LODP) of ca. 200-300 glucose units (depending on the cellulose source).[133] While many reducing ends are already present (particularly in low degree of polymerization cellulosic materials such as CNCs), activation occurs at the interface of crystalline and amorphous regions within cellulose chains and results in the formation of

additional reducing ends.[133] After cellulose activation, cellulose depolymerization and degradation occur through two competitive pathways.[134,135] High temperatures favor the production of a volatile fraction composed of anhydrosugars such as levoglucosan, while low temperatures favor the production of char and gases including carbon dioxide and carbon monoxide.[135,136] Cellulose degree of polymerization therefore plays a critical role in thermal stability: shorter cellulose chains possess more reducing ends and as such are already somewhat "active".[137] For this reason, CNCs, which are made up of cellulose chain lengths at or near their LODP, have lower thermal stabilities than cellulosic materials with longer cellulose chains such as native cellulose,[138] CNFs,[137] and cellulose filaments.[139]

In addition to being made up of shorter cellulose chains, the thermal stability (and overall thermal performance) of CNCs is heavily affected by the introduction of surface charge groups. CNCs made with sulfuric acid typically begin to degrade around 150 °C in their native acid form; however, this can be extended to ca. 300 °C by neutralizing CNCs to the sodium salt form.[95,140] When sulfate groups are present on CNC surfaces at elevated temperatures, desulfation occurs and free sulfate ions combine with water (either bound to the CNCs or released as a by-product of degradation)[141] to produce sulfuric acid.[142] This localized acid further catalyzes the desulfation, degradation and depolymerization of cellulose chains.[138] When the sulfate groups' proton counterions are replaced with sodium ions (via the addition of sodium hydroxide), localized acid is neutralized and thermal stability is improved.[95,139,143] Additionally, removing sulfate groups prior to heating through desulfation procedures can mitigate acid-catalyzed degradation and further improve thermal stability.[138,140] As such, both surface chemistry (of the bound functional group and its associated counterion) and surface charge density play an important role in CNC thermal performance.

While sulfated CNCs are the most widely used, numerous methods exist to produce CNCs with carboxyl groups, both at laboratory and industrial scales (as outlined above). The presence of carboxyl groups on cellulose surfaces significantly alters their thermal performance.[144–146] Perhaps the most important observation is the influence of proton and sodium counterions: while sulfated CNCs are more thermally stable in their native acid form, CNFs with carboxyl groups follow the opposite trend.[145] In acid form, carboxyl groups reduce cellulose thermal stability; however, this phenomena is exacerbated in sodium form, where sodium carbonate is formed as a result of decarboxylation and dehydration reactions.[145] Similarly to the thermal behavior of sulfated CNCs, increased loadings of carboxyl groups on cellulose surfaces further reduce their thermal stability.[147] The surface chemistry of the carboxyl groups is also a relevant factor: carboxyl groups bonded at the C6 position are less thermally stable than, for example, carboxymethylcellulose.[147]

While the thermal performance of sodium form sulfated CNCs (as well as acid form oxidized CNCs) is quite impressive for an organic material, many researchers have sought out new production routes to further improve this property. These efforts are largely motivated by the desire to use CNCs as strengthening agents in melt-processed composites, where material performance will suffer if the polymer melting point is greater than the onset

of thermal degradation of the CNCs. Generally, attempts to improve CNC thermal performance involve a modified hydrolysis procedure using weak acids. For example, phosphoric acid has been used to produce CNCs with phosphate groups which performed noticeably better than sulfated CNCs at high temperatures.[48] However, in later work, we attributed the increased thermal stability to the low density of phosphate groups on CNC surfaces resulting from the weak acid hydrolysis.[39] In fact, Fiss et al. demonstrated that CNCs with higher loadings of phosphate groups (produced via ball milling with phosphorus pentoxide and urea) acted as flame-retardants and began to degrade at much lower temperatures than typical sulfated CNCs.[148] As such, the introduction of phosphate groups does dot directly improve CNC thermal stability; rather, improvements are a result of weaker hydrolysis conditions resulting in lower surface charge densities and likely longer CNCs. This theory is in line with optimization efforts on sulfuric acid hydrolyzed CNCs, whereby CNCs produced in less harsh reaction conditions (shorter reaction time, lower temperature, or weaker acid) are generally more thermally stable.[95]

Organic acid hydrolyses have also been used to produce CNCs with seemingly increased thermal stability.[47,52,77] Unfortunately, the extent of the improvements, as well as the CNC properties which cause them, are often unclear. The morphology, degree of crystallinity, and colloidal stability of CNCs made with organic acids (e.g., oxalic, maleic, citric acids) differ from those of CNCs made with sulfuric acid (Table 2.1). As such, the increased thermal stability of CNCs made with organic acids appears to follow the trend discussed above: CNCs subject to weaker hydrolysis procedures are generally more thermally stable. CNCs produced with organic acids, however, possess carboxylate functional groups,[47,52] which are known to reduce the thermal stability of CNCs in sodium form.[144,145] Nevertheless, the thermal performance of CNCs produced with organic acids is often compared to sulfuric acid hydrolyzed CNCs using a single counterion for both CNC types. Since sulfated CNCs are more thermally stable in acid from, such comparisons are misleading and can cause researchers to attribute improvements in thermal performance to CNCs themselves rather than to the selection of a favorable counterion. As a result, it is difficult to draw conclusions from the literature. Furthermore, these difficulties are exacerbated when thermal performance is compared between laboratories where sample preparation, instruments, and standard operating procedures differ[132].

In addition to exploring new production routes, researchers have investigated surface modifications or simple additives which can improve CNC (or CNF) thermal performance in the dry state. These efforts include reduction of reducing ends with NaBH₄,[133] acetylation of surface hydroxy groups,[137] counterion exchange with methyl(triphenyl)phosphonium,[149] coating with ionic liquids,[150] and coupling amine-terminated polyethylene glycol to carboxyl groups.[151] These modifications and additives target the weak points of CNC thermal performance: reducing ends, vulnerable surface charge groups, and unstable counterions. It is therefore obvious that they rely on a fundamental understanding of cellulose thermal degradation mechanisms and on the effects of various CNC properties and surface chemistries on these mechanisms. As new production routes emerge in both laboratory and industrial scale processes, our understanding of these principles must deepen to expand the usage of CNCs in high temperature applications.

2.3.2 Thermal performance of cellulose nanocrystal suspensions

While the high temperature performance of CNCs is most often evaluated on dried CNCs (recognizing that "dry" nanocelluloses always encompasses a certain amount of residual moisture on the order of 2-5 %),[152] these results are irrelevant for applications looking to incorporate CNCs into aqueous formulations. The thermal stability of CNC suspensions can limit their use in aqueous high temperature applications such as fluids for enhanced oil recovery. At temperatures as low as 110 ºC, bulk suspension properties, particularly pH, colloidal stability and rheology, begin to change.[153,154] These changes in bulk suspension properties stem from desulfation of surface sulfate groups, which can occur at temperatures as low as 4°C.[142] Desulfation further progresses at higher temperatures, whereby significant decreases in surface sulfate groups are observed around 40-50 °C.[155] Upon losing their anionic charge groups, the electrostatic repulsion between neighboring CNCs decreases and attractive van der Waals forces begin to dominate interparticle interactions. At this stage, CNC aggregates[154] or percolated gel networks[156] can form, therefore altering the rheological behavior of CNC-containing fluids.[156,157]

In addition to altering bulk suspension properties via desulfation, high temperatures can cause structural changes to the CNCs themselves. Discoloration, for example, has been observed upon heating CNC suspensions to 120-150 °C;[154,156] however, the extent to which it occurs is dependent on the initial concentration of the suspension. Discoloration is typically attributed to the production of furfural and hydroxymethylfurfural;[154] however, it is not necessarily indicative of extensive degradation of cellulose chains. Overall, relatively few studies have evaluated the effects of high temperatures on CNC suspensions; as such, further studies are required to determine what changes, if any, are occurring in CNC structure and morphology.

2.3.3 Outlook on cellulose nanocrystal thermal performance

Overall, it is evident that CNC morphology and structure, in addition to the presence of surface charge groups and their respective counterions, all play a role in CNC thermal performance. As new CNC types continue to emerge at both laboratory and industrial scales, a thorough understanding of the effects of CNC properties on their behavior at high temperatures is a necessity. Obtaining this understanding requires systematic studies which directly compare multiple CNC types, therefore avoiding differences in sample preparation, instruments, and standard operating procedures. Furthermore, these systematic studies must evaluate the thermal performance of each CNC type with various counterions. This will prevent the mislabelling of certain CNC types as "thermally superior" when their thermal performance is only attributable to a favorable counterion choice. Similarly, improved thermal performance should not come at the cost of a loss of other key CNC properties, for example, a reduction in surface charge density and therefore colloidal stability, or a decrease in CNC's reinforcement potential. Ultimately, improving our understanding of CNC thermal performance will expand their usage in a variety of applications and will aid in their transition from a technology push to a market pull.

2.4 References

1.   Nickerson, R. F. & Habrle, J. A. Cellulose intercrystalline structure. *Ind. Eng. Chem.* **39**, 1507–1512 (1947).

2.   Rånby, B. G., Banderet, A. & Sillén, L. G. Aqueous colloidal solutions of cellulose micelles. *Acta Chem. Scand.,* **3**, 649–650 (1949).

3.   Rånby, B. G. The Colloidal Properties of Cellulose Micelles. *Discuss. Faraday Soc.* **11**, 158–164 (1951).

4.   Mukherjee, S. M. & Woods, H. J. X-ray and electron microscope studies of the degradation of cellulose by sulphuric acid. *Biochim. Biophys. Acta* **10**, 499–511 (1953).

5.   Nanotechnologies - Standard terms and their definition for cellulose nanomaterial, ISO/TS 20477, International Organization for Standardization 2017, Geneva.

6.   Tashiro, K. & Kobayashi, M. Theoretical evaluation of three-dimensional elastic constants of native and regenerated celluloses: role of hydrogen bonds. *Polymer (Guildf).* **32**, 1516–1526 (1991).

7.   Viet, D., Beck-Candanedo, S. & Gray, D. G. Dispersion of cellulose nanocrystals in polar organic solvents. *Cellulose* **14**, 109–113 (2007).

8.   Revol, J.-F., Bradford, H., Giasson, J., Marchessault, R. H. & Gray, D. G. Helicoidal self-ordering of cellulose microfibrils in aqueous suspension. *Int. J. Biol. Macromol.* **14**, 170–172 (1992).

9.   Roman, M. Toxicity of cellulose nanocrystals: a review. *Ind. Biotechnol.* **11**, 25–33 (2015).

10. Reid, M. S., Villalobos, M. & Cranston, E. D. Benchmarking cellulose nanocrystals: from the laboratory to industrial production. *Langmuir* **33**, 1583–1598 (2017).

11. Miller, J. *Nanocellulose: Producers, Products, and Applications*. (TAPPI Press, 2017).

12. The Global Market for Nanocellulose. *Research and Markets.* https://www.researchandmarkets.com/reports/4827614/the-global-market-for-nanocellulose?utm_code=bcb85m&utm_medium=BW (2019).

13. Favier, V., Chanzy, H. & Cavaillé, J. Y. Polymer nanocomposites reinforced by cellulose whiskers. *Macromolecules* **28**, 6365–6367 (1995).

14. Araki, J., Wada, M. & Kuga, S. Steric stabilization of a cellulose microcrystal suspension by poly(ethylene glycol) grafting. *Langmuir* **17**, 21–27 (2001).

15. Choi, Y. & Simonsen, J. Cellulose nanocrystal-filled carboxymethyl cellulose nanocomposites. *J. Nanosci. Nanotechnol.* **6**, 633–639 (2006).

16. Heath, L. & Thielemans, W. Cellulose nanowhisker aerogels. *Green Chem.* **12**, 1448–1453 (2010).

17. Liew, S. Y., Thielemans, W. & Walsh, D. A. Electrochemical capacitance of nanocomposite polypyrrole/cellulose films. *J. Phys. Chem. C* **114**, 17926–17933 (2010).

18.   Jackson, J. K. *et al.* The use of nanocrystalline cellulose for the binding and controlled release of drugs. *Int. J. Nanomedicine* **6**, 321–330 (2011).

19.   Kalashnikova, I., Bizot, H., Cathala, B. & Capron, I. New pickering emulsions stabilized by bacterial cellulose nanocrystals. *Langmuir* **27**, 7471–7479 (2011).

20.   Cao, Y., Weiss, W. J., Youngblood, J., Moon, R. & Zavattieri, P. Performance-enhanced cementitious materials by cellulose nanocrystal additions. *Prod. Appl. Cellul. Nanomater.* 135–136 (2013).

21.   Lu, P. & Hsieh, Y. Lo. Preparation and properties of cellulose nanocrystals: Rods, spheres, and network. *Carbohydr. Polym.* **82**, 329–336 (2010).

22.   Foster, E. J. *et al.* Current characterization methods for cellulose nanomaterials. *Chem. Soc. Rev.* **47**, 2609–2679 (2018).

23.   Brinkmann, A. *et al.* Correlating cellulose nanocrystal particle size and surface zrea. *Langmuir* **32**, 6105–6114 (2016).

24.   Van De Ven, T. G. M. & Sheikhi, A. Hairy cellulose nanocrystalloids: A novel class of nanocellulose. *Nanoscale* **8**, 15101–15114 (2016).

25.   Lin, K.-H. *et al.* An analysis on the electrophoretic mobility of cellulose nanocrystals as thin cylinders: relaxation and end effect. *RSC Adv.* **9**, 34032–34038 (2019).

26.   Bhattacharjee, S. DLS and zeta potential - What they are and what they are not? *J. Control. Release* **235**, 337–351 (2016).

27.   Eichhorn, S. J. *et al.* Review: Current international research into cellulose nanofibres and nanocomposites. *J. Mater. Sci.* **45**, 1–33 (2010).

28.   Phan-Xuan, T. *et al.* Aggregation behavior of aqueous cellulose nanocrystals: the effect of inorganic salts. *Cellulose* **23**, 3653–3663 (2016).

29.   Cherhal, F., Cousin, F. & Capron, I. Influence of charge density and ionic strength on the aggregation process of cellulose nanocrystals in aqueous suspension, as revealed by small-angle neutron scattering. *Langmuir* **31**, 5596–5602 (2015).

30.   Fraschini, C. *et al.* Critical discussion of light scattering and microscopy techniques for CNC particle sizing. *Nord. Pulp Pap. Res. J.* **29**, 31–40 (2014).

31.   Boluk, Y. & Danumah, C. Analysis of cellulose nanocrystal rod lengths by dynamic light scattering and electron microscopy. *J. Nanoparticle Res.* **16**, (2014).

32.   Ogawa, Y. & Putaux, J. L. Transmission electron microscopy of cellulose. Part 2: technical and practical aspects. *Cellulose* **26**, 17–34 (2019).

33.   Sèbe, G., Ham-Pichavant, F., Ibarboure, E., Koffi, A. L. C. & Tingaut, P. Supramolecular structure characterization of cellulose II nanowhiskers produced by acid hydrolysis of cellulose i substrates. *Biomacromolecules* **13**, 570–578 (2012).

34.   Yue, Y. *et al.* Comparative properties of cellulose nano-crystals from native and mercerized cotton fibers. *Cellulose* **19**, 1173–1187 (2012).

35.   Agarwal, U. P., Ralph, S. A., Reiner, R. S. & Baez, C. Probing crystallinity of never-dried wood cellulose with Raman spectroscopy. *Cellulose* **23**, 125–144 (2016).

36.   Park, S., Baker, J. O., Himmel, M. E., Parilla, P. A. & Johnson, D. K. Cellulose crystallinity index: Measurement techniques and their impact on interpreting cellulase performance. *Biotechnol. Biofuels* **3**, 1–10 (2010).

37.   Segal, L., Creely, J. J., Martin, A. E. & Conrad, C. M. An empirical method for estimating the degree of crystallinity of native cellulose using the X-ray diffractometer. *Text. Res. J.* **29**, 786–794 (1959).

38.   Kedzior, S. A., Zoppe, J. O., Berry, R. M. & Cranston, E. D. Recent advances and an industrial perspective of cellulose nanocrystal functionalization through polymer grafting. *Curr. Opin. Solid State Mater. Sci.* **23**, 74–91 (2019).

39.   Vanderfleet, O. M. *et al.* Insight into thermal stability of cellulose nanocrystals from new hydrolysis methods with acid blends. *Cellulose* **26**, 507–528 (2019).

40.   Teixeira, E. de M. *et al.* Sugarcane bagasse whiskers: Extraction and characterizations. *Ind. Crops Prod.* **33**, 63–66 (2011).

41.   Bano, S. & Negi, Y. S. Studies on cellulose nanocrystals isolated from groundnut shells. *Carbohydr. Polym.* **157**, 1041–1049 (2017).

42.   Melikoğlu, A. Y., Bilek, S. E. & Cesur, S. Optimum alkaline treatment parameters for the extraction of cellulose and production of cellulose nanocrystals from apple pomace. *Carbohydr. Polym.* **215**, 330–337 (2019).

43.   Kontturi, E. *et al.* Degradation and crystallization of cellulose in hydrogen chloride vapor for high-yield isolation of cellulose nanocrystals. *Angew. Chemie - Int. Ed.* **55**, 14455–14458 (2016).

44.   Lu, Q. *et al.* Extraction of cellulose nanocrystals with a high yield of 88% by simultaneous mechanochemical activation and phosphotungstic acid hydrolysis. *ACS Sustain. Chem. Eng.* **4**, 2165–2172 (2016).

45.   Yu, H. *et al.* Facile extraction of thermally stable cellulose nanocrystals with a high yield of 93% through hydrochloric acid hydrolysis under hydrothermal conditions. *J. Mater. Chem. A* **1**, 3938–3944 (2013).

46.   Novo, L. P., Bras, J., García, A., Belgacem, N. & Curvelo, A. A. S. Subcritical water: a method for green production of cellulose nanocrystals. *ACS Sustain. Chem. Eng.* **3**, 2839–2846 (2015).

47.   Chen, L. *et al.* Highly thermal-stable and functional cellulose nanocrystals and nanofibrils produced using fully recyclable organic acids. *Green Chem.* **18**, 3835–3843 (2016).

48.   Camarero Espinosa, S. *et al.* Isolation of thermally stable cellulose nanocrystals by phosphoric acid hydrolysis. *Biomacromolecules* **14**, 1223–1230 (2013).

49.   Sadeghifar, H., Filpponen, I., Clarke, S. P., Brougham, D. F. & Argyropoulos, D. S. Production of cellulose nanocrystals using hydrobromic acid and click reactions on their surface. *J. Mater. Sci.* **46**, 7344–7355 (2011).

50.   Li, D., Henschen, J. & Ek, M. Esterification and hydrolysis of cellulose using oxalic acid dihydrate in a solvent-free reaction suitable for preparation of surface-functionalised cellulose nanocrystals with high yield. *Green Chem.* **19**, 5564–5567 (2017).

51.   Boujemaoui, A., Mongkhontreerat, S., Malmström, E. & Carlmark, A. Preparation and characterization of functionalized cellulose nanocrystals. *Carbohydr. Polym.* **115**, 457–464 (2015).

52.   Yu, H.-Y., Zhang, D.-Z., Lu, F.-F. & Yao, J. New approach for single-step extraction of carboxylated cellulose nanocrystals for their use as adsorbents and flocculants. *ACS Sustain. Chem. Eng.* **4**, 2632–2643 (2016).

53.   Zhou, Y., Saito, T., Bergström, L. & Isogai, A. Acid-free preparation of cellulose nanocrystals by TEMPO oxidation and subsequent cavitation. *Biomacromolecules* **19**, 633–639 (2018).

54.   Leung, A. C. W. *et al.* Characteristics and properties of carboxylated cellulose nanocrystals prepared from a novel one-step procedure. *Small* **7**, 302–305 (2011).

55.   Filson, P. B., Dawson-Andoh, B. E. & Schwegler-Berry, D. Enzymatic-mediated production of cellulose nanocrystals from recycled pulp. *Green Chem.* **11**, 1808–1814 (2009).

56.   Siqueira, G., Tapin-Lingua, S., Bras, J., da Silva Perez, D. & Dufresne, A. Morphological investigation of nanoparticles obtained from combined mechanical shearing, and enzymatic and acid hydrolysis of sisal fibers. *Cellulose* **17**, 1147–1158 (2010).

57.   Sacui, I. A. *et al.* Comparison of the properties of cellulose nanocrystals and cellulose nanofibrils isolated from bacteria, tunicate, and wood processed using acid, enzymatic, mechanical, and oxidative methods. *ACS Appl. Mater. Interfaces* **6**, 6127–6138 (2014).

58.   Abushammala, H., Krossing, I. & Laborie, M. P. Ionic liquid-mediated technology to produce cellulose nanocrystals directly from wood. *Carbohydr. Polym.* **134**, 609–616 (2015).

59.   Man, Z. *et al.* Preparation of cellulose nanocrystals using an ionic liquid. *J. Polym. Environ.* **19**, 726–731 (2011).

60.   Miao, J., Yu, Y., Jiang, Z. & Zhang, L. One-pot preparation of hydrophobic cellulose nanocrystals in an ionic liquid. *Cellulose* **23**, 1209–1219 (2016).

61.   Sirviö, J. A., Visanko, M. & Liimatainen, H. Acidic Deep Eutectic Solvents As Hydrolytic Media for Cellulose Nanocrystal Production. *Biomacromolecules* **17**, 3025–3032 (2016).

62.   Jiang, J. *et al.* High Production Yield and More Thermally Stable Lignin-Containing Cellulose Nanocrystals Isolated Using a Ternary Acidic Deep Eutectic Solvent. 2–11 (2020) doi:10.1021/acssuschemeng.0c01724.

63.   Trache, D., Hussin, M. H., Haafiz, M. K. M. & Thakur, V. K. Recent progress in cellulose nanocrystals: Sources and production. *Nanoscale* **9**, 1763–1786 (2017).

64.   Xiang, Q., Lee, Y. Y., Pettersson, P. O. & Torget, R. W. Heterogeneous aspects of acid hydrolysis of α-cellulose. in *Applied Biochemistry and Biotechnology* vols 105–108 505–

514 (2003).

65.   Battista, O. A., Coppick, S., Howsmon, J. A., Morehead, F. F. & Sisson, W. A. Level-off degree of polymerization. *Ind. Eng. Chem.* **48**, 333–335 (1956).

66.   Vanderfleet, O. M., Osorio, D. A. & Cranston, E. D. Optimization of cellulose nanocrystal length and surface charge density through phosphoric acid hydrolysis. *Philos. Trans. R. Soc. London A Math. Phys. Eng. Sci.* **376**, 1–7 (2018).

67.   Henschen, J., Li, D. & Ek, M. Preparation of cellulose nanomaterials via cellulose oxalates. *Carbohydr. Polym.* **213**, 208–216 (2019).

68.   Bian, H., Chen, L., Dai, H. & Zhu, J. Y. Effect of fiber drying on properties of lignin containing cellulose nanocrystals and nanofibrils produced through maleic acid hydrolysis. *Cellulose* **24**, 4205–4216 (2017).

69.   Du, H. *et al.* Preparation and characterization of thermally stable cellulose nanocrystals via a sustainable approach of FeCl3-catalyzed formic acid hydrolysis. *Cellulose* **23**, 2389–2407 (2016).

70.   Chen, L. *et al.* Tailoring the yield and characteristics of wood cellulose nanocrystals (CNC) using concentrated acid hydrolysis. *Cellulose* **22**, 1753–1762 (2015).

71.   Dong, S., Bortner, M. J. & Roman, M. Analysis of the sulfuric acid hydrolysis of wood pulp for cellulose nanocrystal production: A central composite design study. *Ind. Crops Prod.* **93**, 1–12 (2016).

72.   Guo, J., Guo, X., Wang, S. & Yin, Y. Effects of ultrasonic treatment during acid hydrolysis on the yield, particle size and structure of cellulose nanocrystals. *Carbohydr. Polym.* **135**, 248–255 (2016).

73.   Araki, J., Wada, M., Kuga, S. & Okano, T. Flow properties of microcrystalline cellulose suspension prepared by acid treatment of native cellulose. *Colloids Surfaces A Physicochem. Eng. Asp.* **142**, 75–82 (1998).

74.   Salajková, M., Berglund, L. A. & Zhou, Q. Hydrophobic cellulose nanocrystals modified with quaternary ammonium salts. *J. Mater. Chem.* **22**, 19798–19805 (2012).

75.   Liu, Y. *et al.* A novel approach for the preparation of nanocrystalline cellulose by using phosphotungstic acid. *Carbohydr. Polym.* **110**, 415–422 (2014).

76.   Vasconcelos, N. F. *et al.* Bacterial cellulose nanocrystals produced under different hydrolysis conditions: Properties and morphological features. *Carbohydr. Polym.* **155**, 425–431 (2017).

77.   Spinella, S. *et al.* Concurrent cellulose hydrolysis and esterification to prepare a surface-modified cellulose nanocrystal decorated with carboxylic acid moieties. *ACS Sustain. Chem. Eng.* **4**, 1538–1550 (2016).

78.   Braun, B. & Dorgan, J. R. Single-step method for the isolation and surface functionalization of cellulosic nanowhiskers. *Biomacromolecules* **10**, 334–341 (2009).

79.   Cheng, M., Qin, Z., Chen, Y., Liu, J. & Ren, Z. Facile one-step extraction and oxidative carboxylation of cellulose nanocrystals through hydrothermal reaction by using mixed

inorganic acids. *Cellulose* **24**, 3243–3254 (2017).

80. Leguy, J. *et al.* Periodate oxidation followed by NaBH4 reduction converts microfibrillated cellulose into sterically stabilized neutral cellulose nanocrystal suspensions. *Langmuir* **34**, 11066–11075 (2018).

81. Andrews, M. P. & Morse, T. Method for producing functionalized nanocrystalline cellulose and functionalized nanocrystalline cellulose thereby produced. (2017).

82. Tan, X. Y., Abd Hamid, S. B. & Lai, C. W. Preparation of high crystallinity cellulose nanocrystals (CNCs) by ionic liquid solvolysis. *Biomass and Bioenergy* **81**, 584–591 (2015).

83. Novo, L. P., Bras, J., García, A., Belgacem, N. & Curvelo, A. A. S. Subcritical water: a method for green production of cellulose nanocrystals. *ACS Sustain. Chem. Eng.* **3**, 2839–2846 (2015).

84. Nelson, K. & Retsina, T. Innovative nanocellulose process breaks the cost barrier. *Tappi J.* **13**, 19–23 (2014).

85. Castro-Guerrero, C. F. & Gray, D. G. Chiral nematic phase formation by aqueous suspensions of cellulose nanocrystals prepared by oxidation with ammonium persulfate. *Cellulose* **21**, 2567–2577 (2014).

86. Montanari, S., Roumani, M., Heux, L. & Vignon, M. R. Topochemistry of carboxylated cellulose nanocrystals resulting from TEMPO-mediated oxidation. *Macromolecules* **38**, 1665–1671 (2005).

87. Habibi, Y., Chanzy, H. & Vignon, M. R. TEMPO-mediated surface oxidation of cellulose whiskers. *Cellulose* **13**, 679–687 (2006).

88. Wu, B., Wang, S., Tang, J. & Lin, N. Nanocellulose in high-value applications for reported trial and commercial products. in *Advanced Functional Materials from Nanopolysaccharides* (eds. Lin, N., Tang, J., Dufresne, A. & Tam, M. K. C.) 389–409 (Springer Singapore, 2019). doi:10.1007/978-981-15-0913-1_11.

89. Habibi, Y. Key advances in the chemical modification of nanocelluloses. *Chem. Soc. Rev.* **43**, 1519–1542 (2014).

90. Filson, P. B. & Dawson-Andoh, B. E. Sono-chemical preparation of cellulose nanocrystals from lignocellulose derived materials. *Bioresour. Technol.* **100**, 2259–2264 (2009).

91. Bondeson, D., Mathew, A. & Oksman, K. Optimization of the isolation of nanocrystals from microcrystalline cellulose by acid hydrolysis. *Cellulose* **13**, 171–180 (2006).

92. Dong, X. M., Revol, J.-F. & Gray, D. G. Effect of microcrystallite preparation conditions on the formation of colloid crystals of cellulose. *Cellulose* **5**, 19–32 (1998).

93. Beck-Candanedo, S., Roman, M. & Gray, D. G. Effect of reaction conditions on the properties and behavior of wood cellulose nanocrystal suspensions. *Biomacromolecules* **6**, 1048–1054 (2005).

94. Hamad, W. Y. & Hu, T. Q. Structure-process-yield interrelations in nanocrystalline cellulose extraction. *Can. J. Chem. Eng.* **88**, 392–402 (2010).

95.   Kargarzadeh, H. *et al.* Effects of hydrolysis conditions on the morphology, crystallinity, and thermal stability of cellulose nanocrystals extracted from kenaf bast fibers. *Cellulose* **19**, 855–866 (2012).

96.   Wang, Q., Zhao, X. & Zhu, J. Y. Kinetics of strong acid hydrolysis of a bleached kraft pulp for producing cellulose nanocrystals (CNCs). *Ind. Eng. Chem. Res.* **53**, 11007–11014 (2014).

97.   Bouchard, J., Méthot, M., Fraschini, C. & Beck, S. Effect of oligosaccharide deposition on the surface of cellulose nanocrystals as a function of acid hydrolysis temperature. *Cellulose* **23**, 3555–3567 (2016).

98.   Novo, L. P., Bras, J., García, A., Belgacem, N. & Curvelo, A. A. da S. A study of the production of cellulose nanocrystals through subcritical water hydrolysis. *Ind. Crops Prod.* **93**, 88–95 (2016).

99.   Hemmati, F., Jafari, S. M., Kashaninejad, M. & Barani Motlagh, M. Synthesis and characterization of cellulose nanocrystals derived from walnut shell agricultural residues. *Int. J. Biol. Macromol.* **120**, 1216–1224 (2018).

100.   Prasad Reddy, J. & Rhim, J. W. Isolation and characterization of cellulose nanocrystals from garlic skin. *Mater. Lett.* **129**, 20–23 (2014).

101.   Santos, R. M. dos *et al.* Cellulose nanocrystals from pineapple leaf, a new approach for the reuse of this agro-waste. *Ind. Crops Prod.* **50**, 707–714 (2013).

102.   Jiang, F. & Hsieh, Y. Lo. Cellulose nanocrystal isolation from tomato peels and assembled nanofibers. *Carbohydr. Polym.* **122**, 60–68 (2015).

103.   Johar, N., Ahmad, I. & Dufresne, A. Extraction, preparation and characterization of cellulose fibres and nanocrystals from rice husk. *Ind. Crops Prod.* **37**, 93–99 (2012).

104.   Schütz, C. *et al.* Effect of source on the properties and behavior of cellulose nanocrystal suspensions. *ACS Sustain. Chem. Eng.* **6**, 8317–8324 (2018).

105.   Nishiyama, Y. *et al.* Periodic disorder along ramie cellulose microfibrils. *Biomacromolecules* **4**, 1013–1017 (2003).

106.   Cudjoe, E. *et al.* Miscanthus Giganteus: A commercially viable sustainable source of cellulose nanocrystals. *Carbohydr. Polym.* **155**, 230–241 (2017).

107.   Cao, X., Ding, B., Yu, J. & Al-Deyab, S. S. Cellulose nanowhiskers extracted from TEMPO-oxidized jute fibers. *Carbohydr. Polym.* **90**, 1075–1080 (2012).

108.   Brito, B. S. L., Pereira, F. V., Putaux, J. L. & Jean, B. Preparation, morphology and structure of cellulose nanocrystals from bamboo fibers. *Cellulose* **19**, 1527–1536 (2012).

109.   Yoshiharu, N., Shigenori, K., Masahisa, W. & Takeshi, O. Cellulose microcrystal film of high uniaxial orientation. *Macromolecules* **30**, 6395–6397 (1997).

110.   El Achaby, M., Kassab, Z., Aboulkas, A., Gaillard, C. & Barakat, A. Reuse of red algae waste for the production of cellulose nanocrystals and its application in polymer nanocomposites. *Int. J. Biol. Macromol.* **106**, 681–691 (2018).

111. Sugiyama, J., Vuong, R. & Chanzy, H. Electron diffraction study on the two crystalline phases occurring in native cellulose from an algal cell wall. *Macromolecules* **24**, 4168–4175 (1991).

112. Chanzy, H. & Henrissat, B. Electron microscopy study of the enzymic hydrolysis of Valonia cellulose. *Carbohydr. Polym.* **3**, 161–173 (1983).

113. Hirai, A., Inui, O., Horii, F. & Tsuji, M. Phase separation behavior in aqueous suspensions of bacterial cellulose nanocrystals prepared by sulfuric acid treatment. *Langmuir* **25**, 497–502 (2009).

114. Pääkkönen, T. *et al.* Sustainable High Yield Route to Cellulose Nanocrystals from Bacterial Cellulose. *ACS Sustain. Chem. Eng.* **7**, 14384–14388 (2019).

115. Cranston, E. D. Overview of Canada. in *TAPPI International Conference on Nanotechnology for Renewable Materials, Tokyo, Japan* (2019).

116. Ngo, T., Danumah, C. & Ahvazi, B. Production of cellulose nanocrystals at InnoTech Alberta. in *Nanocellulose and Sustainability* 269–287 (CRC Press, 2018). doi:10.1201/9781351262927-2.

117. The Process Development Center. https://umaine.edu/pdc/nanocellulose/.

118. Beck, S., Bouchard, J. & Berry, R. Dispersibility in water of dried nanocrystalline cellulose. *Biomacromolecules* **13**, 1486–1494 (2012).

119. Lockhart, J. Continuous compressed cellulose CNC reactor demonstration at low acid ratios. in *TAPPI International Conference on Nanotechnology for Renewable Materials, Tokyo, Japan* (2019).

120. McAlpine, S. & Nakoneshny, J. Production of crystalline cellulose. (2019).

121. Retsina, T. & Pylkkannen, V. Method for the production of fermentable sugars and cellulose from lignocellulosic material. (2011).

122. Retsina, T., Pylkkannen, V. & van Heiningen, A. Method for vapor phase pulping with alcohol, sulfur dioxide and ammonia. (2011).

123. Retsina, T., Pylkkannen, V. & van Heiningen, A. Method for vapor phase pulping with alcohol and sulfur dioxide. (2012).

124. Retsina, T. & Pylkkannen, V. Separation of lignin from hydrolyzate. (2013).

125. Cellulose nanomaterials - Test methods for characterization, CAN/CSA-Z5100-17, Standards Council of Canada 2017, Ottawa.

126. Cellulose nanomaterials - Blank detail specification, CAN/CSA-Z5200-17, Standards Council of Canada 2017, Ottawa.

127. Nanotechnologies - Characterization of cellulose nanocrystals, ISO/TR 19716, International Organization for Standardization 2016, Geneva.

128. Pulp - Determination of cellulose nanocrystal sulfur and sulfate half-ester content, ISO 21400, International Organization for Standardization 2018, Geneva.

129. Crystallinity of cellulose nanomaterials by powder X-ray diffraction, ISO/TC 229 – PWI 23361, International Organization for Standardization (Preliminary Work Item), Geneva.

130. Nanotechnologies - Health and safety practices in occupational settings relevant to nanotechnologies, ISO/TR 12885, International Organization for Standardization 2008, Geneva.

131. Nanotechnologies - Exposure Control Program for Engineered Nanomaterials in Occupational Settings, CAN/CSA Z12885-12, Standards Council of Canada 2017, Ottawa.

132. Grønli, M., Antal, M. J. & Várhegyi, G. A round-robin study of cellulose pyrolysis kinetics by thermogravimetry. *Ind. Eng. Chem. Res.* **38**, 2238–2244 (1999).

133. Matsuoka, S., Kawamoto, H. & Saka, S. What is active cellulose in pyrolysis? An approach based on reactivity of cellulose reducing end. *J. Anal. Appl. Pyrolysis* **106**, 138–146 (2014).

134. Shafizadeh, F. & Bradbury, a G. W. Thermal-Degradation Of Cellulose In Air And Nitrogen At Low-Temperatures. *J. Appl. Polym. Sci.* **23**, 1431–1442 (1979).

135. Bradbury, A. G. W., Sakai, Y. & Shafizadeh, F. A kinetic model for pyrolysis of cellulose. *J. Appl. Polym. Sci.* **23**, 3271–3280 (1979).

136. Lin, Y., Cho, J., Tompsett, G. a, Westmoreland, P. R. & Huber, G. W. Kinetics and Mechanism of Cellulose Pyrolysis Kinetics and Mechanism of Cellulose Pyrolysis. *Cellulose* 20097–20107 (2009) doi:10.1021/jp906702p.

137. Agustin, M. B., Nakatsubo, F. & Yano, H. The thermal stability of nanocellulose and its acetates with different degree of polymerization. *Cellulose* **23**, 451–464 (2016).

138. Roman, M. & Winter, W. T. Effect of sulfate groups from sulfuric acid hydrolysis on the thermal degradation behavior of bacterial cellulose. *Biomacromolecules* **5**, 1671–1677 (2004).

139. D'Acierno, F., Hamad, W. Y., Michal, C. A. & Maclachlan, M. J. Thermal Degradation of Cellulose Filaments and Nanocrystals. *Biomacromolecules* **21**, 3374–3386 (2020).

140. Lin, N. & Dufresne, A. Surface chemistry, morphological analysis and properties of cellulose nanocrystals with gradiented sulfation degrees. *Nanoscale* **6**, 5384–5393 (2014).

141. Scheirs, J., Camino, G. & Tumiatti, W. Overview of water evolution during the thermal degradation of cellulose. *Eur. Polym. J.* **37**, 933–942 (2001).

142. Beck, S. & Bouchard, J. Auto-Catalyzed acidic desulfation of cellulose nanocrystals. *Nord. Pulp Pap. Res. J.* **29**, 6–14 (2014).

143. Wang, N., Ding, E. & Cheng, R. Thermal degradation behaviors of spherical cellulose nanocrystals with sulfate groups. *Polymer (Guildf).* **48**, 3486–3493 (2007).

144. Fukuzumi, H., Saito, T., Okita, Y. & Isogai, A. Thermal stabilization of TEMPO-oxidized cellulose. *Polym. Degrad. Stab.* **95**, 1502–1508 (2010).

145. Lichtenstein, K. & Lavoine, N. Toward a deeper understanding of the thermal degradation mechanism of nanocellulose. *Polym. Degrad. Stab.* **146**, 53–60 (2017).

146. Fukuzumi, H., Saito, T., Iwata, T., Kumamoto, Y. & Isogai, A. Transparent and high gas barrier films of cellulose nanofibers prepared by TEMPO-mediated oxidation. *Biomacromolecules* **10**, 162–165 (2009).

147. Sharma, P. R. & Varma, A. J. Thermal stability of cellulose and their nanoparticles: Effect of incremental increases in carboxyl and aldehyde groups. *Carbohydr. Polym.* **114**, 339–343 (2014).

148. Fiss, B. G., Hatherly, L., Stein, R. S., Friščić, T. & Moores, A. Mechanochemical phosphorylation of polymers and synthesis of flame-retardant cellulose nanocrystals. *ACS Sustain. Chem. Eng.* **7**, 7951–7959 (2019).

149. Fox, D. M. *et al.* Simultaneously Tailoring Surface Energies and Thermal Stabilities of Cellulose Nanocrystals Using Ion Exchange: Effects on Polymer Composite Properties for Transportation, Infrastructure, and Renewable Energy Applications. *ACS Appl. Mater. Interfaces* **8**, 27270–27281 (2016).

150. Song, X. *et al.* Simultaneous improvement of thermal stability and redispersibility of cellulose nanocrystals by using ionic liquids. *Carbohydr. Polym.* **186**, 252–259 (2018).

151. Lavoine, N., Bras, J., Saito, T. & Isogai, A. Improvement of the Thermal Stability of TEMPO-Oxidized Cellulose Nanofibrils by Heat-Induced Conversion of Ionic Bonds to Amide Bonds. *Macromol. Rapid Commun.* **37**, 1033–1039 (2016).

152. Peng, Y. *et al.* Influence of drying method on the material properties of nanocellulose I: Thermostability and crystallinity. *Cellulose* **20**, 2379–2392 (2013).

153. Heggset, E. B., Chinga-Carrasco, G. & Syverud, K. Temperature stability of nanocellulose dispersions. *Carbohydr. Polym.* **157**, 114–121 (2017).

154. Molnes, S. N., Paso, K. G., Strand, S. & Syverud, K. The effects of pH, time and temperature on the stability and viscosity of cellulose nanocrystal (CNC) dispersions: implications for use in enhanced oil recovery. *Cellulose* (2017) doi:10.1007/s10570-017-1437-0.

155. Dong, X. M. & Gray, D. G. Effect of counterions on ordered phase formation in suspensions of charged rodlike cellulose crystallites. *Langmuir* **13**, 2404–2409 (1997).

156. Lewis, L., Derakhshandeh, M., Hatzikiriakos, S. G., Hamad, W. Y. & MacLachlan, M. J. Hydrothermal Gelation of Aqueous Cellulose Nanocrystal Suspensions. *Biomacromolecules* **17**, 2747–2754 (2016).

157. Abitbol, T., Kam, D., Levi-Kalisman, Y., Gray, D. G. & Shoseyov, O. Surface Charge Influence on the Phase Separation and Viscosity of Cellulose Nanocrystals. *Langmuir* **34**, 3925–3933 (2018).

Chapter 3

Benchmarking cellulose nanocrystals part II: New industrially produced materials

_____

This chapter evaluates the properties and performance of four industrially produced CNC samples. As new CNC producers emerge, the range of available CNC types, and therefore the range of available CNC properties, increases. Herein, we provide commercial CNC users a guide to select the ideal CNC for their desired application.

In this work, I led the project conceptualization and experimental planning jointly with Gwendoline Delepierre (M.Sc.) and Dr. Elina Niinivaara. CNC samples were received from industrial producers and jointly purified by the afore-mentioned co-authors. I carried out zeta potential and dynamic light scattering measurements, as well as conductometric titrations. Jointly with Dr. Elina Niinivaara, I solubilised the cellulose samples for size exclusion chromatography. Gwendoline Delepierre prepared the lab-made CNCs, observed CNC liquid crystalline behaviour, and carried out thermogravimetric analysis and polarized optical microscopy. Dr. Elina Niinivaara carried out atomic force microscopy and CNC particle sizing, as well as quart-crystal microbalance measurements. Behzad Zakani (MASc) carried out rheological measurements and a technician was responsible for X-Ray diffraction measurements. Myself, Gwendoline Delepierre, and Dr. Elina Niinivaara jointly performed data analysis and wrote the manuscript with assistance from Dr. Emily Cranston. This chapter has been submitted to *Langmuir* for publication.

Delepierre, G.,[‡] Vanderfleet, O.M.,[‡] Niinivaara, E.,[‡] Zakani, B., Cranston, E.D., "Benchmarking cellulose nanocrystals part II: New industrially produced materials", *Langmuir*, submitted, Manuscript ID: la-2021-00550w.

[‡]These authors contributed equally.

3.1 Abstract

The demand for industrially produced cellulose nanocrystals (CNCs) has been growing since 2012, when CelluForce Inc. opened its inaugural demonstration plant with a production capacity of one tonne per day. Currently, there are ten industrial CNC producers worldwide, each producing a unique material. Thus, academic researchers and commercial users alike must consider the properties of all available CNCs and carefully select the material which will optimize the performance of their desired application. To support these efforts, this article presents a thorough characterization of four new industrially produced CNCs including sulfated CNCs from NORAM Engineering and Constructors Ltd. (in cooperation with InnoTech Alberta and Alberta-Pacific Forest Industries Inc.) and Melodea Ltd. as well as carboxylated CNCs from Anomera Inc. and Blue Goose Biorefineries Inc. These materials were benchmarked against typical lab-made, sulfated CNCs. While all CNCs were similar in size, shape, crystallinity and suspension quality, the sulfated CNCs had a higher surface charge density than their carboxylated counterparts, leading to higher colloidal stability. Additionally, significant differences in the rheological profiles of aqueous CNC suspensions, as well as CNC thermal stability and self-assembly behavior were observed. As such, this article highlights both the subtle and significant differences between five CNC types and acts as a guide for end users looking to optimize the performance of CNC-based materials.

3.2 Introduction

In the past 8 years, the market demand for cellulose nanocrystals (CNCs) has increased dramatically as they are an environmentally friendly alternative to many petroleum-based materials, and can significantly improve existing products, often at very low loadings.[1] CNCs are attractive as a bio-based material due to their high strength, low density, unique optical properties, high aspect ratio, functionalizability, and biodegradability.[2–4] CNCs have gained popularity in both academia and industry due to their potential in both commodity applications and advanced functional materials. In academia, this is reflected in the growing number of publications and patents on this remarkable crystalline polysaccharide nanoparticle (Figure 3.1). In fact, on average 2.5 papers are published per day, with topics ranging from the fundamental understanding of CNC production and properties, to their potential applications. Similarly, the use of CNCs in commercial products (e.g., oil and gas fluids, cement and concrete, adhesives, water remediation technologies, coatings, etc.) continues to expand, making industrially produced CNCs an essential requirement for further market development.

Fortunately, there has been an increase in the large-scale production of CNCs worldwide, with new industrial manufacturers entering the market, and the construction of larger pilot, demonstration and commercial plants in new and existing facilities. While some envisioned applications are high-value and may only be produced in relatively small quantities (e.g. biomedical devices, tissue engineering, drug delivery), others, such and industrial processing fluids and rheological modifiers, are necessarily high-volume.[5] Selecting the appropriate CNC type, and any needed surface modification, for the intended usage remains a challenge for end-users due to the range of nanocelluloses available and conflicting

reports in the literature. At the very minimum, for academics, industrial researchers and product developers, access to a complete and direct comparison of industrially produced CNCs is essential.
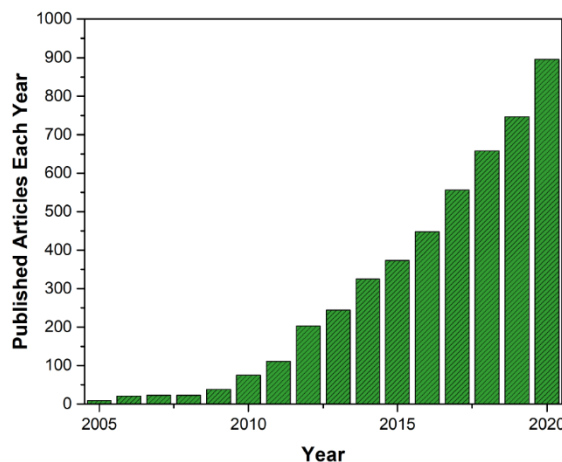
Figure 3.1. Number of published articles on CNCs per year between 2005 and 2020 (not cumulative) according to SciFinder Jan. 2021 (Keywords: "cellulose nanocrystal", "cellulose nanowhisker" and "nanocrystalline cellulose").

In 2017, our group published a research article in which commercially available (at the time), sulfuric acid hydrolyzed CNCs (namely those produced by CelluForce Inc., Alberta Innovates Technology Futures and the USDA Forest Products Laboratory) were comprehensively benchmarked against "typical" CNCs prepared at the laboratory scale.[6] The work provided a comparison between the seemingly similar CNCs, highlighted the value of understanding their fundamental properties and suggested characterization and cleaning procedures to have a "known starting material". The paper concluded that when sulfuric acid hydrolysis is used to produce sulfated CNCs, that changes in protocol, scale, and starting material only lead to small variations in the physical and chemical properties of the CNCs. Consistent and reproducible materials, with minimal batch-to-batch variability can be sourced industrially, and for many applications, further purification is unnecessary. The most significant differences in the CNCs were their crystal structure (with some materials containing cellulose II), their aspect ratio and their surface charge density. However, these were all within a suitable range to meet the Standard definition of CNCs.[7,8] With over 230 citations (as of January 2020), this work has significantly added to the available literature on CNC characterization, and emphasizes the importance of works of its type. With the emergence of new, industrially produced (and some commercially available) CNCs, there is a demand to extend this benchmarking study so that CNC users have access to up-to-date information, and can continue to select materials that best fit their research and application needs.

CNC properties, and their subsequent performance in various formulations, are directly related to the methods used to produce them.[9] CNCs are isolated from natural cellulosic materials using a top-down approach, most typically through a controlled sulfuric acid

hydrolysis,[10] in which dislocations in the cellulose microfibril are degraded, leaving intact individual, and highly crystalline, rod-shaped nanoparticles. The hydrolysis process also leads to the esterification of some of the surface hydroxy groups on the nanocrystals, resulting in charged sulfate half-ester groups which render CNCs colloidally stable in polar solvents.[6,11] While CNCs can also be isolated from tunicates, algae or bacterial cellulose, the most commonly used source is higher plants, especially wood pulp. Depending on the source material, CNCs will typically have lengths ranging from 50 to 3000 nm, and diameters ranging from 3 to 20 nm.[12,13] Because of this variation in CNC properties, it is important to fully characterize them prior to their use, as slight differences can affect their performances, for example, in nanocomposites and emulsions, and as thickening agents and dispersants.[6]

Despite the prevalence and widespread industrial production of sulfated CNCs using batch processes, other production routes exist to further tune CNC properties and/or reduce production costs. For example, NORAM Engineering and Constructors Ltd. has a new continuous CNC production process,[14] whereas Melodea Ltd. has a simplified CNC purification process. While strong and weak mineral acids (e.g. hydrochloric acid,[15–17] phosphoric acid[18,19]), as well as organic acids (e.g. oxalic acid,[20] maleic acid,[20,21] formic acid[22]), and acid blends[23,24] have been demonstrated to produce CNCs at the laboratory scale, these modified production routes generally fall short on producing high quality CNCs. Specifically, their end products often lack colloidal stability, causing them to form large aggregates negating the "nano-advantages" seen from typical CNCs and leading to unpredictable performance. Interestingly, researchers have also explored numerous acid-free production routes, the most promising of which are oxidation reactions[25–28] capable of producing CNCs that are well-dispersed, colloidally stable and, in some cases, highly crystalline. The success of such methods at the laboratory scale is mirrored by recent ventures which demonstrate the production of carboxylated CNCs through oxidative routes, namely those pioneered by Anomera Inc.[29] and Blue Goose Biorefineries Inc.[30] The industrial availability of carboxylated CNCs, potentially at a lower cost than sulfated CNCs, represents an exciting opportunity for end users, including access to a wider range of CNC properties (specifically surface chemistries) which can tune the performance of their products in new and exciting ways.

In this work, we build on our 2017 benchmarking study, by introducing four new "key players" on the CNC market who are manufacturing CNCs on a scale of over 10 tonnes per year. Benchmarked here – against sulfated, laboratory made CNCs – are two newly industrially produced sulfated CNCs by NORAM in cooperation with InnoTech Alberta and Alberta-Pacific Forest Industries Inc.[14,31] and Melodea Ltd.[32], alongside two commercially available carboxylated CNCs, namely DextraCel[TM] from Anomera Inc.[29] and BGB Ultra™ from Blue Goose Biorefineries Inc.[33] As in the original benchmarking paper, all five types of CNCs were thoroughly characterized including morphology, surface charge, degree of crystallinity, thermal and colloidal stability, liquid crystalline properties and self-assembly behavior. In addition, the cellulose degree of polymerization (DP), the water adsorption capacity and the rheological behavior of these materials were analyzed. This allows for a more in-depth investigation of how CNC properties are linked to, for

example, thermal stability,[23] which is relevant for nanocomposites with high processing temperatures; water interactions, which are particularly important for rheological modifiers;[34] the ability to modify the particle surface chemistry for added functionality; and processability. Furthermore, dialysis was performed on all received CNC types, in order to understand if residual salt, acid, oligosaccharides or other additives had an influence on the characterized properties.

3.3 Materials & methods

Materials. Whatman cotton ashless filter aid was purchased from GE Healthcare Canada. Sulfuric acid, hydrochloric acid (1 N), sodium hydroxide (1 N), sodium chloride, poly(allylamine hydrochloride) (PAH, $M = 120\,000-200\,000$ g/mol), dialysis tubing (cut-off = 14 kDa), phenyl isocyanate, dimethyl sulfoxide (DMSO), ethanol (EtOH), methanol (MeOH), deuterium oxide (D_2O) and strong acid cation (SAC) exchange resin were purchased from Sigma Aldrich. All chemicals were used as-received. The water used was MilliQ-grade water with a resistivity of 18.2 MΩ·cm.

CNC Samples. Four CNC types were obtained from four different companies. NORAM Engineering and Constructors Ltd. and Melodea Ltd. provided sulfated CNCs. Anomera Inc. and Blue Goose Biorefineries Inc. provided carboxylated CNCs. These four samples were compared to lab-made sulfated CNCs (CNC-LM). Half of the as-received samples, were diluted to ~3 wt% and dialyzed (cut-off = 14 kDa) against purified water until the pH and conductivity of the washwater were stable. The pH and conductivity of CNC suspensions at 0.2 wt%, before and after dialysis are reported in Appendix 3, Table S1. The dialyzed CNCs (~3 wt%) were then sonicated using a Branson Sonifier SFX550 (Thomas Scientific, Swedesboro, NJ, USA) in batches of 20 mL in an ice bath at 55% amplitude, for 1 min. The CNCs were filtered through a Whatman® glass microfiber filter (Grade GF/A, with pore size of 1.6 µm). The CNC suspensions as-received and dialyzed were stored in the fridge. For analysis requiring dried samples, 3 wt% suspensions were freeze-dried after adjusting the pH to 7 with a 10 mM NaOH solution, so that all the charged groups on the surface of the CNCs have a sodium counter ion. The samples were then put in the freezer overnight and freeze-dried (Labconco, USA).

NORAM Engineering and Constructors Ltd. sulfated CNCs are produced by this Canadian company (Vancouver, British Columbia), via a continuous process that has been developed in cooperation with InnoTech Alberta, Alberta Innovates and Alberta-Pacific Forest Industries Inc. The continuous reactor has been demonstrated at a 0.5 tonnes/day scale using two different wood pulps. The CNC samples generated for this work were made from knife-milled dissolving pulp. The acid hydrolysis takes place at a very low acid:pulp mass ratio of 2.7:1 with 61% sulfuric acid, at 55 °C, for 120 min. This acid:pulp ratio represents a 2 to 3-fold reduction in acid compared to published current practices using batch processes.[14,31] The CNCs were received as a 3 wt% suspension at pH 6.8 (i.e., in the neutralized sodium-form). The CNCs are referred to as "NORAM" and "NORAM-D", for the as-received and dialyzed form, respectively.

Melodea Ltd. uses sulfuric acid hydrolysis to produce sulfated CNCs in a batch process. This Israeli company (Rehovot), will produce more than 10 tonnes/year in 2020. The Melodea production process includes a proprietary Sulfuric Acid Recovery Procedure (SARP™), which further facilitates the sustainable and economical production of CNCs. The source materials that can be used are various bleached hard and softwood pulps and agricultural residue and the hydrolysis process is weaker than the conventional lab-made CNC protocol. The CNCs tested here were made from dissolving pulp and received as a gel at 3.5 wt%, at pH 4.5 (i.e., in-between acid and sodium-form). The CNCs are referred to as "Melodea" and "Melodea-D", for the as-received and dialyzed form, respectively.

Anomera Inc. produces carboxylated CNCs using a batch process with dilute hydrogen peroxide oxidation.[29] The production facility is situated in Mississauga, Ontario, Canada with headquarters in Montreal, Quebec, Canada. The CNCs, which are commercially known as DextraCel™, are currently produced from softwood pulp on a 30 kg/day scale but with expansion underway to reach 1 tonne/day production in Temiscaming, Quebec, Canada in 2021.[29] Anomera CNCs were received as a spray-dried powder in sodium-form and dispersed in purified water with probe sonication for 5 minutes at 60% amplitude. A 1 wt% suspension has a pH of 6.9 (i.e., in the neutralized sodium-form). The CNCs are referred to as "Anomera" and "Anomera-D", for the as-received and dialyzed form, respectively.

Blue Goose Biorefineries Inc. uses a transition metal catalyzed oxidative method to produce carboxylated CNCs in a batch process.[33,35] This Canadian company (Saskatoon, Saskatchewan) uses viscose grade hardwood pulp as their starting material and currently produces 10 kg of CNCs per day under the trade name BGB Ultra™. The primary step of their process consists of a transition metal catalyzed redox reaction of sodium hypochlorite and cellulose at 75 °C, where hypohalite is reduced and cellulose is oxidized, forming carboxylic acids. This is followed by an alkaline extraction with NaOH, and a second oxidation step.[30] The CNCs are purified by diafiltration followed by a concentration step. Blue Goose CNCs were received as a gel at ~8 wt%, at a pH of 5.8 (i.e., in the neutralized sodium-form). The CNCs are referred to as "BGB" and "BGB-D", for the as-received and dialyzed form, respectively.

Lab-made cellulose nanocrystals (CNC-LM) were produced by sulfuric acid hydrolysis of cotton from Whatman ashless filter aid (40 g) with sulfuric acid (64 wt%, 700 mL, acid:pulp mass ratio 27:1) at 45 °C using a previously published protocol.[36] The filter aid pads were shredded in a blender and oven dried overnight at 80 °C prior to being added to the sulfuric acid, the reaction was performed for 45 min under mechanical stirring. The reaction was quenched by 10-fold dilution with ice-cold purified water, followed by three subsequent centrifugation and redispersion steps until the CNCs no longer sedimented. The CNCs were then transferred to pre-washed cellulose membrane dialysis tubes (cut-off = 14 kDa) and dialyzed against purified water until the pH of the suspension and the conductivity of the dialysis water were constant. The final suspension was probe-sonicated for 5 min at 55% amplitude and filtered through Whatman glass microfiber filters (GF/A grade). The CNC suspension was stored at 1.3 wt% at pH 3.4 in acid-form.

Atomic force microscopy (AFM). Samples for AFM imaging were prepared by first cleaning silicon wafers in a piranha solution of 3:1 concentrated sulfuric acid to hydrogen peroxide. The silicon wafers were spin coated (WS-650-23 Spin Coater, Laurell Technologies, North Wales, PA, USA) with a 0.1 wt% PAH solution, followed by rinsing with purified water. Dilute CNC suspensions (0.001 - 0.005 wt%) (both as-received and dialyzed) were made from stock 1 wt% suspensions, redispersed from their freeze-dried form (probe sonicated 5 min at 55% amplitude and filtered through Whatman glass microfiber filters (GF/A grade)).[37] The suspensions were spin coated onto the PAH-coated silicon wafers. Each spin coating step was performed at 3000 rpm and 2300 rpm s^{-1} acceleration for 30 s. Images were acquired using a Bruker Multimode 8 AFM (Bruker, Santa Barbara, CA, USA), in tapping mode at room temperature, using Al coated silicon probes with a 42 N/m spring constant and 350 kHz resonance frequency (NCHR probes from Asylum Research – Oxford Instruments, Santa Barbara, CA, USA). Imaging was carried out at a scan rate of 0.25 Hz with a resolution of 512 measurements per line (512 lines). All images were processed with a standard third order polynomial flattening using the NanoScope analysis software v.8.10. CNC dimensions, i.e., length and cross-section (measured from the particle height) for $N_{CNC}=100$ non-touching particles, were measured on flattened height images using Gwyddion v.2.55 freeware. A lower bound of 100 nm in particle length was defined in order to not include any small by-products/contaminants from the production process into the particle size analysis. Furthermore, not measuring particles shorter than 100 nm for all samples eliminated user bias in particle selection. While this lower bound was applied consistently to all measurements herein, it shifts the average particle lengths slightly higher than other reports.[6,38] The presented confidence intervals are the standard deviation of the average particle dimensions.

Dynamic light scattering (DLS). Apparent size measurements were performed following a standard method on a Malvern Panalytical Zetasizer Nano-ZS (Malvern, United Kingdom).[37] DLS measurements were performed on 0.025 wt% CNC suspensions with no added salt and particle sizes were calculated from hydrodynamic radii using Stokes-Einstein equation and the assumption of spherical particles. For each sample, ten measurements were performed in triplicate. The number average of each particle distribution was calculated, and the confidence interval presented is the standard deviation of three separate samples.

X-ray diffraction (XRD). XRD was measured on freeze-dried as-received CNC samples in sodium-form with a Bruker D8 Davinci diffractometer (Bruker, USA) with a cobalt sealed tube source ($\lambda_{avg} = 1.79026$ Å), 35 kV, 45 mA with a parallel focus Goebel Mirror, Vantec 500 area detector, and 0.5 mm microslit and 0.5 mm short collimator over a 2θ range of 8−45°. The degree of crystallinity of the CNCs was quantified using Rietveld refinement.[6,39–41] The spectra were deconvoluted using a cellulose I single crystal information file, an amorphous peak was fixed at 24.1°. The peak shapes were fitted with a pseudo-Voight function with a linear background. The peak intensity was fitted with a March Dollase preferred orientation function model. The error within the deconvolution method is taken to be *ca.* 5%. Note that the reported crystallinity values are relative[42] and

only comparable within this study or with our previously published articles using the same procedure (Reid *et al.*).[6]

Cellulose degree of polymerization (DP). The DP of cellulose chains in the CNCs was measured following a derivatization procedure reported by Bouchard *et al.*[34] Freeze-dried, sodium-form CNCs were placed in an oven at 80 °C for 1 h to remove residual moisture. Then, 25 mg of CNCs were placed in a glass vial, to which 10 mL of DMSO and 1 mL of phenyl isocyanate were added. The vials were placed in a preheated oil bath at 70 °C and the reaction proceeded for 40 h, with manual agitation occurring every 5-10 h. The reaction was quenched by adding 2 mL of methanol to each vial. Afterwards, the vials were opened to allow excess methanol to evaporate. Size exclusion chromatography (SEC) measurements were performed on an Agilent 1100 instrument equipped with an Agilent 1260 ISO pump and Styragel HR 4, HR 3 and HR 1 columns. DMSO with 0.5% LiBr was used as the eluting solvent. Prior to injection, the carbanilated cellulose solutions, which contained 2.5 mg of cellulose per mL, were filtered with a 0.45 μm polytetrafluoroethylene syringe filter (Chromspec Syringe Filters, Chromatographic Specialties Inc. Brockville, Canada), the samples were injected into the column using an auto-injector at an eluting rate of 0.5 mL/min. The results were collected using a refractive index detector and processed using ASTRA 6.0. Polystyrene sulfonate standards with molecular weights of 891, 2000, 4290, 10000, 29500 and 140000 Da were used to calibrate the SEC. The cellulose DP was calculated by dividing the weight-average molecular weight (M_w) by the molecular weight of a tricarbanilated anhydroglucose unit (519 g/mol).[23,43] The average chain length dispersity (Đ) was calculated by dividing the weight average molecular weight by the number average molecular weight of the samples.

ζ-Potential. ζ-potential measurements were performed following a standard method on a Malvern Panalytical Zetasizer Nano-ZS (Malvern, United Kingdom).[32] Following the protocol from our previous benchmarking study, 0.25 wt% CNC suspensions with 10 mM NaCl were used to measure electrophoretic mobility.[6] The suspensions were not adjusted for pH, the pH values of the suspensions at a concentration of 0.2 wt% can be found in Appendix 3, Table S1. The Melodea and BGB CNCs produced error messages citing high count rates at this concentration; as such, these two CNC types were measured on 0.1 wt% CNC suspensions with 5 mM NaCl. The electrophoretic mobilities were then converted to ζ-potentials for comparison to literature values, following Smoluchowski theory, despite the assumptions inherent to this method.[44] The confidence interval is the standard deviation of triplicate measurements.

Conductometric titrations. As-received and dialyzed CNC suspensions were first fully protonated by passing the suspensions through a column containing Dowex Marathon C hydrogen form strong acid cation exchange resin at a ratio of 12 g of resin per g of CNCs.[45,46] Sulfated CNCs, which include the lab-made CNCs, as well as those industrially produced by NORAM and Melodea, were titrated against a 10 mM NaOH solution. The carboxylated CNCs, produced by Anomera and BGB, were titrated differently, first, a known amount of 0.1 M HCl was added to lower the pH of the suspensions, as is common with weak acid titrations.[37] Afterwards, the titrations were performed with the same

concentration of NaOH (10 mM) as for the sulfated CNCs.[46] Three titrations were performed for each sample and the average of the three values was reported as the total charge content of the CNCs with standard deviation. The surface charge density of each type of CNC was calculated by normalizing by the CNC surface area assuming a cylindrical model with round cross-section, using the average length and cross-section measured via AFM.[47]

Thermogravimetric analysis (TGA). Pellets of sodium-form and acid-form CNCs were made by weighing 7 ± 2 mg of CNCs into a 1 mL plastic syringe. The CNCs were compressed into a pellet between two rubber plunging heads to produce samples with consistent densities. TGA was performed on a Mettler-Toledo STAR system, at a heating rate of 10 °C/min, between 50 °C and 500 °C. The TGA was purged with a sample purge flow rate of 80 mL/min N_2 and a balance flow rate of 20 mL/min N_2. An additional measurement was performed on the as-received Melodea CNCs and CNC-LM in sodium-form, at a heating rate of 10°C/min in N_2, between 25 and 800 °C, to investigate the remaining char content. All the curves were smoothed on Origin using a Savitzky-Golay method.

Rheology. Each CNC type was concentrated to 3 wt% and probe sonicated for 90 s at 60% amplitude and filtered using 1.6 µm pore size glass fibre filters to remove any metal particles from the sonicator probe. All samples, besides those that were too gelled (i.e., Melodea) were filtered after sonication. The as-received samples were then diluted to 2 wt% suspensions, while the dialyzed samples were pH adjusted to pH 7 with NaOH (to put them in the sodium-form) and then diluted to 2 wt%. The rheological measurements were all performed with a Kinexus Ultra+ rotational rheometer. The rheometry was performed under controlled shear rate mode, using a 4°/40 mm cone and plate measuring system. In order to avoid evaporation during measurements, silicone oil was applied on the periphery of the samples and the measurement environment was also saturated with water using a solvent trap. Steady state viscometry was performed in the shear rate range of 0.001-1000 s^{-1}. The samples were measured in duplicate and the average of both measurements was reported.

Quartz-crystal microbalance with dissipation monitoring (QCM-D). Silicon dioxide coated QCM-D sensors (Biolin Scientific, Gothenburg, Sweden) were first cleaned with nitrogen and then cleaned in a UV Ozone Cleaner - ProCleaner™ (BioForce Nanosciences) for 15 min. A dialyzed and as-received 1 wt% CNC suspension was spin coated onto the QCM-D sensors, at 3000 rpm (2300 rpm s^{-1} acceleration) for 60 s. After carefully cleaning the back of the sensors with EtOH, the spin coated films were annealed overnight in the oven at 80 °C. The sensors were placed in a flow cell (QSense Analyzer, Biolin Scientific, Gothenburg, Sweden) and equilibrated in purified water overnight with a constant flow rate of 0.2 mL/min at RT, in order to obtain a stable baseline. A water/D_2O solvent exchange was carried out to determine the amount of water bound in the CNC films.[48,49] A purified water baseline was recorded for 20 min, after which the solvent was exchanged for D_2O and changes in resonance frequency (Δf) were recorded for an additional 20 min. A solvent exchange back to purified water was then done for a final 20 min of data aquisition. The

amount of bound surface water (Γ_{H2O}) was calculated according to Equation 1, the Sauerbrey equation:[48–50]

$$\Gamma_{H2O} = -C \left(\frac{\Delta f}{n}\right)_{film,H_2O} \qquad \text{Equation 1}$$

Where C is the sensitivity constant of the sensor (0.177 mg m^{-2} Hz^{-1}), n is the measurement harmonic (n = 1, 3, 5, 7…) (here we have analyzed the 3rd harmonic). Equation 2 describes the calculation for $\Delta f_{film\,H2O}$:

$$\Delta f_{film,H_2O} = \left(\frac{\left(\frac{\Delta f}{n}\right)_{film} - \left(\frac{\Delta f}{n}\right)_{bare\,substrate}}{\left(\frac{\rho_{D_2O}}{\rho_{H_2O}}\right) - 1}\right) \qquad \text{Equation 2}$$

where Δf_{film} is the measured change in resonance frequency of the CNC film due to the solvent exchange, $\Delta f_{bare\,sensor}$ is the measured change in resonance frequency of a pristine SiO$_2$ coated QCM sensor (-54 Hz) due to the solvent exchange, ρ_{D2O} is the density of D$_2$O (1.104 g cm^{-3} at 25 °C) and ρ_{H2O} is the density of water (0.977 g cm^{-3} at 25 °C). Γ_{H2O} was normalized to the thickness of the CNC film (as measured by AFM scratch-height analysis).[49] The samples were measured in triplicate, and the error is represented by the standard deviation.

Liquid crystalline (LC) phase separation. CNC suspensions (as-received and dialyzed samples in acid form) were concentrated by slow evaporation of water at RT whilst stirring with a magnetic stir bar. Additionally, a 10 mL Millipore stirred cell was used to concentrate the CNC suspensions further to their gel point (different for every CNC type). For carboxylated CNCs, the highest concentration suspension containing 1 mM of NaCl that could be tested was 5 wt% due to the inability to fill the capillaries at higher viscosities. The concentrated CNC suspensions were diluted into vials using purified water and an NaCl solution (30 mM) to obtain the targeted concentration of CNCs ranging from 0.3 to 10 wt% with 1 mM NaCl, depending on the CNC type. The suspensions were added to small flat glass capillary tubes obtained from VitroTubes (0.6 × 0.3 × 5 mm) and left to self-assemble/phase separate.[10,51] The suspensions in the capillaries were equilibrated for 7 days prior to taking the photographs in between crossed polarizers. For as-received carboxylated CNCs, capillary tubes were also prepared without any NaCl in order to see the effect of salt on their phase behavior and/or gelation. Additionally, the gelling point of the suspensions containing 1 mM of NaCl was determined by inverting vials containing CNC suspensions of increasing concentration for 48 h. If the suspension remained at the (now) top of the vial, the suspension was considered to have reached its gel-like state.

Polarized optical microscopy (POM). POM images of the capillary tubes filled with CNC suspensions (as described above) were acquired in reflection mode on an Olympus BX41 microscope equipped with a digital camera and for some images a 530 nm retardation plate was added. Polarized optical microscopy images were collected with crossed linear polarizers, which were oriented horizontally and vertically relative to the analyzer and, if used, the 530 nm wave plate was aligned from the bottom right direction to top left of the

images. Additionally, a droplet of concentrated CNC suspension was observed during slow drying under the POM for each CNC type, in order to observe tactoid formation.

3.4 Results and discussion

Four industrial CNC types, including sulfated CNCs from NORAM (produced in collaboration with InnoTech Alberta and Alberta-Pacific Forest Industries Inc.) and Melodea Ltd., and carboxylated CNCs, DextraCel[TM] from Anomera Inc. and BGB Ultra™ from Blue Goose Biorefineries Inc. were benchmarked against sulfated lab-made CNCs (CNC-LM). Each CNC type was extensively characterized to determine: i) nanoparticle dimensions, ii) apparent size and degree of dispersion in aqueous suspension, iii) crystal structure, iv) cellulose degree of polymerization, v) surface charge density and colloidal stability, vi) thermal stability, vii) rheological behavior, viii) water binding capacity, and ix) liquid crystalline and self-assembly behavior (Table 3.1 and Table 3.2). In Reid e*t al.*[6] we showed that Soxhlet extraction did not have a significant impact on the properties and behavior of CNCs, therefore this purification method was not used in the current work. Herein, dialysis was employed as it can remove water soluble salts and residual reagents that may be present depending on the production methods used.[52] Thus, most characterization was carried out on both 'as-received' samples, and after dialysis against purified water. Dialyzed samples are designated with a 'D' suffix throughout.

Table 3.1. Summary of CNC properties in their as-received and dialyzed (D) form.

	CNC-LM	NORAM		Melodea		Anomera		BGB	
		as-received	D	as-received	D	as-received	D	as-received	D
Length (nm)	190±40	160±30	190±40	210±60	230±50	150±30	170±40	210±50	220±50
Cross-section (nm)	8±2	5±1	5±2	4±1	4±1	5±2	6±2	5±2	5±2
Aspect Ratio	27±8	40±10	40±10	70±30	80±40	30±10	30±10	40±20	50±20
Apparent Size (nm)	81±1	81±1	81±1	96±1	76±1	81±1	80±1	101±1	92±1
χ_c (%)	91	82		79		80		93	
DP	235	71		130		46		40	
Đ	4.1	3.1		3.2		4.4		3.5	
Total charge (mmol/kg CNC)	269±3	274±7	255±4	168±1	440±5	141±10	121±4	130±5	116±3
Surface Charge Density (e/nm^2)[a]	0.49	0.31	0.29	0.15	0.40	0.16	0.16	0.15	0.13
ζ-potential (mV)	-33±1	-34±2	-31±2	-31±1	-31±1	-21±1	-24±1	-28±2	-25±2
Normalized mass of bound water (ng cm^{-2} nm^{-1})	2.7±0.3	5.1±0.3	5.6±0.3	8.5±0.5	4.8±0.2	4.2±0.4	4.3±0.3	2.8±0.2	2.5±0.1
Viscosity @ 2 wt%, 10 s^{-1} (mPa·s)	0.97	3.5	2.5	650	130	1.6	2.1	25	18

[a] Surface charge density was calculated by normalizing by the CNC surface area assuming a cylindrical model with round cross-section, using the average length and cross-section measured via AFM (ref. 47)

Physical appearance of CNC suspensions. Figure 3.2 shows photographs of 1 wt% suspensions of the as-received CNCs, to compare their physical appearance. Like CNC-LM, NORAM, Anomera, and BGB CNCs form uniform and colloidally stable suspensions with a blueish hue.[37] Conversely, the Melodea CNC suspension exhibits a gel-like behavior with trapped air bubbles; this can be attributed to the high viscosity of the sample, which will be further discussed below.
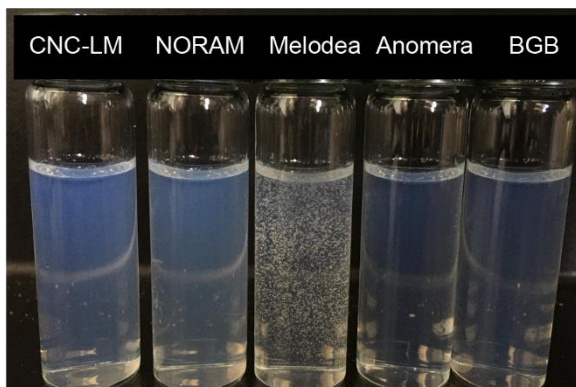
Figure 3.2. Photograph of 1 wt% as-received CNC suspensions. From left to right: lab made CNCs (CNC-LM), NORAM, Melodea, Anomera, and BGB CNCs.

Nanoparticle size and structure. The dimensions of CNCs play an important role in the performance of CNC-based materials. For example, high aspect ratio CNCs have a lower percolation threshold than those with a low aspect ratio, making them more promising as reinforcement agents in nanocomposites.[53] Likewise, the critical concentration for liquid crystalline phase separation is lower for high aspect ratio CNCs, and as such their dimensions play a significant role in their self-assembly behavior.[54] To better understand the behavior of the five CNC types included in this study, their average particle sizes were measured using atomic force microscopy (AFM) before and after dialysis ($N_{CNC} = 100$) (Figure 3.3 and Figure 3.4).[37]
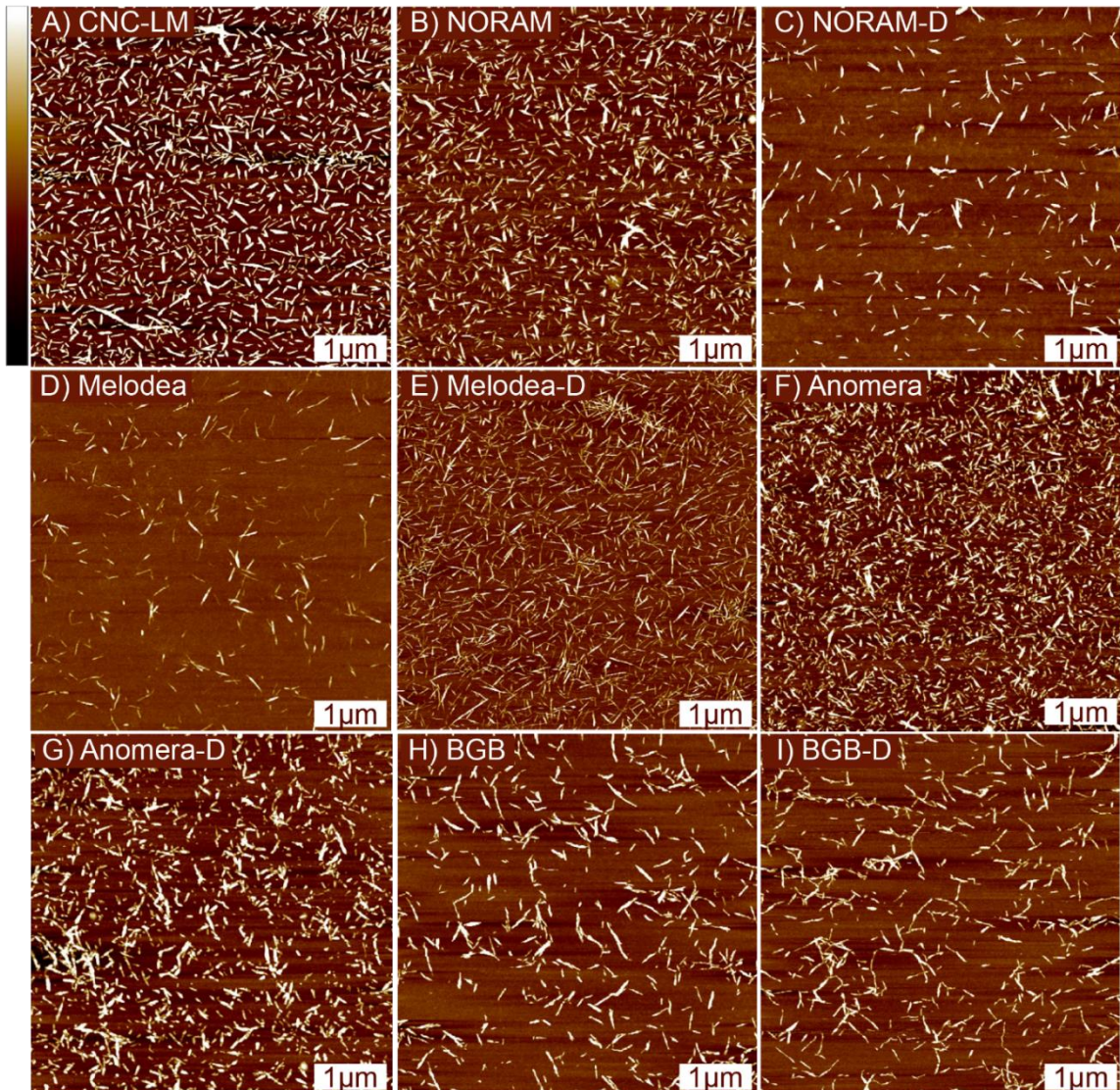
Figure 3.3. Atomic force microscopy (AFM) height images of A) CNC-LM B) NORAM, C) NORAM-D, D) Melodea, E) Melodea-D, F) Anomera, G) Anomera-D, H) BGB and I) BGB-D CNCs on Si wafers. The CNC dimensions measured are considered within the standard range. All images have a height scale from -5 to 5 nm, which is indicated on the left of panel A.
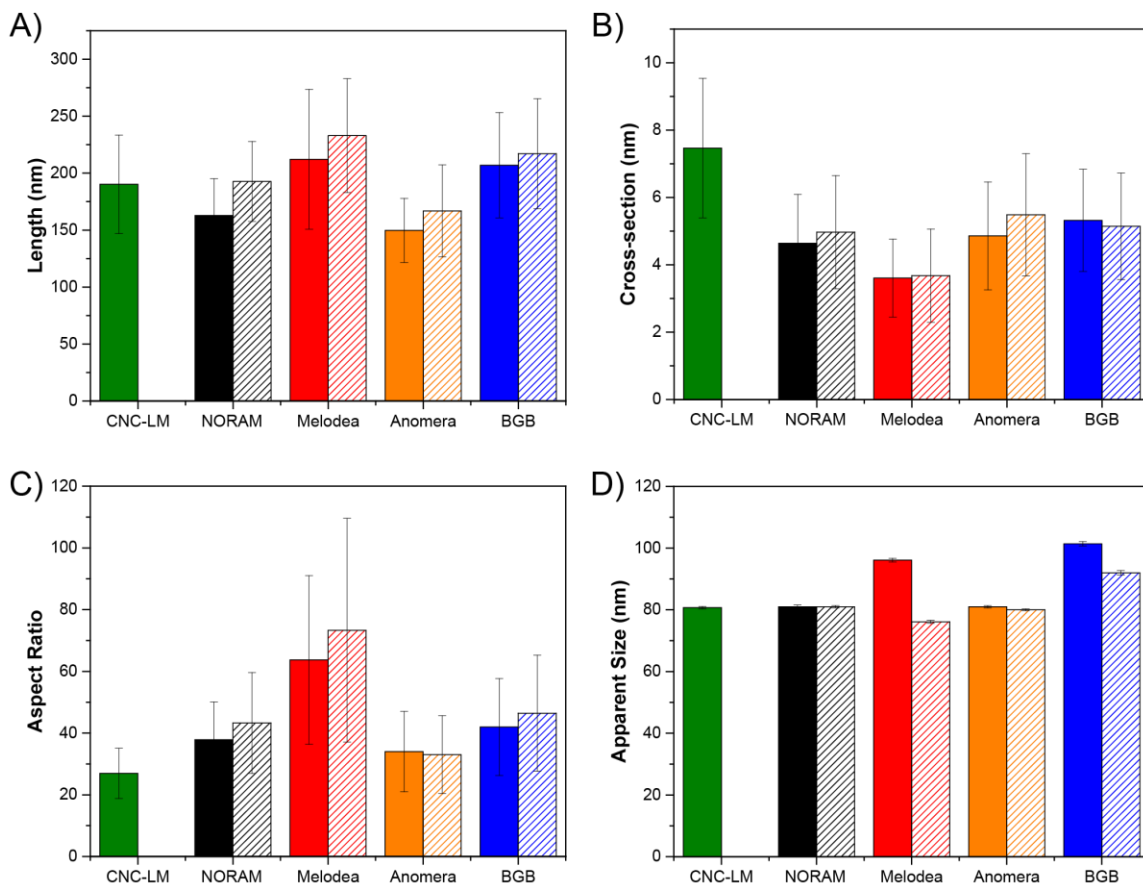
Figure 3.4. Comparison of the A) length, B) cross-section and C) aspect ratio of industrially produced CNCs (as-received (solid) and dialyzed (striped)) to CNC-LM as measured by AFM, and D) the apparent particle size in suspension of the different CNC types as determined by DLS. The standard deviation values are primarily an indirect measure of the particle size polydispersity (N_{CNC} = 100), not the precision of the measurements.

All samples (both as-received and dialyzed) resembled "typical" CNCs: rod-shaped nanoparticles with average lengths between 120 and 280 nm and average cross-sections between 3 and 10 nm were observed (Figure 3.4).[8,37,38] While the differences in particle lengths and cross-sections are not statistically significant, there were substantial differences in the breadth of the particle size distributions (Appendix 3, Figure A3.1). Melodea and BGB CNCs had the largest length distribution (100 – 400 nm and 100 – 350 nm, respectively). Furthermore, Melodea CNCs appear longer and thinner, resulting in a much higher average aspect ratio (*ca.* 70) in comparison to the other CNC types (*ca.* 27 – 50). As discussed above, CNCs with higher aspect ratios have lower percolation thresholds and therefore have lower critical gelation and self-assembly concentrations. As such, Melodea's longer and thinner CNCs results in their suspensions appearing more viscous than the other samples (Figure 3.1). This propensity to percolate and form a network structure at low CNC loadings makes Melodea CNCs particularly promising as viscosity modifiers and reinforcing nanofillers in composites.

53

The values obtained here for the average particle length and cross-section for CNC-LM by AFM are slightly larger than the ones obtained in our previous benchmarking work[6] and a recent interlaboratory study on CNC size.[38] This is due to our imposed lower size threshold (of 100 nm) and in general, the subjectivity of the user in selecting individual particles, which is always an issue when manually measuring AFM images.[37] Furthermore, AFM is sensitive to tip effects such as the broadening of the probe over time.[38]

The apparent size of CNCs and their dispersion quality in suspension were evaluated using DLS (Figure 3.4D, Table 3.1). While we refer to DLS measurements as CNC apparent size, we would like to emphasize that this does not refer to a specific particle dimension and is in fact more representative of the degree of aggregation of CNCs in suspension. The apparent sizes of NORAM and Anomera CNCs were the same as CNC-LM (*ca.* 81 nm). These results are comparable with the size measured in our previous benchmarking study, even though a different instrument was used.[6] Melodea and BGB CNCs have larger apparent sizes closer to 100 nm; this increase agrees with the larger lengths measured by AFM, yet is also likely indicative of some CNC aggregation. The apparent sizes of the Melodea and BGB CNCs decreased after dialysis, suggesting the removal of residual reagents or ions from the suspension or a further liberation of individual CNCs. The presence of residual ions, which would screen the surface charge on CNCs and induce aggregation, was further confirmed for Melodea CNCs by the decrease in suspension conductivity which occurred after dialysis (Appendix 3, Table A3.1). Despite these minor differences in apparent size, all of the CNC suspensions were uniform dispersions without significant particle aggregation (apart from some lateral aggregation[55] and the innate polydispersity expected for particles extracted from natural materials). As the Anomera CNCs were the only samples received dry (spray dried, the others were in dispersion/gel never-dried forms), these results demonstrate that the material has excellent redispersibility in water upon probe sonication.

Appendix 3, Figure A3.2 shows the XRD spectra for each of the CNC types, which indicate that all five samples consist solely of cellulose I (the native cellulose crystal structure). Interestingly, Reid *et al.*[6] reported in the previous benchmarking paper, that some industrially produced CNCs were a mixture of cellulose I and cellulose II; further emphasizing the importance of extensively characterizing one's chosen material. The crystal allomorph provides insight into the production process and whether cellulose dissolution, regeneration and/or mercerization occurs, which is not the case for any of the CNC types studied here.

The degree of crystallinity (χ_c) of each sample was calculated through a Rietveld refinement, which is commonly used for crystalline cellulose.[39,42] Degree of crystallinity is related to the mechanical performance of CNCs, which is crucial for composites but also has implications in water interactions, and rheology as discussed further below. As shown in Table 3.1, each CNC type was highly crystalline with χ_c ranging from 79 – 93 %. It must be noted, however, that χ_c values are relative, and as such the values shown here may deviate from those reported in the literature due to differences in sample preparation, instrumental setup and data fitting routines.[42] Overall, these results show that CNC-LM and

BGB CNCs have the highest χ_c values (91 and 93%, respectively). Out of the sulfated CNCs, CNC-LM likely were made following the harshest hydrolysis conditions (that removed the most disordered cellulose) resulting in the higher crystallinity. Similarly, out of the carboxylated CNCs, BGB CNCs had a higher crystallinity than Anomera CNCs, indicating that metal catalyzed oxidation is more efficient at degrading non-crystalline cellulose than peroxides.

The molecular weight (M) distribution of the cellulose chains that make-up the CNCs was analyzed by size exclusion chromatography after derivatization (carbanilation) and complete dissolution in DMSO (Table 3.1). Figure 3.5 shows the shape and the number of peaks which can be analyzed to elucidate CNC composition. The CNC-LM molecular weight distribution showed a clear bimodality with the main peak starting at log M=3.5 and a shorter peak starting at log M =5.5. The high molecular weight peak is somewhat surprising as this peak has not been observed in our previous work where the same hydrolysis conditions were used.[23,56] This might be the result of less uniform mixing/mass transfer compared to previously used lab and industrial processes. However, we note that the amount of high molecular weight chains in CNC-LM is not as pronounced as it appears; the peak at high molecular weight is skewed by the fact that the higher molecular weight cellulose also has a larger SEC response.

Interestingly, at log M=3, an extra shoulder for CNC-LM can also be observed, indicating that the hydrolysis conditions were conducive to the formation and precipitation of oligosaccharides.[34,57] Oligosaccharides with DP values above 7 are soluble in acidic solutions yet insoluble in water,[57] and have been shown to irreversibly precipitate onto CNC surfaces during the quenching stage of the hydrolysis.[34,58] Seemingly, the conditions under which NORAM and Melodea CNCs were produced did not result in the precipitation of surface oligosaccharides, i.e., they had no low molecular weight shoulder (Figure 3.5). CNCs with oligosaccharide-free surfaces could result from higher temperature hydrolyses (which degrade oligosaccharides into water-soluble sugars) or a modified purification route which alters the quenching step to maintain oligosaccharide solubility. The presence of oligosaccharides on CNCs (or lack thereof) can greatly influence the water binding capacity and rheological behavior of their suspensions, which will be discussed below.

The shape of the molecular weight distributions for carboxylated CNCs differs from the sulfated CNCs; the distribution shows a significant portion of lower molecular weight cellulose chains over a larger range of molecular weights, compared to sulfated CNCs, implying significant cleavage of cellulose during oxidative processes. While the sulfuric acid hydrolysis of cellulose preferentially breaks the β-1-4 glycosidic (ether) bond in the less ordered regions of cellulose,[12] these oxidation routes break the C2-C3 bond of glucose (not necessarily in the disordered regions), prior to chain cleavage (catalyzed by alkaline conditions),[26,59] leading to shorter cellulose chains and more chain ends within the CNCs.
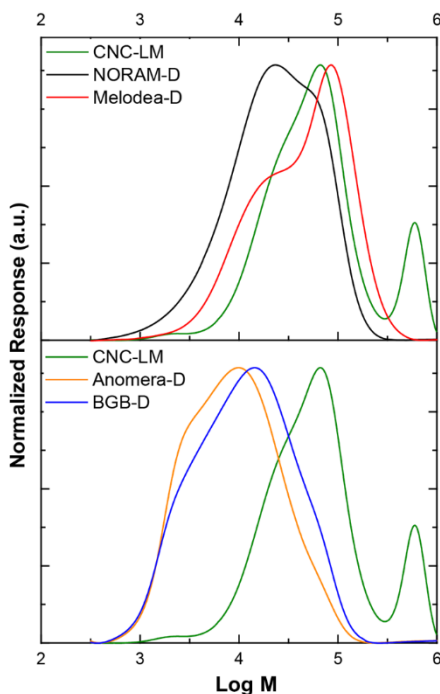
Figure 3.5. Molecular weight (M) distribution of cellulose chains from the different CNC types.

Overall, the average cellulose chain lengths within carboxylated CNCs trended towards lower M_w (DP≈40) compared to sulfated CNCs.[26] NORAM, Melodea and CNC-LM had average DP values of 71, 130 and 235, respectively. If the high molecular weight peak that skews the distribution for CNC-LM is not included, the average DP for the majority of the chains making up the CNC-LM is 117, implying these CNCs are most similar to Melodea CNCs. The differences within the sulfated CNCs can be attributed to their respective starting materials (containing more or less disordered cellulose) and production routes (time, temperature and acid concentration).[60–62]

Comparing the DP of sulfated CNCs produced at a large scale, Melodea CNCs were made up of longer cellulose chains than NORAM CNCs, which indicates that a weaker hydrolysis (e.g., lower temperature, time, or acid concentration) was used to produce them. This is in line with the results discussed above, whereby Melodea CNCs were found to be less crystalline and longer, again, suggesting that the hydrolysis has not been pushed to its limit and some disordered cellulose regions remain. We note that the DP values measured here for sulfated CNCs fall near the range of predicted levelling off degree of polymerization values for cotton linters (140 – 180) and commercial wood pulps (100 – 300),[63,64] however, the carboxylated CNCs have a lower DP, demonstrating that oxidation of cellulose is a less selective process than acid hydrolysis.

Looking at the breadth of the molecular weight distributions (Figure 3.5 and Table 3.1), all CNC types have large dispersity (Đ) values. For sulfated CNCs, CNC-LM had the highest Đ (4.1) compared to NORAM (3.1) and Melodea (3.2), indicating that CNC-LM contains

the least uniform cellulose chain lengths, as a result of their bimodality. It is interesting to note that NORAM and Melodea CNCs have similar dispersity values but the M_w is much higher for Melodea CNCs. For the carboxylated CNCs, Anomera has both the larger Đ (4.4) and M_w values, compared to BGB (Đ = 3.5).

Surface charge and colloidal stability. The surface charge and the surface potential of CNCs can be inferred through conductometric titrations and electrophoretic mobility measurements, respectively. These parameters are important as they regulate colloidal stability, and also affect thermal stability and self-assembly behavior.[19,23,65] The CNC surface charge is a direct result of the introduction of the functional groups (-OSO_3^- and -COO^-) during the production process. The sulfate half-ester groups are deprotonated under all working solution conditions (strong acid groups) whereas the carboxyl groups are weak acid groups, deprotonated above pH ~ 4.5.[66,67] In contrast, surface hydroxy groups on cellulose are not deprotonated (pKa > 12) and do not contribute to CNC surface charge as degradation and/or mercerization would be expected under such conditions.[37,68]

In general, electrophoretic mobility (typically reported as ζ-potential for CNCs using the Smoluchowski approximation or, more recently, the modified Oshima-Overbeek equation[44]) provides an indication of CNC suspension colloidal stability. Particles with ζ-potentials above |10| mV are considered colloidally stable as there is sufficient electrostatic repulsion between particles to prevent aggregation.[66] Even higher ζ-potentials (e.g., above |20| mV) are generally desirable, as sulfated CNCs undergo desulfation over time or can be exposed to salts, both of which induce aggregation.[69,70] Here, all five CNC types had ζ-potential values between -36 and -24 mV, indicating that they all formed colloidally stable suspensions in water (Figure 3.6). The ζ-potential values of sulfated CNCs, however, were more negative than their carboxylated counterparts. NORAM and Melodea CNCs were comparative to that of the CNC-LM (-33 ± 1 mV), while Anomera and BGB CNCs had ζ-potentials of -21 ± 1 mV and -28 ± 2 mV, respectively. As such, carboxylated CNCs are slightly less colloidally stable and more sensitive to pH than sulfated CNCs.

The ζ-potential values measured here for the sulfated CNCs are comparable to those in our previous benchmarking paper even though a different instrument was used.[6] Note that we decreased the amount of NaCl added to Melodea and BGB CNCs (i.e., 5 mM instead of 10 mM), because for these CNC types 10 mM salt was sufficient to induce some aggregation due to their high viscosity (discussed below) and led to errors in the measurement signal indicating that the sample was changing over time. Dialysis of the suspensions (which mainly removes ions) did not cause notable changes to the ζ-potential of the CNCs as the measurements were performed after "re-addition" of 5 mM (for Melodea and BGB CNCs) or 10 mM salt (for CNC-LM, NORAM and Anomera CNCs).
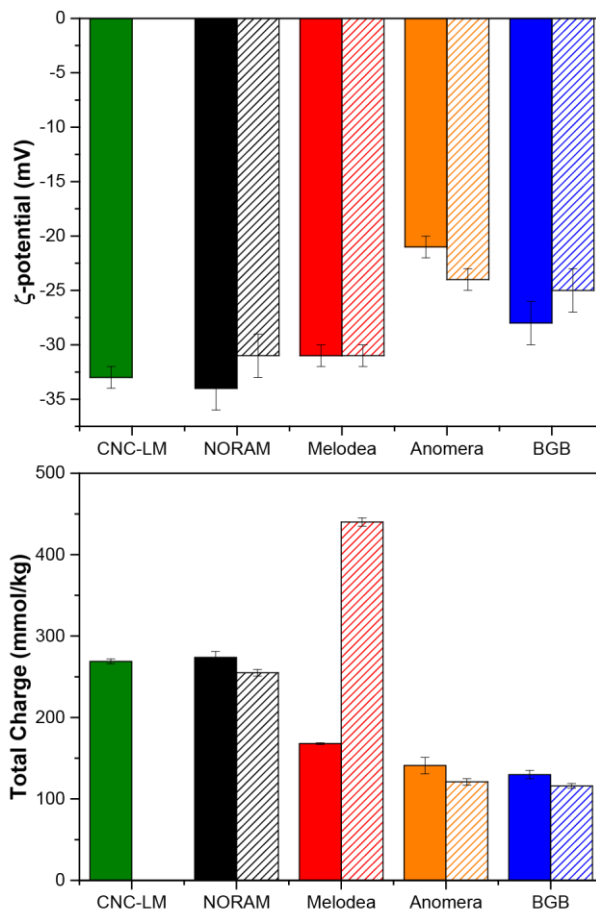
Figure 3.6. Comparison of the ζ-potential and total charge content of industrially produced CNCs (as-received (solid) and dialyzed (striped)) to those of CNC-LM. The error bars represent the standard deviation of the average value of triplicate measurements.

Conductometric titrations were performed to determine the total charge content of the CNCs (Table 3.1). Previous benchmarking efforts within our group found industrially produced and lab-made sulfated CNCs to have sulfur contents between 206 and 335 mmol S/kg CNC.[6] The lab-made CNCs used in this study, as well as the NORAM CNCs, were found to have sulfur contents within this range (274 ± 7 mmol S/kg CNC for NORAM and 269 ± 3 mmol S/kg CNC for CNC-LM). Interestingly, NORAM CNCs were produced with a 10-fold smaller acid to pulp ratio than the CNC-LM, but still had a similar total charge content. This production route presents a promising path towards greener (and likely cheaper) sulfated CNCs, as it reduces sulfuric acid usage and enforces the principle of atom economy (i.e., a higher percentage of the sulfur in the sulfuric acid will be incorporated into the sulfate half-ester groups on the CNCs).[71]

Unlike NORAM CNCs and CNC-LM, the total sulfur content of Melodea CNCs did not align with expected values: the as-received sample had a total charge content of 168 ± 1 mmol/kg CNC, which then increased almost 3-fold to 440 ± 5 mmol/kg after dialysis.

Furthermore, this increase did not align with the measured ζ-potential of the Melodea CNCs, which did not change after dialysis and gave similar values to the other sulfated CNCs. The change in charge content after dialysis may result from ions in the as-received sample, the way in which this sample interacts with the ion exchange resin that must be used prior to titration,[46] and the accessibility of sulfate groups to be titrated. We suspected the as-received samples contained excess free ions; which was confirmed by measuring the conductivity of their suspensions, which decreased from 32.6 µS cm^{-1} to 8.74 µS cm^{-1} after dialysis. Note that 32.6 µS cm^{-1} was by far the highest conductivity measured amongst all samples in sodium-form (Appendix 3, Table A3.1). Furthermore, the char value for the as-received Melodea CNCs (6.3 %) was higher than that of CNC-LM (2.1 %) when performing TGA at high temperatures (800 °C), indicating a higher number of incombustible inorganics are present in the Melodea CNC samples (Appendix 3, Figure A3.3).

We speculate that the salts/ions in Melodea samples are residual Na_2SO_4 (as stated in their certificate of analysis) and divalent cations such as calcium or magnesium (which are prevalent in industrial process water). Divalent cations can act as counterions for sulfate half-ester groups on neighboring CNCs, therefore forming bridges between particles. Whereas the sulfate salts may enable the formation of CNC-salt complexes. When subject to an ion-exchange resin column, the sulfate half-ester counterions in question may not be accessible to the resin beads due to their locations within aggregates/complexes or not being at the outermost surface of the CNCs (i.e., slightly buried) and thus are likely not exchanged to a H^+ counterion.[46] As such, without first dialyzing suspensions to remove the excess free ions, the true number of surface sulfate groups could not be determined using titrations. This theory agrees with the higher apparent DLS size of the Melodea CNCs before dialysis (as bridging between neighboring CNCs would result in larger apparent sizes). Further evidence of a "CNC-superstructure" and cation-induced bridging in the Melodea CNCs will be discussed in the rheology and water binding capacity sections below.

The total charge content of the carboxylated CNCs was much lower than sulfated CNCs: Anomera and BGB CNCs had total charge contents of 141 ± 10 mmol/kg CNC and 130 ± 5 mmol/kg CNC, respectively. This result was in line with the ζ-potentials of the carboxylated CNC suspensions, which were less negative than those for the sulfated CNCs. Furthermore, both Anomera and BGB CNCs showed negligible changes in charge content after dialysis, which suggests that few additional ions were present in the as-received samples.

The total charge obtained by conductometric titrations was further normalized by the surface area of the CNCs in order to obtain the surface charge density (Table 3.1).[47,72] As all the CNCs have a similar surface area, the trend in surface charge density remained similar to the trend in total charge content. In short, carboxylated CNCs showed a lower surface charge density (about 1 charge per 6 nm^2) compared to sulfated CNCs (about 1 charge per 2-3 nm^2). While high colloidal stability is important for CNCs in general, less surface charge can be advantageous for some applications. For example, Kalashnikova *et al.*[73] showed that CNCs with a lower surface charge density enhance the interfacial activity

of the CNCs, leading to more stable emulsions. Anomera Inc. has used this property to their advantage by making microparticles with CNCs and proteins.[74] Furthermore, a lower surface charge density gives the advantage of more non-functionalized hydroxy groups on the surface of the CNCs, which are (in addition to the carboxylic acid groups) accessible for chemical modification.[3,75]

Thermal stability. The thermal stability of the CNCs was investigated using TGA. Cellulose and more so, highly crystalline CNCs, is relatively thermally stable for an organic material with thermal degradation occurring above 200 °C.[9,23,76] This makes CNCs a good candidate to be used as reinforcing fillers in nanocomposites (e.g. melt processing with plastics >110°C),[77] in engineering fluids (e.g. oil extraction fluids that must function >150°C),[78–80] and in separation processes.[9] Knowing the range over which CNCs are thermally stable is thus of importance. TGA was performed on dialyzed freeze-dried CNCs in both acid and sodium-forms as the counterion has been shown to significantly affect CNC thermal stability.[23]

In their acid-form, the sulfated CNCs demonstrated a lower thermal stability compared to their sodium-form (Figure 3.7A and 3.7B). In the acid-form, desulfation from the CNC surface is uninhibited, the sulfate groups and water released during pyrolysis react to produce localized and concentrated sulfuric acid which promotes cellulose degradation.[23,76] This low temperature pyrolysis process favors char formation,[81] which further protects the remaining cellulose structure and results in higher mass fractions at the end of the thermal sweep. Conversely, when neutralizing the surface sulfate half-ester groups, CNCs in sodium-form degrade at higher temperatures, and form volatile compounds rather than char. As a result, the final sample weight (or char value) was significantly lower for sodium-form CNCs (Figure 3.7A).
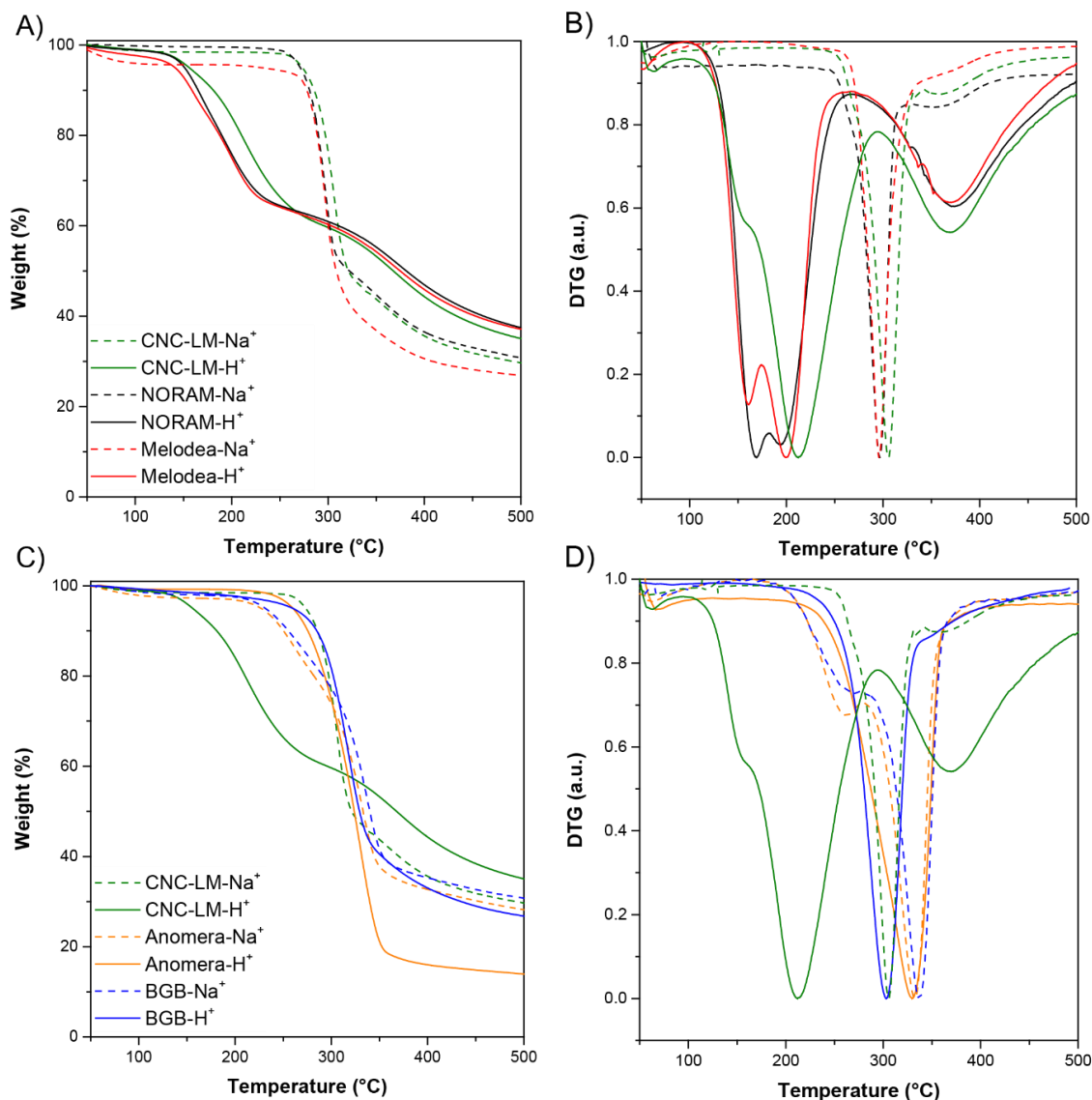
Figure 3.7. TGA and DTG curves for the five types of CNCs in acid and sodium-form. A) TGA curves for sulfated CNCs; B) DTG curves for sulfated CNCs; C) TGA curves for carboxylated CNCs compared to CNC-LM, D) DTG curves for carboxylated CNCs compared to CNC-LM. Solid lines are acid-form and dotted lines are sodium-form CNCs.

Although all sulfated CNCs showed higher thermal stability in their sodium-form compared to acid-form, slight differences in their overall thermal behavior was observed. The NORAM and Melodea CNCs were slightly less thermally resistant than the CNC-LM in sodium-form; their maximum rate of thermal decomposition occurred at 295°C *vs*. 305°C for CNC-LM. Furthermore, the shape of the derivative thermogravimetry (DTG) curves vary amongst the acid-form sulfated CNC samples (Figure 3.7B). The primary pyrolysis stage, which generally occurs between 150 °C – 250 °C for acid-form sulfated CNCs, is the result of the degradation of the sulfated surface and the depolymerization of the

cellulose chains, catalyzed by sulfuric acid.[76] The temperature at which this primary pyrolysis stage occurs is heavily dependent on both the number of sulfate groups as well as the number of reducing ends (which activate cellulose pyrolysis)[82] present in the CNC samples.[23] This stage occurred at a slightly lower temperature for the NORAM and Melodea CNCs compared to CNC-LM. This can be primarily attributed to the differences in the DP of the cellulose chains that make up the CNCs. They have a shorter average chain length, and more reducing ends than the CNC-LM and thus degrade faster. Nevertheless, the three sulfated CNCs tested in this work displayed similar thermal properties and would likely exhibit indistinguishable thermal performance in most CNC-based applications.

The carboxylated CNCs demonstrated a different thermal behavior. Most noticeably, the differences between their acid and sodium-form thermal performance were less significant than those observed among the sulfated CNCs (Figure 3.7C and 3.7D). This behavior can be attributed to their relatively low total charge contents (Table 3.1); if more carboxyl groups were present, the difference in thermal behavior between the acid and sodium-form would likely be more pronounced. Nevertheless, differences were observed in the onset of thermal degradation, which occurred at a lower temperature in sodium-form for both Anomera and BGB CNCs (*ca.* 200 °C in sodium-form *vs. ca.* 250 °C in acid-form). This behavior has been observed in other carboxylated nanocelluloses and is indicative of a reaction between the carboxyl group and the sodium ions which catalyzes the degradation of cellulose.[23]

Overall, the Anomera and BGB CNCs were more thermally stable than their sulfated counterparts. This is somewhat surprising since the Anomera and BGB CNCs have substantially lower DP values, which would typically reduce their thermal stability.[23] The length of the cellulose chains therefore must be overshadowed by the differences in surface chemistry. The CNC-LM, which have more surface charge groups, are less thermally stable than the Anomera and BGB CNCs, which have less surface charge groups. Nevertheless, these differences are reduced when all CNC types are compared with their most favorable counterions. As such, these results outline the importance of selecting an appropriate counterion for each CNC type to maximize thermal performance and expand their suitability for high temperature applications.

Rheology. Rheometry is a useful method for analyzing the behavior of colloidal suspensions,[83–90] and reports have linked changes in the rheology of CNC suspensions to parameters such as sonication treatment,[88,91] ionic strength,[85,86] surface charge density,[92] surface modification,[93] aspect ratio,[94] temperature,[83,95] and hydrolysis conditions.[96] Figure 3.8 shows the shear viscosity of each CNC type (at 2 wt% before and after dialysis) as a function of shear rate; values at 10 s^{-1} are tabulated in Table 3.1. The rheological behavior varied significantly between samples, however, no obvious correlation between surface chemistry (i.e., sulfated or carboxylated) and viscosity was observed. The rheological behavior of NORAM and Anomera CNC suspensions, both before and after dialysis, resembled that of CNC-LM. Each of these materials exhibited typical Newtonian behavior. CNC-LM had the lowest steady state viscosity (0.97 mPas·s at 10s[-1]) likely due to it having the lowest aspect ratio. The Newtonian properties of these CNCs make them suitable in

industrial and medical applications where fluids with constant viscosities over a range of shear rates are required.[97–99]

BGB and Melodea CNC suspensions demonstrated significantly higher viscosities than the aforementioned samples. BGB CNC suspensions, showed an isotropic behavior.[100] Its corresponding flow curve exhibited a constant viscosity (at low shear rates), followed by a shear-thinning behavior (at intermediate shear rates). On the other hand, Melodea CNCs exhibited rheological properties atypical for 2 wt% CNC suspensions.[100–102] For example, the shear thinning behavior of Melodea CNCs, particularly the as-received sample, is more representative of a CNC gel than a relatively dilute suspension.[103] Interestingly, the high aspect ratio of Melodea CNCs seems to result in rheological properties closer to those reported for cellulose nanofibers,[104] and would thus be an appropriate choice for applications where designing yield stress fluids are required.[105,106]

While high aspect ratio and low surface charge are known to lead to more viscous CNC suspensions,[107,108] the viscosity measured here did not show a clear trend with either factor indicating that both properties, amongst other factors like dispersion quality, intermolecular interactions, and purity have a compound effect on rheology. The influence of purification via dialysis on the rheological behavior of CNC suspensions was evaluated. Minimal changes were observed for NORAM, Anomera, and BGB CNC suspensions. The removal of residual reagents or excess salt/ions, as shown through conductivity measurements (Appendix 3, Table A3.1) likely contributed to the slight differences between the as-received and dialyzed samples.[109,110] Melodea CNCs, on the other hand, demonstrated a significant decrease in viscosity upon dialysis. Again, this can be attributed to the removal of Na_2SO_4 salt, other excess (multivalent) ions and "CNC-super-structures" from the as-received suspension, as mentioned above and supported by the marked decrease in conductivity after dialysis (Appendix 3, Table A3.1). Bridging with multivalent ions can lead to highly percolated CNC networks, resulting in a highly viscous or gel-like suspension. Similar increases in viscosity have been observed through the addition of calcium chloride to carboxymethyl cellulose solutions as well as cellulose nanocrystal suspensions.[111,112]
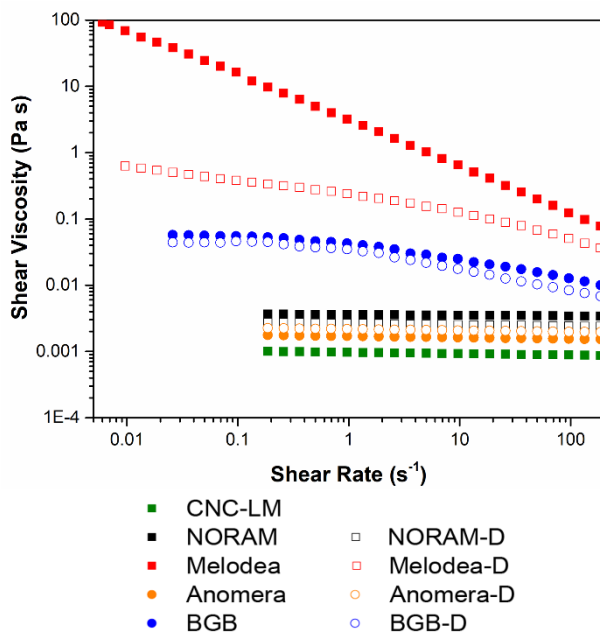
Figure 3.8. Shear viscosity of the different sulfated and carboxylated CNC types at different shear rates. The suspensions were analyzed both in their as-received (closed symbols) and dialyzed form with a sodium counterion (open symbols).

Water binding capacity. QCM-D was used to determine the water adsorption capacity of the CNCs following a solvent exchange protocol whereby H_2O is exchanged for D_2O (Appendix 3, Table A3.2, Figure A3.4).[48] CNC-water interactions not only play a decisive role in their colloidal stability, rheological behavior and self-assembly, but are also important for their functionalization, processing, and storage.[34,46,56,113] Numerous works have been carried out to probe CNC interactions with water and water vapor, and while all cellulosics and CNCs have strong interactions with water,[114] the magnitude of the interaction is dependent on the source material, the surface charge and chemistry.[48,49,115,116] Figure 3.9 shows the adsorbed water content (normalized by the film thickness) of spin coated CNC films produced from the as-received and dialyzed samples. Overall, the water binding capacity of BGB CNCs is comparative to CNC-LM, however, NORAM, Melodea, and Anomera CNCs all bind more water.

Interestingly, Bouchard *et al.*[34] reported an inverse correlation between the amount of oligosaccharides on the surface of CNCs to their viscosity in suspension. They hypothesized that the viscosity of CNC suspensions increases with the thickness of the bound water layer on the particle surface due to a subsequent increase in 'effective' particle size. Conversely, the presence of precipitated oligosaccharides would disrupt the bound water layer, and as such, CNCs with larger amounts of surface oligosaccharides are predicted to have lower suspension viscosities. It is thus interesting that CNC-LM, which has a shoulder in the lower molecular weight region of Figure 3.5 (that is most likely

precipitated oligosaccharides on the surface of the CNCs), has a low water binding capacity.

BGB CNCs also had a low water binding capacity (Figure 3.9, Table 3.1). As described above, we attribute this to the carboxylated CNCs having a significant portion of low molecular weight cellulose chains, making the surface of the CNCs less ordered[26] and leading to less water bound on the surface. This effect is less pronounced for Anomera CNCs as water binding is also strongly affected by the specific surface area and Anomera CNCs being smaller, have a significantly higher specific surface area that can bind more water.
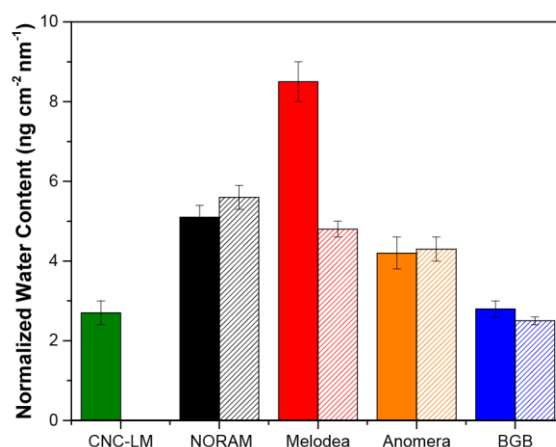
Figure 3.9. Comparison of the normalized bound water content of the different CNC types. Films were prepared from suspensions in their as-received (solid) and dialyzed form with a sodium counterion (striped).

While the QCM and SEC results show that a decrease in surface oligosaccharides corresponded to an increase in water binding capacity, a direct comparison between the rheological properties and bound water content of the different CNC types cannot be made due to their significantly different particle size and charge. However, for the CNCs most similar in size (i.e., 81 nm by DLS for CNC-LM, NORAM, and Anomera CNCs) there is a linear correlation between bound water content and viscosity (Table 3.1). Also noteworthy, is the decrease in the water binding capacity of Melodea CNCs upon dialysis, which corresponds to the most significant decrease in viscosity; the mass of bound water in the Melodea CNC films decreased by a factor of 1.8 as a result of dialysis. We believe this is direct result of the removal of residual salts and divalent ions, which have a strong kosmotropic nature (e.g. calcium or magnesium), meaning the ions themselves are highly hydrated and could increase the packing of water molecules at the CNC surface according to the Hoftmeister series.[117–119] Upon removal of these ions by dialysis, the ordering of water, and the subsequent water binding capacity of the CNCs, would decrease. This theory follows trends in conductivity, apparent size, total charge content, and viscosity of Melodea CNCs, all of which suggest the presence of Na_2SO_4 and divalent ions in the as-received

sample. Conversely, the changes in water uptake capacity for NORAM, Anomera, and BGB CNCs as a result of dialysis are considered negligible.

Liquid crystalline properties and self-assembly. Due to their anisotropic nature and colloidal stability, CNCs display shear birefringence at low concentrations and can self-assemble forming liquid crystals above a critical concentration (c*);[51] these properties have garnered interest for optical and decorative applications.[4,108] The self-assembly behavior of CNCs is dependent on their size and surface charge density, as well as suspension ionic strength and the cellulose source.[4,72] To evaluate this behavior, liquid crystalline phase separation of the industrial CNCs, both as-received and dialyzed, was compared to CNC-LM. Flat capillary tubes were filled with suspensions ranging from 0.3 to 10 wt% (Appendix 3, Figures A3.5-A3.9) and the electrostatic double layer thickness was adjusted to be constant for all samples at *ca.* 9.7 nm by adding 1 mM of NaCl. Phase separation of the suspensions within the capillaries was photographed through cross-polarizers after a week of equilibration.[108] Table 3.2 summarizes the liquid crystalline properties of each CNC type before and after dialysis. The capillaries filled with increasing CNC concentration reveal c*, above which the suspensions phase separate into an (upper) isotropic and (lower) anisotropic phase. Additionally, the point at which the CNCs reach a gel-like state was determined.[107]

Table 3.2**.** Self-assembly behavior of CNCs in their as-received and dialyzed (D) form, with a final salt concentration of 1 mM. Imaging of drying droplets was performed on as-received carboxylated CNCs without the addition of salt. CNT and NT indicate chiral nematic tactoids and nematic tactoids, respectively.

		CNC-LM	NORAM		Melodea		Anomera		BGB	
Form		D	as-received	D	as-received	D	as-received	D	as-received	D
Filled Capillary Tubes	**Critical concentration (wt%)**	9	6	5	-	-	-	-	-	-
	Chiral nematic phase	Yes	Yes	Yes	No	No	No	No	No	No
	Gelling point (wt%)	15	8	7	2	2	5	2	4	2
Drying Droplet	**LC properties**	CNT	CNT	CNT	NT	NT	CNT	/	CNT	/

All five CNC types showed shear birefringence at low concentration as a result of their anisotropic shape. Yet, under the conditions investigated in this work, only CNC-LM and NORAM CNCs (in the as-received and the dialyzed-form) showed a distinct phase separation into a dark isotropic phase and a bright anisotropic phase when imaged between cross-polarizers (Appendix 3, Figures A3.5 – A3.9). This agrees with the phase separation behavior seen for sulfated CNCs in our previous benchmarking study.[6] The phase separation occurred at a lower concentration for NORAM CNCs compared to CNC-LM; this is attributed to their larger aspect ratio and lower surface charge density, which are both known to reduce c*.[54,65,107] After dialysis, the c* for NORAM CNCs reduced from 6 to 5 wt%, which is expected as a result of the reduction in surface charge (Table 3.1).[65] These c* values generally agree with the literature where c* with or without salt normally ranges from 0.5-8 wt% for sulfated CNCs, depending on the factors described above.[65,108] Above c*, the anisotropic phase for sulfated CNCs most commonly takes on a chiral nematic liquid crystalline texture with a characteristic "fingerprint" structure. This was observed for both CNC-LM and NORAM CNCs (Figure 3.10 A-C).

For Melodea CNCs, lower concentrations (0.3 – 3 wt%) were used to fill the capillary tubes due to their inherently high viscosity (Table 3.2 and Appendix 3, Figure A3.7). Despite this, Melodea CNCs did not show any liquid crystalline phase separation in the as-received or dialyzed form; this is likely due to the formation of a kinetically arrested gel-like state, where the orientation of rod-like particles to a liquid crystalline phase is inhibited.[100,108] Previously, phase separation at low concentrations (c* under 1 wt%) was reported for CNCs produced following a very similar protocol to that used by Melodea.[65,120] However, there are small differences in the hydrolysis and purification processes used in these reports, which are also known to affect the liquid crystalline properties.[4] Dialysis of Melodea CNCs had the inverse effect of what was expected: the CNCs formed a uniform birefringent phase at lower CNC concentrations after dialysis (2 wt% *vs.* 3 wt%) (Appendix 3, Figure A3.7 B *vs.* D). We hypothesize that the removal of excess free ions by dialysis reduced the screening of the surface charge groups, allowing the particles to interact with each other over larger distances, resulting in long-range orientational order which appears birefringent in between crossed polarizers.

As expected from the lack of phase separation, no chiral nematic ordering was observed for Melodea CNCs at concentrations considered high for this CNC type (Figure 3.10 D-F). Furthermore, when observing a drying droplet of a 0.5 wt% suspension via POM, *nematic* tactoids were observed at the edge of the droplet (Figure 3.10 F). As such, while the high viscosity of Melodea CNCs likely inhibits the formation of fingerprint structures, these suspensions still demonstrate interesting self-assembly behavior.

Unlike their sulfated counterparts, phase separation has not been studied widely for carboxylated CNC suspensions. While the anisotropic shape of both Anomera and BGB CNCs should encourage the formation of a lyotropic liquid crystalline phase,[54] their weak-acid surface groups clearly affected their self-assembly behavior.[121] The capillary tubes filled with increasing concentrations of carboxylated CNCs (with 1 mM salt) did not phase separate. As-received Anomera CNCs did not exhibit birefringence as their self-assembly

was inhibited by the relatively early onset of gelation when salt was added (Table 3.2). However, after dialysis, the capillaries with Anomera CNCs above 2 wt% developed long-range orientational order and birefringence (Appendix 3, Figures A3.8 A and B).

For BGB CNCs, birefringence was observed in the capillaries containing both as-received (above 3 wt%) and dialyzed (above 2 wt%) CNCs (Appendix 3, Figures A3.9 A and B). The behavior of the dialyzed carboxylated CNCs is similar to the dialyzed Melodea CNCs, where the onset of birefringence appeared at *lower* concentrations for the dialyzed samples likely due to the increased repulsion between CNCs upon removal of excess ions.

It is known that in some cases birefringence (as a result of long-range orientational order and gelation) can be induced by the addition of salt, as observed by Honoratio-Rios *et al.* for sulfated CNCs.[107] However, for the carboxylated CNCs (as-received) no significant difference was seen with or without 1 mM NaCl (Figure A3.8, A *vs*. C, and Figure A3.9, A *vs*. C). In the field of polymeric colloids, sulfate stabilization allows colloids to more reliably assemble into highly ordered structures, whereas weak-acid carboxyl group stabilization is less effective as a result of their lower degree of ionization and their "weaker" interactions in general.[121] Ruling out the effect of salt, we hypothesize that the weaker repulsion between particles in the carboxylated CNC suspensions results in a smaller drive towards phase separation because there is less of an entropic gain, compared to sulfated CNCs. In the carboxylated samples, CNCs can approach each other more easily and form locally ordered regions (as long as they do not aggregate significantly). We note that adding salt would further reduce the interparticle repulsion and exacerbate the factors opposing phase separation, provided the salt concentration was below that which induces aggregation and sedimentation of CNCs. Alternatively or in conjunction, weaker repulsion and higher sample viscosity could imply that carboxylated CNCs reach a kinetically trapped gel-like state at low concentrations precluding phase separation.[108]

Upon observing drying droplets of carboxylated CNC suspensions (without salt), however, chiral nematic tactoids *were* identified (Figure 3.10 I and L). This suggests that the inability to see chiral nematic structures in the capillary tubes may be because the pitch was below the resolution of the optical microscope or because the CNCs had gelled before ordering.[108]

To the best of our knowledge, only Gray and co-workers have previously investigated the self-assembly behavior of carboxylated CNCs. They demonstrated a chiral nematic liquid crystalline phase for carboxylated CNCs prepared by ammonium persulfate oxidation of cotton.[122] This self-assembly was contrasted with CNCs extracted from wood pulp via the same method (but at a larger scale), which did not exhibit a chiral nematic structure – this highlights the intricacies of carboxylated CNC self-assembly. Overall, these results suggest that further research should be conducted to deepen our understanding of the effects of surface chemistry on the self-assembly behavior of CNCs.
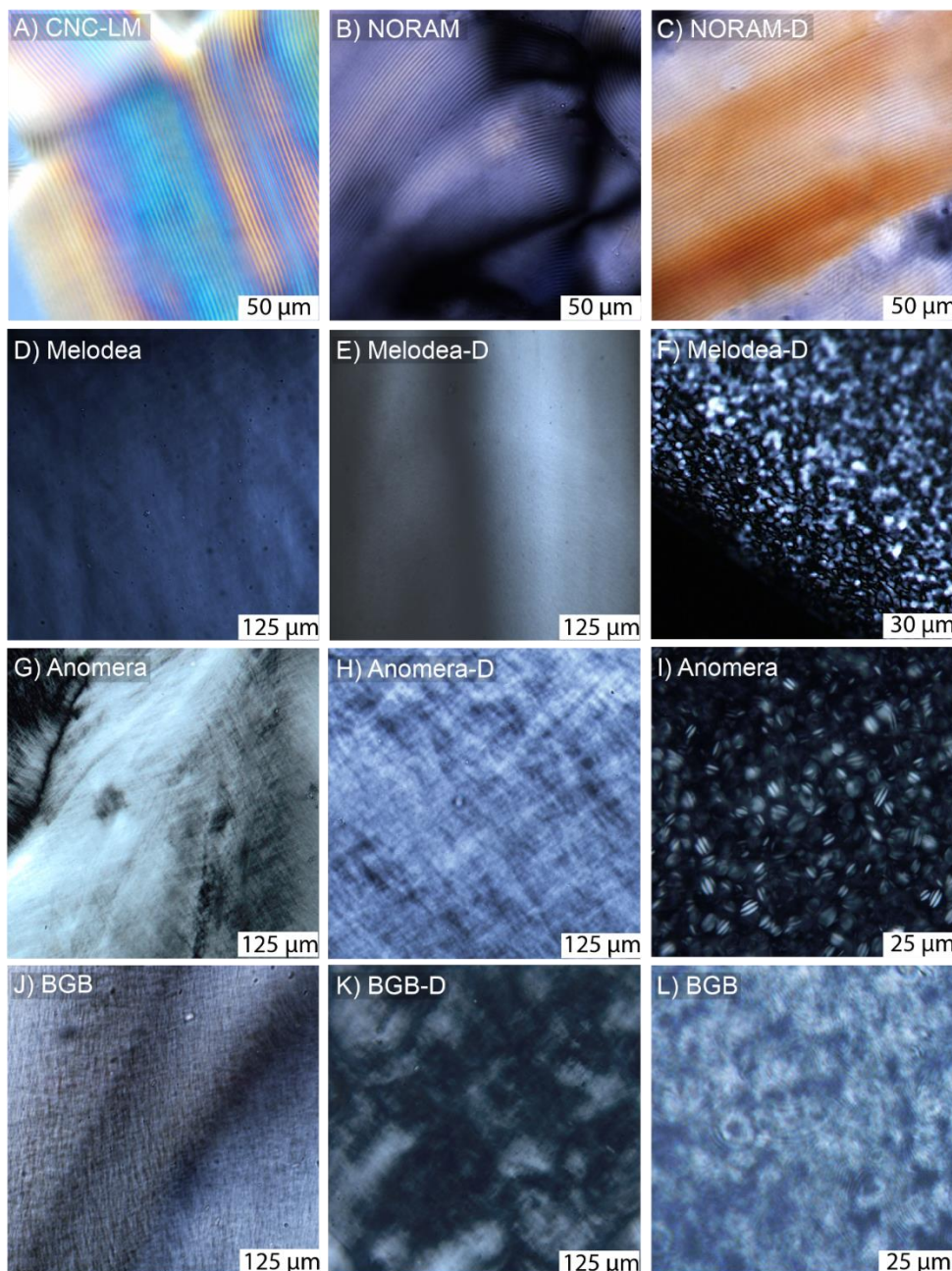
Figure 3.10. Polarized optical microscopy images of A) CNC-LM at 10 wt%, 1 mM NaCl, B) NORAM at 6 wt%, 1 mM NaCl, C) NORAM-D at 6 wt%, 1 mM NaCl, D) Melodea at 3 wt%, 1 mM NaCl, E) Melodea-D at 2 wt%, 1 mM NaCl, F) nematic tactoids form in a drying droplet of Melodea-D at 0.5 wt% starting concentration, G) Anomera at 4 wt%, no salt, H) Anomera-D at 3 wt%, 1 mM NaCl, I) chiral nematic tactoids observed in a drying droplet of Anomera CNCs with a concentration of 3 wt%, J) BGB at 5 wt%, 1 mM NaCl, K) BGB-D at 3 wt%, 1 mM NaCl, L) chiral nematic fingerprints can be observed in a drying droplet of BGB at 4 wt%.

3.5 Conclusions

This work has benchmarked four new industrially produced CNCs against sulfated lab-made CNCs. Together with our previously published benchmarking paper,[6] all current industrially produced CNCs have now been analyzed in a comparable fashion, providing an overview of the properties of the different CNC types. Additionally, this work has allowed us to answer the following questions which we believe are pertinent for future research and product development:

What are the main differences between industrially produced sulfated and carboxylated CNCs? Sulfated CNCs from NORAM, Melodea Ltd. and those made in-house were compared to carboxylated CNCs from Anomera Inc. and Blue Goose Biorefineries Inc. All CNC types were rod-shaped, highly crystalline, well-dispersed and colloidally stable (at low ionic strength); the biggest differences were their surface charge densities, thermal properties and self-assembly behavior. The carboxylated CNCs had a lower surface charge density compared to the sulfated CNCs. Furthermore, carboxylated CNCs were slightly more thermally stable, making them interesting for applications where high temperatures are needed. Sulfated CNCs (except for Melodea CNCs) showed a liquid crystalline phase separation (under the investigated conditions) into an isotropic and a chiral nematic anisotropic phase, that carboxylated CNCs did not, making sulfated CNCs more relevant for optical applications where liquid crystals are beneficial over mere shear birefringence.

What is the effect of process modifications on the properties of sulfated CNCs? The CNCs from NORAM are produced with a lower acid-to-pulp ratio in a continuous process, which is in contrast to the conventional sulfuric acid hydrolysis batch process. Nevertheless, the CNCs have very similar properties to lab-made CNCs and the previously characterized commercial sulfated CNCs.[6] This is promising for the future production of sulfated CNCs, as this could significantly reduce cost and environmental impact. Melodea Ltd. also uses a simplified cost-saving purification process, resulting in CNCs with slightly different properties. Furthermore, Melodea's process includes a proprietary Sulfuric Acid Recovery Procedure (SARP™) which enables the recovery of the sulfuric acid used during the hydrolysis. For example, the Melodea CNCs had a significantly higher aspect ratio and showed cellulose nanofiber-type rheology, making these CNCs particularly suited for reinforcing and rheological applications. Thus, the acid hydrolysis process and work-up can lead to changes in CNC properties and an optimized process should be chosen based on the intended use of the CNCs.

How does the CNC production process impact their performance and potential applications? As described above, some differences were observed for sulfated and carboxylated CNCs. The carboxylated CNCs were produced following novel non-traditional routes, i.e., Anomera and BGB CNCs were produced via a hydrogen peroxide oxidation method and a transition metal catalyzed oxidation method, respectively. The different surface chemistry provides a "handle" through which to chemically modify the CNCs, as reviewed elsewhere.[12,123,124] Previously, post-synthesis carboxylation of sulfated

CNCs has been extensively applied as an intermediate step prior to surface functionalization, implying that this surface chemistry is highly desirable. The direct production of carboxylated CNCs by these oxidative methods fulfill a number of the tenants of Green Chemistry, including using less hazardous reagents and catalyzed reactions, preventing waste, and minimizing derivatives/intermediates (in the context of producing functionalized CNCs).

We have analyzed CNC performance in three categories we identified as promising for applications, namely, thermal stability, rheology, and liquid crystalline self-assembly. The conclusions are as follows:

Thermal performance. Anomera and BGB CNCs showed a slightly higher thermal stability, in both their acid and sodium-form, compared to sulfated CNCs. Nevertheless, the thermal stability of the sulfated CNCs could be increased by choosing the right counterion, i.e., Na^+ *vs.* H^+. Overall, CNCs are suitable for many high temperature applications (below *ca.* 300 ºC) in both dried and suspension form but their thermal degradation is sensitive to the environment/media in which they are heated and the kinetics of heating.

Rheology. Whilst CNC-LM, NORAM and Anomera CNCs showed Newtonian rheological behavior, BGB CNCs had a typical isotropic behavior. Unexpectedly, Melodea CNCs exhibited cellulose nanofiber-type rheological behavior, and formed gels at very low concentrations. All CNC-types are thus interesting for rheological applications where a variety of viscosities and gelling behaviors are needed and can benefit from a bio-based thickening agent that is non-toxic and potentially edible.

Liquid crystalline self-assembly. The self-assembly behavior of CNCs can be exploited to be used in optical materials such as decorative coatings, anticounterfeiting applications, sensors, waveguides/gratings, optical filters or as hierarchical templates.[4,125] NORAM CNCs phase separated at low concentrations (5 wt%), showing a characteristic chiral nematic fingerprint structure. The two types of carboxylated CNCs showed chiral nematic tactoids, but with a much shorter pitch likely as a result of their weaker electrostatic repulsion. Depending on the target optical application, the ability to manipulate light at different wavelengths based on the range of pitches available from different CNC types could be advantageous.

In short, this research serves as a guide for both academic and commercial users looking to use industrially produced CNCs or compare their lab-made CNCs to what is available currently on the market and suggests how differences in CNC performance may benefit a range of applications.

3.6 References

(1)   Research and Markets. *The Global Market for Nanocellulose - Research and Markets*; 2019.

(2)   Kontturi, E.; Laaksonen, P.; Linder, M. B.; Nonappa; Gröschel, A. H.; Rojas, O. J.; Ikkala, O. Advanced Materials through Assembly of Nanocelluloses. *Advanced Materials* **2018**, *30* (24), 1703779. https://doi.org/10.1002/adma.201703779.

(3)   Wohlhauser, S.; Delepierre, G.; Labet, M.; Morandi, G.; Thielemans, W.; Weder, C.; Zoppe, J. O. Grafting Polymers *from* Cellulose Nanocrystals: Synthesis, Properties, and Applications. *Macromolecules* **2018**, *51* (16), 6157–6189. https://doi.org/10.1021/acs.macromol.8b00733.

(4)   Parker, R. M.; Guidetti, G.; Williams, C. A.; Zhao, T.; Narkevicius, A.; Vignolini, S.; Frka-Petesic, B. The Self-Assembly of Cellulose Nanocrystals: Hierarchical Design of Visual Appearance. *Advanced Materials* **2018**, *30* (19), 1704477. https://doi.org/10.1002/adma.201704477.

(5)   Lafitte, V.; Lee, J. C.; James, S. G.; Valle, J. F. D.; Yakovlev, A. V.; Panga, M. K. R.; Szabo, G. H. Fluids and Methods Including Nanocellulose. US20150072902A1, March 12, 2015.

(6)   Reid, M. S.; Villalobos, M.; Cranston, E. D. Benchmarking Cellulose Nanocrystals: From the Laboratory to Industrial Production. *Langmuir* **2017**, *33* (7), 1583–1598. https://doi.org/10.1021/acs.langmuir.6b03765.

(7)   International Organization for Standardization. Nanotechnologies — Standard terms and their definition for cellulose nanomaterial. ISO/TS 20477:2017 https://www.iso.org/cms/render/live/en/sites/isoorg/contents/data/standard/06/81/68153.html (accessed Jun 17, 2020).

(8)   International Organization for Standardization. Nanotechnologies - Characterization of cellulose nanocrystals ISO/TR 19716:2016 https://www.iso.org/cms/render/live/en/sites/isoorg/contents/data/standard/06/61/66110.html (accessed Jun 17, 2020).

(9)   Vanderfleet, O. M.; Cranston, E. D. Production Routes to Tailor the Performance of Cellulose Nanocrystals. *Nature Reviews Materials* **2020**, 1–21. https://doi.org/10.1038/s41578-020-00239-y.

(10)   Dong, X. M.; Kimura, T.; Revol, J.-F.; Gray, D. G. Effects of Ionic Strength on the Isotropic−Chiral Nematic Phase Transition of Suspensions of Cellulose Crystallites. *Langmuir* **1996**, *12* (8), 2076–2082. https://doi.org/10.1021/la950133b.

(11)   Habibi, Y. Key Advances in the Chemical Modification of Nanocelluloses. *Chemical Society Reviews* **2014**, *43* (5), 1519–1542. https://doi.org/10.1039/C3CS60204D.

(12)   Habibi, Y.; Lucia, L. A.; Rojas, O. J. Cellulose Nanocrystals: Chemistry, Self-Assembly, and Applications. *Chem. Rev.* **2010**, *110* (6), 3479–3500. https://doi.org/10.1021/cr900339w.

(13)   Moon, R. J.; Martini, A.; Nairn, J.; Simonsen, J.; Youngblood, J. Cellulose Nanomaterials Review: Structure, Properties and Nanocomposites. *Chem. Soc. Rev.* **2011**, *40* (7), 3941–3994. https://doi.org/10.1039/C0CS00108B.

(14)   Lockhart, J.; Eng, P.; Gattrell, M.; Anderson, J.; Eng, P. Demonstration of CNC Production at Dramatically Lower Acid Ratios, 2019.

(15)   Nickerson, R. F.; Habrle, J. A. Cellulose Intercrystalline Structure. *Ind. Eng. Chem.* **1947**, *39* (11), 1507–1512. https://doi.org/10.1021/ie50455a024.

(16)   Yu, H.; Qin, Z.; Liang, B.; Liu, N.; Zhou, Z.; Chen, L. Facile Extraction of Thermally Stable Cellulose Nanocrystals with a High Yield of 93% through Hydrochloric Acid Hydrolysis under Hydrothermal Conditions. *J. Mater. Chem. A* **2013**, *1* (12), 3938–3944. https://doi.org/10.1039/C3TA01150J.

(17)   Araki, J.; Wada, M.; Kuga, S.; Okano, T. Flow Properties of Microcrystalline Cellulose Suspension Prepared by Acid Treatment of Native Cellulose. *Colloids and Surfaces A: Physicochemical and Engineering Aspects* **1998**, *142* (1), 75–82. https://doi.org/10.1016/S0927-7757(98)00404-X.

(18)   Espinosa, S. C.; Kuhnt, T.; Foster, E. J.; Weder, C. Isolation of Thermally Stable Cellulose Nanocrystals by Phosphoric Acid Hydrolysis https://pubs.acs.org/doi/full/10.1021/bm400219u (accessed Apr 9, 2020). https://doi.org/10.1021/bm400219u.

(19)   Vanderfleet, O. M.; Osorio, D. A.; Cranston, E. D. Optimization of Cellulose Nanocrystal Length and Surface Charge Density through Phosphoric Acid Hydrolysis. *Philosophical Transactions of the Royal Society A: Mathematical, Physical and Engineering Sciences* **2018**, *376* (2112), 20170041. https://doi.org/10.1098/rsta.2017.0041.

(20)   Chen, L.; Zhu, J. Y.; Baez, C.; Kitin, P.; Elder, T. Highly Thermal-Stable and Functional Cellulose Nanocrystals and Nanofibrils Produced Using Fully Recyclable Organic Acids. *Green Chem.* **2016**, *18* (13), 3835–3843. https://doi.org/10.1039/C6GC00687F.

(21)   Bian, H.; Chen, L.; Dai, H.; Zhu, J. Y. Effect of Fiber Drying on Properties of Lignin Containing Cellulose Nanocrystals and Nanofibrils Produced through Maleic Acid Hydrolysis. *Cellulose* **2017**, *24* (10), 4205–4216. https://doi.org/10.1007/s10570-017-1430-7.

(22)   Du, H.; Liu, C.; Wang, D.; Zhang, Y.; Yu, G.; Si, C.; Li, B.; Mu, X.; Peng, H. Sustainable Preparation and Characterization of Thermally Stable and Functional

Cellulose Nanocrystals and Nanofibrils via Formic Acid Hydrolysis. **2017**, 6. https://doi.org/10.21967/jbb.v2i1.68.

(23)   Vanderfleet, O. M.; Reid, M. S.; Bras, J.; Heux, L.; Godoy-Vargas, J.; Panga, M. K. R.; Cranston, E. D. Insight into Thermal Stability of Cellulose Nanocrystals from New Hydrolysis Methods with Acid Blends. *Cellulose* **2019**, *26* (1), 507–528. https://doi.org/10.1007/s10570-018-2175-7.

(24)   Spinella, S.; Maiorana, A.; Qian, Q.; Dawson, N. J.; Hepworth, V.; McCallum, S. A.; Ganesh, M.; Singer, K. D.; Gross, R. A. Concurrent Cellulose Hydrolysis and Esterification to Prepare a Surface-Modified Cellulose Nanocrystal Decorated with Carboxylic Acid Moieties. *ACS Sustainable Chem. Eng.* **2016**, *4* (3), 1538–1550. https://doi.org/10.1021/acssuschemeng.5b01489.

(25)   Zhou, Y.; Saito, T.; Bergström, L.; Isogai, A. Acid-Free Preparation of Cellulose Nanocrystals by TEMPO Oxidation and Subsequent Cavitation. *Biomacromolecules* **2018**, *19* (2), 633–639. https://doi.org/10.1021/acs.biomac.7b01730.

(26)   van de Ven, T. G. M.; Sheikhi, A. Hairy Cellulose Nanocrystalloids: A Novel Class of Nanocellulose. *Nanoscale* **2016**, *8* (33), 15101–15114. https://doi.org/10.1039/C6NR01570K.

(27)   Leung, A. C. W.; Hrapovic, S.; Lam, E.; Liu, Y.; Male, K. B.; Mahmoud, K. A.; Luong, J. H. T. Characteristics and Properties of Carboxylated Cellulose Nanocrystals Prepared from a Novel One-Step Procedure. *Small* **2011**, *7* (3), 302–305. https://doi.org/10.1002/smll.201001715.

(28)   Leguy, J.; Diallo, A.; Putaux, J.-L.; Nishiyama, Y.; Heux, L.; Jean, B. Periodate Oxidation Followed by NaBH$_4$ Reduction Converts Microfibrillated Cellulose into Sterically Stabilized Neutral Cellulose Nanocrystal Suspensions. *Langmuir* **2018**, *34* (37), 11066–11075. https://doi.org/10.1021/acs.langmuir.8b02202.

(29)   Andrews, M. P.; Morse, T. Method for Producing Functionalized Nanocrystalline Cellulose and Functionalized Nanocrystalline Cellulose Thereby Produced. US20170260298A1, September 14, 2017.

(30)   Blue Goose Biorefineries Inc. Process https://bluegoosebiorefineries.com/process/ (accessed Aug 4, 2020).

(31)   Lockhart, J. M.; Wearing, J. T.; Gulamhusein, A.; Hobenshield, E. J.; Devries, D. Process for Making Partly-Hydrolyzed Cellulose Using Compressed Cellulosic Materials. WO2014043781, March 27, 2014.

(32)   Melodea Ltd. Technology https://melodea.eu/technology/ (accessed Aug 10, 2020).

(33)   McAlpine, S.; Nakoneshny, J. Production of Crystalline Cellulose. WO2017127938A1, August 3, 2017.

(34)   Bouchard, J.; Méthot, M.; Fraschini, C.; Beck, S. Effect of Oligosaccharide Deposition on the Surface of Cellulose Nanocrystals as a Function of Acid Hydrolysis Temperature. *Cellulose* **2016**, *23* (6), 3555–3567. https://doi.org/10.1007/s10570-016-1036-5.

(35)   McAlpine, S.; Nakoneshny, J. Production of Crystalline Cellulose. US20190040158A1, February 7, 2019.

(36)   Cranston, E. D.; Gray, D. G. Morphological and Optical Characterization of Polyelectrolyte Multilayers Incorporating Nanocrystalline Cellulose. *Biomacromolecules* **2006**, *7* (9), 2522–2530. https://doi.org/10.1021/bm0602886.

(37)   Foster, E. J.; Moon, R. J.; Agarwal, U. P.; Bortner, M. J.; Bras, J.; Camarero-Espinosa, S.; Chan, K. J.; Clift, M. J. D.; Cranston, E. D.; Eichhorn, S. J.; Fox, D. M.; Hamad, W. Y.; Heux, L.; Jean, B.; Korey, M.; Nieh, W.; Ong, K. J.; Reid, M. S.; Renneckar, S.; Roberts, R.; Shatkin, J. A.; Simonsen, J.; Stinson-Bagby, K.; Wanasekara, N.; Youngblood, J. Current Characterization Methods for Cellulose Nanomaterials. *Chem. Soc. Rev.* **2018**, *47* (8), 2609–2679. https://doi.org/10.1039/C6CS00895J.

(38)   Bushell, M.; Meija, J.; Chen, M.; Batchelor, W.; Browne, C.; Cho, J.-Y.; Clifford, C. A.; Al-Rekabi, Z.; Vanderfleet, O. M.; Cranston, E. D.; Lawn, M.; Coleman, V. A.; Nyström, G.; Arcari, M.; Mezzenga, R.; Park, B. C.; Shin, C.; Ren, L.; Bu, T.; Saito, T.; Kaku, Y.; Wagner, R.; Johnston, L. J. Particle Size Distributions for Cellulose Nanocrystals Measured by Atomic Force Microscopy: An Interlaboratory Comparison. *Cellulose* **2021**. https://doi.org/10.1007/s10570-020-03618-4.

(39)   Thygesen, A.; Oddershede, J.; Lilholt, H.; Thomsen, A. B.; Ståhl, K. On the Determination of Crystallinity and Cellulose Content in Plant Fibres. *Cellulose* **2005**, *12* (6), 563. https://doi.org/10.1007/s10570-005-9001-8.

(40)   De Figueiredo, L. P.; Ferreira, F. F. The Rietveld Method as a Tool to Quantify the Amorphous Amount of Microcrystalline Cellulose. *Journal of Pharmaceutical Sciences* **2014**, *103* (5), 1394–1399. https://doi.org/10.1002/jps.23909.

(41)   Ju, X.; Bowden, M.; Brown, E. E.; Zhang, X. An Improved X-Ray Diffraction Method for Cellulose Crystallinity Measurement. *Carbohydrate Polymers* **2015**, *123*, 476–481. https://doi.org/10.1016/j.carbpol.2014.12.071.

(42)   Ahvenainen, P.; Kontro, I.; Svedström, K. Comparison of Sample Crystallinity Determination Methods by X-Ray Diffraction for Challenging Cellulose I Materials. *Cellulose* **2016**, *23* (2), 1073–1086. https://doi.org/10.1007/s10570-016-0881-6.

(43)   Stålbrand, H.; Mansfield, S. D.; Saddler, J. N.; Kilburn, D. G.; Warren, R. A. J.; Gilkes, N. R. Analysis of Molecular Size Distributions of Cellulose Molecules during Hydrolysis of Cellulose by Recombinant Cellulomonas Fimi β-1,4-Glucanases. *Applied and Environmental Microbiology* **1998**, *64* (7), 2374. https://doi.org/10.1128/AEM.64.7.2374-2379.1998.

(44)   Lin, K.-H.; Hu, D.; Sugimoto, T.; Chang, F.-C.; Kobayashi, M.; Enomae, T. An Analysis on the Electrophoretic Mobility of Cellulose Nanocrystals as Thin Cylinders: Relaxation and End Effect. *RSC Adv.* **2019**, *9* (58), 34032–34038. https://doi.org/10.1039/C9RA05156B.

(45)   Abitbol, T.; Kloser, E.; Gray, D. G. Estimation of the Surface Sulfur Content of Cellulose Nanocrystals Prepared by Sulfuric Acid Hydrolysis. *Cellulose* **2013**, *20* (2), 785–794. https://doi.org/10.1007/s10570-013-9871-0.

(46)   Beck, S.; Méthot, M.; Bouchard, J. General Procedure for Determining Cellulose Nanocrystal Sulfate Half-Ester Content by Conductometric Titration. *Cellulose* **2015**, *22* (1), 101–116. https://doi.org/10.1007/s10570-014-0513-y.

(47)   Lin, N.; Dufresne, A. Surface Chemistry, Morphological Analysis and Properties of Cellulose Nanocrystals with Gradiented Sulfation Degrees. *Nanoscale* **2014**, *6* (10), 5384–5393. https://doi.org/10.1039/C3NR06761K.

(48)   Kittle, J. D.; Du, X.; Jiang, F.; Qian, C.; Heinze, T.; Roman, M.; Esker, A. R. Equilibrium Water Contents of Cellulose Films Determined via Solvent Exchange and Quartz Crystal Microbalance with Dissipation Monitoring. *Biomacromolecules* **2011**, *12* (8), 2881–2887. https://doi.org/10.1021/bm200352q.

(49)   Niinivaara, E.; Faustini, M.; Tammelin, T.; Kontturi, E. Water Vapor Uptake of Ultrathin Films of Biologically Derived Nanocrystals: Quantitative Assessment with Quartz Crystal Microbalance and Spectroscopic Ellipsometry. *Langmuir* **2015**, *31* (44), 12170–12176. https://doi.org/10.1021/acs.langmuir.5b01763.

(50)   Craig, V. S. J.; Plunkett, M. Determination of Coupled Solvent Mass in Quartz Crystal Microbalance Measurements Using Deuterated Solvents. *Journal of Colloid and Interface Science* **2003**, *262* (1), 126–129. https://doi.org/10.1016/S0021-9797(03)00210-8.

(51)   Revol, J.-F.; Bradford, H.; Giasson, J.; Marchessault, R. H.; Gray, D. G. Helicoidal Self-Ordering of Cellulose Microfibrils in Aqueous Suspension. *International Journal of Biological Macromolecules* **1992**, *14* (3), 170–172. https://doi.org/10.1016/S0141-8130(05)80008-X.

(52)   Banerjee, M.; Saraswatula, S.; Williams, A.; Brettmann, B. Effect of Purification Methods on Commercially Available Cellulose Nanocrystal Properties and TEMPO Oxidation. *Processes* **2020**, *8* (6), 698. https://doi.org/10.3390/pr8060698.

(53)   Sacui, I. A.; Nieuwendaal, R. C.; Burnett, D. J.; Stranick, S. J.; Jorfi, M.; Weder, C.; Foster, E. J.; Olsson, R. T.; Gilman, J. W. Comparison of the Properties of Cellulose Nanocrystals and Cellulose Nanofibrils Isolated from Bacteria, Tunicate, and Wood Processed Using Acid, Enzymatic, Mechanical, and Oxidative Methods. *ACS Appl. Mater. Interfaces* **2014**, *6* (9), 6127–6138. https://doi.org/10.1021/am500359f.

(54)   Onsager, L. The Effects of Shape on the Interaction of Colloidal Particles. *Annals of the New York Academy of Sciences* **1949**, *51*, 627–659. https://doi.org/10.1111/j.1749-6632.1949.tb27296.x.

(55)   Chen, M.; Parot, J.; Hackley, V. A.; Zou, S.; Johnston, L. J. AFM Characterization of Cellulose Nanocrystal Height and Width Using Internal Calibration Standards. *Cellulose* **2021**. https://doi.org/10.1007/s10570-021-03678-0.

(56)   Delepierre, G.; Eyley, S.; Thielemans, W.; Weder, C.; Cranston, E. D.; Zoppe, J. O. Patience Is a Virtue: Self-Assembly and Physico-Chemical Properties of Cellulose Nanocrystal Allomorphs. *Nanoscale* **2020**, 17480–17493. https://doi.org/10.1039/D0NR04491A.

(57)   Tolonen, L. K.; Juvonen, M.; Niemelä, K.; Mikkelson, A.; Tenkanen, M.; Sixta, H. Supercritical Water Treatment for Cello-Oligosaccharide Production from Microcrystalline Cellulose. *Carbohydrate Research* **2015**, *401*, 16–23. https://doi.org/10.1016/j.carres.2014.10.012.

(58)   Labet, M.; Thielemans, W. Improving the Reproducibility of Chemical Reactions on the Surface of Cellulose Nanocrystals: ROP of ε-Caprolactone as a Case Study. *Cellulose* **2011**, *18* (3), 607–617. https://doi.org/10.1007/s10570-011-9527-x.

(59)   Clayden, J.; Greeves, N.; Warren, S. *Organic Chemistry - Jonathan Clayden, Nick Greeves, Stuart Warren - Google Books*, 2nd ed.; Oxford University Press.

(60)   Beck-Candanedo, S.; Roman, M.; Gray, D. G. Effect of Reaction Conditions on the Properties and Behavior of Wood Cellulose Nanocrystal Suspensions. *Biomacromolecules* **2005**, *6* (2), 1048–1054. https://doi.org/10.1021/bm049300p.

(61)   Elazzouzi-Hafraoui, S.; Nishiyama, Y.; Putaux, J.-L.; Heux, L.; Dubreuil, F.; Rochas, C. The Shape and Size Distribution of Crystalline Nanoparticles Prepared by Acid Hydrolysis of Native Cellulose. *Biomacromolecules* **2008**, *9* (1), 57–65. https://doi.org/10.1021/bm700769p.

(62)   Dong, X.; Revol, J.-F.; Gray, D. Effect of Microcrystallite Preparation Conditions on the Formation of Colloid Crystals of Cellulose. *Cellulose* **1998**, *5* (1), 19–32. https://doi.org/10.1023/A:1009260511939.

(63)   Kontturi, E.; Vuorinen, T. Indirect Evidence of Supramolecular Changes within Cellulose Microfibrils of Chemical Pulp Fibers upon Drying. *Cellulose* **2009**, *16* (1), 65–74. https://doi.org/10.1007/s10570-008-9235-3.

(64)   Comprehensive Cellulose Chemistry. Volume 1. Fundamentals and Analytical Methods By D. Klemm, B. Philipp, T. Heinze, U. Heinze, and W. Wagenknecht. Wiley: Weinheim, Germany. 1998. 260 Pp. $236.25. ISBN 3-527-29413-9. *J. Am. Chem. Soc.* **1999**, *121* (37), 8677–8677. https://doi.org/10.1021/ja9857514.

(65)   Abitbol, T.; Kam, D.; Levi-Kalisman, Y.; Gray, D. G.; Shoseyov, O. Surface Charge Influence on the Phase Separation and Viscosity of Cellulose Nanocrystals. *Langmuir* **2018**, *34* (13), 3925–3933. https://doi.org/10.1021/acs.langmuir.7b04127.

(66)   Bhattacharjee, S. DLS and Zeta Potential – What They Are and What They Are Not? *Journal of Controlled Release* **2016**, *235*, 337–351. https://doi.org/10.1016/j.jconrel.2016.06.017.

(67)   Fall, A. B.; Lindstr, S. B. Colloidal Stability of Aqueous Nanofibrillated Cellulose Dispersions. **2011**, 7.

(68)   Bhattacharyya, L.; Rohrer, J. S. *Applications of Ion Chromatography for Pharmaceutical and Biological Products | Wiley*; John Wiley & Sons, Inc.: Hoboken, NJ, USA, 2012.

(69)   Beck, S.; Bouchard, J. Auto-Catalyzed Acidic Desulfation of Cellulose Nanocrystals. *Nordic Pulp & Paper Research Journal* **2014**, *29* (1), 6–14. https://doi.org/10.3183/npprj-2014-29-01-p006-014.

(70)   Cherhal, F.; Cousin, F.; Capron, I. Influence of Charge Density and Ionic Strength on the Aggregation Process of Cellulose Nanocrystals in Aqueous Suspension, as Revealed by Small-Angle Neutron Scattering. *Langmuir* **2015**, *31* (20), 5596–5602. https://doi.org/10.1021/acs.langmuir.5b00851.

(71)   Trost, B. M. The Atom Economy--a Search for Synthetic Efficiency. *Science* **1991**, *254* (5037), 1471–1477. https://doi.org/10.1126/science.1962206.

(72)   Schütz, C.; Van Rie, J.; Eyley, S.; Gençer, A.; van Gorp, H.; Rosenfeldt, S.; Kang, K.; Thielemans, W. Effect of Source on the Properties and Behavior of Cellulose Nanocrystal Suspensions. *ACS Sustainable Chem. Eng.* **2018**, *6* (7), 8317–8324. https://doi.org/10.1021/acssuschemeng.8b00334.

(73)   Kalashnikova, I.; Bizot, H.; Cathala, B.; Capron, I. Modulation of Cellulose Nanocrystals Amphiphilic Properties to Stabilize Oil/Water Interface. *Biomacromolecules* **2012**, *13* (1), 267–275. https://doi.org/10.1021/bm201599j.

(74)   Andrews, M. P.; Morse, T.; Rak, M.; Wu, J.; Hu, Z. Microparticles Comprising Cellulose Nanocrystals Aggregated with Proteins and Cosmetic Uses Thereof. WO2020227814, November 19, 2020.

(75)   Eyley, S.; Thielemans, W. Surface Modification of Cellulose Nanocrystals. *Nanoscale* **2014**, *6* (14), 7764–7779. https://doi.org/10.1039/C4NR01756K.

(76)   D'Acierno, F.; Hamad, W. Y.; Michal, C. A.; MacLachlan, M. J. Thermal Degradation of Cellulose Filaments and Nanocrystals. *Biomacromolecules* **2020**, *21* (8), 3374–3386. https://doi.org/10.1021/acs.biomac.0c00805.

(77)   Nagalakshmaiah, M.; Rajinipriya, M.; Afrin, S.; Ansari, M. A.; Asad, M.; Karim, Z. Cellulose Nanocrystals-Based Nanocomposites. In *Bio-based Polymers and*

Nanocomposites : Preparation, Processing, Properties & Performance; Sanyang, M. L., Jawaid, M., Eds.; Springer International Publishing: Cham, 2019; pp 49–65. https://doi.org/10.1007/978-3-030-05825-8_3.

(78)   Ramasamy, J.; Amanullah, M. Nanocellulose for Oil and Gas Field Drilling and Cementing Applications. *Journal of Petroleum Science and Engineering* **2020**, *184*, 106292. https://doi.org/10.1016/j.petrol.2019.106292.

(79)   Hall, L. J.; Deville, J. P.; Araujo, C. S.; Li, S.; Rojas, O. J. Nanocellulose and Its Derivatives for High-Performance Water-Based Fluids. In *SPE International Conference on Oilfield Chemistry*; Society of Petroleum Engineers: Montgomery, Texas, USA, 2017. https://doi.org/10.2118/184576-MS.

(80)   Fluorocarbon Company Ltd. What is HPHT? High Pressure, High Temperature https://fluorocarbon.co.uk/news-and-events/post/32/what-is-hpht-high-pressure-high-temperature (accessed Feb 8, 2021).

(81)   Bradbury, A. G. W.; Sakai, Y.; Shafizadeh, F. A Kinetic Model for Pyrolysis of Cellulose. *Journal of Applied Polymer Science* **1979**, *23* (11), 3271–3280. https://doi.org/10.1002/app.1979.070231112.

(82)   Matsuoka, S.; Kawamoto, H.; Saka, S. What Is Active Cellulose in Pyrolysis? An Approach Based on Reactivity of Cellulose Reducing End. *Journal of Analytical and Applied Pyrolysis* **2014**, *106*, 138–146. https://doi.org/10.1016/j.jaap.2014.01.011.

(83)   Shafiei-Sabet, S.; Hamad, W. Y.; Hatzikiriakos, S. G. Rheology of Nanocrystalline Cellulose Aqueous Suspensions. *Langmuir* **2012**. https://doi.org/10.1021/la303380v.

(84)   Derakhshandeh, B.; Petekidis, G.; Shafiei Sabet, S.; Hamad, W. Y.; Hatzikiriakos, S. G. Ageing, Yielding, and Rheology of Nanocrystalline Cellulose Suspensions. *Journal of Rheology* **2013**. https://doi.org/10.1122/1.4764080.

(85)   Xu, Y.; Atrens, A. D.; Stokes, J. R. "liquid, Gel and Soft Glass" Phase Transitions and Rheology of Nanocrystalline Cellulose Suspensions as a Function of Concentration and Salinity. *Soft Matter* **2018**. https://doi.org/10.1039/c7sm02470c.

(86)   Xu, Y.; Atrens, A. D.; Stokes, J. R. Rheology and Microstructure of Aqueous Suspensions of Nanocrystalline Cellulose Rods. *Journal of Colloid and Interface Science* **2017**. https://doi.org/10.1016/j.jcis.2017.02.020.

(87)   Lu, A.; Hemraz, U.; Khalili, Z.; Boluk, Y. Unique Viscoelastic Behaviors of Colloidal Nanocrystalline Cellulose Aqueous Suspensions. *Cellulose* **2014**. https://doi.org/10.1007/s10570-014-0173-y.

(88)   Gicquel, E.; Bras, J.; Rey, C.; Putaux, J.-L.; Pignon, F.; Jean, B.; Martin, C. Impact of Sonication on the Rheological and Colloidal Properties of Highly Concentrated Cellulose Nanocrystal Suspensions. *Cellulose* **2019**. https://doi.org/10.1007/s10570-019-02622-7.

(89)   Bercea, M.; Navard, P. Shear Dynamics of Aqueous Suspensions of Cellulose Whiskers. *Macromolecules* **2000**. https://doi.org/10.1021/ma000417p.

(90)   Ureña-Benavides, E. E.; Ao, G.; Davis, V. A.; Kitchens, C. L. Rheology and Phase Behavior of Lyotropic Cellulose Nanocrystal Suspensions. *Macromolecules* **2011**. https://doi.org/10.1021/ma201649f.

(91)   Beck, S.; Bouchard, J.; Berry, R. Controlling the Reflection Wavelength of Iridescent Solid Films of Nanocrystalline Cellulose. *Biomacromolecules* **2011**. https://doi.org/10.1021/bm1010905.

(92)   Shafeiei-Sabet, S.; Hamad, W. Y.; Hatzikiriakos, S. G. Influence of Degree of Sulfation on the Rheology of Cellulose Nanocrystal Suspensions. *Rheologica Acta* **2013**, *52* (8–9), 741–751.

(93)   Lenfant, G.; Heuzey, M.-C.; van de Ven, T. G. M.; Carreau, P. J. A Comparative Study of ECNC and CNC Suspensions: Effect of Salt on Rheological Properties. *Rheologica Acta* **2017**, *56* (1), 51–62.

(94)   Xu, Y.; Atrens, A.; Stokes, J. R. A Review of Nanocrystalline Cellulose Suspensions: Rheology, Liquid Crystal Ordering and Colloidal Phase Behaviour. *Advances in colloid and interface science* **2020**, *275*, 102076.

(95)   Liu, D.; Chen, X.; Yue, Y.; Chen, M.; Wu, Q. Structure and Rheology of Nanocrystalline Cellulose. *Carbohydrate Polymers* **2011**. https://doi.org/10.1016/j.carbpol.2010.11.039.

(96)   Araki, J.; Wada, M.; Kuga, S.; Okano, T. Flow Properties of Microcrystalline Cellulose Suspension Prepared by Acid Treatment of Native Cellulose. *Colloids and Surfaces A: Physicochemical and Engineering Aspects* **1998**. https://doi.org/10.1016/S0927-7757(98)00404-X.

(97)   Ali, D.; Sen, S. Permeability and Fluid Flow-Induced Wall Shear Stress of Bone Tissue Scaffolds: Computational Fluid Dynamic Analysis Using Newtonian and Non-Newtonian Blood Flow Models. *Computers in Biology and Medicine* **2018**, *99*, 201–208. https://doi.org/10.1016/j.compbiomed.2018.06.017.

(98)   Jammalamadaka, U.; Tappa, K. Recent Advances in Biomaterials for 3D Printing and Tissue Engineering. *Journal of Functional Biomaterials* **2018**, *9* (1), 22. https://doi.org/10.3390/jfb9010022.

(99)   Guntzburger, Y.; Fontaine, A.; Fradette, L.; Bertrand, F. An Experimental Method to Evaluate Global Pumping in a Mixing System: Application to the Maxblend^{TM} for Newtonian and Non-Newtonian Fluids. *Chemical Engineering Journal* **2013**, *214*, 394–406. https://doi.org/10.1016/j.cej.2012.10.041.

(100)   Shafiei-Sabet, S.; Hamad, W. Y.; Hatzikiriakos, S. G. Rheology of Nanocrystalline Cellulose Aqueous Suspensions. *Langmuir* **2012**, *28* (49), 17124–17133. https://doi.org/10.1021/la303380v.

(101)   Xu, Y.; Atrens, A. D.; Stokes, J. R. Rheology and Microstructure of Aqueous Suspensions of Nanocrystalline Cellulose Rods. *Journal of Colloid and Interface Science* **2017**, *496*, 130–140. https://doi.org/10.1016/j.jcis.2017.02.020.

(102)   Gicquel, E.; Bras, J.; Rey, C.; Putaux, J.-L.; Pignon, F.; Jean, B.; Martin, C. Impact of Sonication on the Rheological and Colloidal Properties of Highly Concentrated Cellulose Nanocrystal Suspensions. *Cellulose* **2019**, *26* (13), 7619–7634. https://doi.org/10.1007/s10570-019-02622-7.

(103)   Zakani, B.; Grecov, D. Yield Stress Analysis of Cellulose Nanocrystalline Gels. *Cellulose* **2020**, *27* (16), 9337–9353. https://doi.org/10.1007/s10570-020-03429-7.

(104)   Nazari, B.; Kumar, V.; Bousfield, D. W.; Toivakka, M. Rheology of Cellulose Nanofibers Suspensions: Boundary Driven Flow. *Journal of Rheology* **2016**, *60* (6), 1151–1159. https://doi.org/10.1122/1.4960336.

(105)   Moberg, T.; Sahlin, K.; Yao, K.; Geng, S.; Westman, G.; Zhou, Q.; Oksman, K.; Rigdahl, M. Rheological Properties of Nanocellulose Suspensions: Effects of Fibril/Particle Dimensions and Surface Characteristics. *Cellulose* **2017**, *24* (6), 2499–2510. https://doi.org/10.1007/s10570-017-1283-0.

(106)   Nechyporchuk, O.; Belgacem, M. N.; Pignon, F. Current Progress in Rheology of Cellulose Nanofibril Suspensions. *Biomacromolecules* **2016**, *17* (7), 2311–2320. https://doi.org/10.1021/acs.biomac.6b00668.

(107)   Honorato-Rios, C.; Lehr, C.; Schütz, C.; Sanctuary, R.; Osipov, M. A.; Baller, J.; Lagerwall, J. P. F. Fractionation of Cellulose Nanocrystals: Enhancing Liquid Crystal Ordering without Promoting Gelation. *NPG Asia Mater* **2018**, *10* (5), 455–465. https://doi.org/10.1038/s41427-018-0046-1.

(108)   Schütz, C.; Bruckner, J. R.; Honorato-Rios, C.; Tosheva, Z.; Anyfantakis, M.; Lagerwall, J. P. F. From Equilibrium Liquid Crystal Formation and Kinetic Arrest to Photonic Bandgap Films Using Suspensions of Cellulose Nanocrystals. *Crystals* **2020**, *10* (3), 199. https://doi.org/10.3390/cryst10030199.

(109)   Shafiei-Sabet, S.; Hamad, W. Y.; Hatzikiriakos, S. G. Ionic Strength Effects on the Microstructure and Shear Rheology of Cellulose Nanocrystal Suspensions. *Cellulose* **2014**. https://doi.org/10.1007/s10570-014-0407-z.

(110)   Xu, Y.; Atrens, A. D.; Stokes, J. R. Rheology and Microstructure of Aqueous Suspensions of Nanocrystalline Cellulose Rods. *Journal of Colloid and Interface Science* **2017**. https://doi.org/10.1016/j.jcis.2017.02.020.

(111)   Lopez, C. G.; Richtering, W. Influence of Divalent Counterions on the Solution Rheology and Supramolecular Aggregation of Carboxymethyl Cellulose. *Cellulose* **2019**, *26*, 1517–1534. https://doi.org/10.1007/s10570-018-2158-8.

(112)   Chau, M.; Sriskandha, S. E.; Pichugin, D.; Thérien-Aubin, H.; Nykypanchuk, D.; Chauve, G.; Méthot, M.; Bouchard, J.; Gang, O.; Kumacheva, E. Ion-Mediated Gelation

of Aqueous Suspensions of Cellulose Nanocrystals. *Biomacromolecules* **2015**, *16* (8), 2455–2462. https://doi.org/10.1021/acs.biomac.5b00701.

(113)   Garg, M.; Linares, M.; Zozoulenko, I. Theoretical Rationalization of Self-Assembly of Cellulose Nanocrystals: Effect of Surface Modifications and Counterions. *Biomacromolecules* **2020**, *21* (8), 3069–3080. https://doi.org/10.1021/acs.biomac.0c00469.

(114)   Nishiyama, Y. Molecular Interactions in Nanocellulose Assembly. *Philosophical Transactions of the Royal Society A: Mathematical, Physical and Engineering Sciences* **2018**, *376* (2112), 20170047. https://doi.org/10.1098/rsta.2017.0047.

(115)   Reid, M. S.; Villalobos, M.; Cranston, E. D. Cellulose Nanocrystal Interactions Probed by Thin Film Swelling to Predict Dispersibility. *Nanoscale* **2016**, *8* (24), 12247–12257. https://doi.org/10.1039/C6NR01737A.

(116)   Aulin, C.; Ahola, S.; Josefsson, P.; Nishino, T.; Hirose, Y.; Österberg, M.; Wågberg, L. Nanoscale Cellulose Films with Different Crystallinities and Mesostructures—Their Surface Properties and Interaction with Water. *Langmuir* **2009**, *25* (13), 7675–7685. https://doi.org/10.1021/la900323n.

(117)   Liu, Z.; Zhang, C.; Liu, R.; Zhang, W.; Kang, H.; Li, P.; Huang, Y. Dissolution of Cellobiose in the Aqueous Solutions of Chloride Salts: Hofmeister Series Consideration. *Cellulose* **2016**, *23* (1), 295–305. https://doi.org/10.1007/s10570-015-0827-4.

(118)   Collins, K. D.; Washabaugh, M. W. The Hofmeister Effect and the Behaviour of Water at Interfaces. *Quarterly Reviews of Biophysics* **1985**, *18* (4), 323–422. https://doi.org/10.1017/S0033583500005369.

(119)   Traube, J. The Attraction Pressure. *J. Phys. Chem.* **1910**, *14* (5), 452–470. https://doi.org/10.1021/j150113a003.

(120)   Facchine, E. G.; Jin, S.-A.; Spontak, R. J.; Khan, S. A.; Rojas, O. J. Quantitative Calorimetric Studies of the Chiral Nematic Mesophase in Aqueous Cellulose Nanocrystal Suspensions. *Langmuir* **2020**. https://doi.org/10.1021/acs.langmuir.0c01871.

(121)   Oncsik, T.; Trefalt, G.; Csendes, Z.; Szilagyi, I.; Borkovec, M. Aggregation of Negatively Charged Colloidal Particles in the Presence of Multivalent Cations. *Langmuir* **2014**, *30* (3), 733–741. https://doi.org/10.1021/la4046644.

(122)   Castro-Guerrero, C. F.; Gray, D. G. Chiral Nematic Phase Formation by Aqueous Suspensions of Cellulose Nanocrystals Prepared by Oxidation with Ammonium Persulfate. *Cellulose* **2014**, *21* (4), 2567–2577. https://doi.org/10.1007/s10570-014-0308-1.

(123)   Peng, B. L.; Dhar, N.; Liu, H. L.; Tam, K. C. Chemistry and Applications of Nanocrystalline Cellulose and Its Derivatives: A Nanotechnology Perspective. *The Canadian Journal of Chemical Engineering* **2011**, *89* (5), 1191–1206. https://doi.org/10.1002/cjce.20554.

(124)   Kedzior, S. A.; Zoppe, J. O.; Berry, R. M.; Cranston, E. D. Recent Advances and an Industrial Perspective of Cellulose Nanocrystal Functionalization through Polymer Grafting. *Current Opinion in Solid State and Materials Science* **2019**, *23* (2), 74–91. https://doi.org/10.1016/j.cossms.2018.11.005.

(125)   Lagerwall, J. P. F.; Scalia, G. A New Era for Liquid Crystal Research: Applications of Liquid Crystals in Soft Matter Nano-, Bio- and Microtechnology. *Current Applied Physics* **2012**, *12* (6), 1387–1412. https://doi.org/10.1016/j.cap.2012.03.019.

Appendix 3

Table A3.1. pH and conductivity values of 0.2 wt% suspensions in their as-received and dialyzed (-D) form.

	pH	Conductivity (μS cm^{-1})
MilliQ Water	5.38	0.79
CNC-LM	3.43	38.8
NORAM-AlPac	6.30	5.06
NORAM-AlPac-D	5.01	6.28
Melodea	5.28	32.6
Melodea-D	5.14	8.74
Anomera	7.03	9.14
Anomera-D	6.10	4.38
BGB	6.48	7.55
BGB-D	6.55	7.12
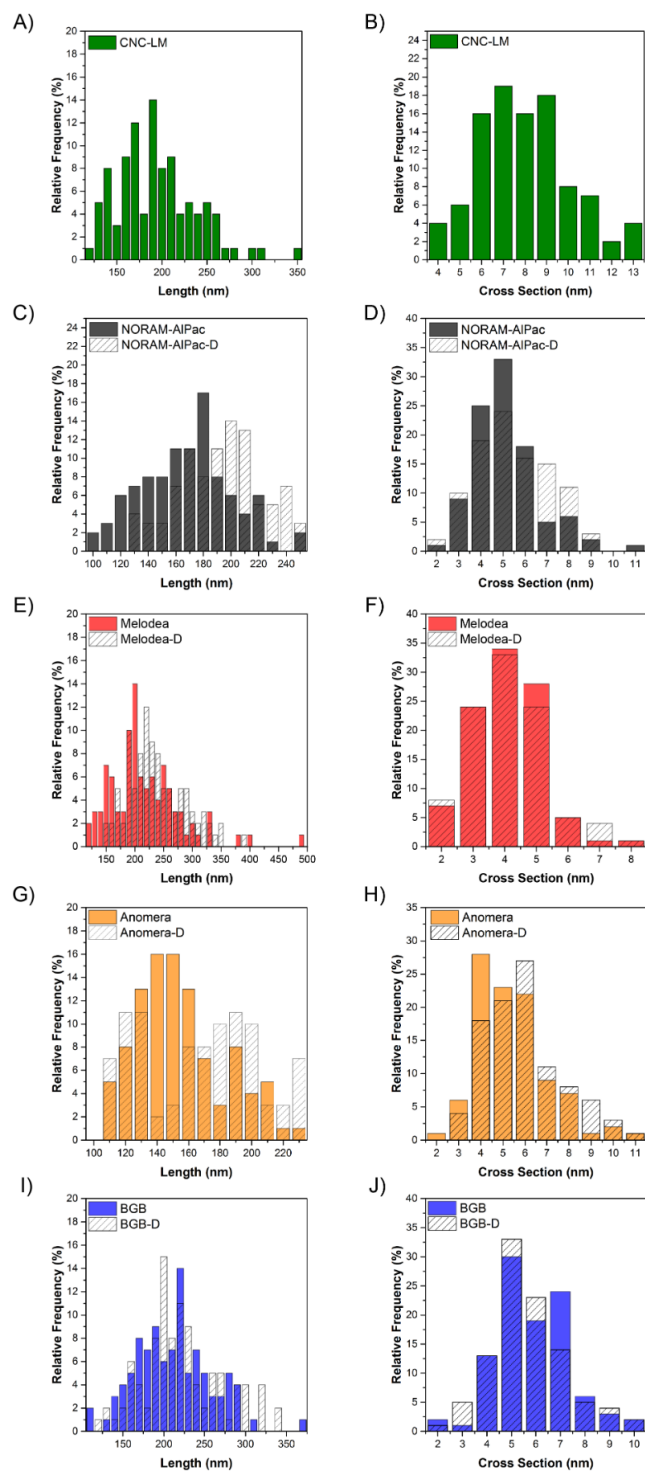
Figure A3.1. Particle length A), C), E), G) and I) distributions of CNCs from the different types of CNCs in their as-received and dialyzed form as measured by AFM. Particle cross section B), D), F), H) and J) from as-received and dialyzed CNC samples.
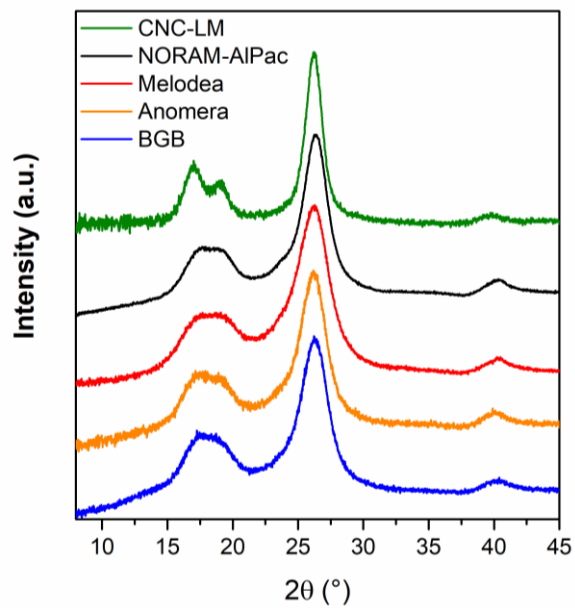
Figure A3.2. Plot supporting the native cellulose I crystal structure of the five CNC types.
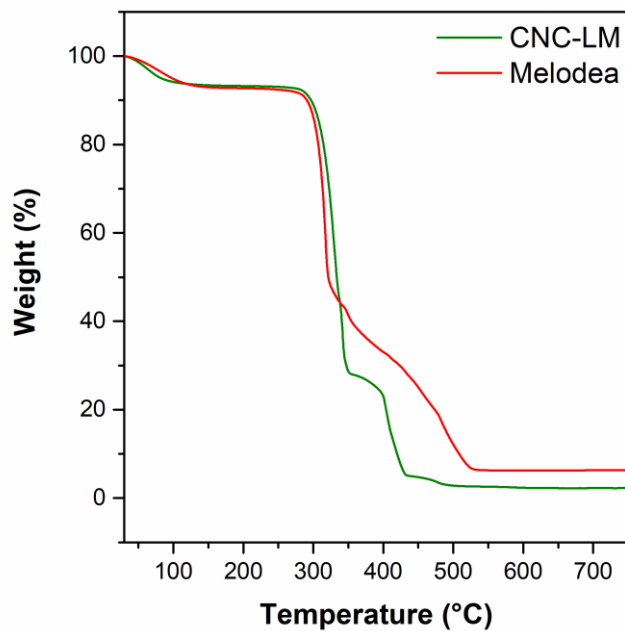
Figure A3.3. TGA curves for CNC-LM and Melodea CNCs (both in sodium-form) at high temperature.

Table A3.2. Water binding capacity of the five CNC types.

	CNC-LM	NORAM-AlPac		Melodea		Anomera		BGB	
Form		A.R.	D	A.R.	D	A.R.	D	A.R.	D
Δf_{film} (Hz)	-78.9	-94.1	-104.1	-177.9	-110.6	-92.6	-87.3	-77.6	-74.8
Δf_{water} (Hz)	-239.8	-382.0	-475.3	-1166.6	-536.2	-368.1	-318.2	-227.4	-201.2
Γ_{water} (ng/cm^2)	42.4	67.6	84.1	206.5	94.9	65.2	56.3	40.3	35.6
Normalized mass of water (ng cm^{-2} nm^{-1})	2.7 ± 0.3	5.1 ± 0.3	5.6 ± 0.3	8.5 ± 0.5	4.8 ± 0.2	4.2 ± 0.4	4.3 ± 0.3	2.8 ± 0.2	2.5 ± 0.1
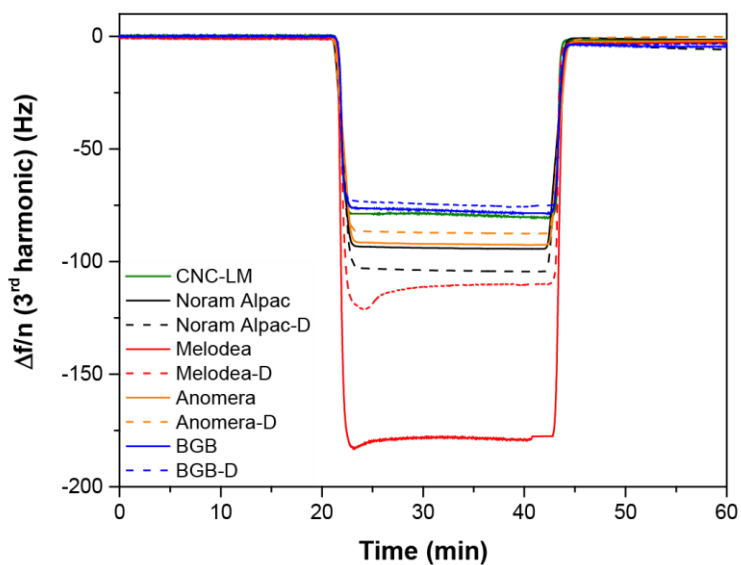
Figure A3.4. Changes in quartz crystal sensor resonance frequency as a function of time during a water/deuterium oxide solvent exchange measurement carried out using quartz crystal microgravimetry with dissipation monitoring. A decrease in frequency indicates an increase in bound water mass.

Figure A3.5. Photograph of aqueous CNC-LM suspensions (with 1 mM NaCl) containing 1 – 10 wt% (labelled at top in white) taken between crossed linear polarizers. The photograph was taken after one week of equilibration. A birefringent phase can be observed in the capillaries containing 9 and 10 wt%.
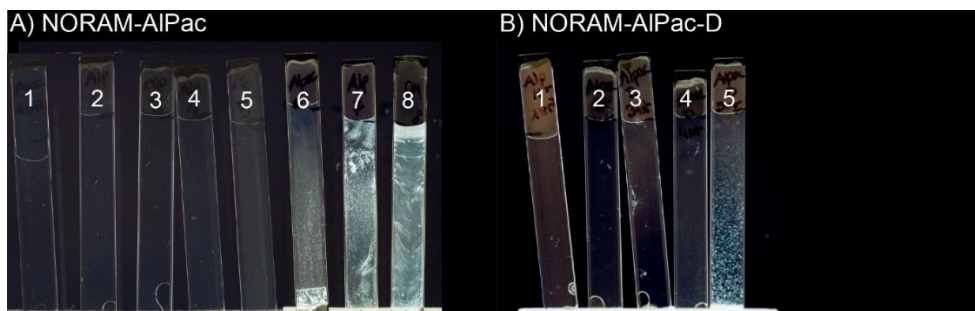
Figure A3.6. Photograph of aqueous NORAM-AlPac CNC suspensions in their as-received A) and dialyzed B) form (with 1 mM NaCl) containing 1 – 8 wt% and 1 – 5 wt%, respectively. The photographs were taken between crossed linear polarizers after one week of equilibrating at room temperature. A birefringent phase can be observed in the capillaries containing A) 6 – 8 wt% and B) 5 wt%.
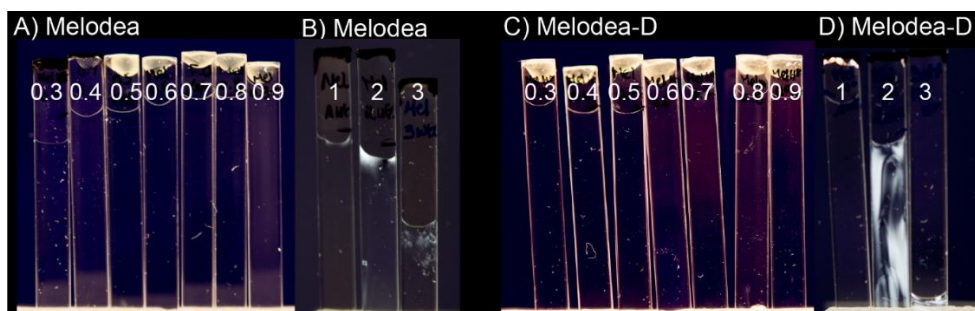
Figure A3.7. Photograph of aqueous Melodea CNC suspensions in their as-received form A) at low concentration, and B) at high concentration, and dialyzed form C) at low concentration, and D) at high concentration (all containing 1 mM NaCl).The photographs were taken between crossed linear polarizers after one week of equilibrating at room temperature. Birefringence can only be observed in D) at 2 and 3 wt%. Note that the non-

linear white-ish reflection in the capillaries filled with low concentration is not a phase separation but is due to the reflection of the white paper holder underneath the capillaries.
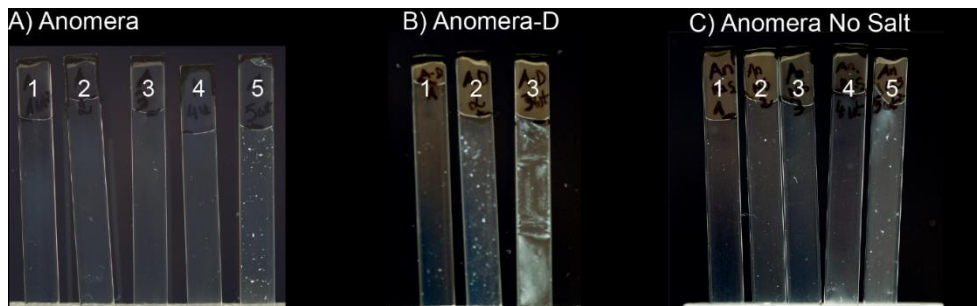
Figure A3.8. Photograph of aqueous Anomera CNC suspensions in their as-received A) and dialyzed B) form (with 1 mM NaCl) containing 1 – 5 wt% and 1 – 3 wt%, respectively. The capillaries in C) were filled with as-received suspension of 1 – 5 wt% and no salt was added to the suspension. The photographs were taken between crossed linear polarizers after one week of equilibrating at room temperature. Birefringence can only be observed in C) at 3 wt%.
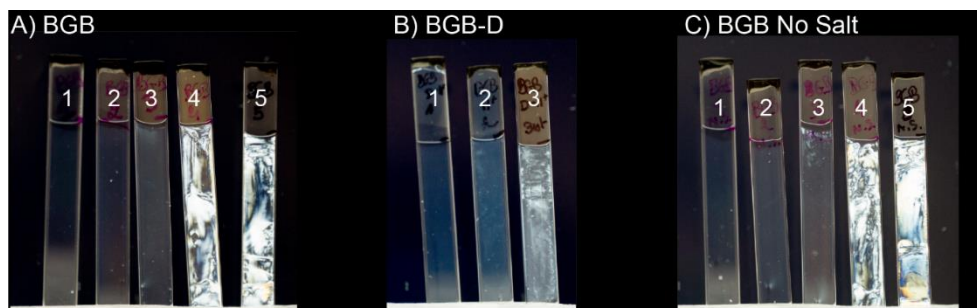
Figure A3.9. Photograph of aqueous BGB CNC suspensions in their as-received A) and dialyzed B) form (with 1 mM NaCl) containing 1 – 5 wt% and 1 – 3 wt%, respectively. The capillaries in C) were filled with as-received suspensions from 1 – 5 wt%, and no salt was added to the suspension. The photographs were taken between crossed linear polarizers after one week of equilibrating at room temperature. Birefringence can be observed in A) and C) at 4 – 5 wt% and in B) at 3 wt%. Note that the non-linear white-ish reflection in the capillaries filled with low concentration is not a phase separation but is due to the reflection of the white paper holder underneath the capillaries.

Chapter 4

Optimization of cellulose nanocrystal length and surface charge density through phosphoric acid hydrolysis

_____

Currently, only sulfated and carboxylated CNCs are produced on an industrial scale. Nevertheless, numerous other CNC production methods exist; for example, a phosphoric acid hydrolysis can be used to produce thermally stable phosphated CNCs. Herein, a design of experiments approach is used to determine optimal phosphoric acid hydrolysis conditions and to gain a better understanding of the range of CNC properties which can be achieved using this method.

In this work, I led the project conceptualization and experimental planning. I prepared the CNC samples with a fellow graduate student (Daniel Osorio, MASc). I carried out CNC imaging and particle size analysis using atomic force microscopy, colorimetric determination of CNC phosphate content, and thermogravimetric analysis. I also completed the statistical analysis of the results and wrote the manuscript with assistance from my supervisor, Dr. Emily Cranston. Daniel Osorio, MASc, carried out the zeta potential and dynamic light scattering experiments. A technician carried out the X-Ray diffraction experiments. This chapter is reproduced with permission from the Royal Society © 2017.

4.1 Abstract

Cellulose nanocrystals (CNCs) are emerging nanomaterials with a large range of potential applications. CNCs are typically produced through acid hydrolysis with sulfuric acid; however, phosphoric acid has the advantage of generating CNCs with higher thermal stability. This paper presents a design of experiments approach to optimize the hydrolysis of CNCs from cotton with phosphoric acid. Hydrolysis time, temperature and acid concentration were varied across nine experiments and a linear least squares regression analysis was applied to understand the effects of these parameters on CNC properties. In all but one case, rod-shaped nanoparticles with a high degree of crystallinity and thermal stability were produced. A statistical model was generated to predict CNC length, and trends in phosphate content and zeta potential were elucidated. The CNC length could be tuned over a relatively large range (238-475 nm) and the polydispersity could be narrowed most effectively by increasing the hydrolysis temperature and acid concentration. The CNC phosphate content was most affected by hydrolysis temperature and time, however the charge density and colloidal stability was considered low compared to sulfuric acid hydrolysed CNCs. This study provides insight into weak acid hydrolysis and proposes "design rules" for CNCs with improved size uniformity and charge density.

4.2 Introduction

The extraction of cellulose nanocrystals (CNCs) via hydrolysis of wood and cotton with sulfuric acid was first reported by Nickerson and Habrle in 1947, followed by Rånby in 1949.[1,2] The hydrolysed particles were found to be highly crystalline and colloidally stable in water.[2] This work inspired Mukherjee and Woods, who were the first to image CNCs with transmission electron microscopy.[3] Rod-like particles with lengths of approximately 200 nm and widths of 10-20 nm were observed.[3] The CNC particles tended to form large sheet-like aggregates; however, by increasing the hydrolysis time and temperature, more individualized nanocrystals were obtained.[3] CNCs have since gained popularity both as an academic curiosity and model system to study rod-shaped particles and cellulose interactions, and as an emerging commercial nanomaterial with many potential applications. Importantly, the hydrolysis procedure to produce CNCs from natural cellulose sources is not complex and industry has succeeded in producing ton per day quantities of reproducible and high quality nanoparticles.[4] Furthermore, the process is relatively green since the starting materials are renewable, the degraded sugar by-products can be fermented for biofuels and the acid can be recycled.

Cellulose nanocrystals have many interesting properties; for example, they have a high specific Young's modulus similar to Kevlar and steel, are non-toxic, form lyotropic liquid crystals, and due to their amphiphilic nature and high aspect ratio they are promising reinforcing agents, rheological modifiers and interface stabilizers (e.g., in emulsions, gels and foams).[5] The colloidal stability of CNCs is another crucial property for most applications and is attributed to the charged surface groups that are grafted onto CNCs during production.[5] Most commonly, CNCs are made by hydrolysis with sulfuric acid, which yields sulfate half-ester groups on the surface, or by strong oxidation which imparts carboxylate groups.[6] Other acids have been used to hydrolyse cellulose, including strong

acids such as hydrochloric and hydrobromic acid, as well as weak acids such as phosphoric, citric, oxalic and maleic acid.[7–10] This paper focuses on CNCs produced via phosphoric acid hydrolysis and examines the range of properties attainable using this procedure.

CNCs have potential applications spanning composites, food, cosmetics, packaging, construction, oil & gas, paints, coatings and biomedical devices, to name just a few. While water-based applications and processing methods are the most straightforward for CNCs, there are also many surface modification routes to improve their dispersibility in polymer matrices and increase their compatibility with hydrophobic materials and non-polar solvents.[11,12] For most applications, CNCs with narrow size distributions, tailorable charge content and high yield and crystallinity are required. Although CNCs can be produced from many cellulose sources and under a wide range of hydrolysis conditions,[6] the yield and charge content can be very low or the CNCs can be large and aggregated if the conditions are not optimal. For these reasons, past studies have aimed to optimize the sulfuric acid hydrolysis of CNCs,[13–20] which is the most widespread hydrolysis procedure and is currently the method of choice for industrial production. These studies have demonstrated that the hydrolysis time, hydrolysis temperature, sulfuric acid concentration, and the acid-to-pulp ratio have the most significant effects on CNC properties and end uses.

In general, the optimization and modelling of sulfuric acid hydrolysed CNCs show the same trends and some broad conclusions can be drawn: by increasing the harshness of the hydrolysis (i.e., increasing time, temperature, acid concentration or acid-to-pulp ratio), smaller CNCs with higher sulfate content are typically produced and in higher yield.[13–20] However, if the harshness of the hydrolysis increases beyond a certain point, CNC crystallinity is compromised and the cellulose is degraded into sugars, which can proceed further to form furfurals.[18] This causes the CNC yield to decrease, while the yield of by-products increases.[19] The optimal hydrolysis conditions for the production of CNCs depends on the desired output parameter, as higher CNC yields have been obtained by lowering the sulfuric acid concentration; however, this resulted in CNCs with lower surface charge density and reduced colloidal stability.[19]

Thermal stability of CNCs is another important consideration for many applications, specifically in oil and gas extraction fluids and in the fabrication of nanocomposites which are often processed at high temperatures. The effects of hydrolysis conditions on the thermal stability of sulfuric acid hydrolysed CNCs have been studied and it has been shown that longer hydrolysis times produce CNCs that degrade at lower temperatures.[17] Although improved thermal stability was achieved with very low hydrolysis times, the CNCs produced were larger with lower colloidal stability.[17] Recently, hydrolysis procedures with acids other than sulfuric acid have been used to produce CNCs with increased thermal stability.[7,10] Chen et al. used oxalic acid to produce thermally stable CNCs functionalized with carboxyl groups; however, the CNC yield was very low.[10] Work by Camarero-Espinosa et al. has demonstrated that CNCs hydrolysed with hydrochloric acid or phosphoric acid have significantly higher thermal degradation temperatures than those hydrolysed with sulfuric acid.[7] Unfortunately, CNCs hydrolysed with HCl are uncharged and largely aggregated, do not form colloidal suspensions in water, and as a result are

difficult to handle and disperse. Conversely, CNCs hydrolysed with phosphoric acid have anionic phosphate half-ester groups grafted to their surfaces and form stable suspensions, though the colloidal stability of these suspensions does not rival that of CNCs produced with sulfuric acid.[7]

The significant improvement in thermal stability of phosphoric acid hydrolysed CNCs is a potential solution for many applications requiring temperature resistance. Furthermore, phosphorylation of (macro)cellulose and cellulose derivatives has been shown to impart flame retardancy.[21–24] On a nano-scale, phosphorylated cellulose nanofibrils (CNFs) have also been demonstrated to possess self-extinguishing properties.[25] We also have interest in CNCs hydrolysed with phosphoric acid because they have potential advantages over their sulfuric acid counterparts as bone scaffolding materials. Other phosphorylated cellulose substrates have demonstrated potential as biomedical materials that promote the formation of hydroxyapatite, which is the inorganic component of bone.[26–29] Thus, not only are CNCs hydrolysed with phosphoric acid stable at high temperatures and potentially flame-retardant, they could ideally be used in bone scaffolding applications to encourage new bone growth.

To facilitate the use of CNCs hydrolysed with phosphoric acid in some of the applications described above, the hydrolysis procedure needs to be optimized and better understood. Although this method has been used in the literature,[30,31] the resulting particles are often larger than sulfuric acid hydrolysed CNCs and tend to aggregate due to their low surface charge density.[7,32,33] These shortcomings make the CNCs difficult to work with; post-processing purification such as filtration of CNCs after sonication becomes extremely difficult and results in the loss of material as the aggregates are unable to pass through the normal paper or glass microfiber filters. We hypothesize that the previously demonstrated phosphoric acid hydrolysis protocols are not harsh enough to fully degrade the less ordered cellulose regions to yield individualized nanoparticles and do not functionalize the nanocrystal surfaces with a sufficient density of phosphate groups. The goal of this project is to optimize the hydrolysis to extract phosphated CNCs that have greater colloidal stability and more uniform size distributions (and thus more predictable performance). A design of experiments approach was selected to screen the effects of hydrolysis time, temperature and acid concentration on the morphology, charge content, thermal stability, crystallinity and colloidal stability of CNCs hydrolysed with phosphoric acid.

4.3 Materials & methods

Materials. Phosphoric acid (85 wt%), sodium hydroxide (96 wt%) and sodium chloride (salt) were purchased from Caledon Laboratories Ltd (Georgetown, Canada) and used as received. Dialysis tubing (14 kDa MWCO) was purchased from Sigma-Aldrich. Whatman ashless filter aid (catalog no.1703-050) and Whatman glass microfiber filter paper was obtained from GE Healthcare Life Sciences Canada. Phospher 3 Phosphate Reagent Powder Pillows were obtained from Hach Canada. Poly(allylamine hydrochloride) (PAH, Mw 120 000-200 000 g/mol) was purchased from PolySciences (Warrington, USA) and used without further purification. All water used had a resistivity of 18.2 MΩ·cm and was

purified by a Barnstead GenPure Pro water purification system from Thermo Fisher Scientific (Waltham, USA).

Experimental design. A 3-factor design of experiments (DOE) was chosen to study the effects of hydrolysis time (x_1), temperature (x_2) and phosphoric acid concentration (x_3) on CNC properties. A full factorial of experiments was performed to gain information on the individual effects of the three parameters as well as their two-factor interactions. This full factorial required the extraction of eight batches of CNCs and an additional center point with conditions (0, 0, 0) was performed as well. The hydrolysis time, temperature and acid concentration had low and high values of 80 min and 120 min, 100 °C and 120 °C and 70 wt% and 75 wt%, respectively. All three parameters were selected to vary within ranges that would generate a reliable model that could accurately predict CNC properties. The goal of these experiments was to assess which parameters affected the desired outputs most and to determine the direction for future experiments. For this reason, the hydrolysis time, temperature and acid concentration were varied over relatively narrow ranges. Additionally, some constraints further restricted the selected values (like the solubility of cellulose in H_3PO_4). The range of hydrolysis temperatures was initially set to vary from 80°C-120°C; however, acid hydrolysis of cotton at 80°C failed to produce particles with nanoscale dimensions and coagulated/partially digested cellulose was obtained. As discussed below, sample discoloration and burning was observed at 120 °C such that higher temperatures could not be used. Furthermore, the range of acid concentrations considered in this paper is narrow because the hydrolysis conditions had to be harsher than those presented by Camarero-Espinosa et al. without causing the cellulose to dissolve, which occurs around 80 wt% phosphoric acid.[7,34] For all hydrolyses, CNC length, height, apparent size by dynamic light scattering, phosphate content, thermal stability, crystallinity and zeta potential were measured, however statistical analysis was only carried out for properties that changed outside of the measurement precision. As such, a linear least squares regression as a function of the three input parameters was performed for three outputs: CNC length, phosphate content and zeta potential. This statistical analysis was performed in R version 3.2.3, which is a free and open source statistical computing and graphics program available online (https://cran.r-project.org/).

Phosphoric acid hydrolysis. Cellulose nanocrystals were hydrolysed with phosphoric acid roughly following the procedure outlined by Camarero-Espinosa et al.[7] A total of nine hydrolyses were completed with the reaction parameters indicated in Table 4.1 and the naming of samples follows "hydrolysis time, temperature, acid concentration", i.e., sample 120-120-75 was produced through a 120 minute hydrolysis, at 120˚C with 75 wt% phosphoric acid. In general, a cotton pulp was first produced by blending 2 g of Whatman ashless filter aid with varying amounts of water, depending on the desired acid concentration. The size of this pulp (with dry density ca. 0.23 g/mL) and morphology of its fibers (with diameters ca. 25 µm) are shown in Appendix 4, Figure A4.1. The pulp was placed in a 500 mL round-bottom flask, to which phosphoric acid was added (total volume

361 mL) and the mixture was heated in an oil bath under constant stirring with a magnetic stir bar. Following the hydrolysis, the suspension was cooled in an ice bath and quenched with 600 mL water. The suspension was evenly divided into six 250 mL Nalgene bottles and centrifuged for 15 minutes at 3600 rpm in a Sorvall RC-5 superspeed refrigerated centrifuge from Dupont. The resulting supernatant was poured off, an additional 600 mL of water was added to the remaining suspension and the centrifugation cycle was repeated. After two centrifugation cycles, the remaining suspension was placed in dialysis. CNCs were dialysed against purified water (suspension:water volume ratio = 20:1) changing the water daily until the pH of the suspension no longer changed (ca. 15 days). Once removed from dialysis, the CNC suspensions were sonicated for 15 minutes at 60% output with a probe sonicator (Sonifier 450, Branson Ultrasonics) in an ice bath to maintain the temperature below 30 $^{\circ}$C, and filtered with a glass microfiber filter with 1 µm pore size. CNCs were then converted to the sodium-salt form by adding sodium hydroxide until the samples reached a pH of 7.

Atomic force microscopy (AFM). CNCs were imaged by AFM to study particle morphology. Silica wafers were cleaned with a piranha solution (3:1 sulfuric acid to hydrogen peroxide), followed by a rinsing step with water and a drying step with nitrogen. A thin layer of 0.1 wt% PAH was spin-coated (G3P spin-coater, Specialty Coating Systems Inc.) onto the wafers at 4000 rpm for 30 seconds to prevent aggregation of the CNCs. Following the deposition of PAH, water was spin-coated to rinse the substrate. Lastly, a dilute CNC suspension (0.01 wt% or 0.005 wt%) was spin-coated onto the wafers. Images were collected on a MFP-3D AFM (Asylum Research an Oxford Instruments Company, Santa Barbara, USA) in tapping mode. FMR cantilevers, with a force constant of 2.8 ± 0.7 N/m and a resonance frequency of 75 ± 15 Hz, were purchased from NanoWorld and used to collect images. Post-processing of the images was performed with the Asylum Research 13.17 software, in conjunction with Igor Pro 6.37. Images were flattened with the Magic Mask feature and the particle size distributions were obtained using the built-in particle analysis tool in the Asylum Research software. All edge particles were ignored and any particles with areas less than 25 nm^2 were not measured. CNC particle length and particle cross section (from the height profile) were measured on the height images.[35] The particle size distributions shown here and in Appendix 4 are all the result of particle counts greater than 100, over multiple AFM images. Due to the nature of the samples and the presence of large aggregates, the median CNC length was selected rather than the average CNC length to best represent CNC size. Further justification for choosing the median CNC length for statistical modelling is described in Appendix 4 Figure A4.2 (as tested on shorter and more dispersed sulfuric acid hydrolysed CNCs).

Dynamic light scattering (DLS). Apparent CNC size in suspension was obtained by DLS with a Malvern ZetaSizer Nano at 25°C for 0.025 wt% CNC suspensions. The term "apparent" is used to recognize the limitation of DLS which assumes spherical particles; since CNCs are rod-shaped the DLS values can only be used as a relative measure but do provide insight regarding size, size distribution and degree of aggregation of CNCs in suspension.[36] Three particle size estimates were obtained for each sample; each estimate is an average particle size obtained from a distribution of values collected over 10-15

measurements. The sample average with 95% confidence (assuming normal distribution) is reported from three measurements.

Colorimetric determination of phosphate. Colorimetric methods have been used to detect phosphate levels in solution for decades.[37–39] Readily available powder pillows from Hach are commonly used to detect phosphates in water samples with a portable spectrophotometer. This method is comparable to standard procedures outlined in the literature.[40] Dilute CNC suspensions of 0.1 wt% were prepared for phosphate content analysis. The CNC suspension was placed in the Hach DR 2800 portable spectrophotometer and the absorbance of the sample at a wavelength of 880 nm was measured. This absorbance was used as a blank. A PhosVer 3 Ascorbic Acid Powder Pillow from Hach was added to a separate CNC suspension. This sample was vigorously mixed for 30 seconds, followed by a 2-minute wait time for the reaction to proceed to completion. The reactive orthophosphate in the CNC sample reacts with the molybdate from the powder pillows under acidic conditions to form a phosphomolybdic complex, which appears blue in color. The absorbance of this sample was measured at 880 nm and translated to a phosphate content. The sample average with 95% confidence (assuming normal distribution) is reported from three measurements.

Zeta potential. Zeta potential was used to assess the colloidal stability of the CNCs in suspension and was measured with a ZetaPlus zeta potential analyzer from Brookhaven Instruments. All zeta potential measurements were performed on 0.1 wt% CNC suspensions with 5 mM NaCl added. Three measurements were performed on each sample and the electrophoretic mobility was converted to zeta potential following Smoluchowski theory. The sample average with 95% confidence (assuming normal distribution) is reported from three measurements.

X-Ray diffraction (XRD). XRD was used to determine the degree of crystallinity for CNCs. Freeze-dried CNCs were compressed into small disks and mounted on a silicon wafer. A Bruker D8 Discover diffractometer with Davinci Design was used to collect 2D frames at a detector distance of 14 cm. The X-ray source was a cobalt sealed tube emitting an electron beam with a wavelength of 1.79026 Å with a 35 kV and 45 mA power source. The sample was properly positioned with a vertical D8 θ-θ goniometer, while a 0.5 mm micro slit and a 0.5 mm short collimator were used to adjust the beam. 1D frames were obtained by integrating the 2D frames with Diffrac.eva 4.0 and subtracting frames collected on an empty silicon wafer. Rietveld refinement was used to match theoretical models to the measured diffraction spectra for both the crystalline and amorphous phases.[41,42] The amorphous phase was modelled with a Pseudo-Voigt function and a manually inserted fixed peak at 24.1° for all samples. Crystallinity index was obtained by comparing the contribution of the crystalline peaks to the diffraction spectrum of the sample. The measurement error is taken to be ca. 5%.

Thermogravimetric analysis (TGA). Thermogravimetric analysis was performed on freeze-dried CNCs with a TA Instruments Q50 thermal analyzer. To get reproducible TGA results, a round pellet was formed by placing 3.0 mg of dried CNCs between two plastic stoppers in a 1.0 mL syringe. The CNCs were compressed to form a pellet, which was

placed in an argon-filled chamber. The mass of the sample was monitored as the temperature in the analyzer was raised to 600 °C from room temperature at a rate of 10 °C/min under argon.

4.4 Results and discussion

Nine phosphoric acid hydrolyses covering the desired parameter space were performed to produce phosphated CNCs with a range of properties. (In the following discussion, samples are named according to the convention "hydrolysis time, temperature, acid concentration".) CNCs were fully characterized and the zeta potential, apparent particle size, phosphate content, median particle length and crystallinity index are shown in Table 4.1. While AFM length and apparent size by DLS are both size measurements, we include both because one is a physical size but a 2D projection of a 3D system, and the other provides insight into the dispersion of nanoparticles in suspension. In general, the two size measurements show the same trend with hydrolysis conditions – the CNCs produced are shorter with increasing hydrolysis harshness. AFM median lengths span 238-475 nm and apparent size by DLS ranges from 163-250 nm which implies that nanoparticles are being produced and that there is no significant aggregation in suspension.

As expected, almost all hydrolysis conditions produced rod-like nanoparticles, as shown in Figure 4.1, except for the harshest hydrolysis (i.e., 120-120-75). The particles extracted from this hydrolysis can be seen in Figure 4.1i; they appear to be aggregates of over-hydrolysed, degraded and re-precipitated cellulose and larger micron size clumps were also observed but difficult to image by AFM. We do not consider the 120-120-75 CNCs to be true CNCs based on size, the low degree of crystallinity,[4] and the brown color observed after hydrolysis. At first, harsher acid hydrolysis conditions (increased time, temperature and acid concentration) have resulted in increased CNC crystallinity due to degradation of the amorphous regions into oligosaccharides.[18] Beyond a certain point, however; crystallinity has been shown to decrease due to damage to the crystalline region,[17] which has likely occurred with 120-120-75. An attempt was made to introduce a cellulose II phase for the 120-120-75 sample. The peaks observed in the x-ray diffraction spectra of this sample were very broad and, while some peaks resemble those of a cellulose II phase, this cannot be stated with absolute certainty. The X-ray diffractometry profile can be seen in Figure A4.3 of the Appendix 4. Furthermore, the brown color of the CNCs hydrolysed at the harshest condition is likely due to the formation of fufural and 5-hydroxymethyl-2-furfural (HMF), which are degradation products from the hydrolysis of cellulose nanocrystals. The reaction pathways leading to the formation of these compounds have been discussed in several papers[18,43] and the presence of HMF has previously been quantified via high pressure liquid chromatography.[44–46] As such, due to the presence of large aggregates and the apparent degradation of crystalline regions, the median length/size distribution and statistical analyses were not performed on 120-120-75. The eight remaining samples were used in the DOE modelling and are considered sufficient to obtain model results with confidence levels that can be calculated and do not span zero.

Zeta potential is a measure of colloidal stability, where absolute values over 20 mV are generally taken as colloidally stable suspensions.[36] The CNCs produced using phosphoric

acid do not meet this criterion yet appear well dispersed in water and remain stable over time by eye. Small additions of salt (~10 mM) however, will cause the particles to coagulate and settle which supports the zeta potential values reported. The zeta potential is a function of the phosphate content (i.e., surface charge density, see Table A4.1 in Appendix 4 for surface charge density approximations calculated from phosphate content and AFM particle dimensions) and the particle size and is discussed further below in the modelling section.

The degree of crystallinity for CNCs is important because the mechanical properties, response to electromagnetic fields and chemical resistance are directly related to the organization and packing of polymer chains in the nanoparticles. The degree of crystallinity also relates to the harshness of the hydrolysis where too little or too much hydrolysis of cellulose could lead to significant changes in the crystal structure. All CNCs produced had a high degree of crystallinity, over 93% (except for 120-120-75). From Table 4.1, the crystallinity values are within the assumed measurement error (5%) and were therefore not included in any statistical analysis. We conclude that phosphoric acid hydrolysis yields highly crystalline CNCs, similar to sulfated CNCs, but that within the range of hydrolysis time, temperature and acid concentrations tested we cannot tailor CNC crystallinity to a significant degree.

Table 4.1. Properties of CNCs hydrolysed with phosphoric acid with varying hydrolysis time, temperature and acid concentration.

Sample Name	Time, x_1 (min)	Temp., x_2 (°C)	Acid Conc., x_3 (wt%)	Zeta Potential (mV)	Apparent DLS Size (nm)	Phosphate Content (mmol/kg CNC)	Median Particle Length (nm)	Crystallinity Index (%)
80-100-70	80	100	70	-10.8±0.6	240±11	15±2	475	96
80-120-70	80	120	70	-11.7±0.5	243±8	31±1	284	97
80-100-75	80	100	75	-9.8±0.7	246±8	8±1	312	96
80-120-75	80	120	75	-17.3±0.8	163±3	13±3	238	96
100-110-72.5	100	110	72.5	-9.0±0.5	215±9	13±1	325	93
120-100-70	120	100	70	-9.8±0.7	250±2	10±1	391	97
120-120-70	120	120	70	-12.4±0.5	200±10	44±2	268	94
120-100-75	120	100	75	-12.4±0.4	179±7	18±11	315	93
120-120-75	120	120	75	-11±1	351±6	17±8	N/A	65
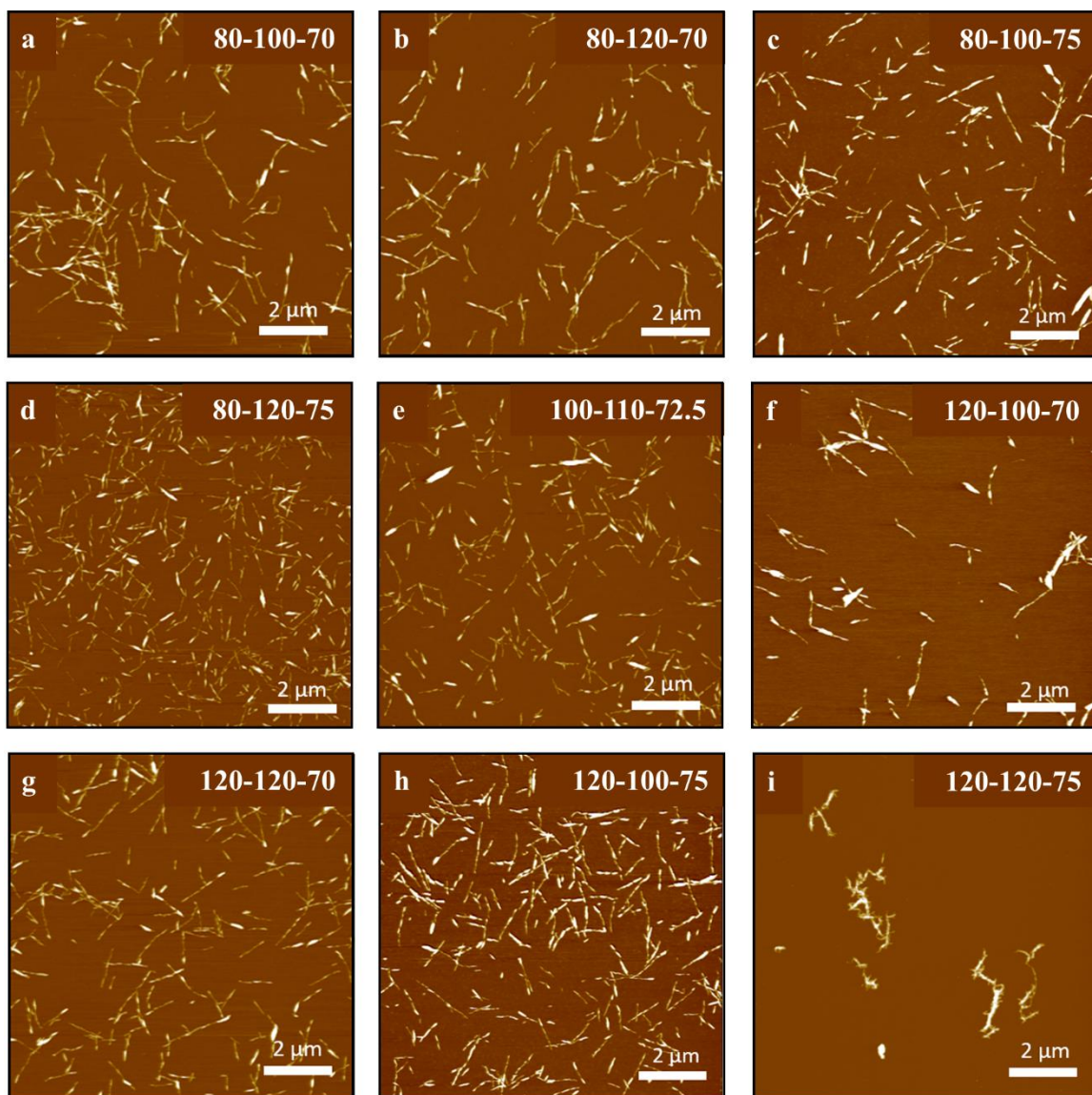
Figure 4.1. Atomic force microscopy height images of CNCs hydrolysed with phosphoric acid with varying hydrolysis time, temperature and acid concentration (as indicated within each image). Images a-i roughly follow the order of increasing acid hydrolysis harshness. All scale bars are 2 μm.

A primary reason to produce CNCs by phosphoric acid hydrolysis is to obtain more thermally stable CNCs. The TGA curves in Figure 4.2 indicate that all CNCs showed significant increases in thermal stability when compared to CNCs hydrolysed with sulfuric acid (S-CNCs). S-CNCs in the sodium form are known to be more stable than in the acid form[47] and this is also the case for phosphoric acid hydrolyzed CNCs. While the results in Figure 4.2 are for sodium form CNCs, a separate study was performed on CNCs hydrolysed for 90 minutes at 100 °C with 70 wt% phosphoric acid. In acid form, the CNCs from this

sample had a maximum rate of thermal decomposition of 331 °C, which is significantly lower than the 392 °C observed for the same CNCs in sodium form. Interestingly however, very similar thermal degradation patterns were observed for all phosphated CNCs and the thermal stability was not changed in a statistically significant way by changing the hydrolysis conditions. As such, the generation of a model for thermal stability is not included in this paper; future studies will examine thermal degradation mechanisms of CNCs produced with different acids in more detail. The following sections present the DOE models for properties that can be tailored significantly though phosphoric acid hydrolysis and that generate models with high confidence. In order of decreasing model accuracy, CNC length, phosphate content and zeta potential (colloidal stability) are presented below.
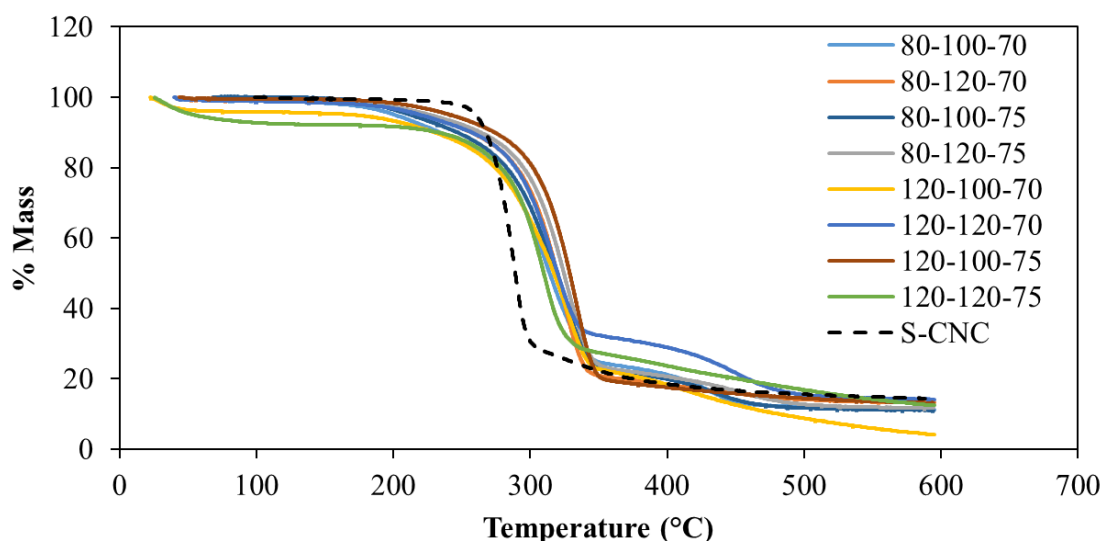
Figure 4.2 Thermal degradation curves of CNCs hydrolysed with phosphoric acid with varying hydrolysis time, temperature and acid concentration. The dashed black line shows the thermal degradation curve for CNCs hydrolysed with sulfuric acid.

Median particle length model. The median particle lengths for each CNC sample were obtained by automated particle detection on AFM images as described above. The *median* particle length was chosen to represent CNC size because it is not heavily affected by aggregates. The particle size distributions were measured for eight samples (all samples except for 120-120-75). CNCs hydrolysed with phosphoric acid have the potential to be tailored over a larger range of lengths compared to CNCs hydrolysed with sulfuric acid, whose lengths do not vary as significantly. Within the range of hydrolysis conditions tested, median length of CNCs hydrolysed with phosphoric acid varied within 238-475 nm. Conversely, research shows that CNCs produced through various sulfuric acid hydrolysis conditions have lengths that either do not change with any statistical significance, or change within a smaller range of values (e.g., 130-281 nm).[17,19] A multiple linear least squares regression was performed in R and the following model (Equation 1) was generated to predict the median particle length (Y) based on hydrolysis time (x_1), hydrolysis temperature (x_2) and phosphoric acid concentration (x_3).

$$Y = 200.65 - 24.51x_1 - 30.18x_2 - 35.81x_3 - 10.00x_1x_2 - 19.38x_2x_3 - 16.99x_1x_3$$
(Equation 1)

The R^2 (coefficient of determination) for this model is 1 and the p-value is 0.003, suggesting that the null hypothesis should be rejected and this model accurately describes the effects of hydrolysis parameters on median CNC length. The coefficients for the parameters of this model are shown in Figure 4.3.
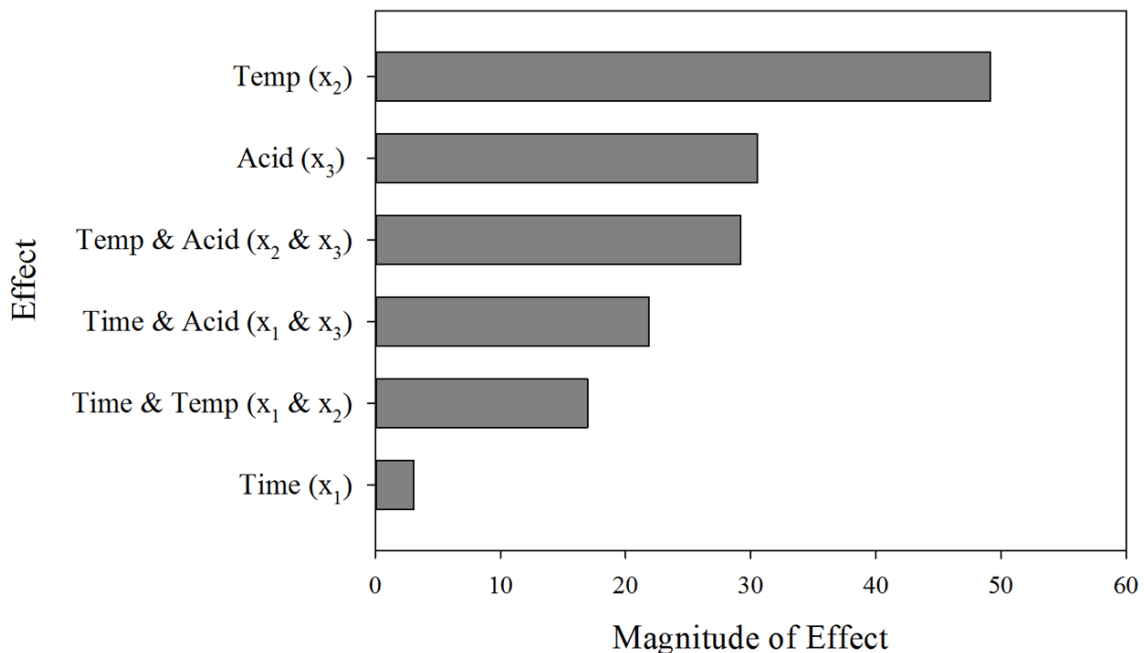
Figure 4.3. Coefficients for the parameters in a model predicting median CNC length. All coefficients are negative (i.e., an increase in the input parameter results in a decrease of the output property).

The most significant effects on median CNC length were observed by changing the hydrolysis temperature and acid concentration. Previous work by Chen et al. has similarly discussed a strong dependence of CNC length on the sulfuric acid concentration used in the hydrolysis.[19] CNCs hydrolysed with phosphoric acid appear to follow the same trend; increasing the acid concentration allows for the extraction of CNCs with a lower median length. Hydrolysis temperature, as well as the interaction between temperature and acid concentration, also play significant roles in determining median CNC length. The strong effect of temperature on CNC length is likely a result of a higher rate constant for the acid hydrolysis of cellulose.[48] Higher rate constants result in faster hydrolysis of glycosidic linkages and lower degree of polymerization of cellulose, which correlates with nanocellulose length.[49] The exact reason for the increase in reaction rate remains unclear; however, both increased diffusion of acid into cellulose fibers and a higher acidity function of phosphoric acid could be responsible.[50] The strong interaction between temperature and acid concentration is evident from both Figure 4.3 and the factor interaction profiles in

Figure 4.4. The slopes of the median length vs hydrolysis temperature at low and high acid concentrations have very different magnitudes, indicating a strong interaction between acid concentration and temperature. At a low acid concentration, changes in hydrolysis temperature have greater effects on median CNC length than at a high acid concentration. Similarly, a plot of median length vs acid concentration shows that, at lower temperatures, small changes in acid concentration cause larger decreases in median CNC length. Strong interactions between hydrolysis temperatures and acid concentrations have been observed in other work with sulfated CNCs.[18,20] The degree of hydrolysable cellulose has been shown to increase with increasing reaction harshness; a parameter that was used to designate the combined effect of temperature and acid concentration in a sulfuric acid hydrolysis.[18] The degree of hydrolysable cellulose was defined as the fraction of cellulose that could be de-polymerized at given hydrolysis conditions.[18] A higher degree of hydrolysable cellulose is reflected in shorter CNCs; this was also observed in the CNCs hydrolysed with phosphoric acid. By increasing both the temperature and acid concentration of the hydrolysis, a lower polydispersity of cellulose nanocrystals was observed. Figure 4.5 shows particle size distributions collected from AFM images of samples 80-100-70 and 80-120-75 which are the least harsh and most harsh hydrolysis conditions with an 80 minute hydrolysis time, respectively. (Figure A4.4 in Appendix shows particle size distributions for all samples.) By increasing both the temperature and the acid concentration, the particle size distribution becomes narrower and fewer large CNCs or CNC aggregates are observed. This is also apparent in the AFM images in Figure 4.1.
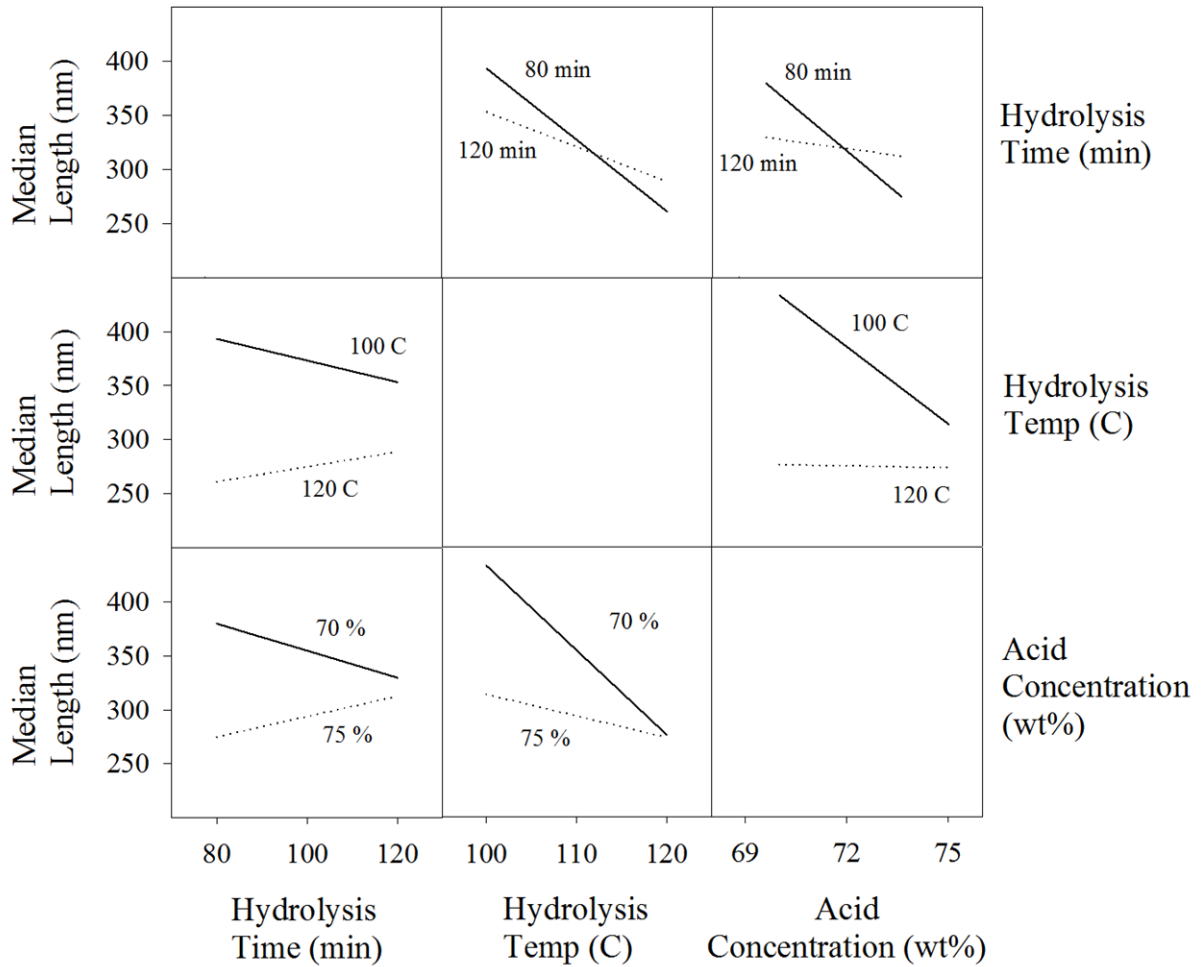
Figure 4.4. Factor interaction profiles describing the interactions of two hydrolysis parameters and their combined effects on median CNC length.

Conversely, Figure 4.3 shows that hydrolysis time on its own does not significantly affect median CNC length over the range of hydrolysis times tested in this study. This is in line with findings by Kargarzadeh et al., where CNCs were hydrolysed with sulfuric acid for 20-120 minutes and no discerning changes in CNC length were observed.[17] It is possible; however, that a hydrolysis time significantly lower than 80 minutes could result in much longer CNCs. The range of hydrolysis times selected for this set of experiments are likely within a plateau region where no further decreases in CNC length can be observed with increasing hydrolysis times.
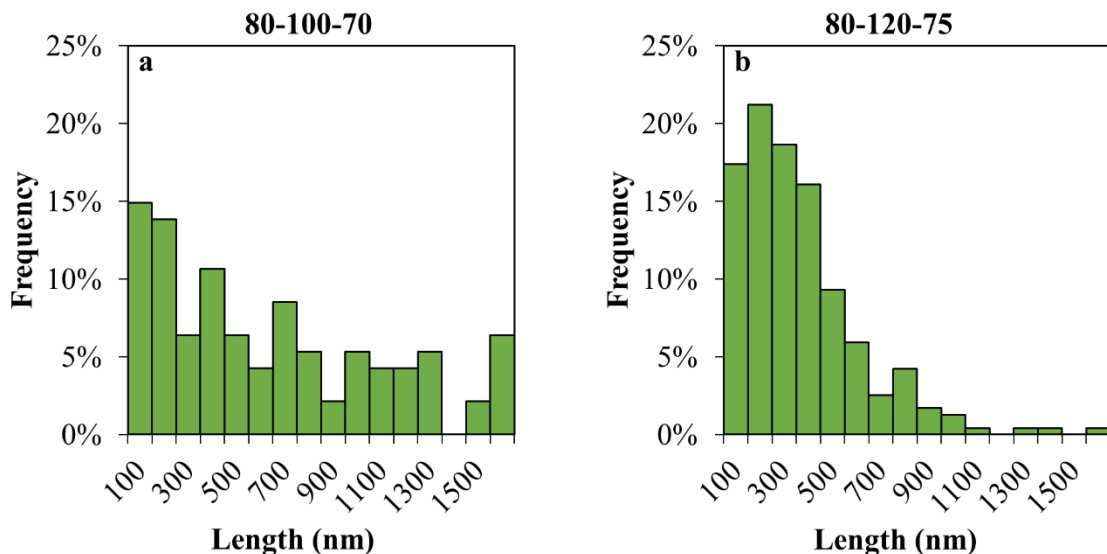
Figure 4.5. Particle size distributions obtained from AFM image analysis for two CNC batches hydrolysed under different conditions as indicated above the histogram.

Phosphate content model. The phosphate content for each sample can be seen in Table 4.1 and the charge density is calculated in Appendix 4, Table A4.1. The lowest and highest observed phosphate contents were 8.2 mmol/kg and 44.5 mmol/kg, respectively. The surface charge densities span 0.01-0.05 e/nm^2 which are low compared to sulfated CNCs (80-350 mmol/kg or ca. 0.1-1 e/nm^2).[51–53,4,14] A multiple linear least squares regression was performed and the following model (Equation 2) was generated to predict the phosphate content (Y) based on hydrolysis time (x_1), hydrolysis temperature (x_2) and acid concentration (x_3).

$$Y = 23.28 + 6.34x_1 + 8.33x_2 - 1.29x_3 + 4.28x_1x_2 - 3.72x_2x_3 + 5.93x_1x_3$$

(Equation 2)

The R^2 for this model is 0.8844 and the p-value is 0.59, meaning that there is not enough evidence to reject the null hypothesis. This model cannot fully predict CNC phosphate content; however, it can provide key insights into the main factors affecting charge content on CNCs hydrolysed with phosphoric acid. The coefficients for the parameters of this model are shown in Figure 4.6.
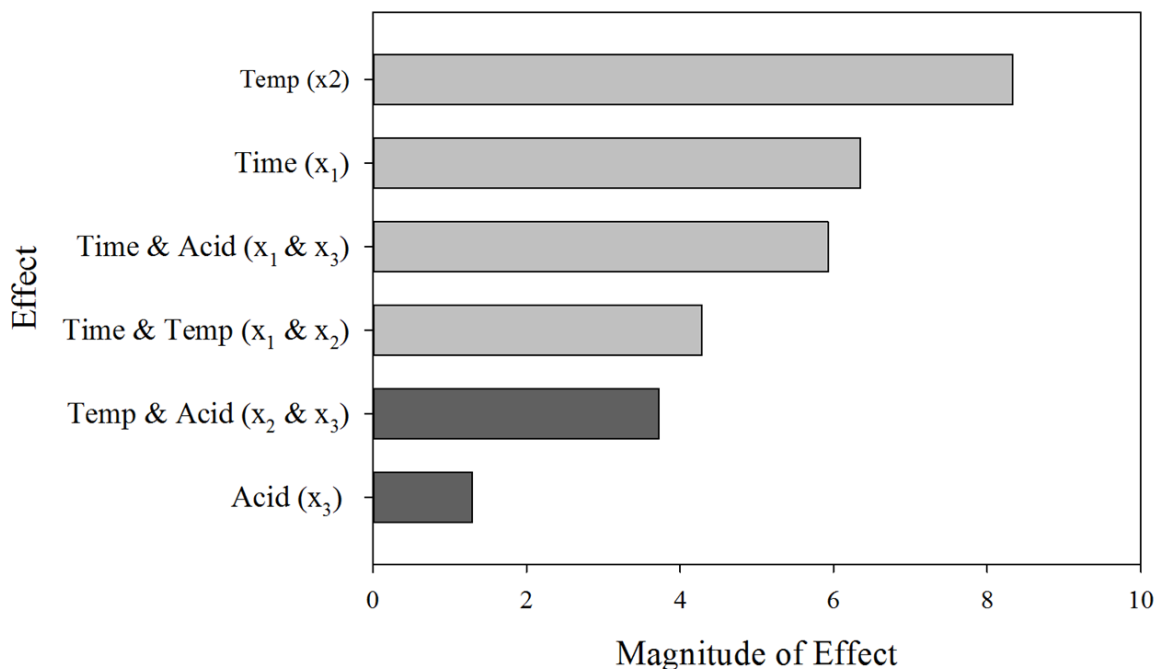
Figure 4.6. Coefficients for the parameters in a model predicting CNC phosphate content. Light grey bars indicate positive coefficients, while dark grey bars indicate negative coefficients.

Changes in hydrolysis temperature between 100°C and 120°C have the most significant effects on CNC phosphate content, while the effect of changing acid concentration on its own is minor. Furthermore, the Pareto plot in Figure 4.6 and the sign of the coefficients in the model's equation show that increasing the acid concentration causes phosphate content to slightly decrease, while increasing the hydrolysis time or temperature causes phosphate content to increase. The factor interaction profiles can be found in Figure A4.5 in Appendix 4. This does not follow previously demonstrated trends for the hydrolysis of CNCs with sulfuric acid. Work by Dong et al. concluded that acid concentration had the most significant effect on CNC sulfate content, while hydrolysis temperature had a moderate effect and hydrolysis time had a negligible effect.[20] Chen et al. showed that acid concentration has the most drastic effect on CNC sulfate content, though hydrolysis time and temperature were also shown to be important factors.[19] At low acid concentrations, the effects of hydrolysis time were shown to be more significant, as the formation of sulfate half esters on CNC surfaces occurs relatively slowly. At high acid concentrations, the effects of time are less significant, as CNC sulfate content increases sharply and levels off.[19] The strong effect of acid concentration on the sulfate content for S-CNCs is directly related to the fact that sulfuric acid is a strong acid and is known to catalyze the esterification of cellulose.[54]

As mentioned, CNCs hydrolysed with phosphoric acid have roughly one tenth of the surface charge density of those hydrolysed with sulfuric acid. This is likely related to the

fact that phosphoric acid is a weaker acid that is not entirely dissociated in solution and does not catalyze esterification to the same extent as sulfuric acid. Furthermore, to reach the same H^+ concentration in the reaction as is present with ~65 wt% sulfuric acid (the most common protocol)[55] would require a phosphoric acid concentration over 15 M (assuming a dissociation constant of ca. 0.618);[56] this concentration would dissolve cellulose.[34] (The ratio of ionic species from phosphoric acid dissociation at high concentrations and high temperatures is also somewhat debated.)[57,58] We can also infer that our hydrolysis never reaches the same severity in terms of acid concentration, since we do not observe a significant leveling off or decrease in phosphate content, as has been observed with sulfuric acid. Finally, the small changes in phosphate content overall may be a result of insignificant changes in H^+ concentration over the 70-75 wt% range of acid conditions tested. The hydrolysis time and temperature have far more significant effects on phosphate content within this DOE. From these results, we conclude that the most significant effect of the acid strength (strong vs. weak acid) is apparent in the ability of the acid to impart surface charge density which unfortunately leads to phosphated CNCs which are not sufficiently charged or colloidally stable for some of the intended applications.

Zeta potential model. As discussed, zeta potential relates to colloidal stability and is a function of the surface charge density and CNC size – the value is calculated from the electrophoretic mobility of the particles in suspension. The zeta potential values are given in Table 4.1 and range from -17.3 mV to -9.0 mV, respectively. The zeta potential was measured at pH 7, which is below the second pK_a of phosphoric acid; however, the effect of pH on zeta potential was found to be negligible as shown in Figure A4.6 in Appendix 4. A multiple linear least squares regression was performed and the following model (Equation 3) was generated to predict the zeta potential (Y) based on hydrolysis time (x_1), hydrolysis temperature (x_2) and acid concentration (x_3).

$$Y = -12.40 - 0.41x_1 - 2.11x_2 - 1.64x_3 - 0.03x_1x_2 - 1.23x_2x_3 - 0.49x_1x_3$$

(Equation 3)

The R^2 for this model is 0.6969 and the p-value is 0.8426, meaning that there is not enough evidence to reject the null hypothesis. This model cannot fully predict CNC zeta potential. Furthermore, since all zeta potentials are within a small range and they indicate a general lack of colloidal stability for phosphoric acid hydrolysed CNCs, this model will not be discussed extensively. A Pareto plot demonstrating the effects of hydrolysis time, temperature and acid concentration can be seen in Appendix 4 Figure A4.7 and factor interaction profiles are included in the Appendix 4 Figure A4.8. Overall, temperature and acid concentration affect the zeta potential the most (which are also the most significant parameters affecting the CNC length) which implies that with the low charge content values obtained here, the size is a dominant factor in predicting how CNCs move in an electric field.

4.5 Conclusions

This design of experiments study provided significant insight into the effects of hydrolysis time, temperature and acid concentration on the morphology and surface charge density of CNCs hydrolysed with phosphoric acid. Three main outputs were statistically analyzed; CNC length, phosphate content and zeta potential. The intention was to perform a screening study and understand the range of properties attainable through phosphoric acid hydrolysis of cellulose, not to develop a predictive model, as has been done elegantly, for example, in the central composite design study of sulfuric acid hydrolysed CNCs by Dong et al..[20] We also did not investigate the yield from these hydrolyses but observed that in all cases the yield of CNCs produced was >40% and could likely be improved.

The data collected generated models with high confidence for CNC length but could not fully describe the phosphate content and zeta potential results for phosphoric acid hydrolysed CNCs. Nonetheless, general trends were observed to understand which parameters had the greatest effects on these CNC properties. The hydrolysis temperature and phosphoric acid concentration have the greatest effect on median CNC length and on the overall particle size distribution. Increasing both temperature and acid concentration increases the reaction harshness and results in CNCs with a narrower particle size distribution and smaller median length. Hydrolysis time and temperature had the greatest effects on CNC phosphate content, while the effect of acid concentration was negligible. This is because only a small percentage of phosphoric acid is dissociated and small changes in the acid concentration have little effect on the ability to graft phosphate half-esters onto the CNC surfaces. CNCs extracted with phosphoric acid similarly have small zeta potentials which indicates low colloidal stability. Furthermore, the zeta potential values measured did not vary significantly with changing hydrolysis parameters.

Overall, this design of experiments provided general "rules" for tailoring CNC size showing that we could control CNC length over a significantly larger range than for sulfated CNCs. This is particularly useful for controlling CNC reinforcement, rheological modification and interface stabilizing abilities. The use of a weak acid gave an expanded range of properties by not degrading the cellulose too quickly under mild hydrolysis conditions. The downfall of using a weak acid is that low phosphate content and low colloidal stability was inevitable. Although the surface charge density and zeta potential could be better modelled by increasing the number of runs and adding second-order variables to the model, the resultant model implied that higher phosphate content can be imparted by using harsher hydrolysis conditions (most importantly, by increasing the hydrolysis temperature). All of the CNCs produced in this work have high crystallinity and thermal stability and we believe this is a good first step towards tailoring phosphated CNC properties to maximize their potential in high temperature applications and biomedical devices.

4.6 References

1.   Nickerson, R. F. & Habrle, J. A. Cellulose intercrystalline structure. *Ind. Eng. Chem.* **39**, 1507–1512 (1947).

2.   Rånby, B. G., Banderet, A. & Sillén, L. G. Aqueous colloidal solutions of cellulose micelles. *Acta Chem. Scand.,* **3**, 649–650 (1949).

3.   Mukherjee, S. M. & Woods, H. J. X-ray and electron microscope studies of the degradation of cellulose by sulphuric acid. *Biochim. Biophys. Acta* **10**, 499–511 (1953).

4.   Reid, M. S., Villalobos, M. & Cranston, E. D. Benchmarking Cellulose Nanocrystals: From the Laboratory to Industrial Production. *Langmuir* **33**, 1583–1598 (2017).

5.   Habibi, Y., Lucia, L. A. & Rojas, O. J. Cellulose Nanocrystals : Chemistry , Self-Assembly , and Applications. **110**, 3479–3500 (2010).

6.   Sacui, I. A. *et al.* Comparison of the Properties of Cellulose Nanocrystals and Cellulose Nanofibrils Isolated from Bacteria, Tunicate, and Wood Processed Using Acid, Enzymatic, Mechanical, and Oxidative Methods. *ACS Appl. Mater. Interfaces* **6**, 6127–6138 (2014).

7.   Camarero Espinosa, S., Kuhnt, T., Foster, E. J. & Weder, C. Isolation of Thermally Stable Cellulose Nanocrystals by Phosphoric Acid Hydrolysis. *Biomacromolecules* **14**, 1223–1230 (2013).

8.   Sadeghifar, H., Filpponen, I., Clarke, S. P., Brougham, D. F. & Argyropoulos, D. S. Production of cellulose nanocrystals using hydrobromic acid and click reactions on their surface. *J. Mater. Sci.* **46**, 7344–7355 (2011).

9.   Yu, H.-Y., Zhang, D.-Z., Lu, F.-F. & Yao, J. New approach for single-step extraction of carboxylated cellulose nanocrystals for their use as adsorbents and flocculants. *ACS Sustain. Chem. Eng.* **4**, 2632–2643 (2016).

10.   Chen, L., Y. Zhu, J., Baez, C., Kitin, P. & Elder, T. Highly thermal-stable and functional cellulose nanocrystals and nanofibrils produced using fully recyclable organic acids. *Green Chem.* **18**, 3835–3843 (2016).

11.   Peng, B. L., Dhar, N., Liu, H. L. & Tam, K. C. Chemistry and applications of nanocrystalline cellulose and its derivatives: A nanotechnology perspective. *Can. J. Chem. Eng.* **89**, 1191–1206 (2011).

12.   Habibi, Y. Key advances in the chemical modification of nanocelluloses. *Chem. Soc. Rev.* **43**, 1519–1542 (2014).

13.   Dong, X. M., Revol, J.-F. & Gray, D. G. Effect of microcrystallite preparation conditions on the formation of colloid crystals of cellulose. *Cellulose* **5**, 19–32 (1998).

14. Beck-Candanedo, S., Roman, M. & Gray, D. G. Effect of reaction conditions on the properties and behavior of wood cellulose nanocrystal suspensions. *Biomacromolecules* **6**, 1048–1054 (2005).

15. Bondeson, D., Mathew, A. & Oksman, K. Optimization of the isolation of nanocrystals from microcrystalline cellulose by acid hydrolysis. *Cellulose* **13**, 171–180 (2006).

16. Hamad, W. Y. & Hu, T. Q. Structure–process–yield interrelations in nanocrystalline cellulose extraction. *Can. J. Chem. Eng.* **88**, 392–402 (2010).

17. Kargarzadeh, H. *et al.* Effects of hydrolysis conditions on the morphology, crystallinity, and thermal stability of cellulose nanocrystals extracted from kenaf bast fibers. *Cellulose* **19**, 855–866 (2012).

18. Wang, Q., Zhao, X. & Zhu, J. Y. Kinetics of strong acid hydrolysis of a bleached kraft pulp for producing cellulose nanocrystals (CNCs). *Ind. Eng. Chem. Res.* **53**, 11007–11014 (2014).

19. Chen, L. *et al.* Tailoring the yield and characteristics of wood cellulose nanocrystals (CNC) using concentrated acid hydrolysis. *Cellulose* **22**, 1753–1762 (2015).

20. Dong, S., Bortner, M. J. & Roman, M. Analysis of the sulfuric acid hydrolysis of wood pulp for cellulose nanocrystal production: A central composite design study. *Ind. Crops Prod.* **93**, 76–87 (2016).

21. Kandola, B. K., Horrocks, A. R., Price, D. & Coleman, G. V. Flame-Retardant Treatments of Cellulose and Their Influence on the Mechanism of Cellulose Pyrolysis. *J. Macromol. Sci. Part C* **36**, 721–794 (1996).

22. Shi, Y., Belosinschi, D., Brouillette, F., Belfkira, A. & Chabot, B. Phosphorylation of Kraft fibers with phosphate esters. *Carbohydr. Polym.* **106**, 121–127 (2014).

23. Blanchard, E. J. & Graves, E. E. Phosphorylation of Cellulose with Some Phosphonic Acid Derivatives. *Text. Res. J.* **73**, 22–26 (2003).

24. Božič, M., Liu, P., Mathew, A. P. & Kokol, V. Enzymatic phosphorylation of cellulose nanofibers to new highly-ions adsorbing, flame-retardant and hydroxyapatite-growth induced natural nanoparticles. *Cellulose* **21**, 2713–2726 (2014).

25. Ghanadpour, M., Carosio, F., Larsson, P. T. & Wågberg, L. Phosphorylated Cellulose Nanofibrils: A Renewable Nanomaterial for the Preparation of Intrinsically Flame-Retardant Materials. *Biomacromolecules* **16**, 3399–3410 (2015).

26. Hong, L. *et al.* Hydroxyapatite/bacterial cellulose composites synthesized via a biomimetic route. *Mater. Lett.* **60**, 1710–1713 (2006).

27.   Wan, Y. Z. *et al.* Synthesis and characterization of hydroxyapatite–bacterial cellulose nanocomposites. *Compos. Sci. Technol.* **66**, 1825–1832 (2006).

28.   Wan, Y. Z. *et al.* Biomimetic synthesis of hydroxyapatite/bacterial cellulose nanocomposites for biomedical applications. *Mater. Sci. Eng. C* **27**, 855–864 (2007).

29.   Yamaguchi, K. *et al.* Highly dispersed nanoscale hydroxyapatite on cellulose nanofibers for bone regeneration. *Mater. Lett.* **168**, 56–61 (2016).

30.   Koshizawa, T. Degradation of Wood Cellulose and Cotton Linters in Phosphoric Acid. *Japan Tappi J.* **14**, 455-458,475 (1960).

31.   Usuda, M., Suzuki, O., Nakano, J. & Migita, N. Acid Hydrolysis of Cellulose in Concentrated Phosphoric Acid; Influences of Modified Groups of Cellulose on the Rate of Hy drolysis. *J. Soc. Chem. Ind. Japan* **70**, 349–352 (1967).

32.   Li, S. *et al.* Fabrication of nano-crystalline cellulose with phosphoric acid and its full application in a modified polyurethane foam. *Polym. Degrad. Stab.* **98**, 1940–1944 (2013).

33.   Tang, Y. *et al.* Extraction of cellulose nano-crystals from old corrugated container fiber using phosphoric acid and enzymatic hydrolysis followed by sonication. *Carbohydr. Polym.* **125**, 360–366 (2015).

34.   Zhang, Y.-H. P., Cui, J., Lynd, L. R. & Kuang, L. R. A transition from cellulose swelling to cellulose dissolution by o-phosphoric acid: evidence from enzymatic hydrolysis and supramolecular structure. *Biomacromolecules* **7**, 644–648 (2006).

35.   Brinkmann, A. *et al.* Correlating cellulose nanocrystal particle size and surface zrea. *Langmuir* **32**, 6105–6114 (2016).

36.   Bhattacharjee, S. DLS and zeta potential - What they are and what they are not? *J. Control. Release* **235**, 337–351 (2016).

37.   Briggs, A. P. A Colorimetric Method for the Determination of Homogentisic Acid in Urine. *J. Biol. Chem.* **51**, 453–454 (1922).

38.   Berenblum, I. & Chain, E. An improved method for the colorimetric determination of phosphate. *Biochem. J.* **32**, 295–298 (1938).

39.   Dickman, S. R. & Bray, R. H. Colorimetric Determination of Phosphate. *Ind. Eng. Chem. Anal. Ed.* **12**, 665–668 (1940).

40.   Ormaza-González, F. I. & Villalba-Flor, A. P. The measurement of nitrite, nitrate and phosphate with test kits and standard procedures: A comparison. *Water Res.* **28**, 2223–2228 (1994).

41.   Driemeier, C. & Calligaris, G. A. Theoretical and experimental developments for accurate determination of crystallinity of cellulose I materials. *J. Appl. Crystallogr.*

44, 184–192 (2011).

42.   Ahvenainen, P., Kontro, I. & Svedström, K. Comparison of sample crystallinity determination methods by X-ray diffraction for challenging cellulose I materials. *Cellulose* **23**, 1073–1086 (2016).

43.   Sasaki, M. *et al.* Cellulose hydrolysis in subcritical and supercritical water. *J. Supercrit. Fluids* **13**, 261–268 (1998).

44.   Mijares, R. M., Park, G. L., Nelson, D. B. & McIVER, R. C. HPLC Analysis of HMF in Orange Juice. *J. Food Sci.* **51**, 843–844 (1986).

45.   Porretta, S. & Sandei, L. Determination of 5-(hydroxymethyl)-2-furfural (HMF) in tomato products: Proposal of a rapid HPLC method and its comparison with the colorimetric method. *Food Chem.* **39**, 51–57 (1991).

46.   Zappalà, M., Fallico, B., Arena, E. & Verzera, A. Methods for the determination of HMF in honey: a comparison. *Food Control* **16**, 273–277 (2005).

47.   Wang, N., Ding, E. & Cheng, R. Thermal degradation behaviors of spherical cellulose nanocrystals with sulfate groups. *Polymer (Guildf).* **48**, 3486–3493 (2007).

48.   Daruwalla, E. H. & Shet, R. T. Heterogeneous Acid Hydrolysis of Alpha-Cellulose from Sudanese Cotton. *Text. Res. J.* **32**, 942–954 (1962).

49.   Shinoda, R., Saito, T., Okita, Y. & Isogai, A. Relationship between Length and Degree of Polymerization of TEMPO-Oxidized Cellulose Nanofibrils. *Biomacromolecules* **13**, 842–849 (2012).

50.   Fengel, D. & Wegener, G. *Wood: chemistry, ultrastructure, reactions*. (Walter de Gruyter, 1983).

51.   Jiang, F., Esker, A. R. & Roman, M. Acid-Catalyzed and Solvolytic Desulfation of H2SO4-Hydrolyzed Cellulose Nanocrystals. *Langmuir* **26**, 17919–17925 (2010).

52.   Abitbol, T., Kloser, E. & Gray, D. G. Estimation of the surface sulfur content of cellulose nanocrystals prepared by sulfuric acid hydrolysis. *Cellulose* **20**, 785–794 (2013).

53.   Cherhal, F., Cousin, F. & Capron, I. Influence of charge density and ionic strength on the aggregation process of cellulose nanocrystals in aqueous suspension, as revealed by small-angle neutron scattering. *Langmuir* **31**, 5596–5602 (2015).

54.   Mao, R. L. Van, Zhao, Q., Dima, G. & Petraccone, D. New Process for the Acid-Catalyzed Conversion of Cellulosic Biomass (AC3B) into Alkyl Levulinates and Other Esters Using a Unique One-Pot System of Reaction and Product Extraction. *Catal. Letters* **141**, 271–276 (2011).

55.   Revol, J.-F., Bradford, H., Giasson, J., Marchessault, R. H. & Gray, D. G.

Helicoidal self-ordering of cellulose microfibrils in aqueous suspension. *Int. J. Biol. Macromol.* **14**, 170–172 (1992).

56. Cherif, M., Mgaidi, A., Ammar, N., Vallée, G. & Fürst, W. A New Investigation of Aqueous Orthophosphoric Acid Speciation Using Raman Spectroscopy. *J. Solution Chem.* **29**, 255–269 (2000).

57. Mesmer, R. E. & Baes, C. F. Phosphoric acid dissociation equilibria in aqueous solutions to 300 C. *J. Solution Chem.* **3**, 307–322 (1974).

58. Elmore, K. L., Hatfield, J. D., Dunn, R. L. & Jones, A. D. Dissociation of Phosphoric Acid Solutions at 25°1. *J. Phys. Chem.* **69**, 3520–3525 (1965).

Appendix 4

a)

b)
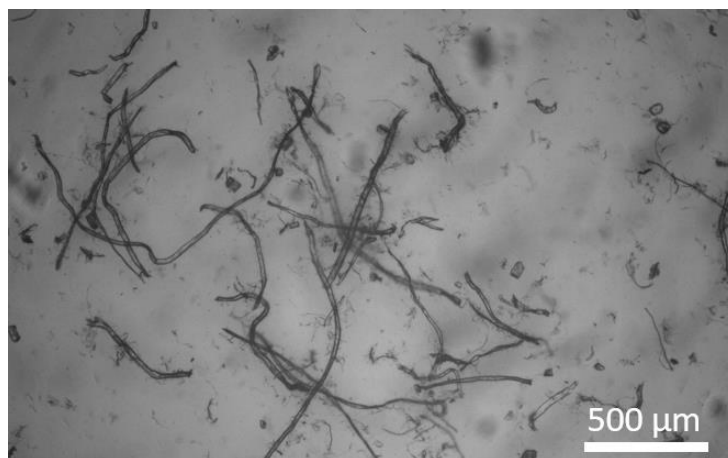
Figure A4.1. (a) Pulp made by blending 2g of Whatman ashless filter aid with 100 mL Milli-Q water and (b) fibers in pulp, which have macroscale diameters (4x magnification).
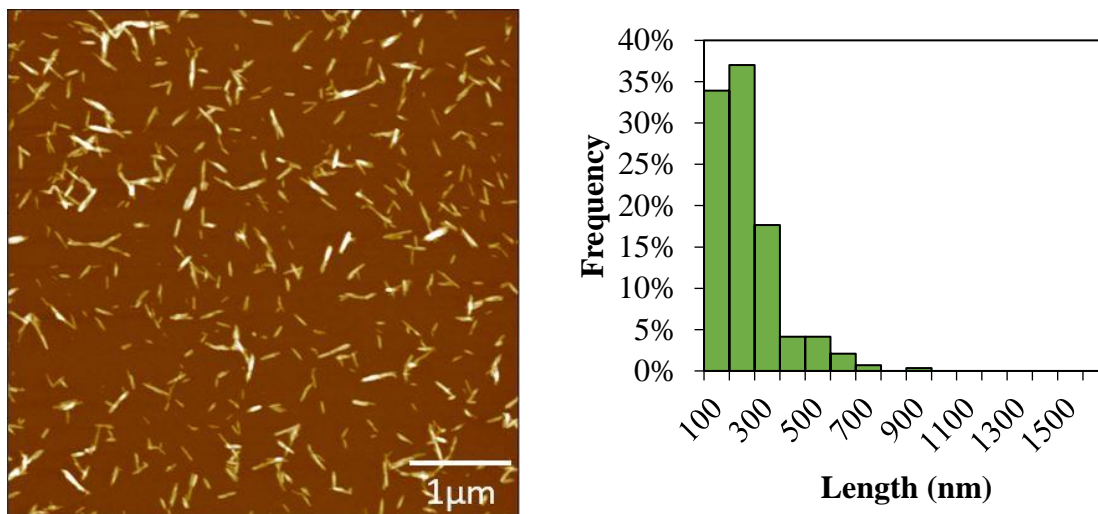
Average particle length by manually measuring individual S-CNCs: 127±55 nm

Median S-CNC particle length determined using Asylum Research Igor Pro software particle analysis tool: 127 nm

Figure A4.2. Comparison of CNC length obtained by manually selecting and measuring length vs. using the automated particle sizing software (for sulfuric acid hydrolysed CNCs).

Table A4.1. Phosphate content, dimensions and calculated surface charge density (assuming CNCs are cylindrical in shape with a density of 1.6 g/mL) of CNCs hydrolysed with phosphoric acid at varying hydrolysis conditions.

Sample	x_1 (min)	x_2 (°C)	x_3 (wt%)	Phosphate Content (mmol /kg CNC)	Median Particle Length (nm)	Median Particle Height (nm)	Surface Charge Density (e/nm^2)
80-100-70	80	100	70	15±2	475	7.5	0.027±0.004
80-120-70	80	120	70	31±1	284	6.7	0.049±0.002
80-100-75	80	100	75	8±1	312	7.1	0.014±0.002
80-120-75	80	120	75	13±3	238	4.9	0.015±0.004
100-110-72.5	100	110	72.5	13±1	325	7.2	0.022±0.002
120-100-70	120	100	70	10±1	391	6.5	0.016±0.002
120-120-70	120	120	70	44±2	268	7.2	0.075±0.003
120-100-75	120	100	75	18±11	315	6.7	0.03±0.02
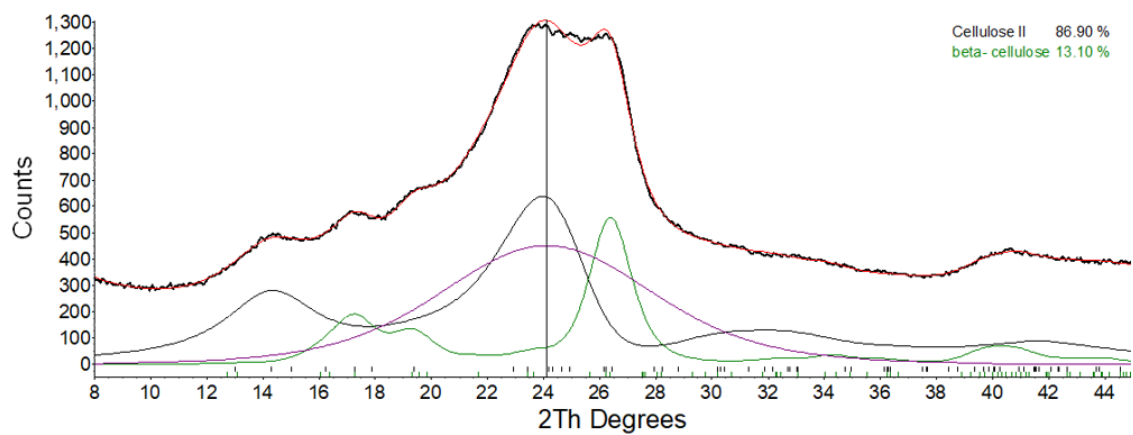
Figure A4.3. X-Ray Diffractometry profile for ample 120-120-75
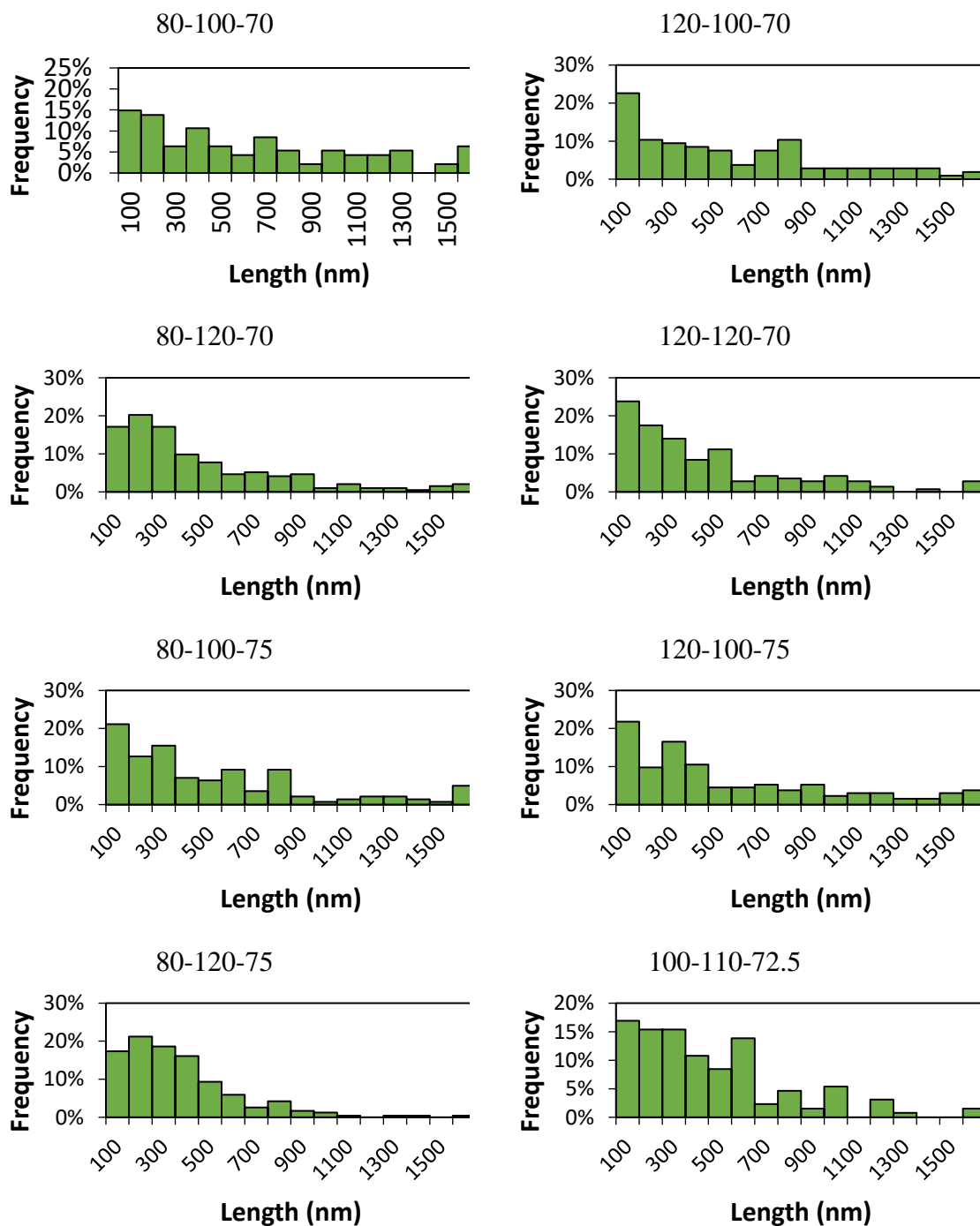
Figure A4.4. Particle length distributions for CNCs hydrolysed with phosphoric acids with varying hydrolysis times, temperatures and acid concentrations (labelled above each histogram), measured using the automated Asylum Research Igor Pro sizing software on >100 particles from multiple AFM height images (similar to those shown in Figure 4.1).
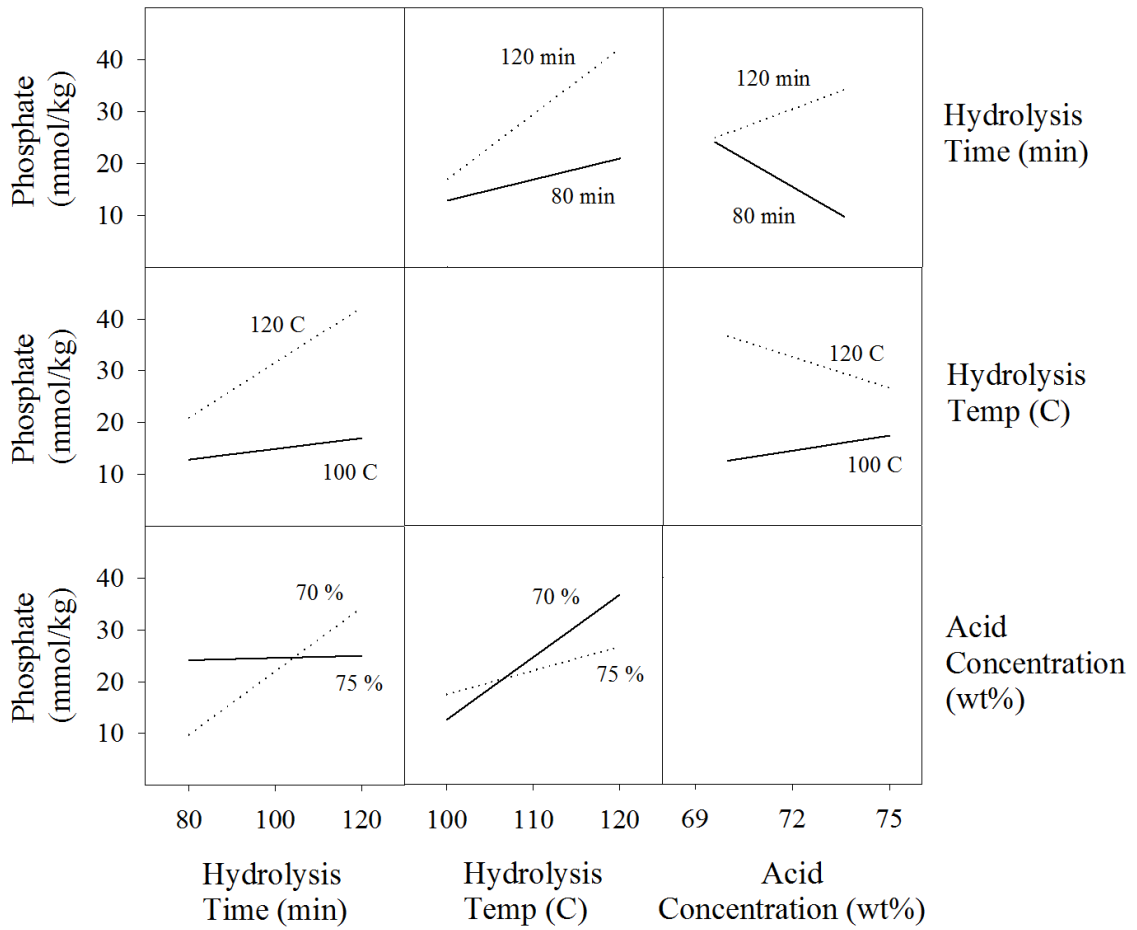
Figure A4.5. Factor interaction profiles describing the interactions of two hydrolysis parameters and their combined effects on CNC phosphate content.
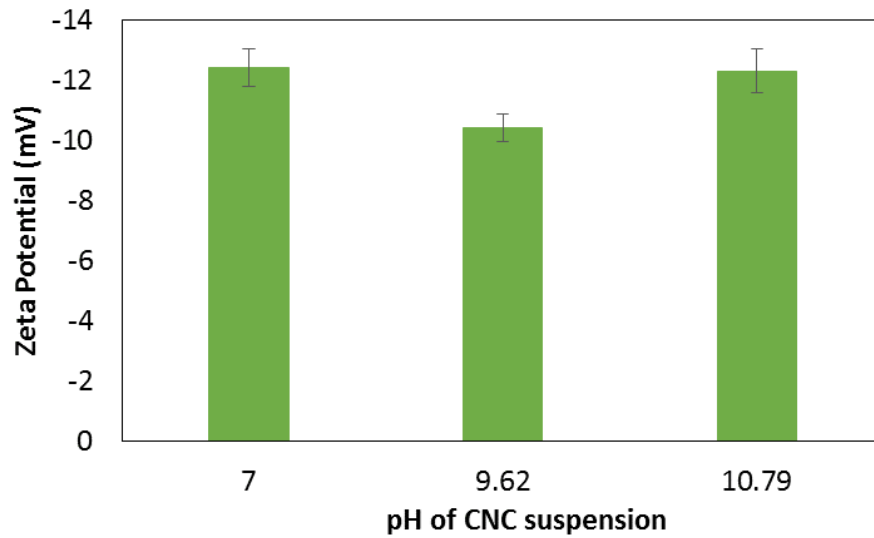
Figure A4.6. Zeta potential of 120-120-70 CNCs at pH above and below the second pK_a of phosphoric acid (7.2).
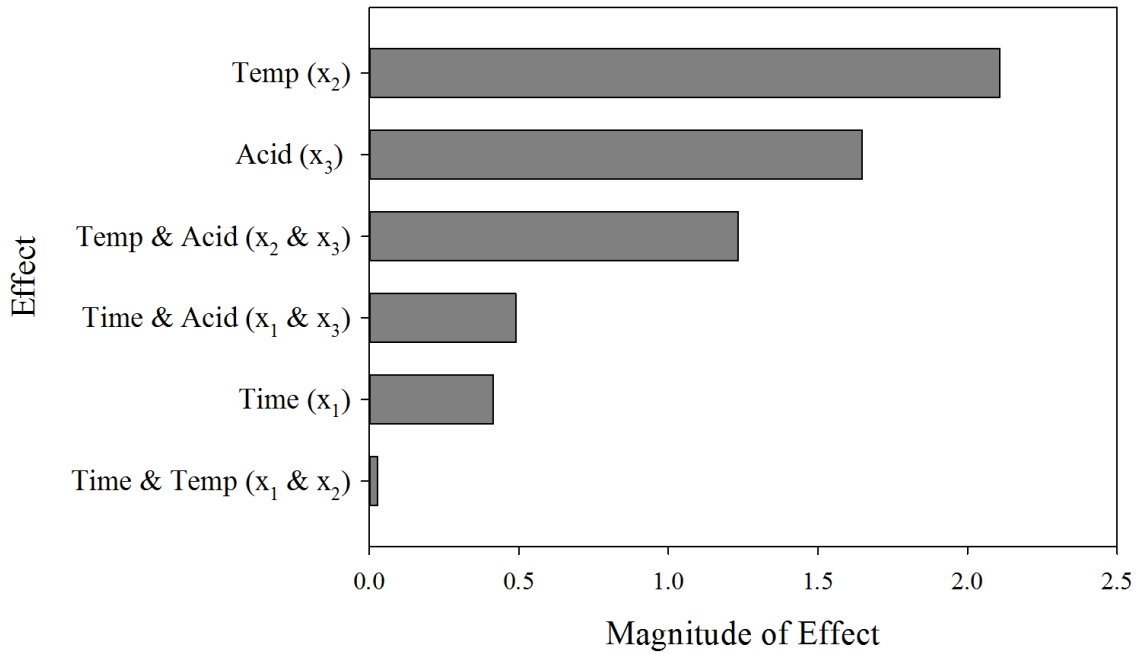
Figure A4.7. Coefficients for the parameters in a model predicting CNC zeta potential. Dark grey bars indicate negative coefficients.
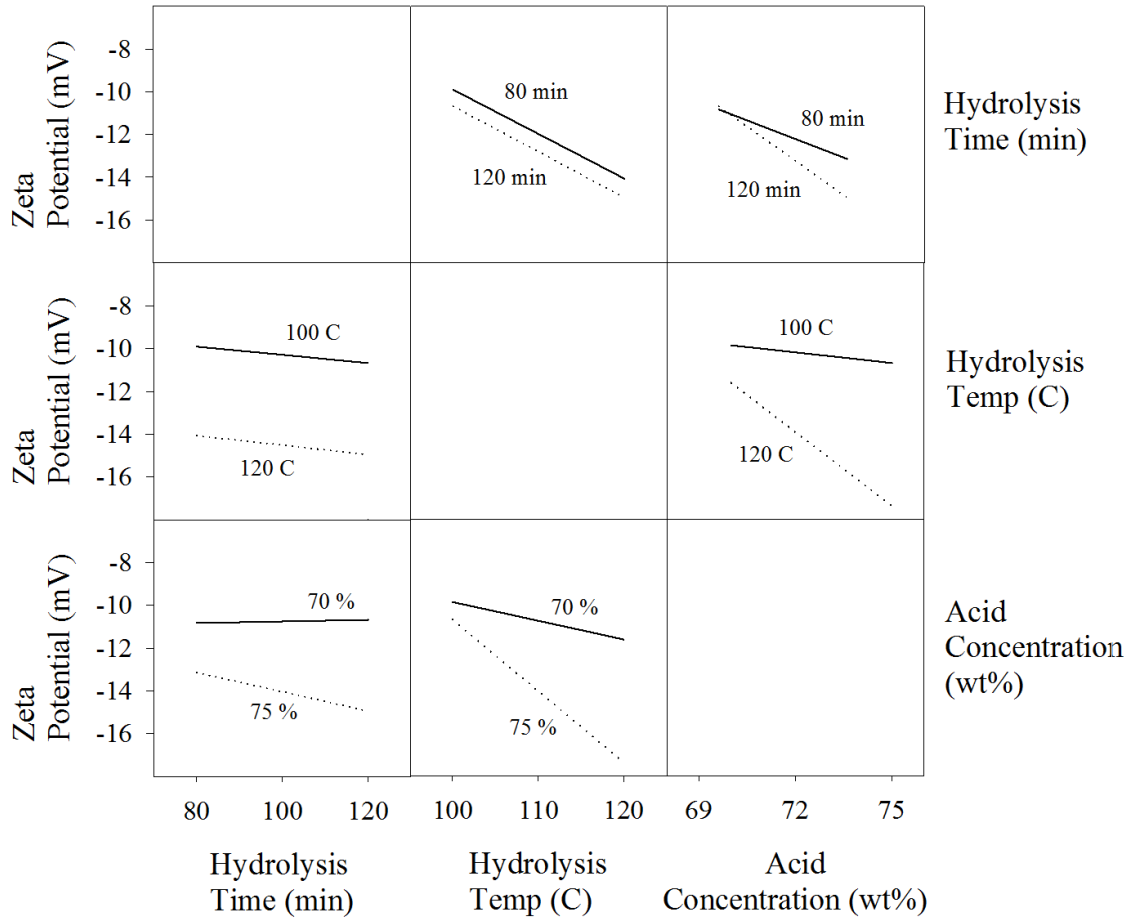
Figure A4.8. Factor interaction profiles describing the interactions of two hydrolysis parameters and their combined effects on CNC zeta potential.

Chapter 5

Tuning physicochemical properties of cellulose nanocrystals through an in-situ oligosaccharide surface modification method

_____

This chapter presents a highly tunable surface modification method which can be easily implemented into industrial CNC production processes and does not require extensive purifications or reaction steps. As such, this method is capable of further tuning the properties of industrially produced CNCs, and therefore has the potential to add to the range of CNC properties presented in Chapter 3. Furthermore, this method adds phosphate groups onto CNC surfaces (via deposition of cellulose phosphate oligosaccharides) without sacrificing CNC colloidal stability or dispersibility.

In this work, I led the project conceptualization and experimental planning jointly with Dr. Elina Niinivaara. Together, we optimized the surface modification method, prepared the oligosaccharides and CNC samples, performed rheological measurements, and solubilised the cellulose samples for gel permeation chromatography. I carried out conductometric titrations, atomic force microscopy, and thermogravimetric analysis. Dr. Elina Niinivaara carried out zeta potential and DLS measurements, quartz crystal microgravimetry, and particle size analysis. Elemental analysis and X-Ray diffraction measurements were performed by technicians. Dr. Elina Niinivaara and I jointly analysed the resulting data and prepared the manuscript with editorial assistance from Dr. Emily Cranston and Dr. Eero Kontturi. This chapter has been submitted to *Biomacromolecules* for publication.

Niinivaara, E.,[‡] Vanderfleet, O.M.,[‡] Kontturi, E., Cranston, E.D., "Tuning physicochemical properties of cellulose nanocrystals through an *in-situ* surface modification method", *Biomacromolecules,* submitted.

[‡]These authors contributed equally.
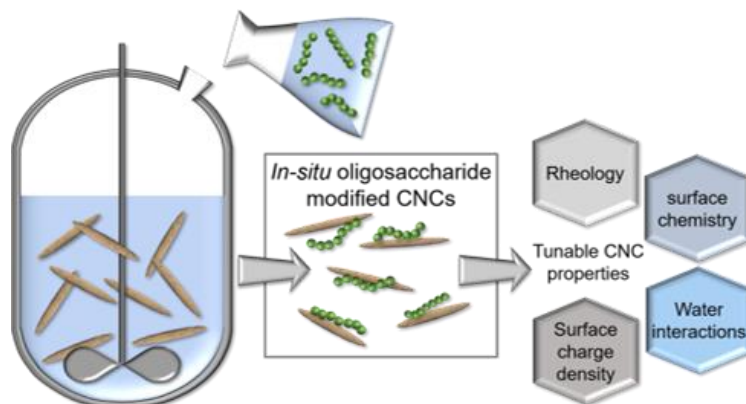
5.1 Abstract

The necessity to replace petroleum-based products with sustainable alternatives has shifted research efforts towards plant-based materials such as cellulose nanocrystals (CNCs). CNCs show promise in numerous applications (e.g., composites and rheological modifiers), however, maximizing their performance often requires surface modifications with complex chemistries and purification steps. Presented here is a novel surface modification method which tunes CNC properties through the *in-situ* deposition of cellulose phosphate oligosaccharides during CNC production. This was achieved by leveraging the selective solubility of oligosaccharides, which are soluble at low pH (during the CNC hydrolysis) yet become insoluble and precipitate onto CNC surfaces upon increasing pH during quenching. Oligosaccharide-coated CNCs demonstrated higher surface charge densities, and lower water adsorption capacities and viscosities than their unmodified counterparts. CNC surface coverage was tuned by controlling oligosaccharide degree of polymerization. Overall, this fundamental study introduces an easily scalable modification route that opens the door for expanded CNC functionality and applications.

5.2 Introduction

Advanced materials incorporating plant-based cellulose nanocrystals (CNCs) are at the forefront of current research efforts for greener and more sustainable solutions.[1–3] CNCs have been proposed in a wide range of application suites including biomedical devices,[4,5] adhesives,[6–14] food/cosmetics,[15–20] composites,[21,22] electronics,[23] and oil and gas extraction fluids.[24–26] However, the full potential of CNCs in many targeted applications has yet to be realized. The hygroscopic nature of cellulose impairs the wet strength of CNC-based materials, and the incompatibility of CNCs with non-polar solvents and polymers is a significant drawback in designing functional materials. Furthermore, the sensitivity of CNC colloidal stability to factors such as ionic strength, heat and other chemicals limits their usage in many liquid formulated products. Fortunately, however, various CNC surface modification methods have been proposed to circumvent these issues, including new production routes[27] and numerous chemistries to improve CNC steric stability[28–32] and alter their surface wettability.[33–38]

Although many of the reported CNC surface modification methods are efficient in overcoming the aforementioned challenges, they often involve complex synthetic solutions

based on harsh, environmentally detrimental solvents and reagents, and lengthy purification steps. Demonstrated here is a previously unreported CNC surface modification route, whereby oligosaccharide precipitation modifies CNCs *in-situ* during the acid hydrolysis production process. This modification method takes advantage of the existing variations in pH during the cellulose hydrolysis to alter oligosaccharide solubility; thereby eliminating the need for the use of additional chemicals.

Oligosaccharides can be tailor-made to tune the performance and processability of CNCs by altering the surface chemistry and charge density (colloidal stability), molecular weight (M) distribution, thermal stability, water binding capacity, and suspension viscosity of the CNCs. Herein we demonstrate the potential of this modification method using cellulose phosphate oligosaccharides of varying degree of polymerization (DP) and degree of substitution (DS) to modify CNCs. Moreover, this proof-of-concept study suggests that this modification method can be extended to further tune nanocellulose properties by utilizing oligosaccharides with targeted functionalities.

From a commercialization perspective, this novel *in-situ* CNC surface modification method is easily scalable and requires only those processes already available in the industrial production of CNCs.[27,39,40] The production of oligosaccharides from cellulosic materials would not require the implementation of any harsher chemicals than those already used in general cellulose research (and the pulp and paper industry), and the *in-situ* nature of this modification method would allow it to be easily implemented in CNC manufacturing facilities, without alterations to the existing production lines.

5.3 Materials and methods

Materials. Whatman ashless filter-aid and Whatman glass microfiber filter paper (GF/B and GF/D) were purchased from GE Healthcare Life Sciences Canada. The following chemicals and consumables were purchased from Sigma-Aldrich (Canada): Avicel PH-101 microcrystalline cellulose, Cellulose membrane dialysis tubing (14 kDa cut-off), 85 wt% H_3PO_4, 96 wt% H_2SO_4, NaCl, D_2O (99.9 Atom % D), NaOH, 30 % H_2O_2, DMSO, methanol and phenyl isocyanate (> 98%). Poly(allylamine hydrochloride) (PAH) (M: 120 000 – 200 000 g mol^{-1}) was purchased from PolySciences (PA, USA) and used as received. All water used was MilliQ grade (Barnstead™ GenPure™ Pro, Thermo Fisher Scientific, Waltham, USA) with a resistivity of 18.2 MΩ·cm (referred to henceforth as 'purified water').

Oligosaccharide preparation. Oligosaccharides were prepared through a H_3PO_4 hydrolysis of microcrystalline cellulose as previously reported by Bouchard et al..[41] First, 48 g of microcrystalline cellulose (MCC) (Avicel PH-101) was wetted with 35 mL purified water, and the mixture was then added to 900 mL of 85 wt% H_3PO_4. After 18 h, the mixture was filtered using GF/B grade glass fibre filter paper to remove any inaccessible cellulose fragments. Aliquots of 300 mL were taken at two ($Oligo_2$), four ($Oligo_4$), and six ($Oligo_6$) week intervals. Each aliquot was filtered using a Buchner funnel with a GF/D grade glass fibre filter paper to remove any un-hydrolyzed cellulose. Next, 900 mL of purified water was added to the oligosaccharide solution to precipitate the oligosaccharides, and the water

was then removed via filtration with a Buchner funnel and GF/B grade glass fibre filter paper. The precipitated oligosaccharides were collected and diluted with purified water. The suspensions were then placed into cellulose membrane dialysis tubing and dialyzed against purified water to remove any residual acid.

CNC preparation. Control CNCs (CNC$_{65}$) were isolated from Whatman ashless filter-aid through a H$_2$SO$_4$ hydrolysis. A thoroughly optimized procedure was used;[42] however, the temperature was increased to 65°C to avoid the production of non water-soluble oligosaccharide by-products.[41] First, 10 g of Whatman ashless filter-aid was finely ground using a compact blender and dried at 80°C overnight. Next, 175 mL of 64 wt% H$_2$SO$_4$ was heated to 65°C and added to the ground filter-aid. The hydrolysis reaction was carried out for 45 min at 65°C with constant mechanical stirring. To quench the hydrolysis reaction, the CNC-acid slurry was diluted with 2 L of ice-cold water (i.e., a ten-fold dilution). The suspension was left to sediment for ca. 30 min, and the supernatant was decanted. The CNCs were cleansed of the remaining acid through multiple rinses with purified water and subsequent centrifugations (10 min, 6000 rpm) in a Sorvall RC-5 Superspeed Refrigerated centrifuge (Dupont). Centrifugation was performed until the CNCs no longer sedimented and remained colloidally stable in suspension. The CNC suspensions were then dialyzed in cellulose membrane dialysis tubing against purified water to remove any residual acid. Once the pH of the CNC suspension had stabilized (to pH 5.5), the suspensions were sonicated (Sonifier 450 Probe Sonicator, Branson Ultrasonics, Connecticut, USA) to ensure proper CNC dispersion; 1 L of CNC suspension was sonicated at a time, and each sonication was carried out for 15 min at 60 % output in an ice bath. Finally, the sonicated samples were filtered using a glass microfiber filter (pore size 1 µm) to remove any metal contaminants from the sonicator probe. A portion of the CNCs were converted from their native acid form (H$^+$ counterion) to their sodium form (Na$^+$ counterion) by neutralizing the CNC suspension (to pH 7) through the addition of NaOH. Unless otherwise mentioned, all characterization was carried out on CNCs in their acid form.

Oligosaccharide precipitation onto CNCs. Surface modification of CNCs through oligosaccharide precipitation was carried out *in-situ* as part of the CNC hydrolysis (Figure 5.1). As such, the reaction conditions, quenching, and purification for the surface modified CNCs are all as described previously in the '*CNC preparation*' section. The only modification to the reaction was the addition of the oligosaccharides in the final stages of the CNC hydrolysis. At the 40 min time mark of the hydrolysis, 1 g of oligosaccharides was dissolved in 33 mL 64 wt% H$_2$SO$_4$ at room temperature by bath sonicating the mixture for 3 min. At the 44 min time mark, the 3 wt% oligosaccharide solution was added to the hydrolysis mixture. As such, the original mass ratio of oligosaccharides to cellulose (i.e., Whatman filter aid) was 1:10; however, CNC hydrolysis yields are generally in the range of 20-75 %.[43–45] Due to the high temperature of our CNC hydrolysis (i.e., 65°C), we predicted a yield on the lower end of this range, and therefore anticipated a final oligosaccharide to CNC ratio between 1:2 and 1:5. Continuous mixing during the hydrolysis ensured that the oligosaccharide solution was homogeneously incorporated throughout the hydrolysis mixture. The mixture was then quenched with a ten-fold volume of water to halt the hydrolysis reaction; the sudden change in pH precipitated any non

water-soluble oligosaccharides.[41,46,47] While precipitation onto the CNC surfaces is likely a result of the availability of the large specific surface area of CNCs, the natural affinity of the oligosaccharides to the chemically similar CNCs results in their irreversible deposition onto the CNC surfaces.[46,48,49] This was repeated separately for each oligosaccharide type to yield CNCs modified with "high DP" (CNC_{65}-$Oligo_2$), "medium DP" (CNC_{65}-$Oligo_4$) and "low DP" (CNC_{65}-$Oligo_6$) oligosaccharides.
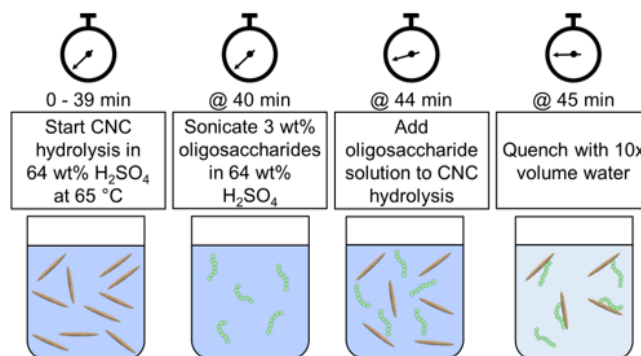
Figure 5.1. Schematic representation of the in-situ CNC surface modification through oligosaccharide precipitation, where the externally produced oligosaccharides are dissolved into 64 wt% H_2SO_4 in a separate beaker, and then added to the CNC hydrolysis mixture prior to quenching.

Redispersing freeze-dried CNCs. CNC suspensions (1 wt%) were prepared by adding freeze-dried CNCs (in their sodium form) to purified water and stirred overnight on a magnetic stir plate. The suspension was then sonicated (Sonifier 450 Probe Sonicator, Branson Ultrasonics, Connecticut, USA) for a total of 150 sec (with 30 sec sonication followed by 30 sec rest for 5 min) at 60% output, to ensure proper CNC dispersion. Sonication was carried out in an ice bath to prevent the CNC suspension from over heating. Finally, the sonicated samples were filtered using a glass microfiber filter (pore size 1 µm) to remove any metal contaminants from the sonicator probe. The re-dispersed CNC suspensions were used to prepare all of the spin coated samples as described below.

Oligosaccharide degradation during hydrolysis. An additional hydrolysis test was done to ensure that the oligosaccharides did not undergo substantial degradation when dissolved and added to the hydrolysis mixture. First, 1 g of oligosaccharides was dissolved in 33 mL 64 wt% H_2SO_4 at room temperature by bath sonicating the mixture for 3 min, followed by a 1 min "reaction". After this, the oligosaccharide solution was quenched with 330 mL of purified water to precipitate the oligosaccharides. The mixture was then filtered with a Buchner funnel and GF/B grade glass fibre filter paper. The precipitated oligosaccharides (here on referred to as S-$Oligo_x$) were collected and diluted with purified water. The suspensions were then placed into cellulose membrane dialysis tubing and dialyzed against purified water to remove any residual acid.

Conductometric titration. Conductometric titrations were carried out to determine the total surface charge of the CNCs. Dilute CNC suspensions were titrated against a 10 mM standardized NaOH using 250 µL increments. Prior to titrating, 0.2 mL of 200 mM NaCl

was added to the suspension to increase conductivity to a measurable value. Changes in pH and conductivity were monitored simultaneously, and volume corrected conductivity was plotted as a function of volume of NaOH added. The equivalence point of the curve was used to determine CNC surface charge.

Zeta (ζ) potential and dynamic light scattering (DLS). ζ-potential and apparent particle size were determined using a Zetasizer Nano-ZS (Malvern Panalytical, Malvern, UK). The electrophoretic mobility of 0.25 wt% CNC suspensions with 5 mM salt were measured using a Folded Capillary Zeta Cell (Malvern Panalytical, Malvern, UK). Electrophoretic mobility was converted to ζ-potential according to the Smoluchowski theory.[50] DLS measurements were carried out on 0.025 wt% CNC suspensions (no added salt) using polystyrene cuvettes. The measured diffusion coefficient was converted to apparent size using the Stokes-Einstein equation with the assumption that the CNCs are spherical,[51] thereby resulting in merely relative quantities.

Atomic force microscopy (AFM). AFM was used to analyse the size of the CNCs (in their sodium form). First, ca. 1 cm × 1 cm pieces of silica wafer (Purewafer, California, USA) were cleaned using an acidic piranha solution (three parts 96 wt% H_2SO_4: one part 30 % H_2O_2). The silica wafer was then spin-coated at 3000 rpm for 30 sec with an acceleration of 2300 s^{-1} (SPS 150 spin coater, SPS-Europe, Putten, Gerderland, Netherlands) using a 0.1 wt% PAH solution followed by a rinse with purified water. The cationic charge of the PAH adlayer ensures an even distribution of individual CNCs on the substrate upon spin coating.[39,52] Finally, 0.01 wt% CNC suspension was spin coated onto the PAH coated silica substrate (3000 rpm, 2300 s^{-1}, 30 sec). AFM images were acquired using a MFP-3D AFM (Asylum Research, California, USA) in tapping mode. FMR cantilevers (Asylum Research, California, USA) with a nominal force constant of 2.8 ± 0.7 N m^{-1} and resonance frequency of 75 ± 15 Hz were used for imaging. All images were baseline corrected using a standard third order polynomial flattening using the Asylum Research software v. 13.17. Particle size analysis was carried out on flattened AFM images using Gwyddion freeware with a minimum sample size of 100 particles.

AFM was also used to measure the thickness of the spin coated CNC films. Each film was scratched with a fine needle, and the AFM cantilever was then positioned at the edge of the scratch using the optical microscope on the AFM set up. A 15 µm × 15 µm image was taken across the edge of the scratch to show the exposed substrate and the surface of the CNC film. The section tool of the Asylum Research v. 13.17 software was used to measure the height difference between the exposed substrate at the surface of the CNC film. Thicknesses reported are an average of 3 separate measurements on 2 scratches (i.e., a total of 6 film thickness analyses).

Microgravimetry. Quartz crystal microbalance with dissipation monitoring (QCM-D) (QSense Analyzer, Biolin Scientific, Gothenburg, Sweden) was used to quantify the mass of bound water in spin coated CNC (in their sodium form) thin films by using a water/D_2O solvent exchange protocol.[53] Thin films were prepared on silicon dioxide coated quartz crystal sensors (Biolin Scientific, Gothenburg, Sweden), which were first cleaned using dry N_2 followed by 15 min inside a UV Ozone Cleaner - ProCleaner™ (BioForce

Nanosciences). CNC thin films were deposited by spin coating (SPS 150 spin coater, SPS-Europe, Putten, Gerderland, Netherlands) 1 wt% CNC suspensions at 3000 rpm for 60 sec with an acceleration of 2300 s^{-1}. The CNC films were then annealed overnight in an oven at 80°C.

Prior to running the water/D$_2$O exchange measurements, the CNC coated sensors were placed in the measurement chambers and were equilibrated overnight under a constant flow of purified water (0.2 µL min^{-1}). Solvent exchange measurements were conducted by passing purified water through the measurement chamber for 20 min, followed by 20 min of deuterium oxide and then finally 20 min of purified water (all at a flow rate of 0.1 mL min^{-1}). The temperature was kept constant at 25°C throughout the measurement. Changes in the resonance frequency (Δf) and dissipation of resonance (ΔD) of the sensor were collected simultaneously throughout the duration of the measurement.

The amount of bound surface water (Γ_{H_2O}) was calculated according to the Sauerbrey equation:

$$\Gamma_{H2O} = - C \left(\frac{\Delta f}{n}\right)_{film,H_2O} \tag{1}$$

Where C is the sensitivity constant of the sensor (0.177 mg m^{-2} Hz^{-1}), n is the measurement harmonic (n = 1, 3, 5, 7…) (here we have analyzed the 3rd harmonic), and $\Delta f/n_{film,H_2O}$ is as follows:

$$\frac{\Delta f}{n}_{film,H_2O} = \left(\frac{\left(\frac{\Delta f}{n}\right)_{film} - \left(\frac{\Delta f}{n}\right)_{bare\ substrate}}{\left(\frac{\rho_{D_2O}}{\rho_{H_2O}}\right)-1}\right) \tag{2}$$

where $\Delta f/n_{film}$ is the measured change in resonance frequency of the CNC film due to the solvent exchange, $\Delta f/n_{bare\ substrate}$ is the measured change in resonance frequency of a pristine SiO$_2$ coated QCM-D sensor (-54 Hz) due to a H$_2$O/D$_2$O solvent exchange, ρ_{D_2O} the density of D$_2$O (1.104 g cm^{-3} at 25°C) and ρ_{H_2O} the density of water (0.977 g cm^{-3} at 25°C). Γ_{H_2O} was normalized to the thickness of the CNC film as measured using AFM). Normalization is important here, as previous works have demonstrated that water uptake capacity (as measured through QCM-D) is highly dependent on film thickness.[53]

Degree of polymerization (DP) and gel permeation chromatography (GPC). Due to the insolubility of both the oligosaccharides and CNCs in common solvents, a carbanilation derivatization was performed to render the samples soluble in DMSO. The carbanilation was carried out as described elsewhere with conditions optimized for a full phenyl isocyanate substitution (i.e., degree of substitution (DS) of 3) and minimal cellulose degradation.[41] To begin, the samples were dried for 1 h at 80°C to remove any residual moisture. 25 mg of each dried samples was combined with 10 mL DMSO and 1 mL phenyl isocyanate and shaken by hand. The reaction vials were placed into a 70°C oil bath, and the reaction was allowed to progress for 40 h. To ensure a homogeneous derivatization, the vials were shaken by hand every 5 – 10 h. The reaction was terminated by quenching with

2 mL of methanol. Finally, the reaction vials were left open in a fumehood to allow excess methanol to evaporate. The carbanilated samples were filtered prior to GPC measurements using a 0.45 µm pore size syringe filter (Chromatographic Specialties Inc. Brockville, Canada). The concentration of carbanilated samples was 2.5 cellulose g per L DMSO. GPC measurements were performed on an Agilent 1100 GPC (Agilent Technologies, CA, USA) equipped with an autoloader, with a DMSO and 5 % LiBr elution solvent flowing at a rate of 0.5 mL min^{-1}. Samples were analysed using a Wyatt Optilab T-Rex refractive index detector (Wyatt Technologies, CA, USA) with a wavelength of 785 nm at 35°C. Molecular weight of the samples were processed using Wyatt ASTRA 6.0 software (Wyatt Technologies, CA, USA) calibrated with polystyrene sulfonate standards of varying molecular weight (0.891, 2, 4.29, 10, 29.5 and 140 kDa). Weight average degree of polymerization (DP_w) values were based on the assumption of a complete substitution of the anhydroglucose unit (AGU), and calculated by dividing the weight average molecular weight (M_w) of each sample by the molecular weight of a tricarbanilated AGU (519 g mol^{-1}).

Thermal analysis. Thermogravimetric analysis (TGA) was performed to assess CNC thermal stability. The measurements were performed on a Simultaneous Thermal Analyzer (STA) 6000 (PerkinElmer, MA, USA) on freeze-dried CNCs in their sodium form. TGA samples were prepared by compressing 8 ± 2 mg CNC powder between two rubber plunging heads in a 1 mL plastic syringe. The resulting CNC pellets should have similar dimensions and surface area, ensuring comparable results.[54] The pellet was placed in the TGA instrument pan and loaded into the nitrogen filled measurement chamber. The temperature within the chamber was increased from ambient temperature to 600°C at a rate of 10°C min^{-1}, and measurements were carried out under an argon blanket.

Elemental analysis. Elemental analysis was performed for all samples by the Xerox Research Centre of Canada with a Thermo Scientific ICAP 6500 inductively coupled plasma—optical emission spectrometry (ICP-OES) system. Measurements were done by placing 50–60 mg of sample into a Teflon digestion tube with a few drops of purified water, 1 mL of hydrofluoric acid and 6 mL of a 60 – 70 wt% nitric acid solution. The samples were then digested using a Milestone UltraWAVE Digestion System after which they were diluted in purified water to a volume of 25 mL for ICP-OES analysis.

X-ray diffraction. X-ray diffraction (XRD) was used to analyse the crystallinity index of the oligosaccharide and CNC samples. All samples were measured on freeze-dried powders (in their sodium form) and were prepped for XRD by compressing pellets of ca. 10 mg of sample between two rubber plunging heads in a 1 mL plastic syringe. The pellets were then mounted onto a silicon wafer, and positioned using a vertical D8 h-h goniometer. Measurements were carried out using an electron beam with a 1.79026 Å wavelength, acceleration voltage of 35 kV and a probe current of 45 mA emitted from a sealed cobalt. The beam was focused using a 0.5 mm micro slit and a 0.5 mm short collimator. Two-dimensional frames at a detector distance of 14 cm were collected using a Bruker D8 Discover diffractometer with Davinci Design and were then integrated with Diffrac.eva 4.0 to obtain one-dimensional frames (frames collected on an empty silicon wafer were

subtracted). A Rietveld refinement was used to match the measured diffractograms with models for both the crystalline and amorphous phases.[55,56] A Pseudo-Voigt function was used to model the amorphous phase, and its peak was manually fixed at 24.1° for all samples. The crystallinity index was determined as the contribution of the crystalline and amorphous peaks compared to the total diffraction spectrum of the sample. The measurement error is taken to be ca. ± 5%.

Rheology. Rheological measurements were performed on 1 wt% CNC suspensions, redispersed from freeze-dried CNCs in their sodium form. The rheological measurements were all performed with a Discovery Hybrid Rheometer (HR-2, TA Instruments, New Castle, DE, USA) using a 1°/40 mm cone and plate system. Steady shear viscometry was performed between shear rates of 10 and 1000 s^{-1}.

5.4 Results and discussion

Phosphoric acid hydrolyzed oligosaccharides. Three oligosaccharides with varying properties were produced using a controlled H_3PO_4 hydrolysis of microcrystalline cellulose (MCC). This was achieved by increasing hydrolysis time in two week increments from two to six weeks, as indicated by x in the oligosaccharide nomenclature 'Oligo$_x$'. Table 5.1 shows the properties of these oligosaccharides (i.e., short cellulose phosphates), which were later used to modify CNC surfaces. Unsurprisingly, an increased hydrolysis time lead to a decrease in oligosaccharide molecular weight.[57] After two weeks of hydrolysis, the MCC source material (starting $DP_w = 480$)[58] had gone through 47 scissions per cellulose chain (no. of scissions = $DP_{w,MCC}/DP_{w,Oligo}$ - 1), resulting in oligosaccharides with an average DP_w of 10 (with a dispersity (Đ) of 6). Similarly, after four and six weeks, the number of scissions were 79 and 95, resulting in average DP_w values of 6 (Đ = 4) and 5 (Đ = 4), respectively. As such, this verifies that oligosaccharide chain lengths can be readily controlled through H_3PO_4 hydrolysis, albeit over long time periods.

Table 5.1. Physicochemical properties of oligosaccharides hydrolyzed through a controlled H_3PO_4 hydrolysis for 2, 4 and 6 weeks. The starting material for the hydrolyses was Avicel PH-101 MCC with a reported DP_w of 480 (ref. 58) GPC was used to determine oligosaccharide M_w, DP_w and Đ, phosphorus content and degree of substitution (DS) were determined through elemental analysis, and XRD was used to assess crystallinity.

	M_w, g mol^{-1}	Weight average degree of polymeriz-ation, DP_w	Đ	No. scissions per cellulose chain (from starting material)	Phosph-orus content, ppm	Oligosacc-haride phosphor us DS	Degree of Crystallinity, %
Oligo$_2$	5300	10	6	47	414	0.002	56
Oligo$_4$	3200	6	4	79	580	0.003	69
Oligo$_6$	2300	5	4	95	699	0.004	64

This control in molecular weight is a critical factor in the design of oligosaccharides as CNC surface modifiers. The main criterion for using oligosaccharides to modify CNC surfaces through the *in-situ* method presented here, is their selective solubility. The oligosaccharides used in this method should be soluble (and chemically stable) in concentrated acid, yet insoluble in mildly acidic and neutral aqueous environments. This selectivity allows the oligosaccharides to be incorporated as a solution into the CNC hydrolysis mixture, yet precipitate onto CNC surfaces in response to quenching, whereby cold water dilutes the mixture ten-fold and significantly increases its pH. Fortunately, the solubility of oligosaccharides is highly dependent on their DP,[59] and as such, control over their selective solubility is fairly straightforward.

Regardless of the hygroscopic nature of cellulosic materials, cellulose is in fact not soluble in water due to its supramolecular and amphiphilic structure.[60] However, a significant decrease in the DP of the cellulose chains will render the material water-soluble.[59] Previous works have shown that cellulose-based oligosaccharides become water-soluble at DP < 6.[57,61–64] On the other hand, oligosaccharide solubility in highly acidic conditions is less selective, and as such, higher DP oligosaccharides readily dissolve in concentrated acids.[41] While the DP_w values for $Oligo_4$ and $Oligo_6$ are similar to that considered water-soluble (DP ≈ 6) (Table 5.1), they did indeed visually precipitate from a 64 wt% H_2SO_4 solution when diluted 10-fold with water. It is likely that the reported DP_w values here are slightly underestimated, due to the assumption of full substitution of each AGU after the carbanilation (required to solubilize cellulose for GPC analysis).[41] Despite this, the oligosaccharides shown here meet the requirements for selective solubility: they are soluble in highly acidic solutions yet will precipitate upon extensive dilution. It should be noted however, that these oligosaccharides have limited solubility in some concentrations of H_2SO_4. The solubility of the "high DP" oligosaccharides ($Oligo_2$, $DP_w = 10$) was examined visually, and it was found that they were in fact insoluble in ca. 5 wt% H_2SO_4 (pH ≈ 0.3) and only soluble up to 3 wt% in 64 wt% H_2SO_4 (pH ≈ -1). An extensive solubility study was not deemed necessary for this proof-of-concept work, as the solubility of the highest DP oligosaccharide ($Oligo_2$) was the limiting factor in preparing oligosaccharide solutions.

In addition to controlling oligosaccharide DP, the H_3PO_4 hydrolysis time also affected the DS (and therefore charge content) of the oligosaccharides (Table 5.1). Elemental analysis showed a nearly 2-fold increase in phosphorus content from ca. 400 ppm for the $Oligo_2$ to ca. 700 ppm for $Oligo_6$. These phosphorus contents translated to DS values between 0.002 and 0.004. The production of oligosaccharides using H_3PO_4, without completely degrading the cellulose to individual sugars, is made possible by the low hydrolysis temperature and the weak nature of the acid.[57] As a result, however, the ability of the H_3PO_4 to esterify hydroxy groups is also limited, as shown by the relatively low phosphorus contents.

The effect of the H_3PO_4 hydrolysis on the crystal structure of oligosaccharides in dried powder form was also probed. XRD analysis revealed that all three oligosaccharides adopted the cellulose II crystal form when dried (Appendix 5, Figure A5.1). Typically, XRD diffractograms of perfect cellulose II crystals possess three distinct peaks at 12.3° (101 plane reflections), 20.1° (10$\bar{1}$ reflections) and 22.0° (002 reflections).[65–68] These three

distinct peaks are visible in the XRD diffractograms of the oligosaccharides presented here; however, their diffraction angles are all shifted toward higher angles by $2 - 3°$. Such shifts can occur from a tilt in the sample during measurements, possible misalignment from the sample calibration position, or due to potential stresses in the sample occurring as a result of sample preparation.[69] As such, despite the small shift in diffraction angles, oligosaccharides precipitated on their own can be concluded to possess a cellulose II structure.

Native cellulose, including the MCC used to produce the oligosaccharides here, has a cellulose I crystal structure, meaning the cellulose chains run parallel to one another. This allomorph can be irreversibly altered to the more thermodynamically stable cellulose II structure, where the cellulose chains are anti-parallel.[60] Cellulose I readily converts to cellulose II by dissolution followed by precipitation (or regeneration) in an aqueous medium or through mercerization.[60] As shown here, recrystallization (after dissolution and subsequent precipitation) of the oligosaccharides resulted in a cellulose II crystal structure. Recrystallization of the oligosaccharides is likely facilitated by their extremely low DS. Tolonen et al. reported a similar finding when studying uncharged oligosaccharides precipitated from a super critical water hydrolysis.[62] As such, the H_3PO_4 hydrolysis demonstrated herein produced oligosaccharides with a cellulose II structure as well as tunable chain lengths and phosphorus contents. In the following sections, the physicochemical properties of CNCs modified *in-situ* using these oligosaccharides will be examined.

Naturally occurring oligosaccharides on CNC surfaces. It has been previously reported that CNCs produced under a range of conditions have naturally occurring, relatively low DP, oligosaccharides bound to their surface.[41,47] To demonstrate the effects of our CNC surface modification through controlled *in-situ* oligosaccharide precipitation (with externally produced oligosaccharides), CNCs with 'pristine' crystalline surfaces were used as the control sample. Therefore, we opted to use a higher than conventional hydrolysis temperature (65°C) to produce relatively oligosaccharide-free CNCs. The remaining hydrolysis parameters were consistent with the conventional H_2SO_4 hydrolysis protocol for the bench scale isolation of CNCs (i.e., 64 wt% H_2SO_4, a 1:30 cellulose-to-acid mass ratio, and a reaction time of 45 min).[42] The molecular weight distribution of the control CNCs (CNC$_{65}$) and that of CNCs prepared using the conventional hydrolysis temperature, 45°C (CNC$_{45}$), are distinctly different (Figure 5.2).
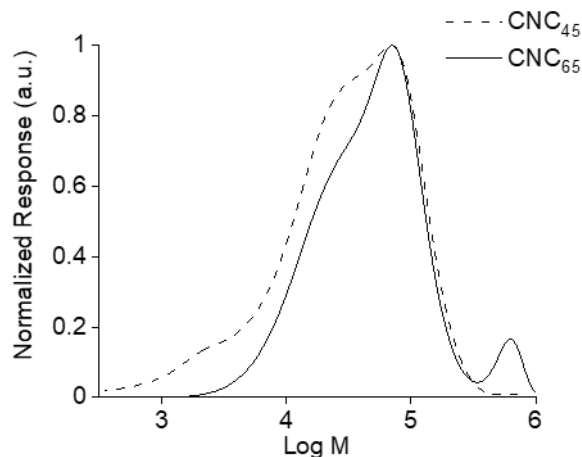
Figure 5.2. Molecular weight (M) distribution of the control CNCs (CNC$_{65}$) compared to that of CNCs hydrolyzed using a more conventional protocol (CNC$_{45}$) (64 wt% H$_2$SO$_4$, 45°C and 45 min).

The CNC$_{65}$ sample possessed a bimodal distribution with a primary maximum molecular weight of 71000 g mol^{-1} corresponding to a DP of 136 of the carbanilated sample. Conversely, the CNC$_{45}$ sample had a broader distribution shifted towards lower molecular weight with a similar primary peak at 71000 g mol^{-1} and an additional shoulder in the lower molecular weight range at ca. 3200 g mol^{-1} (corresponding to a DP of ca. 6); again, we believe the DP values presented here are underestimated (but can be compared relatively). Nevertheless, it is evident that the harsher hydrolysis conditions resulted in 'pristine' CNC surfaces void of detectable precipitated oligosaccharides. Additionally, we note that the increased hydrolysis temperature did not result in further degradation of the crystalline portion of the cellulose, and the CNC$_{65}$ sample was not hydrolyzed beyond the levelling-off degree of polymerization of cotton (i.e., DP 140 – 180).[70–72] On the contrary, the CNC$_{65}$ sample possesses a (highly reproducible) minor second peak at 630 000 g mol^{-1} indicating the presence of a small fraction of longer cellulose chains or undigested chain aggregates. Surprisingly (and somewhat inexplicably), this peak is not present in the CNC$_{45}$ sample, which was produced using weaker hydrolysis conditions. Regardless, the control sample (CNC$_{65}$) appears to be a useful substrate to demonstrate the feasibility of our proposed oligosaccharide surface modification method.

The conventional H$_2$SO$_4$ hydrolysis protocol for the bench scale isolation of CNCs has been optimized to maximize yield while ensuring a complete hydrolysis of accessible cellulose regions, and sufficient esterification of the cellulose surface hydroxy groups.[42–45,73–77] While this protocol has been extensively studied and is optimal in the production of 'standard' CNCs, the conditions are not always sufficiently harsh to fully degrade the oligosaccharides hydrolyzed out of the less ordered regions of cellulose into water-soluble oligosaccharides. As a result, unlike the control CNC$_{65}$ shown here, CNCs isolated using these conditions typically have a layer of bound "by-product" oligosaccharides on their surface (Figure 5.3).[41,46,47]

The presence of these naturally occurring "by-product" oligosaccharides has a distinct effect on the physicochemical properties of CNCs. For example, Bouchard et al. noted that the rheological behavior of CNC suspensions depends on their surface oligosaccharide content (from the "by-product" oligosaccharides).[41] They also demonstrated an increased resistance of suspension colloidal stability to ionic strength,[41] and changes in optical properties of self-assembled CNC films[41,78] with increasing oligosaccharide content. Furthermore, Labet and Thielemans showed that the presence of loosely bound oligosaccharides–along with other hydrolytic by-products–on CNC surfaces negatively affected the reproducibility of CNC surface functionalization with polymers, and required removal through Soxhlet extraction to improve said reproducibility.[47] As is evident from these works, the effects of surface oligosaccharides on CNC properties and performance is multifaceted.
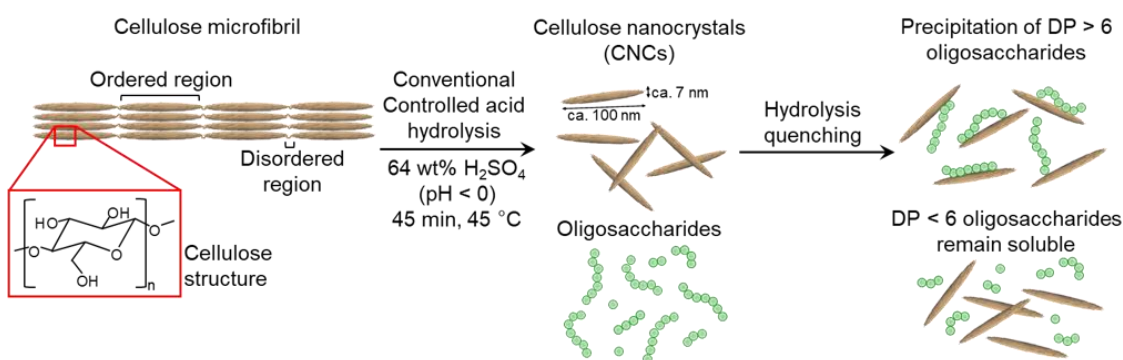
Figure 5.3. Structure of the cellulose AGU and a scheme representing the products of the conventional controlled acid hydrolysis of a cellulose microfibril to produce CNCs, and the precipitation of non-water-soluble oligosaccharides (hydrolysis by-products) onto the surface of CNCs as a result of quenching.

CNC surface modification through oligosaccharide precipitation. Figure 5.4 shows the molecular weight distributions of the control (CNC_{65}) and three CNC samples modified with oligosaccharides of varying DP and DS (CNC_{65}-$Oligo_2$, CNC_{65}-$Oligo_4$ and CNC_{65}-$Oligo_6$). There was a clear difference between the control and the modified samples: the control showed no peak in the oligosaccharide molecular weight range (i.e., log M = 3-4), whereas the modified samples had broader distributions with distinct shoulders in the lower molecular weight regime. In the modified samples, the primary peak (M = 71 000 g mol^{-1}) corresponds to the majority of the cellulose chains which make up the CNC structure, while the shoulders in the lower molecular weight range are associated with the presence of surface oligosaccharides.[41] As can also be seen in Figure 5.4, the structure of the CNC core did not change as a result of oligosaccharide precipitation, and the primary peak in the chromatogram of each modified sample resembled that of the control. For all three modified CNC samples, the molecular weight range of the oligosaccharide shoulder matched the molecular weight range of the oligosaccharides used to perform the surface modification (Figure 5.4 and Appendix 5, Figure A5.2).
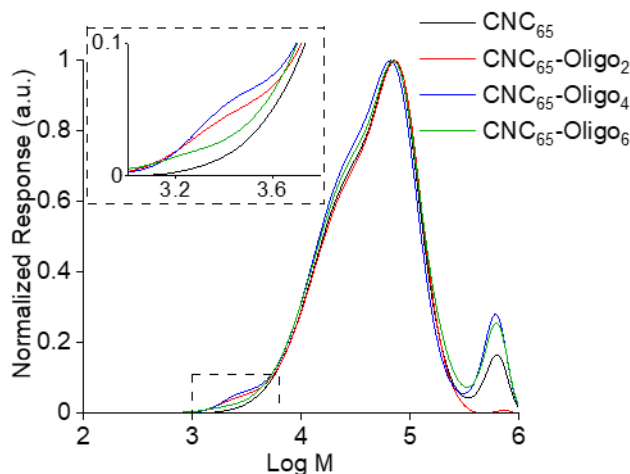
Figure 5.4. Molecular weight (M) distribution of control CNCs (CNC$_{65}$) and CNCs modified with oligosaccharides of varying DP and DS.

As seen in the inset of Figure 5.4, the relative intensity of the oligosaccharide shoulder was greatest for the Oligo$_4$ sample, suggesting the oligosaccharides with "medium DP" provided more CNC surface coverage. It is likely that the precipitation of Oligo$_2$ was sterically hindered due to their comparatively high DP. Conversely, it is possible that as a result of the significant dispersity in the DP$_w$ of the Oligo$_6$ sample, that the lowest DP portion of the material did not in fact precipitate upon quenching, and was removed upon purification, resulting in less available oligosaccharides to cover the CNC surface. Based on the relative intensities of the oligosaccharide peaks in Figure 5.4, CNCs modified with Oligo$_4$ achieved a surface coverage of ca. 84% (assuming single layer coverage) while the corresponding values for CNCs with Oligo$_2$ and Oligo$_6$ are 27 and 10%, respectively (Table 5.2 – see Appendix 5 for details and a sample calculation of CNC surface coverage, Tables A5.1 – A5.3). Overall, the presence of the low molecular weight shoulders in the GPC chromatogram is a clear indication of a successful CNC surface modification. Furthermore, the GPC chromatogram demonstrates the ability to tune CNC surface coverage by controlling oligosaccharide DP.

Table 5.2. Physicochemical properties of control CNCs (CNC$_{65}$) and CNCs modified with oligosaccharides of varying DP and DS. Sulfur and phosphorus contents were determined through elemental analysis, oligosaccharide surface coverage was estimated using M_w data and particle dimensions. Zeta potential and apparent size were measured based on light scattering (Zetasizer Nano-ZS), whereas surface charge of CNCs was determined using conductometric titrations. Water uptake capacity was measured by QCM-D, and normalized changes in resonance frequency were converted to mass of bound water (Normalized Γ_{H_2O}) in each sample and subsequently normalized by thin film thickness (as measured by AFM scratch height analysis). Also shown is the steady shear viscosity of each sample at 1 wt% at a shear rate of 100 s^{-1}.

	Oligosaccharide surface coverage on CNCs*, %	Apparent size by DLS, nm	Zeta potential, mV	Total surface charge, mmol/kg CNC	Sulfur, ppm	Phosphorus, ppm	Normalized Γ_{H_2O}, mg m^{-2} nm^{-1}	Viscosity, mPa·s (1 wt%, 100 s^{-1})
CNC$_{65}$	0	65 ±1	-38 ±1	221 ± 6	8034	0	4.5	0.92
CNC$_{65}$-Oligo$_2$	27	65 ±1	- 36 ±1	320 ±10	9496	24	2.9	0.82
CNC$_{65}$-Oligo$_4$	84	63 ±1	- 39 ±1	260 ± 2	7635	17	2.6	0.86
CNC$_{65}$-Oligo$_6$	10	65 ±1	- 37 ±1	240 ±10	8318	9	3.0	0.88

* See Appendix 5 for details on surface coverage calculation, Tables A5.1 – A5.3.

As mentioned, the selective solubility of the oligosaccharides is the most important parameter for this surface modification method, and the DP of oligosaccharides after exposure to both H$_3$PO$_4$ and H$_2$SO$_4$ must be understood. While the section above characterized oligosaccharides after H$_3$PO$_4$ hydrolysis, subjecting these low DP oligosaccharides to sulfuric acid (during the time required to dissolve and add the solution to the CNC mixture) could potentially further decrease DP and increase solubility outside of a usable range. To verify that exposure to concentrated H$_2$SO$_4$ did not degrade the oligosaccharides to a DP$_w$ below its starting value (Table 5.1), the molecular weight distributions of each sample were compared before and after four minutes of dissolution in 64 wt% H$_2$SO$_4$ (Appendix 5, Figure A5.3). Unexpectedly, regardless of their starting DP$_w$, the oligosaccharides did not undergo any further degradation when exposed to concentrated H$_2$SO$_4$ over the four minutes, as evidenced by the lack of change in their molecular weight distributions. While it is possible, as mentioned earlier, that the lowest molecular weight fragments of the oligosaccharides (particularly in the case of Oligo$_6$), may have been further degraded, GPC showed that the majority of each oligosaccharide sample retained a DP$_w$ above that reported for water-soluble oligosaccharides (Appendix 5, Table A5.4).

While no further significant degradation of the oligosaccharides was detected, the exposure to 64 wt% H_2SO_4 did impact the oligosaccharide chemistries and charge contents (Appendix 5, Table A5.4). Elemental analysis demonstrated the introduction of sulfur, assumed to be in the form of sulfate half esters. Furthermore, the resulting sulfur content far exceeded the original phosphorus content of the oligosaccharides. More than twice the amount of sulfur was introduced during four minutes of exposure to H_2SO_4 as phosphorus in a 6-week hydrolysis. Additionally, after dissolution in H_2SO_4, the phosphorus content of the oligosaccharides decreased. This could indicate that, upon contact with H_2SO_4, the pre-existing phosphate groups became protonated and underwent a nucleophilic substitution with a sulfate half ester. Alternatively, the highly acidic conditions may have prompted de-esterification of CNC phosphate groups.[79]

Despite the broader molecular weight distribution of the cellulose chains that makes up the CNCs after modification, the presence of an oligosaccharide surface layer does not noticeably increase the dimensions of CNCs as observed via AFM (Figure 5.5) or their apparent size and degree of dispersion in water, according to DLS (Table 5.2). Particle size analysis showed that there was no statistically significant difference in the dimensions of the control and modified CNCs (n = 100 particles, Appendix 5, Table A5.5). Additionally, each of the samples were representative of typical CNCs, with average lengths of ca. 200 nm and average cross-sections of ca. 8 nm, as previously reported for cotton-based CNCs.[39,40,80] The apparent size as well as CNC colloidal stability, were all similar (Table 5.2). As such, the proposed oligosaccharide surface modification does not affect CNC suspension quality; CNCs maintain their high aspect ratios and disperse well in aqueous suspensions, factors which are essential in numerous formulations and applications. In future studies, oligosaccharides could be designed that would reduce the sensitivity of CNC colloidal stability to factors such as ionic strength and temperature.
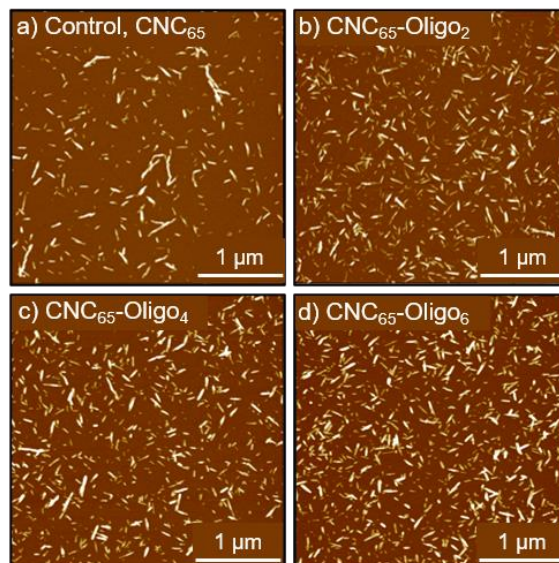
Figure 5.5. AFM height images of (a) control CNCs (CNC$_{65}$) and (b)-(d) CNCs modified with oligosaccharides of varying DP and DS, as labelled. The height scale in each image is -10 nm to 10 nm.

Further evidence of a successful surface modification was demonstrated by changes in CNC surface charge content (as determined through conductometric titration) and chemical composition. When modified with the highest DP oligosaccharides (Oligo$_2$), the total surface charge of the CNCs increased to 320 mmol/kg CNCs; a 100 mmol/kg increase compared to the control sample (Table 5.2). As AFM imaging showed that the surface modification does not change average particle dimensions, the increased surface charge corresponds to an increase in surface charge density, which is particle size dependent.[54] Additionally, CNC$_{65}$-Oligo$_2$ was found to be more highly charged than many industrially-produced sulfated CNCs with similar dimensions.[39,40] Sulfated CNCs produced in pilot/demo/commercial scale have been extensively characterized and tend to have total surface charge contents ranging between 170 and 340 mmol S/kg CNCs, while those isolated using the conventional bench scale protocol have total surface charges of ca. 250 mmol/kg CNCs.[39,40] While CNC surface charge can be substantially increased using, for example, oxidation methods,[81] the high surface charges resulting from our modification method do not rely on additional chemical reactions. Furthermore, the chemical composition of CNCs is also modified through the precipitation of oligosaccharides with phosphate groups. As expected, the CNC$_{65}$ contained only sulfur; however, phosphorus was detected in the modified CNC samples (Table 5.2). Overall, this modification route presents a method to precisely control the surface charge of CNCs, without using harsher hydrolysis conditions and thus preventing unnecessary cellulose degradation.

XRD analysis of all four CNC samples supported a cellulose I crystal structure and similar degrees of crystallinity (Appendix 5, Figure A5.4 and Table A5.5). In a detailed modelling study, Peri et al. showed that oligosaccharides will organize themselves on CNC surfaces in three possible conformations: i) parallel to the CNC surface, ii) at a right angle to the

CNC surface, or iii) at an obtuse angle to the CNC surface, where part of the oligosaccharide is oriented parallel to the CNCs.[46] While the XRD diffractograms only show a cellulose I structure in the oligosaccharide modified CNCs (perhaps due to the lack of resolution in the XRD measurement) it remains unclear whether the oligosaccharides are co-crystallizing or not with the CNC surface. Most importantly, however, the XRD diffractograms show no increase in the amorphous peak at ca. 18°,[66] indicating that the oligosaccharides are indeed crystallizing in some conformation on the CNC surface.

Extensive characterization has thus far demonstrated that the proposed oligosaccharide surface modification method can alter the surface chemistry, surface charge density, and structure (i.e., molecular weight) of typical sulfated CNCs. From a fundamental perspective, this suggests a successful modification. In the following paragraphs, the effects of this modification on CNC performance are discussed. To start, the thermal behavior of both the control and modified CNC samples were evaluated using thermogravimetric analysis (Appendix 5, Figure A5.5a). The degradation behavior of the modified sodium-form CNCs, quantified by the temperature at which the maximum rate of degradation occurs, was not impacted by the presence of oligosaccharides or the resulting increased DS (Appendix 5, Table A5.4). This is in line with previous works on CNC thermal stability, which have shown that cellulose DP is the governing factor in the thermal degradation behavior of sodium-form sulfated CNCs.[82] Because all samples here have a similar DP_w, it is expected that their thermal degradation profiles would be similar.

Additionally, the number of pyrolysis stages undergone by each CNC sample was the same: only one major degradation peak was observed in the derivative thermogravimetry plot (Appendix 5, Figure A5.5b). TGA showed that the maximum degradation of the oligosaccharides occurred at ca. 300°C (Appendix 5, Figure A5.6) compared to 310°C for the control and modified CNCs. The single major degradation peak in the degradation profiles of the modified CNCs indicates that the CNCs are thermally degrading as a single material, rather than a mixture of two separate polysaccharides.[83] While the TGA results do not connect the oligosaccharide surface modifications to any changes in thermal behavior, they do suggest that the modified CNCs act as a homogeneous material. Furthermore, this surface modification method presents an opportunity for future modifications capable of encapsulating CNC surfaces with, for example, flame retardant oligosaccharides to improve thermal resistance. The higher phosphorus content oligosaccharides do show a higher char content (Appendix 5, Figure A5.6) suggesting this as an easy route towards flame retardancy/thermal stability as demonstrated previously for highly phosphated CNCs produced by mechanochemical methods.[84]

CNC-water interactions, which are influenced by bound surface oligosaccharides, can affect CNC self-assembly, colloidal stability and rheological behavior.[41,78,85,86] Here, QCM-D was used to evaluate the water binding capacity of the control and modified CNCs. Because CNCs are nearly impenetrable by water, swelling is considered negligible; making CNCs an ideal material for quantifying bound surface water.[87,88] QCM-D revealed that the presence of oligosaccharides on CNC surfaces hindered their water binding capacity (Appendix 5, Figure A5.7 and Table A5.6). Upon precipitation of oligosaccharides onto

the surface of CNC_{65}, the normalized mass of bound water decreased dramatically from 4.5 mg m^{-2} nm^{-1} to 2.6 – 3.0 mg m^{-2} nm^{-1} (Table 5.2). The QCM-D data also showed a clear trend between CNC oligosaccharide surface coverage and normalized water adsorption capacity. CNC_{65}-Oligo4, which had the highest surface coverage of oligosaccharides (ca. 84%), bound the least amount of water. Furthermore, although minute, the difference in normalized bound surface water between CNC_{65}-Oligo2 and CNC_{65}-Oligo6 (2.9 and 3.0 mg m^{-2} nm^{-1}, respectively) also trends with their oligosaccharide surface coverage (27 and 10%, respectively).

In a detailed molecular dynamics simulation, Matthews et al. demonstrated that water bound to the surface of pristine crystalline cellulose Iβ has a significantly higher mass density than in the bulk.[89] They also reported that water molecules at the surface of the crystalline cellulose hydrogen bond to surface hydroxy groups, resulting in a highly ordered (and dense) layer of water molecules. Similarly, other works have also indicated that water molecules have a tendency to be highly ordered and densely packed along uniform crystal surfaces.[90,91] On the other hand, molecular modelling has also shown that water molecules are less ordered in the vicinity of surface heterogeneities or at the surface of spherical particles (due to their surface curvature).[91] Based on the oligosaccharide adsorption model by Peri at al.,[46] it seems likely that the surface oligosaccharides disrupt the infinitely smooth surface of the crystalline CNC, resulting in a less dense packing of water molecules at the CNC surface, and a lower content of bound surface water (as measured by QCM-D).

The rheological behavior of the control and modified CNC suspensions was probed (Table 5.2) and two distinct observations were made. First, the control CNC suspension had the highest viscosity at 100 s^{-1}, while the suspensions of the modified CNCs were less viscous. While the changes in viscosity among the surface modified CNCs are subtle, the primary finding of our results demonstrates the ability of surface oligosaccharides to reduce the viscosity of CNC suspensions. These findings are in line with those reported by Bouchard et al. who showed a clear linear decrease in viscosity with increasing surface oligosaccharide content.[41] Nevertheless, despite this primary observation in agreement with Bouchard et al., the modified CNCs did not exhibit decreased viscosities with increasing oligosaccharide coverage. Rather, and this is our second observation, a linear trend between total charge content and viscosity at 100 s^{-1} was observed. CNCs with higher total surface charge demonstrated lower viscosities (0.82 mPa·s for CNC_{65}-Oligo2, 0.86 mPa·s for CNC_{65}-Oligo4 and 0.88 mPa·s for CNC_{65}-Oligo6 – Appendix 5, Figure A5.8).

In the case of the work by Bouchard et al., however, the CNCs studied had a constant surface charge regardless of oligosaccharide content.[41] Here, we note a significant increase in total charge content upon CNC modification, and as such the effects of the bound oligosaccharides on CNC viscosity become multifaceted. Surface charge, for example, is known to play a significant role in the viscosity of CNC suspensions where, at high surface charge contents (> 0.3% sulfur), the rheological behavior of CNC suspensions is primarily governed by electroviscous effects.[92–94] These effects are linked to the thickness of the electrical double layer (EDL) of colloidal particles; a smaller EDL will result in lower intrinsic viscosities due to less resistance of the EDL to shear, and less EDL overlapping

of neighboring CNCs.[92–94] Interestingly, Abitbol et al. demonstrated that EDL thickness was inversely proportional to CNC surface charge due to the intrinsic contribution of the CNCs and their counterions to the ionic strength, and a higher CNC surface charge resulted in a decrease in EDL thickness.[92] This phenomenon is likely a contributing factor for the decrease in viscosity with increasing total surface charge demonstrated here.

Overall, the proposed oligosaccharide surface modification method tunes both the water binding capacity of CNC films as well as the viscosity of CNC suspensions by controlling CNC surface coverage and surface charge. These properties can further improve the performance of CNCs in, for example, viscosifying fluids, moisture sensitive biobased packaging, and optical materials, which are governed by the water-interactions and self-assembly of CNCs. Furthermore, the ability to significantly reduce the water binding capacity of CNCs (almost 45% reduction as shown through this modification method) could significantly improve various CNC compounding and drying processes, and produce nanocomposite materials with more consistent properties such as mechanical performance.

5.5 Conclusions

The method demonstrated here is the first proposed CNC surface modification route that can be carried out *in-situ* during the H_2SO_4 hydrolysis process used to produce CNCs. It is also the first report of utilizing the precipitation of externally produced oligosaccharides onto CNC surfaces to tune their physicochemical properties (e.g. surface chemistry, charge content, and water interactions). This strategy is furthermore capable of controlling the loading of oligosaccharides on CNC surfaces by tailoring the oligosaccharide DP. This is expected to broaden CNC potential in commodity and niche applications where water sensitivity, colloidal/thermal stability, rheology, liquid-crystalline behavior and compatibility must be tailored.

We believe that this *in-situ* surface modification method with oligosaccharides is an industrially relevant process that would be easy to implement in existing CNC production facilities and may decrease the environmental burden associated with more traditional modification routes. Moreover, the range of obtainable CNC properties are vast since oligosaccharides can be designed to have functionality targeted for specific applications. As such, a given industrial producer could use a variety of oligosaccharides to produce many "types" of CNCs without upgrading or modifying their equipment.

With the oligosaccharides tested here, we have highlighted the potential to alter CNC-water interactions, which could result in improved processability, increased affinity toward hydrophobic matrixes to produce new composite materials, and decreased water sensitivity for use in highly sensitive applications such as biobased packaging, diagnostic tools and sensors. The proposed modification route and the fundamental understanding of oligosaccharide precipitation has the potential to unlock a new generation of CNC-based materials. Finally, while CNCs were used as model cellulosic substrates because of their impenetrability by water, the wider aim is to expand the application scope of all cellulose-based materials through the implementation of oligosaccharide precipitation as a functionalization method.

5.6 References

1.   Niinivaara, E. & Cranston, E. D. Bottom-up assembly of nanocellulose structures. *Carbohydr. Polym.* **247**, 116664 (2020).

2.   De France, K. J., Hoare, T. R. & Cranston, E. D. A Review of Hydrogels and Aerogels Containing Nanocellulose. *Chem. Mater.* **29**, 4609–4631 (2017).

3.   Kedzior, S. A., Zoppe, J. O., Berry, R. M. & Cranston, E. D. Recent advances and an industrial perspective of cellulose nanocrystal functionalization through polymer grafting. *Curr. Opin. Solid State Mater. Sci.* **23**, 74–91 (2018).

4.   De France, K. J. *et al.* Tissue Response and Biodistribution of Injectable Cellulose Nanocrystal Composite Hydrogels. *ACS Biomater. Sci. Eng.* **5**, 2235–2246 (2019).

5.   Osorio, D. A. *et al.* Cross-linked cellulose nanocrystal aerogels as viable bone tissue scaffolds. *Acta Biomater.* **87**, 152–165 (2019).

6.   Dastjerdi, Z., Cranston, E. D., Berry, R., Fraschini, C. & Dubé, M. A. Polymer nanocomposites for emulsion-based coatings and adhesives. *Macromol. React. Eng.* **13**, 1–15 (2019).

7.   Dastjerdi, Z., Cranston, E. D. & Dubé, M. A. Pressure sensitive adhesive property modification using cellulose nanocrystals. *Int. J. Adhes. Adhes.* **81**, 36–42 (2018).

8.   Dastjerdi, Z., Cranston, E. D. & Dubé, M. A. Adhesive property modification using cellulose nanocrystals. *Int. J. Adhes. Adhes.* submitted (2017).

9.   Ouzas, A., Niinivaara, E., Cranston, E. D. & Dubé, M. A. Synthesis of poly(isobutyl acrylate/n-butyl acrylate/methyl methacrylate)/CNC nanocomposites for adhesive applications via in situ semi-batch emulsion polymerization. *Polym. Compos.* **40**, 1365–1377 (2019).

10.   Ouzas, A., Niinivaara, E., Cranston, E. D. & Dubé, M. A. In situ semibatch emulsion polymerization of 2-ethyl hexyl acrylate/n-butyl acrylate/methyl methacrylate/cellulose nanocrystal nanocomposites for adhesive applications. *Macromol. React. Eng.* **12**, 1–10 (2018).

11.   Niinivaara, E., Ouzas, A., Fraschini, C., Berry, R. M. & Cranston, E. D. How latex film formation and adhesion at the nanoscale correlate to performance of pressure sensitive adhesives with cellulose nanocrystals Abstract Introduction. 1–19.

12.   Pakdel, A. S. *et al.* A sequential design approach for in situ incorporation of cellulose nanocrystals in emulsion-based pressure sensitive adhesives. *Cellulose* **6**, (2020).

13.   Pakdel, A. S., Niinivaara, E., Berry, R. M., Cranston, E. D. & Dubé, M. A. Cellulose nanocrystal (CNC) – latex nanocomposites: The effect of CNC hydrophilicity and charge on rheological, mechanical and adhesive Properties. *Macromol. Rapid Commun.* **In Press**, (2020).

14. Gabriel, V. A., Cranston, E. D. & Dubé, M. A. Pushing the limits with cellulose nanocrystal loadings in latex-based pressure-sensitive adhesive nanocomposites. *Macromol. React. Eng.* **2000027**, 1–9 (2020).

15. Liu, L. *et al.* Effect of Counterion Choice on the Stability of Cellulose Nanocrystal Pickering Emulsions. *Ind. Eng. Chem. Res.* **57**, 7169–7180 (2018).

16. Hu, Z., Marway, H. S., Kasem, H., Pelton, R. & Cranston, E. D. Dried and Redispersible Cellulose Nanocrystal Pickering Emulsions. *ACS Macro Lett.* **5**, 185–189 (2016).

17. Hu, Z., Ballinger, S., Pelton, R. & Cranston, E. D. Surfactant-enhanced cellulose nanocrystal Pickering emulsions. *J. Colloid Interface Sci.* **439**, 139–148 (2015).

18. Kalashnikova, I. *et al.* New pickering emulsions stabilized by bacterial cellulose nanocrystals. *Langmuir* **27**, 7471–7479 (2011).

19. Kalashnikova, I., Bizot, H. H., Cathala, B. & Capron, I. Modulation of cellulose nanocrystals amphiphilic properties to stabilize oil/water interface. *Biomacromolecules* **13**, 267–275 (2012).

20. Capron, I. & Cathala, B. Surfactant-free high internal phase emulsions stabilized by cellulose nanocrystals. *Biomacromolecules* **14**, 291–296 (2013).

21. Favier, V. *et al.* Nanocomposite materials from latex and cellulose whiskers. *Polym. Adv. Technol.* **6**, 351–355 (1995).

22. Favier, V., Chanzy, H. & Cavaillé, J. Y. Polymer Nanocomposites Reinforced by Cellulose Whiskers. *Macromolecules* **28**, 6365–6367 (1995).

23. Liew, S. Y., Thielemans, W. & Walsh, D. A. Electrochemical Capacitance of Nanocomposite Polypyrrole / Cellulose Films. 17926–17933 (2010).

24. Li, M. C. *et al.* Surface-Chemistry-Tuned Cellulose Nanocrystals in a Bentonite Suspension for Water-Based Drilling Fluids. *ACS Appl. Nano Mater.* **1**, 7039–7051 (2018).

25. Li, M. C. *et al.* Overcoming Salt Contamination of Bentonite Water-Based Drilling Fluids with Blended Dual-Functionalized Cellulose Nanocrystals. *ACS Sustain. Chem. Eng.* **8**, 11569–11578 (2020).

26. Li, M. C. *et al.* Cellulose Nanocrystals and Polyanionic Cellulose as Additives in Bentonite Water-Based Drilling Fluids: Rheological Modeling and Filtration Mechanisms. *Ind. Eng. Chem. Res.* **55**, 133–143 (2016).

27. Vanderfleet, O. M. & Cranston, E. D. Production routes to tailor the performance of cellulose nanocrystals. *Nat. Rev. Mater.* (2020) doi:10.1038/s41578-020-00239-y.

28. Yang, H., Chen, D. & van de Ven, T. G. M. Preparation and characterization of

sterically stabilized nanocrystalline cellulose obtained by periodate oxidation of cellulose fibers. *Cellulose* **22**, 1743–1752 (2015).

29. Aïssa, K., Karaaslan, M. A., Renneckar, S. & Saddler, J. N. Functionalizing Cellulose Nanocrystals with Click Modifiable Carbohydrate-Binding Modules. *Biomacromolecules* **20**, 3087–3093 (2019).

30. Azzam, F., Galliot, M., Putaux, J. L., Heux, L. & Jean, B. Surface peeling of cellulose nanocrystals resulting from periodate oxidation and reductive amination with water-soluble polymers. *Cellulose* **22**, 3701–3714 (2015).

31. Leguy, J. *et al.* Periodate Oxidation Followed by NaBH4 Reduction Converts Microfibrillated Cellulose into Sterically Stabilized Neutral Cellulose Nanocrystal Suspensions. *Langmuir* **34**, 11066–11075 (2018).

32. Kloser, E. & Gray, D. G. Surface grafting of cellulose nanocrystals with poly(ethylene oxide) in aqueous media. *Langmuir* **26**, 13450–13456 (2010).

33. Hu, Z., Berry, R. M., Pelton, R. & Cranston, E. D. One-Pot Water-Based Hydrophobic Surface Modification of Cellulose Nanocrystals Using Plant Polyphenols. *ACS Sustain. Chem. Eng.* **5**, 5018–5026 (2017).

34. Nigmatullin, R. *et al.* Thermosensitive supramolecular and colloidal hydrogels via self-assembly modulated by hydrophobized cellulose nanocrystals. *Cellulose* **26**, 529–542 (2019).

35. Yoo, Y. & Youngblood, J. P. Green one-pot synthesis of surface hydrophobized cellulose nanocrystals in aqueous medium. *ACS Sustain. Chem. Eng.* **4**, 3927–3938 (2016).

36. Kedzior, S. A., Graham, L., Moorlag, C., Dooley, B. M. & Cranston, E. D. Poly(methyl methacrylate)-Grafted Cellulose Nanocrystals: One-Step Synthesis, Nanocomposite Preparation, and Characterization. *Can. J. Chem. Eng.* **94**, 811–822 (2016).

37. Salajková, M., Berglund, L. A. & Zhou, Q. Hydrophobic cellulose nanocrystals modified with quaternary ammonium salts. *J. Mater. Chem.* **22**, 19798–19805 (2012).

38. Kontturi, K. S. *et al.* Noncovalent surface modification of cellulose nanopapers by adsorption of polymers from aprotic solvents. *Langmuir* **33**, 5707–5712 (2017).

39. Reid, M. S., Villalobos, M. & Cranston, E. D. Benchmarking cellulose nanocrystals: from the laboratory to industrial production. *Langmuir* **33**, 1583–1598 (2017).

40. Delepierre, G. *et al.* Benchmarking Cellulose Nanocrystals Part II: A Detailed Look at New Industrially-Produced Materials. *Langmuir* **Submitted.**, (2020).

41.   Bouchard, J., Méthot, M., Fraschini, C. & Beck, S. Effect of oligosaccharide deposition on the surface of cellulose nanocrysals as a function of acid hydrolysis temperature. *Cellulose* **23**, 3555–3567 (2016).

42.   Cranston, E. D. & Gray, D. G. Morphological and optical characterization of polyelectrolyte multilayers incorporating nanocrystalline cellulose. *Biomacromolecules* **7**, 2522–2530 (2006).

43.   Chen, L. *et al.* Tailoring the yield and characteristics of wood cellulose nanocrystals (CNC) using concentrated acid hydrolysis. *Cellulose* **22**, 1753–1762 (2015).

44.   Dong, S., Bortner, M. J. & Roman, M. Analysis of the sulfuric acid hydrolysis of wood pulp for cellulose nanocrystal production: A central composite design study. *Ind. Crops Prod.* **93**, 76–87 (2016).

45.   Hamad, W. Y. & Hu, T. Q. Structure-process-yield interrelations in nanocrystalline cellulose extraction. *Can. J. Chem. Eng.* **88**, 392–402 (2010).

46.   Peri, S., Muthukumar, L., Nazmul Karim, M. & Khare, R. Dynamics of cello-oligosaccharides on a cellulose crystal surface. *Cellulose* **19**, 1791–1806 (2012).

47.   Labet, M. & Thielemans, W. Improving the reproducibility of chemical reactions on the surface of cellulose nanocrystals: ROP of ??-caprolactone as a case study. *Cellulose* **18**, 607–617 (2011).

48.   Hayashi, T., Takeda, T., Ogawa, K. & Mitsuishi, Y. Effects of the degree of polymerization on the binding of xyloglucans to cellulose. *Plant Cell Physiol.* **35**, 893–9 (1994).

49.   Hayashi, T., Ogawa, K. & Mitsuishi, Y. Characterization of the adsorption of xyloglucan to cellulose. *Plant Cell Physiol.* **35**, 1199–1205 (1994).

50.   Lin, K. H. *et al.* An analysis on the electrophoretic mobility of cellulose nanocrystals as thin cylinders: Relaxation and end effect. *RSC Adv.* **9**, 34032–34038 (2019).

51.   Bhattacharjee, S. DLS and Zeta Potential - What They Are and What They Are Not? *J. Control. Release* **235**, 337–351 (2016).

52.   Foster, E. J. *et al.* Current characterization methods for cellulose nanomaterials. *Chem. Soc. Rev.* **47**, 2609–2679 (2018).

53.   Kittle, J. D. *et al.* Equilibrium water contents of cellulose films determined via solvent exchange and quartz crystal microbalance with dissipation monitoring. *Biomacromolecules* **12**, 2881–2887 (2011).

54.   Vanderfleet, O. M., Osorio, D. A. & Cranston, E. D. Optimization of cellulose nanocrystal length and surface charge density through phosphoric acid hydrolysis.

Philos. Trans. R. Soc. A Math. Phys. Eng. Sci. **376**, 1–7 (2018).

55.   Driemeier, C. & Calligaris, G. A. Theoretical and experimental developments for accurate determination of crystallinity of cellulose i materials. *J. Appl. Crystallogr.* **44**, 184–192 (2011).

56.   Ahvenainen, P., Kontro, I. & Svedström, K. Comparison of sample crystallinity determination methods by X-ray diffraction for challenging cellulose I materials. *Cellulose* **23**, 1073–1086 (2016).

57.   Hasegawa, M., Isogai, A. & Onabe, F. Preparation of Low-molecular weight cellulose using phosphoric acid. *Carbohydr. Polym.* **20**, 279–283 (1993).

58.   Mittal, A., Katahira, R., Himmel, M. E. & Johnson, D. K. Effects of alkaline or liquid-ammonia treatment on crystalline cellulose: changes in crystalline structure and effects on enzymatic digestibility. *Biotechnol. Biofuels* **4**, 41 (2011).

59.   Taylor, J. B. The water solubilities and heats of solution of short chain cellulosic oligosaccharides. *Trans. Faraday Soc.* **53**, 1198–1203 (1957).

60.   Klemm, D., Philipp, B., Heinze, T., Heinze, U. & Wagenknecht, W. *Comprehensive Cellulose Chemistry. Volume 1: Fundamentals and Analytical Methods.* (Wiley-CVH, 1998).

61.   Kobayashi, S., Kashiwa, K., Kawasaki, T. & Shoda, S. I. Novel Method for Polysaccharide Synthesis Using an Enzyme: The First in Vitro Synthesis of Cellulose via a Nonbiosynthetic Path Utilizing Cellulase as Catalyst. *J. Am. Chem. Soc.* **113**, 3079–3084 (1991).

62.   Tolonen, L. K. *et al.* Supercritical water treatment for cello-oligosaccharide production from microcrystalline cellulose. *Carbohydr. Res.* **401**, 16–23 (2015).

63.   Liebert, T., Seifert, M. & Heinze, T. Efficient method for the preparation of pure, water-soluble cellodextrines. *Macromol. Symp.* **262**, 140–149 (2008).

64.   Zhong, C., Luley-Goedl, C. & Nidetzky, B. Product solubility control in cellooligosaccharide production by coupled cellobiose and cellodextrin phosphorylase. *Biotechnol. Bioeng.* **116**, 2146–2155 (2019).

65.   Fink, H. P., Hofmann, D. & Philipp, B. Some aspects of lateral chain order in cellulosics from X-ray scattering. *Cellulose* **2**, 51–70 (1995).

66.   Nam, S., French, A. D., Condon, B. D. & Concha, M. Segal crystallinity index revisited by the simulation of X-ray diffraction patterns of cotton cellulose Iβ and cellulose II. *Carbohydr. Polym.* **135**, 1–9 (2016).

67.   Langan, P., Nishiyama, Y. & Chanzy, H. X-ray structure of mercerized cellulose II at 1 Å resolution. *Biomacromolecules* **2**, 410–416 (2001).

68.   Nishiyama, Y., Kuga, S. & Okano, T. Mechanism of mercerization revealed by X-

ray diffraction. *J. Wood Sci.* **46**, 452–457 (2000).

69.   Cullity, B. D. *Elements of x-ray diffraction*. (Addison-Wesley Publishing Company Inc., 1978).

70.   Pääkkönen, T. *et al.* From vapour to gas: optimising cellulose degradation with gaseous HCl. *React. Chem. Eng.* 312–318 (2018).

71.   Kontturi, E. *et al.* Degradation and Crystallization of Cellulose in Hydrogen Chloride Vapor for High-Yield Isolation of Cellulose Nanocrystals. *Angew. Chemie - Int. Ed.* **55**, 14455–14458 (2016).

72.   Niinivaara, E., Arshath, S. A. A., Nieminen, K., Bismarck, A. & Kontturi, E. The Effect of Polymorphism on the Kinetics of Adsorption and Degradation: A Case of Hydrogen Chloride Vapor on Cellulose. *Adv. Sustain. Syst.* **2**, 1800026 (2018).

73.   Kargarzadeh, H. *et al.* Effects of hydrolysis conditions on the morphology, crystallinity, and thermal stability of cellulose nanocrystals extracted from kenaf bast fibers. *Cellulose* **19**, 855–866 (2012).

74.   Wang, Q., Zhao, X. & Zhu, J. Y. Kinetics of strong acid hydrolysis of a bleached kraft pulp for producing cellulose nanocrystals (CNCs). *Ind. Eng. Chem. Res.* **53**, 11007–11014 (2014).

75.   Dong, X. M., Revol, J. F. & Gray, D. G. Effect of microcrystallite preparation conditions on the formation of colloid crystals of cellulose. *Cellulose* **5**, 19–32 (1998).

76.   Beck-Candanedo, S., Roman, M. & Gray, D. G. Effect of reaction conditions on the properties and behavior of wood cellulose nanocrystal suspensions. *Biomacromolecules* **6**, 1048–1054 (2005).

77.   Bondeson, D., Mathew, A. & Oksman, K. Optimization of the isolation of nanocrystals from microcrystalline cellulose by acid hydrolysis. *Cellulose* **13**, 171–180 (2006).

78.   Beck, S., Bouchard, J. & Berry, R. Controlling the Reflection Wavelength of Iridescent Solid Films of Nanocrystalline Cellulose. *Biomacromolecules* **12**, 167–172 (2011).

79.   Beck, S. & Bouchard, J. Auto-catalyzed acidic desulfation of cellulose nanocrystals. *Nord. Pulp Pap. Res. J.* **29**, 6–14 (2014).

80.   Elazzouzi-Hafraoui, S. *et al.* The Shape and Size Distribution of Crystalline Nanoparticles Prepared by Acid Hydrolysis of Native Cellulose. *Biomacromolecules* **9**, 57–65 (2008).

81.   Pääkkönen, T. *et al.* Sustainable High Yield Route to Cellulose Nanocrystals from Bacterial Cellulose. *ACS Sustain. Chem. Eng.* **7**, 14384–14388 (2019).

82.   Vanderfleet, O. M. *et al.* Insight into thermal stability of cellulose nanocrystals from new hydrolysis methods with acid blends. *Cellulose* **26**, 507–528 (2019).

83.   Akhlaghi, S. P., Berry, R. C. & Tam, K. C. Surface modification of cellulose nanocrystal with chitosan oligosaccharide for drug delivery applications. *Cellulose* **20**, 1747–1764 (2013).

84.   Fiss, B. G., Hatherly, L., Stein, R. S., Friščić, T. & Moores, A. Mechanochemical Phosphorylation of Polymers and Synthesis of Flame-Retardant Cellulose Nanocrystals. *ACS Sustain. Chem. Eng.* **7**, 7951–7959 (2019).

85.   Delepierre, G. *et al.* Patience is a virtue: self-assembly and physico-chemical properties of cellulose nanocrystal allomorphs. *Nanoscale* **12**, 17480–17493 (2020).

86.   Garg, M., Linares, M. & Zozoulenko, I. Theoretical Rationalization of Self-Assembly of Cellulose Nanocrystals: Effect of Surface Modifications and Counterions. *Biomacromolecules* **21**, 3069–3080 (2020).

87.   Saito, T. & Isogai, A. TEMPO-mediated oxidation of native cellulose. The effect of oxidation conditions on chemical and crystal structures of the water-insoluble fractions. *Biomacromolecules* **5**, 1983–1989 (2004).

88.   Niinivaara, E., Faustini, M., Tammelin, T. & Kontturi, E. Water vapor uptake of ultrathin films of biologically derived nanocrystals: Quantitative assessment with quartz crystal microbalance and spectroscopic ellipsometry. *Langmuir* **31**, 12170–12176 (2015).

89.   Matthews, J. F. *et al.* Computer simulation studies of microcrystalline cellulose Iβ. *Carbohydr. Res.* **341**, 138–152 (2006).

90.   Berlin, E., Kliman, P. G. & Pallansch, M. J. Calorimetry and Thermogravimetry of Bound Water in Dried Milk and Whey Powders. *J. Dairy Sci.* **54**, 300–305 (1971).

91.   Spagnoli, D., Gilbert, B., Waychunas, G. A. & Banfield, J. F. Prediction of the effects of size and morphology on the structure of water around hematite nanoparticles. *Geochim. Cosmochim. Acta* **73**, 4023–4033 (2009).

92.   Abitbol, T., Kam, D., Levi-Kalisman, Y., Gray, D. G. & Shoseyov, O. Surface Charge Influence on the Phase Separation and Viscosity of Cellulose Nanocrystals. *Langmuir* **34**, 3925–3933 (2018).

93.   Wu, Q., Li, X., Fu, S., Li, Q. & Wang, S. Estimation of aspect ratio of cellulose nanocrystals by viscosity measurement: influence of surface charge density and NaCl concentration. *Cellulose* **24**, 3255–3264 (2017).

94.   Boluk, Y., Lahiji, R., Zhao, L. & McDermott, M. T. Suspension viscosities and shape parameter of cellulose nanocrystals (CNC). *Colloids Surfaces A Physicochem. Eng. Asp.* **377**, 297–303 (2011).

95.   Heath, L. & Thielemans, W. Cellulose nanowhisker aerogels. *Green Chem.* **12**, 1448–1453 (2010).

96.   Davidson, T. C., Newman, R. H. & Ryan, M. J. Variations in the fibre repeat between samples of cellulose I from different sources. *Carbohydr. Res.* **339**, 2889–2893 (2004).

Appendix 5
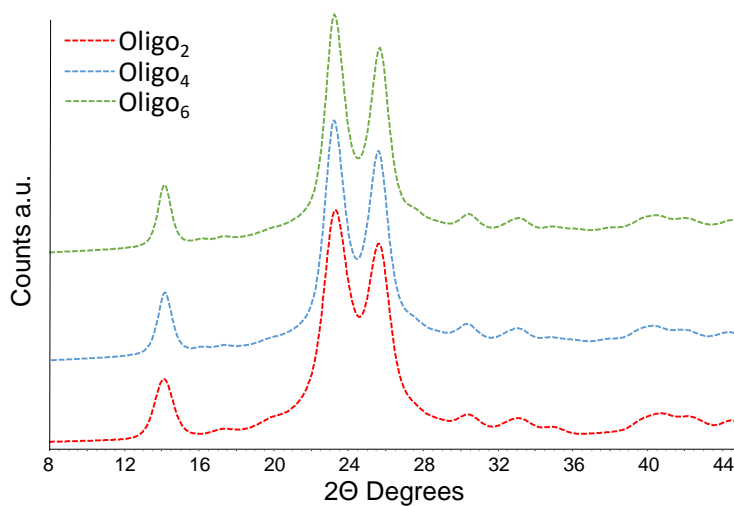
Figure A5.1. XRD diffractograms of oligosaccharides hydrolyzed from microcrystalline cellulose using phosphoric acid (2, 4 and 6-week hydrolysis). XRD was performed on precipitated dry oligosaccharide powders. Diffractograms show that the oligosaccharides are in the form of cellulose II.
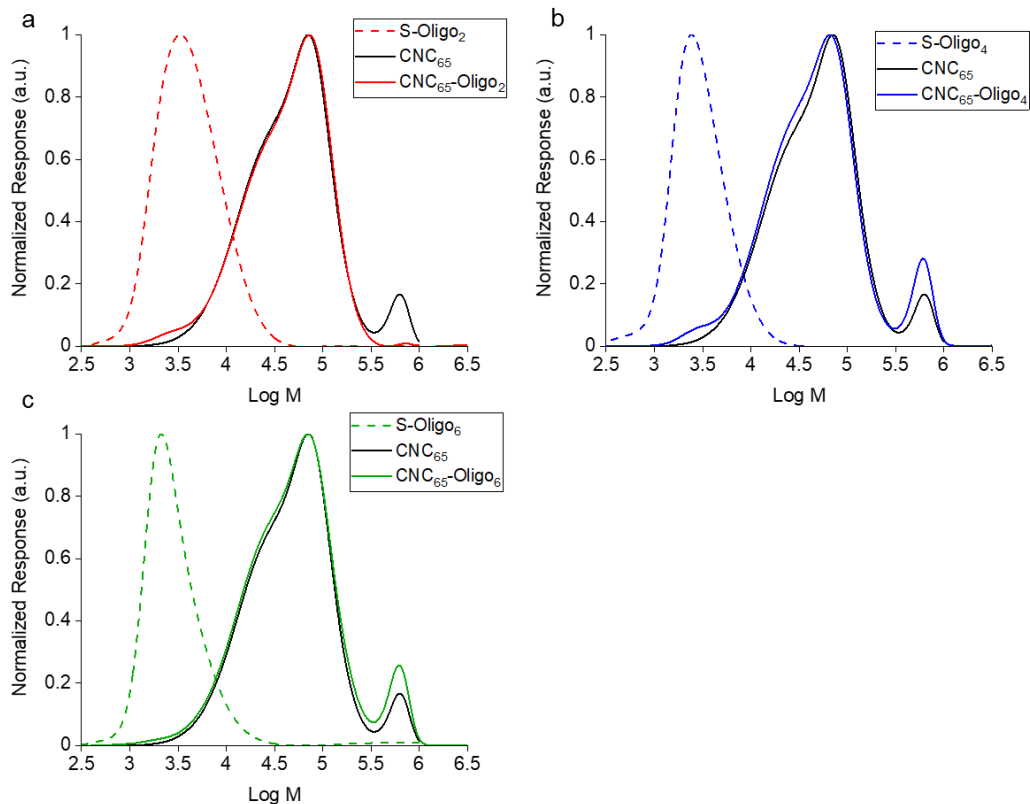
Figure A5.2. Molecular weight distribution of control sample (CNC$_{65}$) compared to CNCs surface modified with (a) Oligo$_2$, (b) Oligo$_4$ and c) Oligo$_6$ in addition to the molecular weight distributions of the corresponding oligosaccharides after 4 min dissolution in 64 wt% H$_2$SO$_4$ (S-Oligo$_x$).

Table A5.1. Physical properties of CNCs, cellobiose and anhydroglucose units (AGU) used in the calculation of oligosaccharide surface coverage of CNCs as a result of surface modification.

Physical property	
Density of CNCs[95]	1.6 g/cm^3
Length of cellobiose[96]	1.031 nm
Width of cellobiose[3]	0.78 nm
Avogadro's number (N$_A$)	6.022x10^{23} mol^{-1}
Molecular weight of AGU	162.14 g mol^{-1}
Length of CNC$_{65}$ (measured from AFM images (N=100, Table A5.5)	200 nm
Width of CNC$_{65}$ (measured from AFM images (N=100, Table A5.5)	8 nm

Table A5.2. Assumed mass of the CNCs and oligosaccharides in the surface modified CNC samples based on their respective peak intensities in the chromatograms of the modified CNCs (Figure A5.2).

	Intensity of oligosaccharide peak in chromatogram of modified CNCs	Intensity of CNC peak in chromatogram of modified CNCs	Assumed mass of CNCs/ oligosaccharides, g
CNC_{65}	n/a	1	1
CNC_{65}-$Oligo_2$	0.0571	1	0.0571
CNC_{65}-$Oligo_4$	0.1788	1	0.1788
CNC_{65}-$Oligo_6$	0.0217	1	0.0217

Table A5.3. Approximate calculations to determine the oligosaccharide surface coverage of modified CNCs (see below for example calculation).

	DP_w	Assumed mass of oligosaccharides, g	Assumed mass of AGUs (in mass of oligosaccharides), g	No. of moles of AGUs (in mass of oligosaccharides)	Total no. of AGUs (in mass of oligosaccharides)	Total no. of oligosaccharides	Surface area[***] of single oligosaccharide nm^2	Total available surface area of oligosaccharides nm^2	Surface coverage, %[**]
S-oligo$_2$[*]	10	0.0571	0.0571	3.5×10^{-4}	2.1×10^{20}	2.1×10^{19}	4.02	8.5×10^{19}	27
S-Oligo$_4$	7	0.1788	0.1788	1.1×10^{-3}	6.6×10^{20}	9.5×10^{19}	2.81	2.7×10^{20}	84
S-Oligo$_6$	7	0.0217	0.0217	1.3×10^{-4}	8.1×10^{19}	1.2×10^{19}	2.81	3.2×10^{19}	10

[*]DP_w of oligosaccharides after 4 min dissolution and subsequent precipitation (i.e., S-Oligo$_x$) were used to determine oligosaccharide surface coverage of CNCs, as these best represent the oligosaccharides found on the CNCs surfaces after the *in-situ* surface modification (Figure A5.2).

[**]Assumption has been made that the oligosaccharides co-crystallize on to the surface of the CNCs in a linear conformation (rather than as a coil, for example). This assumption is made based on molecular modelling shown by Peri et al. (ref. 46).

[***]Surface area of single oligosaccharide only represents the surface area of the hydrophilic plane which would presumably be in contact with the CNC surface.

Calculation for the total available surface area of CNCs (assuming rectangular cuboid shape):

$$Volume_{CNC_{65}} = Length_{CNC_{65}} \times \left(cross\text{-}section_{CNC_{65}}\right)^2 = 200 \text{ nm} \times (8 \text{ nm})^2 = 12800 \text{ nm}^3$$
$$= 1.3 \times 10^{-17} \text{ cm}^3$$

$$Surface\ area_{CNC65} = \left(2 \times \left(cross\text{-}section_{CNC_{65}}\right)^2\right) + \left(4 \times \left(Length_{CNC_{65}} \times cross\text{-}section_{CNC_{65}}\right)\right)$$
$$= (2 \times (8 \text{ nm})^2) + \left(4 \times (200 \text{ nm} \times 8 \text{ nm})\right) = 6528 \text{ nm}^2$$

$$Total\ available\ surface\ area_{CNCs} = \frac{Assumed\ mass\ of\ CNCs}{density_{CNC} \times Volume_{CNC_{65}}} \times surface\ area_{CNC_{65}}$$

$$= \frac{1 \text{ g}}{1.6 \frac{g}{cm^3} \times (1.3 \times 10^{-17} \text{ cm}^3)} \times 6528 \text{ nm}^2 = 3.2 \times 10^{20} \text{ nm}^2$$

Calculation for the total available surface area of Oligosaccharides (values for S-Oligo$_2$ have been used here for demonstrative purposes):

Assumed mass of AGUs = Assumed mass of oligosaccharides from chromatogram

$$\text{No. of moles of AGUs} = \frac{\text{Assumed mass of AGUs}}{\text{Molecular weight of AGU}} = \frac{0.057 \text{ g}}{162.14 \frac{\text{g}}{\text{mol}}} = 3.5 \times 10^{-4} \text{ mol}$$

$$\text{Total no. of AGUs} = \text{No. of moles of AGUs} \times N_A = (3.5 \times 10^{-4} \text{ mol}) \times (6.022 \times 10^{23} \text{ mol}^{-1})$$
$$= 2.1 \times 10^{20} \text{ AGUs}$$

$$\text{Total no. of oligosaccharides} = \frac{\text{Total no. of AGUs}}{\text{DP}_w} = \frac{2.1 \times 10^{20}}{10} = 2.1 \times 10^{19} \text{ oligosaccharides}$$

$$\text{Surface area of single oligosaccharide} = \left(\frac{\text{DP}_w}{2}\right) \times \text{length of cellobiose} \times \text{width of cellobiose}$$
$$= \left(\frac{10}{2}\right) \times 1.031 \text{ nm} \times 0.78 \text{ nm} = 4.02 \text{ nm}^2$$

$$\text{Total available surface area}_{\text{oligosaccharides}}$$
$$= \text{Surface area of single oligosaccharide} \times \text{Total no. of oligosaccharides}$$
$$= 4.02 \text{ nm}^2 \times 2.1 \times 10^{19} = 8.5 \times 10^{19} \text{ nm}^2$$

$$\text{CNC surface coverage} = 100 \times \frac{\text{Total available surface area}_{\text{oligosaccharides}}}{\text{Total available surface area}_{\text{CNCs}}} = 100 \times \frac{(8.5 \times 10^{19} \text{ nm}^2)}{(3.2 \times 10^{20} \text{ nm}^2)}$$
$$= 27\%$$
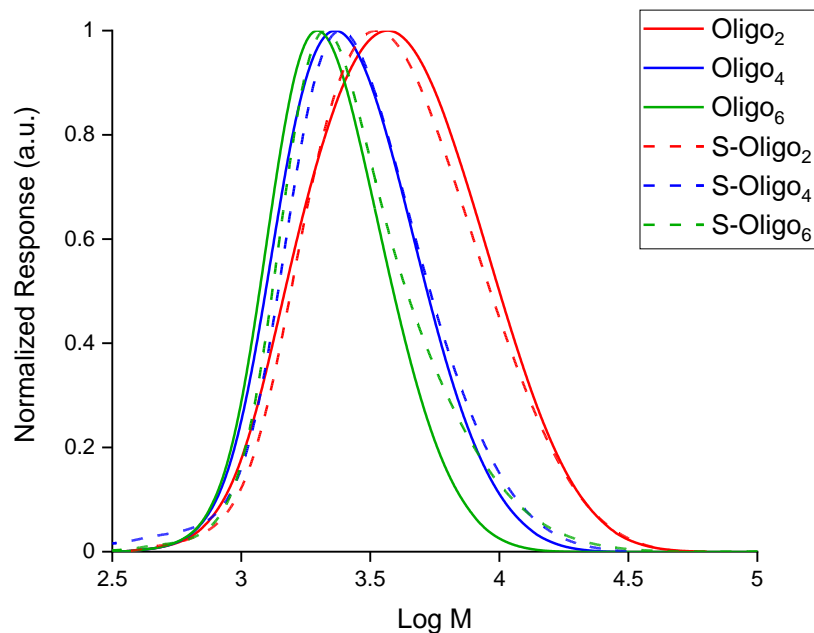
Figure A5.3. Molecular weight distribution of oligosaccharide samples before (Oligo$_x$) and after 4 min dissolution in 64 wt% sulfuric acid (S-Oligo$_x$).

Table A5.4. Elemental sulfur and phosphorus contents of oligosaccharides hydrolyzed through a controlled H_3PO_4 hydrolysis for 2, 4 and 6 weeks ('Oligo$_x$'), and after a 4 min dissolution in 64 wt% H_2SO_4 ('S-Oligo$_x$'). Degree of substitution values were calculated from elemental analysis data.

	Sulfur ppm	Degree of substitution of sulfur	Phosphorus ppm	Degree of substitution of phosphorus	Total degree of substitution	Degree of polymerization, DP_w	$Đ$
Oligo$_2$	0	N/A	414.4	0.0022	0.0022	10	6
Oligo$_4$	0	N/A	580.1	0.0030	0.0030	6	4
Oligo$_6$	0	N/A	699.3	0.0037	0.0037	5	4
S-Oligo$_2$	1199.5	0.0061	217.0	0.0011	0.0072	10	6
S-Oligo$_4$	1552.3	0.0079	332.5	0.0017	0.0097	7	4
S-Oligo$_6$	1847.0	0.0094	413.0	0.0022	0.0116	7	4
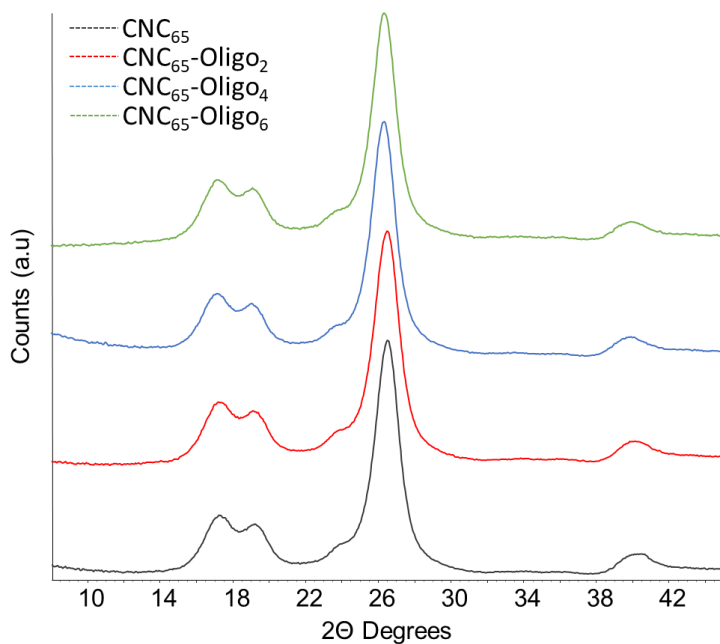
Figure A5.4. XRD diffractograms of control CNCs (CNC$_{65}$) and CNCs modified with oligosaccharides of varying DP and degree of substitution.

Table A5.5. Physicochemical properties of control CNCs (CNC$_{65}$) and CNCs modified with oligosaccharides of varying DP and DS. CNC length and cross-section were measured from AFM images (n = 100 particles). XRD and TGA were used to measure degree of crystallinity and thermal degradation, respectively.

	Length, nm	Cross-section, nm	Degree of crystallinity, %	Temp. max. rate of degradation, °C
CNC$_{65}$	200 ± 40	8 ± 2	94	308
CNC$_{65}$-Oligo$_2$	190 ± 50	6 ± 2	93	310
CNC$_{65}$-Oligo$_4$	220 ± 50	8 ± 3	94	308
CNC$_{65}$-Oligo$_6$	200 ±4 0	9 ± 3	92	309
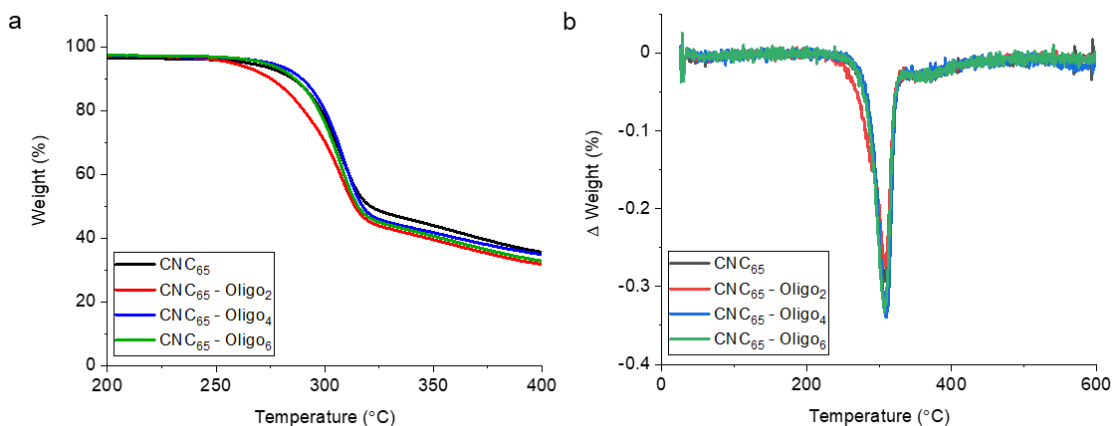
Figure A5.5. Thermogravimetric analysis of control sample (CNC$_{65}$) and CNCs modified with oligosaccharides of varying DP and DS (in their sodium form) with (a) sample mass as a function of temperature and (b) the rate of mass loss as a function on temperature.
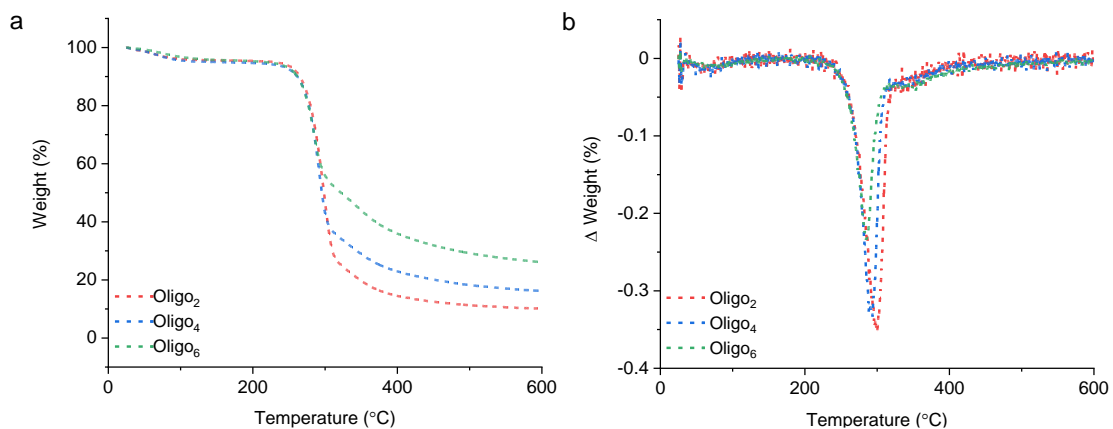
Figure A5.6.Thermogravimetric analysis of phosphoric acid hydrolyzed oligosaccharides with (a) sample mass as a function of temperature and b) the rate of mass loss as a function on temperature.
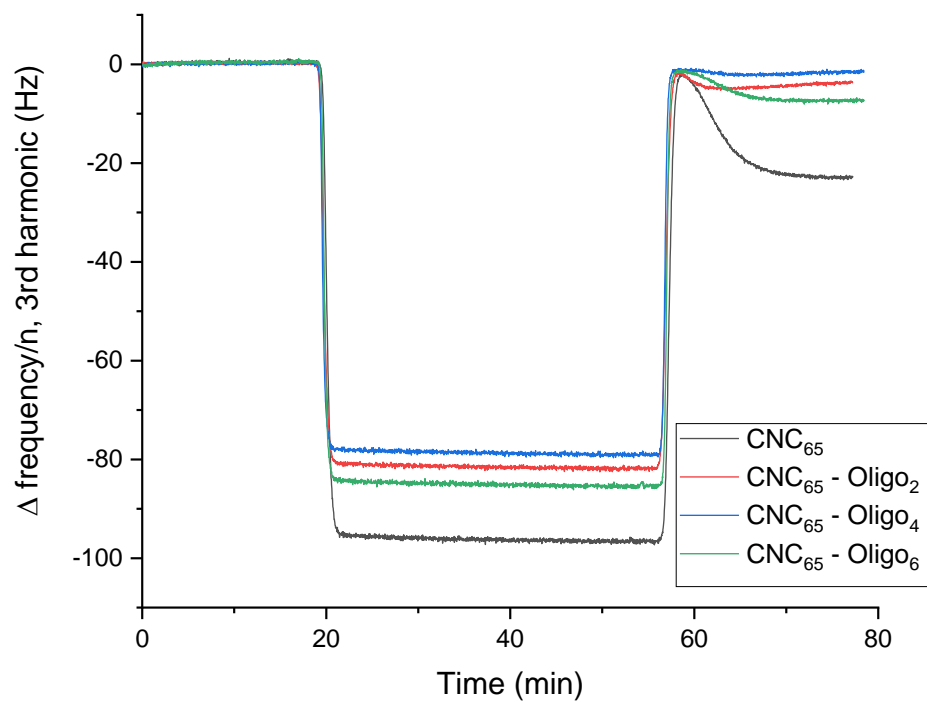
Figure A5.7. Change in normalized resonance frequency (3rd harmonic) as a result of a water/deuterium oxide solvent exchange as measured by quartz crystal microgravimetry, for the control sample (CNC_{65}) and oligosaccharide modified samples.

Table A5.6. Water uptake capacity of CNC_{65} control sample and CNCs modified with oligosaccharides as measured by QCM-D. Normalized changes in resonance frequency were converted to mass of bound water in each sample and subsequently normalized by thin film thickness (as measured by AFM scratch height analysis).

	Δfrequency/n, Hz	Δfrequency$_{H_2O}$/n, Hz	Γ$_{H_2O}$, mg m^{-2}	CNC film thickness, nm
CNC_{65}	-96	-402	71.2	16 ± 1
CNC_{65}-Oligo$_2$	-82	-265	47.0	16 ± 1
CNC_{65}-Oligo$_4$	-79	-239	42.3	16 ± 1
CNC_{65}-Oligo$_6$	-85	-297	52.6	17 ± 1
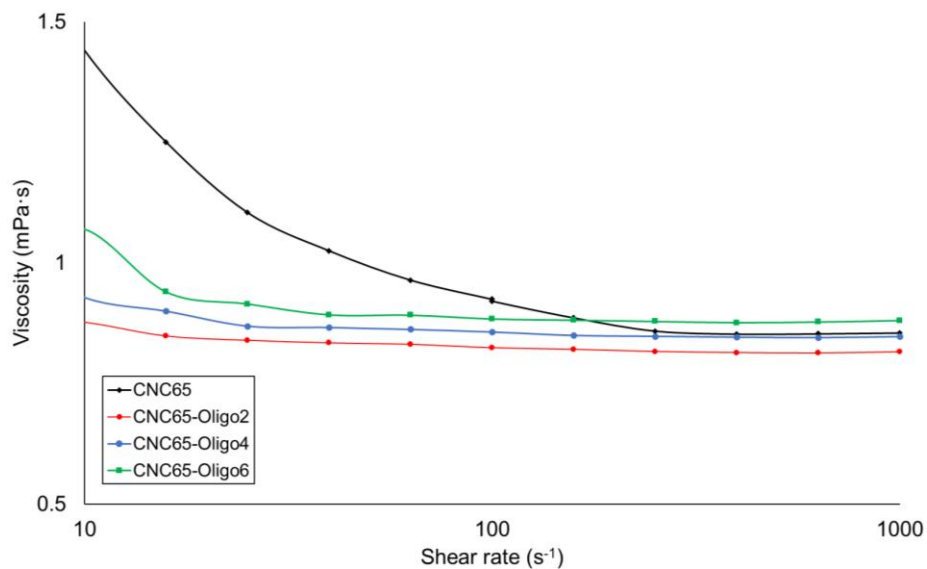
Figure A5.8. Steady shear viscosity as a function of rate of the control sample (CNC_{65}) and oligosaccharide modified samples.

Chapter 6

Insight into thermal stability of cellulose nanocrystals from new hydrolysis methods with acid blends

_____

In Chapters 4 and 5, CNC properties were tailored using new hydrolysis parameters and surface modifications; yet no discernable changes in CNC thermal performance occurred. Herein, a new hydrolysis method is introduced which utilizes blends of phosphoric and sulfuric acid to produce CNCs which have similarly high thermal stabilities to phosphoric acid hydrolysed CNCs, yet also form colloidally stable suspensions. Furthermore, these new CNCs allow for elucidation of dried CNC behavior at high temperatures.

In this work, Dr. Michael Reid and myself jointly conceptualized the experimental matrix and carried out its preliminary experiments including preparation of CNC samples and imaging using atomic force microscopy. Following this, I managed the project and carried out further experiments including CNC surface modification, zeta potential and dynamic light scattering measurements, conductometric titrations, cellulose solubilisation and gel permeation chromatography, and thermogravimetric analysis. I also performed data analysis and wrote the manuscript with assistance from my supervisor, Dr. Emily Cranston. Dr. Laurent Heux carried out NMR experiments. Elemental analysis and X-Ray diffraction experiments were performed by technicians. This chapter is reproduced with permission from Springer Nature © 2018.

Vanderfleet, O.M., Reid, M.S., Bras, J., Heux, L., Godoy-Vargas, J., Panga, M.K.R, Cranston, E.D., "Insight into thermal stability of cellulose nanocrystals from new hydrolysis methods with acid blends", *Cellulose* **2019**, 26: 507–528. https://doi.org/10.1007/s10570-018-2175-7
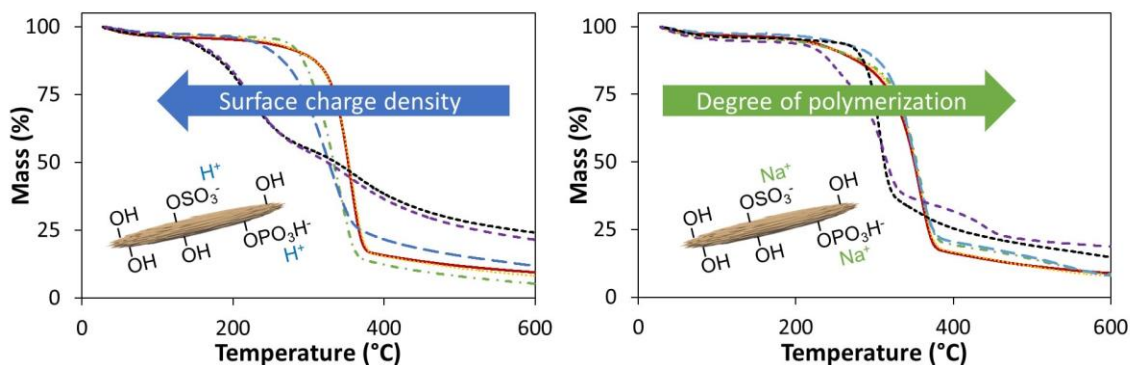
6.1 Abstract

This study provides insight into the thermal degradation of cotton cellulose nanocrystals (CNCs) by tuning their physico-chemical properties through acid hydrolysis using blends of phosphoric and sulfuric acid. CNCs isolated by sulfuric acid hydrolysis are known to degrade at lower temperatures than CNCs hydrolyzed with phosphoric acid; however, the reason for this change is unclear. Although all CNCs are inherently relatively thermally stable, their application in polymer composites and liquid formulations designed to function at high temperatures could be extended if thermal stability was improved. Herein, thermogravimetric analysis was carried out on six types of CNCs (in both acid and sodium form) with different surface chemistry, surface charge density, dimensions, crystallinity and degree of polymerization (DP) to identify the key properties that influence thermal stability of nanocellulose. In acid form, CNC surface charge density was found to be the determining factor in thermal stability due to de-esterification and acid-catalyzed degradation. Conversely, in sodium form, surface chemistry and charge density had a negligible effect on the onset of thermal degradation, however, the DP of the cellulose polymer chains highly influenced stability. The presence of more reducing ends in lower DP nanocrystals is inferred to facilitate thermally-induced depolymerization and degradation. Degree of crystallinity did not significantly affect CNC thermal stability. Studying CNCs produced from single or blends of acids (and changing the counterion) elucidated the thermal behavior of cellulose and furthermore demonstrated new routes to tailor CNCs thermal and colloidal stability.

6.2 Introduction

Cellulose nanocrystals (CNCs) are high aspect ratio nanoparticles made up of ordered cellulose polymer chains. CNCs are isolated from natural cellulose sources, most commonly wood or cotton, via acid hydrolysis or oxidation.[1–3] CNCs were first produced with both hydrochloric and sulfuric acids by Nickerson and Habrle.[4] It was hypothesized that exposure of cellulose to concentrated acid preferentially degrades the disordered regions that link crystalline cellulose units together. The isolated crystalline regions contained cellulose chains of approximately 280 glucose units long (as determined by intrinsic viscosity).[4] Under various hydrolyzing treatments, the degree of polymerization was found to rapidly reduce to a relatively constant value, the so called "level-off degree of polymerization" (LODP).[4,5] Although Nickerson and Habrle found that hydrochloric acid hydrolyzed cellulose more efficiently, it is the sulfuric acid hydrolysis that was further

158

studied since H_2SO_4 imparts surface charge through the grafting of sulfate half-ester groups onto the nanocrystal surface. Rånby demonstrated the production of colloidally stable CNCs with high electrophoretic mobility, again using H_2SO_4.[6] A few years later, CNCs were imaged with transmission electron microscopy (TEM) and demonstrated to have lengths of ca. 200 nm and widths of 10-20 nm, which concretized their high aspect ratio.[7]

More recently, the relationship between LODP and the succession of crystalline and disordered regions along the microfibrils was shown on ramie fibers by small angle neutron scattering, the number of disordered residues being no more than 4-5 glucose units every 300, in very good agreement with the dimensions that can be obtained after the selective hydrolysis of disordered cellulose.[8] Today, the hydrolysis of cellulose with sulfuric acid is widely used and has been scaled up by several companies to produce up to ton per day quantities following a relatively "green" procedure.[9] Furthermore, potential applications of CNCs are numerous; some examples include reinforcing agents for composite and construction materials,[10–13] stabilizers for emulsions,[14] supports and templates in biomedical/optical devices,[15–17] and performance enhancers for pressure sensitive adhesives.[18]

The physico-chemical properties of CNCs are highly dependent on the hydrolysis methods used to produce them. Although the most widely used protocol consists of a 64 wt% sulfuric acid hydrolysis for 45 minutes at 45 °C,[19] many other procedures exist. Subtle variations of this traditional hydrolysis method can be performed to tune CNC properties such as length, crystallinity index and surface charge density.[20–25] To obtain more dramatic changes in CNC properties, the acid used in the hydrolysis can be varied. Not only will this affect the aforementioned properties, it will also alter the surface chemistry. Controlling CNC surface chemistry in general[26] can lead to, for example, drastic differences in compatibility with other composite/hybrid/biological components,[27,28] new options for post-functionalization,[29] tailorable rheological and self-assembly behavior,[30] or enhanced thermal stability.[31] To date, many acids, including both mineral and organic, have been used to isolate CNCs from various cellulose sources. Although the sulfuric acid and hydrochloric acid protocols are the most studied,[32,33] production of CNCs with phosphoric,[34,35] hydrobromic,[36] citric,[37] maleic,[38] and oxalic acids[39] have also been demonstrated.

CNCs hydrolyzed with phosphoric acid (P-CNCs) have gained interest due to their high thermal stability in comparison to CNCs hydrolyzed with sulfuric acid (S-CNCs).[34] Results suggest that the surface charge density may play a role in the thermal degradation behavior of CNCs or that the flame retardant properties of phosphorus could be responsible; however, since there are many other differences between P-CNCs and S-CNCs, the thermal degradation mechanisms remain uncertain. P-CNCs have phosphate half-ester groups on their surfaces as opposed to the sulfate half-ester groups that decorate S-CNCs.[34] P-CNCs also have surface charge densities that are roughly two orders of magnitude lower than typical S-CNCs and increasing the harshness of the phosphoric acid hydrolysis has minimal effects on the phosphate group density.[35] Although their degree of crystallinity is similar, P-CNCs have higher aspect ratios and longer lengths than S-CNCs.[35] Therefore, it is

unclear whether the different thermal properties of these cellulosic materials are due to the surface chemistry, the surface charge density, or the inherent morphological and structural characteristics of the CNCs.

Herein, the term "thermal stability" refers to the ability of CNCs to resist heat-induced degradation, depolymerization, changes in crystalline structure and/or particle size and shape for *dried* CNCs. We emphasize that this is not the same as changes that occur when CNC suspensions are heated, such as changes in colloidal stability and rheological properties.[40–43] Additionally, discoloration may occur when CNCs are oven dried or added to a polymer melt, however, this does not necessarily imply thermally-degraded cellulose and is more likely due to the production of trace amounts of hydroxymethylfurfural.[44] The thermal stability of CNCs is thus highly dependent on the surrounding environment (dry, humid, in water/solvents/polymer) and the behavior of interest for a given application. It is important to note that the inherent dry thermal stability of CNCs is relatively high compared to other organic materials and the onset of degradation is typically reported to occur in the 150-350 °C range.[24,34,45]

To understand the effects of physico-chemical properties on cellulose thermal stability, the pyrolysis of cellulose must first be discussed. The first step upon exposure to heat is the "activation" of cellulose. This corresponds to the initial period in a thermogravimetric analysis (TGA) measurement where no mass is lost.[46] At this stage, the molecular weight distribution of the cellulose sample changes due to decomposition of the reducing ends between the crystalline regions of cellulose.[46] In the case of CNCs, the cellulose is already somewhat "active" because the degree of polymerization (DP) of the cellulose chains is near the LODP and many reducing ends are exposed.[47] Following the activation of cellulose, further depolymerization and degradation of cellulose chains will occur.[48,49] Here, there are two competitive pathways for the degradation of cellulose: a volatile fraction (condensable, low molecular weight products of cellulose degradation such as levoglucosan and anhydro-sugars and oligomers)[50] and a char and gas fraction (water, carbon dioxide and carbon monoxide).[48] At lower temperatures (< 240 °C), the pathway to char and gas production dominates. At higher temperatures, the pathway to volatiles dominates.[48]

The pyrolysis mechanisms of cellulose highlight the importance of structural characteristics such as DP, crystallinity index and crystallite size on thermal degradation. In the case of native/unmodified cellulose, these properties are a function of the cellulose source itself. Higher DP, crystallite length and crystallinity have been correlated with higher thermal stability, specifically for bacterial cellulose, *Halocynthia* cellulose, cotton linters, microcrystalline cellulose and wood flours.[47,51,52] Cellulose with a lower DP will have a greater number of reducing ends for a given mass and have more active sites at which degradation and depolymerization can begin. As such, CNCs typically have lower thermal stability than the cellulose fibers from which they are hydrolyzed. Furthermore, the DP of CNCs is highly dependent on starting material and significant differences in thermal stability of CNCs hydrolyzed from cotton (low DP) versus tunicate (higher DP) could likely be observed. Different cellulose sources will also produce CNCs with different crystallite

length and crystallinity, all of which will play a significant role in their thermal stability. Sulfuric acid hydrolyzed tunicate CNCs have been shown to have a relatively high thermal stability, with an onset of degradation at 150 °C,[53] but a direct comparison to the work here is complicated as it is difficult to separate the effects of structural characteristics, hydrolysis conditions, TGA protocol, and counterions, which all undoubtedly affect thermal stability.

The surface chemistry of cellulosic materials is also important when considering thermal stability since functional groups can enhance or delay thermal degradation of cellulose polymer chains. Cellulose acetate, for example, degrades at higher temperatures than cellulose itself.[47,54,55] It has been suggested that acetyl groups prevent surface hydroxyl groups and cellulose reducing ends from donating protons for hydrogen bond rearrangements that ultimately result in the depolymerization of cellulose.[46,47] The effects of phosphorylation on the thermal stability of water-soluble cellulose derivatives have also been studied. Although cellulose phosphate begins to degrade at lower temperatures than pure cellulose, it has been shown to increase fire-retardancy.[56–58] When cellulose phosphate is heated, dephosphorylation occurs and previously bound phosphate groups combine with water to form phosphoric acid. This further catalyzes the dehydration and decomposition of the cellulose chains and is polymerized to polyphosphorous acid, which forms a protective shield on cellulose surfaces and prevents flame propagation.[56,59] Another example of a cellulose derivative that reduces thermal stability is obtained by 2,2,6,6-tetramethylpiperidinyloxyl radical (TEMPO)-mediated oxidation of cellulose. The introduction of carboxylate groups to cellulose significantly lowers the onset of thermal degradation.[60] Similar results have been demonstrated with carboxymethyl cellulose.[61] The effects of both carboxylate and carboxymethyl groups on the thermal stability of cellulose surfaces can be somewhat mitigated by varying their counterions[60,61] and neutralizing the otherwise acidic surface charge groups. The differing effects of these surface chemistries outlines the need for a deeper understanding of the thermal stability of cellulose, particularly at the nanoscale.

To elucidate the effects of CNC properties on their thermal stability, herein we use a range of production strategies to tailor the surface chemistry, surface charge density, crystallinity and DP of CNCs. Cellulose was hydrolyzed with mixtures of phosphoric acid and sulfuric acid to obtain a range of phosphate and sulfate contents, as well as post-oxidized to introduce carboxylate groups. We hypothesize that by varying the hydrolysis "harshness" that different surface chemistries, morphology and DP will be obtained. TGA was used to identify which parameters have the most significant effects on thermal stability and provide guidance on how to best improve thermal stability of CNCs for future work.

6.3 Materials and methods

Materials. Sulfuric acid (98 wt%), phosphoric acid (85 wt%), hydrochloric acid (36 wt%), sodium hydroxide (96 wt%), sodium chloride (salt), dimethyl sulfoxide (DMSO), dimethyformamide (DMF) and methanol, were purchased from Caledon Laboratories Ltd. (Georgetown, Canada) and used as received. Dialysis tubing (14 kDa MWCO), 2,2,6,6-(tetramethylpiperidin-1-yl)oxyl (TEMPO, 99%), sodium bromide (NaBr, Reagent Plus® >99%), sodium hypochlorite (NaClO, 10-15%) and phenyl isocyanate (> 98%) were

purchased from Sigma-Aldrich (St. Louis, Missouri, USA). Anhydrous ethanol was purchased from Commercial Alcohols (Toronto, Canada). Whatman ashless filter aid (catalog no.1703-050) and Whatman glass microfiber filter paper (both GF/B and GF/D) were obtained from GE Healthcare Life Sciences Canada (Mississauga, Ontario, Canada). Poly(allylamine hydrochloride) (PAH, Mw 120 000-200 000 g/mol) was purchased from PolySciences (Warrington, USA) and used without further purification. All water used ("purified water") had a resistivity of 18.2 MΩ·cm and was purified by a Barnstead GenPure Pro water purification system from Thermo Fisher Scientific (Waltham, USA).

Acid hydrolysis methods. Cellulose nanocrystals were isolated from cotton Whatman ashless filter aid under a variety of conditions. For CNCs hydrolyzed with sulfuric acid, which will be referred to as S-CNCs, a well studied procedure was used.[19] 40 g of dry filter aid was blended with a Magic Bullet® to increase surface area and allow homogeneous wetting with the acid. Figure A6.1 in Appendix 6 shows the filter aid before and after blending. 700 mL of 64 wt% sulfuric acid was pre-heated to 45 °C and added to the filter aid. The reaction proceeded for 45 min with a mechanical stirrer. After the allotted time, the digested cellulose and acid mixture was quenched with 7 L of ice cold water. The suspension was left undisturbed until CNCs began to sediment (ca. 30 minutes). The supernatant was poured off and the remaining suspension was centrifuged for 10 min at 6000 rpm in a Sorvall RC-5 superspeed refrigerated centrifuge from Dupont. Once again, the supernatant was poured off and purified water was added to re-disperse the pellet that had formed. This centrifugation cycle was repeated until the CNCs remained in suspension after centrifugation rather than forming a pellet. The suspension was placed in dialysis tubing.

For CNCs isolated using phosphoric acid, which will be referred to as P-CNCs, a procedure outlined by Camarero-Espinosa et al. was used.[34] A pulp was made by blending 2 g filter aid with 100 mL of purified water in a Magic Bullet®. The pulp was placed in an ice bath and 261 mL of 85 wt% phosphoric acid was added while maintaining the temperature of the mixture below 30 °C. The acid and pulp mixture was placed in a round bottom flask and into an oil bath preheated to 100 °C. The mixture was left to react for 90 min under magnetic stirring. After the hydrolysis, the resulting suspension was quenched in an ice bath and left to cool for 15 min. Following this step, 600 mL of purified water was added to the suspension and it was centrifuged for 15 min at 3600 rpm. The supernatant was poured off, an additional 600 mL of purified water was added, and the centrifugation was performed again. After two centrifugation cycles, the suspension was placed in dialysis tubing.

CNCs produced with acid blends were isolated by adding some sulfuric acid (at 98 wt%) to the hydrolysis procedure used for P-CNCs (with 85 wt% phosphoric acid). These CNCs are referred to as PS-CNCs and three batches were isolated with varying amounts of sulfuric acid. The naming convention includes the molar ratio of phosphoric acid to sulfuric acid used in the hydrolysis; PS-CNC-44, PS-CNC-16 and PS-CNC-8 were isolated with molar ratios of 44:1, 16:1 and 8:1, respectively. In the case of PS-CNC-44, 5 mL of sulfuric acid was added to 256 mL of phosphoric acid and the resulting solution was added to the

cellulose pulp as described above. For PS-CNC-16, the acid solution was composed of 13 mL sulfuric acid and 248 mL phosphoric acid. Lastly, for PS-CNC-8, the acid solution was composed of 26 mL sulfuric acid and 235 mL phosphoric acid. All other steps in the hydrolysis procedure were repeated exactly as described above.

Following the hydrolysis procedure, all samples were dialysed and post-processed in the same way. Dialysis was carried out with purified water and daily water changes were performed until the pH of the dialysis water stabilized (15 rinses at a volume ratio of ca. 1:30 CNCs to purified water). Following this step, the CNC suspensions (ca. 2 L each) were sonicated in an ice bath with a Sonifier 450 probe sonicator from Branson Ultrasonics for 15 min/L of suspension at 60% output. To remove any large particles or contaminants due to the sonicator probe, the suspension was filtered through a glass microfiber filter with 1 µm pore size (for S-CNC) or 2.7 µm pore size (for P-CNC and PS-CNC). To convert CNCs from acid form (H^+ counterion, which is the native form) to sodium form (Na^+ counterion), suspensions were neutralized to pH 7.0 through the addition of NaOH.

TEMPO oxidation of S-CNCs. A TEMPO oxidation was performed on acid form S-CNCs as previously described in the literature.[62] to give the samples referred to as TEMPO-S-CNCs. TEMPO (0.0886 g) and NaBr (0.972 g) were dissolved in 54.5 mL of purified water. Once dissolved, the TEMPO/NaBr solution was added dropwise to 160 mL of 1.88 wt% S-CNCs in a round-bottom flask. Next, 18 g of a 12.5 wt% NaClO solution was added dropwise while ensuring the pH remained constant. The reaction was left to proceed for 3 hours while monitoring the pH of the suspension. Throughout the reaction, the suspension pH was maintained at 10.0 ± 0.2 by correcting with 1 M NaOH when necessary. To stop the reaction, 11 mL of ethanol was added to the flask. The pH of the suspension was then reduced to 2 through the addition of 1 M HCl to quench all remaining TEMPO. To purify the suspension, several centrifugation cycles were performed (15 min at 4500 rpm), followed by dialysis.

Atomic force microscopy (AFM). CNCs were imaged via AFM to observe morphology and, indirectly, CNC dispersion quality. Samples were prepared by first cleaning silica wafers in a piranha solution of 3:1 concentrated sulfuric acid to hydrogen peroxide.[63] Three spin-coating steps were then performed to generate thin CNC films on the silica wafers. Each step was performed at 4000 rpm for 30 s. First, 0.1 wt% PAH was deposited onto the silica wafer, followed by a rinse with water. Lastly, the dilute CNC suspensions (0.01 wt% or 0.005 wt%) were spin-coated onto the wafer. An MFP-3D AFM (Asylum Research an Oxford Instruments Company, Santa Barbara, USA) was used to image the samples in tapping mode with FMR cantilevers, which have a nominal force constant of 2.8 ± 0.7 N/m and a resonance frequency of 75 ± 15 Hz (NanoWorld, Neuchâtel, Switzerland). Asylum Research 13.17 software and Igor Pro 6.37 were used to flatten the images.

Zeta potential and dynamic light scattering (DLS). Light scattering-based zeta potential and apparent size measurements were performed with a Zetasizer Nano ZS from Malvern Instruments (Malvern, United Kingdom). The electrophoretic mobility of 0.1 wt% CNC suspensions with 5 mM NaCl was measured and converted to zeta potential following Smoluchowski theory. DLS measurements were performed on 0.025 wt% CNC

suspensions with no added salt. The results of the DLS measurements are referred to as "apparent CNC size" because the method is based on diffusion coefficients and assumes that the particles are spherical.[64] Since this is not the case for CNCs, these values are used merely as an indication of particle dispersion (or agglomeration) rather than to provide a direct measurement of CNC dimensions. For both DLS and zeta potential measurements, the sample average with 95% confidence (assuming normal distribution) is reported from three measurements.

Elemental analysis (ICP-OES). Elemental analysis was performed for P-CNCs, PS-CNCs and S-CNCs by the Xerox Research Centre of Canada with a Thermo Scientific ICAP 6500 inductively coupled plasma – optical emission spectrometry (ICP-OES) system. Freeze-dried CNCs (50-60 mg) were placed in a Teflon digestion tube with a few drops of purified water, 1 mL of hydrofluoric acid and 6 mL of a 60-70 wt% nitric acid solution. A Milestone UltraWAVE Digestion System was then used to digest the samples. After this, the samples were diluted in purified water to a volume of 25 mL for ICP-OES.

Conductometric titrations. For S-CNCs and TEMPO-S-CNCs, sulfate half-ester content and carboxylate content were determined via conductometric titration.[63] These CNCs were never dried and all reaction and purification steps were performed in purified water; as such, their surface charge groups were fully protonated. For P-CNCs and PS-CNCs, the surface charge density was too low to measure via conductometric titration, hence elemental analysis was performed as described above. S-CNCs were titrated by adding 0.0098 M NaOH in increments of 0.05 mL. To titrate TEMPO-S-CNCs, a known amount of 0.1 M HCl (ca. 0.3 mL) was first added to lower the pH, then the titration was performed by adding 0.0098 M NaOH in 0.05 – 0.1 mL increments. Three titrations were performed for each sample.

Degree of polymerization (DP) measurements. To measure the DP of the cellulose polymer chains that make up the CNCs, a carbanilation reaction was first performed to solubilize the cellulose in organic solvents.[30] Freeze-dried CNCs were placed in an oven at 80°C for 1 hour to remove any residual moisture. Following this, 25 mg of each sample was placed in a glass vial. 10 mL of DMSO and 1 mL of phenyl isocyanate were added to each vial. The vials were quickly mixed by shaking the vials and then placed in an oil bath pre-heated to 70°C. The vials were left in the oil bath for 40 hours with short breaks every 5-10 hours to shake them. After 40 hours, the carbanilation was terminated by adding 2 mL of methanol to each vial. The TEMPO-S-CNC sample appeared cloudy after 40 hours whereas the others were transparent; as such, the reaction was left to proceed for an additional 5 hours, at which point a clear solution was observed. This was done to ensure all cellulose chains were functionalized and fully dissolved in the DMSO. To the best of our knowledge, this carbanilation has not previously been performed on TEMPO oxidized CNCs and the effects of the surface carboxyl groups on the reaction kinetics are unclear. Once the reaction was terminated for each sample, the methanol was evaporated, leaving a solution of carbanilated cellulose chains in DMSO.

To measure the DP, the DMSO solutions were first diluted in DMF with 50 mM LiBr at a volumetric ratio of 3:1 (DMSO:DMF), then filtered with a 0.2 µm syringe filter. Samples

were then injected into a Polymer Laboratories PL-50 gel permeation chromatography (GPC) instrument from Agilent with a refractive index detector (Santa Clara, California, USA). This instrument is equipped with a Phenogel 5 µm linear column of length 300 mm and width 4.6 mm. DMF with 50 mM LiBr is used as the eluent and is eluted at a rate of 0.3 mL/min. The system was calibrated with PEG narrow standards from Polymer Laboratories. The DP of the cellulose chains was calculated by dividing the weight average molecular weight of the sample by 519 g/mol, the molecular weight of the repeat unit of cellulose tricarbanilate. This carbanilation/GPC method is favored for cellulose since it is known not to affect the DP and readily achieves a high degree of substitution compared to other derivatization reactions.[65,66] A degree of substitution of three was assumed, but was not measured. As a result, some cellulose chains may not have been fully substituted with carbanilate groups and the reported DP values may underestimate the actual DP of the samples. Experiments were run twice to confirm each molecular weight distribution.

Thermogravimetric analysis (TGA). Thermogravimetric analysis was performed on freeze-dried CNCs with a Simultaneous Thermal Analyzer (STA) 6000 from PerkinElmer (Waltham, Massachusetts, USA). Although other high temperature characterization techniques exist (differential scanning calorimetry, isothermal treatments and/or heating cellulose films), collecting TGA data while ramping the temperature up provides information over a wide temperature range and is classically used as a preliminary characterization of CNC thermal stability.[45] CNC pellets were made by weighing 8 ± 2 mg of CNCs into a 1 mL plastic syringe with a rubber plunging head. A second rubber plunging head was used to gently compress the CNCs into a pellet. This method is used to ensure that the dimensions of all pellets are consistent as the surface area of the material can affect its thermal degradation profile.[67] To perform the thermogravimetric analysis, a CNC pellet was placed in the instrument pan and was loaded into a chamber filled with nitrogen. The chamber temperature was raised from ambient temperature to 600 °C at a rate of 10 °C/min.

^{13}C CP/MAS NMR spectroscopy (solid state). [13]C Cross-polarization/Magic angle spinning (CP/MAS) experiments were performed with a Bruker Avance III 400 MHz spectrometer operated at 100.6 MHz for [13]C. The specimens were packed into a zirconia specimen rotor. The spinning rate was set at 12 kHz and the cross-polarization contact time at 2 ms. A recycled delay of 2 s was inserted between each cycle. Scans (6000) were accumlated for each spectrum. Degree of crystallinity was calculated by integrating the C4 signal between 93.0-86.5 ppm and 86.5-79.5 ppm for the crystalline and disordered phase, respectively, the degree of crystallinity being the ratio between the crystalline contribution over the sum of the integrals.[63] The measurement error is taken to be ca. $\pm 0.01\%$.

X-Ray diffraction (XRD). The crystallinity index of each sample was measured using X-Ray diffraction. CNC pellets with ca. 10 mg of freeze-dried CNCs were made via compression with two rubber plunging heads as described for TGA measurements. The pellets were mounted on a silicon wafer and positioned with a vertical D8 θ-θ goniometer. A cobalt sealed tube was used as an X-ray source to emit an electron beam with a wavelength of 1.79026 Å, an acceleration voltage of 35 kV and a probe current of 45 mA. This beam was adjusted with a 0.5 mm micro slit and a 0.5 mm short collimator. The Bruker

D8 Discover diffractometer with Davinci Design was used to collect two-dimensional frames at a detector distance of 14 cm. These frames were integrated with Diffrac.eva 4.0 to obtain one-dimensional frames and frames collected on an empty silicon wafer were subtracted. Following data collection, Rietveld refinement was used to match the measured diffraction spectra with models for both the crystalline and amorphous phases.[68,69] Intensity versus two-theta plots, as well as X-Ray diffraction patterns, and the results of the Rietveld refinement are shown for all samples in Figures A6.2, A6.3 and Table A6.1, respectively (Appendix 6). The amorphous phase was modelled with a Pseudo-Voigt function and a manually inserted fixed peak at 24.1° for all samples. Crystallinity index was obtained by comparing the contribution of the crystalline and amorphous peaks to the total diffraction spectrum of the sample. The measurement error is taken to be ca. ± 5%.

6.4 Results and discussion

Physico-chemical characterization of CNCs. Six types of cotton CNCs were prepared and characterized (Table 6.1) to determine the effect of morphology, surface charge density and surface chemistry on the thermal stability of lyophilized nanocellulose. Two CNC types were hydrolyzed with a single acid and their surface chemistries are reflective of the acid used; CNCs hydrolyzed with only phosphoric acid (P-CNCs) or only sulfuric acid (S-CNCs) had phosphate and sulfate half-ester groups, respectively. Additionally, S-CNCs were oxidized with TEMPO (TEMPO-S-CNCs) and contained both carboxylate and sulfate half-ester groups. Lastly, three types of CNCs were hydrolyzed with acid blends of $H_3PO_4:H_2SO_4$ (termed PS-CNCs), in varying molar ratios of 44:1, 16:1 and 8:1, from most to least phosphoric acid. These PS-CNCs had both phosphate and sulfate half-ester surface groups. After proper purification of each CNC type, samples were imaged by AFM to visualise particle size and shape, as well as the degree of agglomeration. Figure 6.1 shows a representative image from each CNC type.
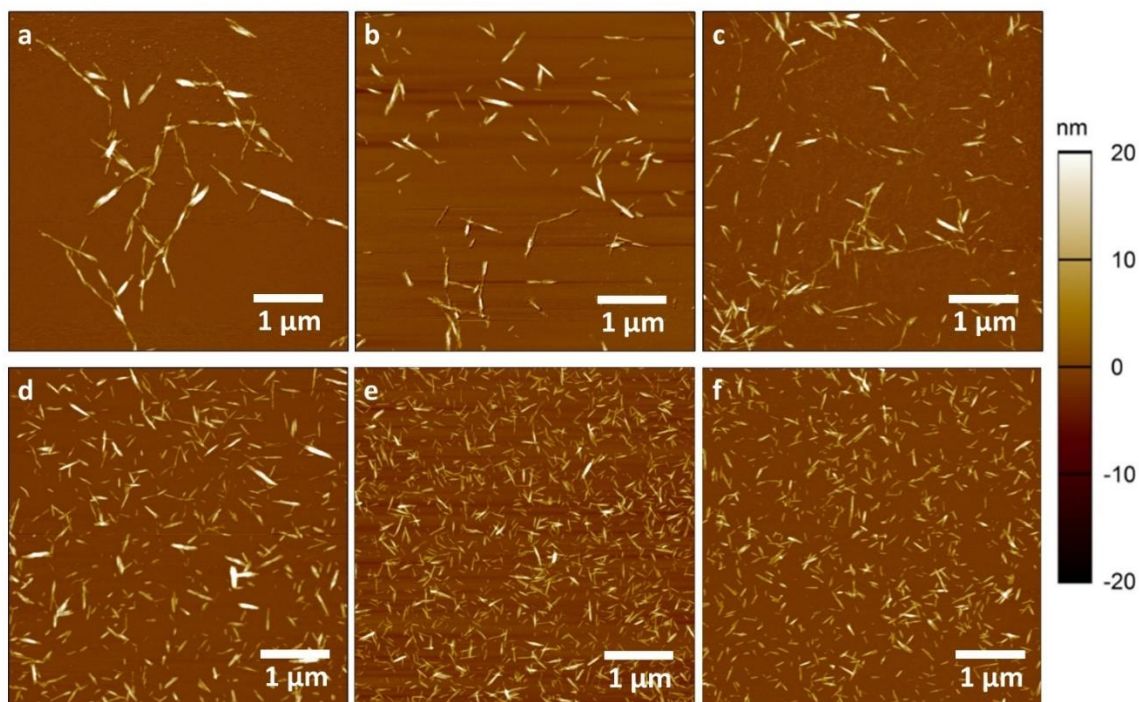
Figure 6.1. AFM of single and mixed-acid CNCs: (a) P-CNC, (b), PS-CNC-44 (c) PS-CNC-16, (d) PS-CNC-8, (e) S-CNC, and (f) TEMPO-S-CNC (ordered from most to least phosphoric acid used in the hydrolysis which corresponds to the least to most sulfuric acid used).

All six AFM images in Figure 6.1 show particles with nanoscale dimensions. Although particle morphologies differ, all hydrolysis conditions and post-functionalization steps produced high aspect ratio nanoparticles. Figure 6.1a shows the morphology of P-CNCs, while images 1e and 1f show the morphology of S-CNCs and TEMPO-S-CNCs, respectively. P-CNCs appear agglomerated or loosely hinged, particularly at their ends, which is different from that of CNCs hydrolyzed with sulfuric acid only. S-CNCs and TEMPO-S-CNCs appear well dispersed and the length of most particles is well under 1 µm (average 100-200 nm), as shown previously for both lab-made and industrially produced S-CNCs.[9] The difference in morphology between P-CNCs and S-CNCs could indicate that the phosphoric acid hydrolysis is incomplete. The LODP may not have been reached and disordered regions may still link crystalline regions together. The larger size of P-CNCs could also be related to partial crosslinking through phosphate groups[70,71] or low charge density which would lead to CNCs that were not colloidally stable in suspension before being deposited onto 2D substrates for AFM imaging.

Interestingly, when small amounts of sulfuric acid were added to the phosphoric acid hydrolyses, significant changes in the morphology of the resulting CNCs were observed. Figure 6.1b, 1c and 1d show CNCs hydrolyzed with acid blends with a decreasing molar ratio of phosphoric acid to sulfuric acid. Figure 6.1b shows sample PS-CNC-44 where few CNCs are loosely hinged and many more individual particles can be seen, compared to

Figure 6.1a. This trend continues as the acid ratio drops to 16:1 and further to 8:1. This last sample, PS-CNC-8 in Figure 6.1d, consists of well-dispersed and uniformly sized CNCs with lengths similar to S-CNCs. Therefore, by "doping" a phosphoric acid hydrolysis with sulfuric acid, significant changes in particle morphology were observed. This is primarily attributed to acid strength which is known to play an important role in cellulose hydrolysis. Protons from the dissociated acid protonate both glucosidic and cyclic oxygens within cellulose polymer chains.[72] Through this, and the addition of water, glucosidic bonds are split and shorter chains are formed. Simultaneously, esterification of hydroxyl groups occurs to form surface charge groups.[72] Phosphoric acid is a weak acid and, even at high concentrations, the phosphate ions are never fully dissociated.[73] Therefore, the concentration of protons is not as high as it would be in a molar equivalent solution of sulfuric acid (a strong acid). The phosphoric acid hydrolysis uses a higher acid concentration, a higher temperature and a longer reaction time than the sulfuric acid hydrolysis and still the resulting P-CNCs are larger than S-CNCs. Further increasing the harshness of the P-CNC hydrolysis only results in small decreases in particle size, likely due to small changes in the concentration of protons.[35] Conversely, by doping the phosphoric acid hydrolysis with small amounts of sulfuric acid, there is a significant increase in protons that results from the addition of a fully ionized acid. Sulfuric acid therefore acts as a catalyst (as proposed previously)[74] and the hydrolysis becomes harsher, and the disordered regions degrade faster, giving smaller nanocrystals within the given hydrolysis time.

The differences in CNC morphology and colloidal stability inferred from AFM are also supported by DLS and zeta potential measurements (Figure 6.2 and Table 6.1)). Figure 6.2a shows the apparent size of the six CNC types. A measured increase in size by DLS could indicate the presence of larger particles, a more agglomerated suspension, or both. Of all the samples, P-CNCs are largest; this is the result of having undergone the least harsh hydrolysis. Once sulfuric acid has been added to this weak hydrolysis, an immediate and significant decrease in size is seen (PS-CNC-44). Following this, further decreases in size are observed since the proportion of sulfuric acid in the acid blend increases (PS-CNC-16 and PS-CNC-8). Lastly, S-CNCs and TEMPO-S-CNCs have the smallest size (ca. 83 nm for both, as seen in Table 6.1) as they have been subjected to the harshest hydrolysis condition. From the AFM images in Figure 6.1, it is evident that increases in DLS apparent size for the six CNC types are due to both larger particles *and* more agglomeration. Thus, the effects of the hydrolysis conditions on the size of CNCs are exaggerated in Figure 6.2a and must be interpreted to include the effect of agglomeration as well.

To understand the agglomeration of CNCs (particularly those hydrolyzed with phosphoric acid), the electrophoretic mobility of particles was measured and the resulting zeta potential values are plotted in Figure 6.2b. P-CNCs have low colloidal stability, even under optimized hydrolysis conditions.[35] A zeta potential of -10 mV indicates the electrostatic repulsion between particles is insufficient to prevent agglomeration and, often, sedimentation, in aqueous suspension.[64] For many applications, CNCs with such low colloidal stability are not desirable as their behavior in suspension is inconsistent and difficult to predict. By adding sulfuric acid to the phosphoric acid hydrolysis, however,

CNCs with increased colloidal stability were obtained. As the H_3PO_4:H_2SO_4 ratio decreased, the magnitude of the zeta potential of the CNCs increased. When using an acid ratio of 8:1, CNCs with a zeta potential of -23 mV were produced. This value approaches the zeta potential of S-CNCs and TEMPO-S-CNCs, which have zeta potential values of ca. -40 mV. Although larger absolute magnitude zeta potential values are generally most desirable, the values of the PS-CNCs (particularly PS-CNC-8) demonstrate sufficient colloidal stability for many potential applications that would utilize CNCs in suspension form, e.g., rheological modifiers and interface stabilizers. Moreover, the enhancement in colloidal stability between P-CNCs and PS-CNC-8 (from -10 mV to -23 mV, where PS-CNC-8 was visibly stable) was achieved merely through the addition of a small amount of sulfuric acid to the hydrolysis (8 wt% sulfuric acid in the reaction mixture). It is therefore still considered to be a relatively weak hydrolysis in comparison to the common protocol used to produce S-CNCs.
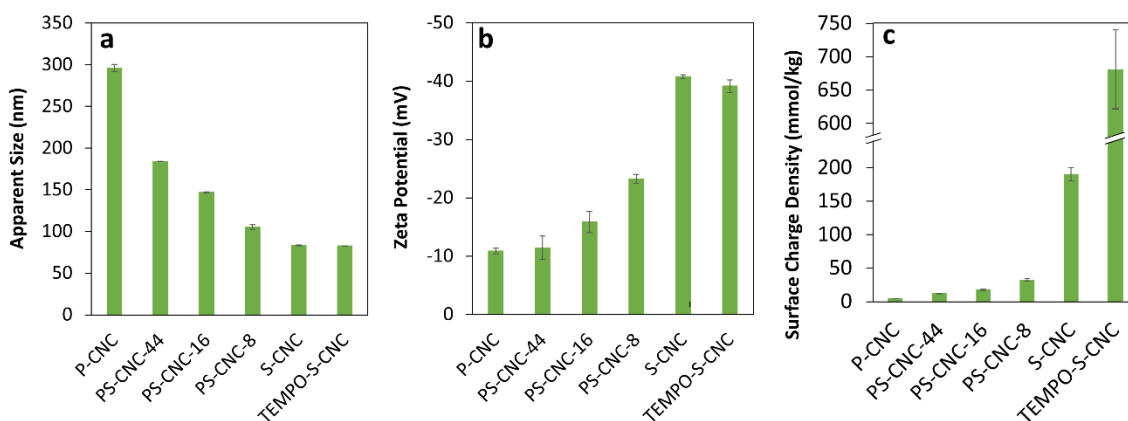
Figure 6.2. (a) Apparent particle size by dynamic light scattering(b) zeta potential of CNCs in acid form (pH values are 5.8, 5.7, 5.1, 4.6, 3.4, and 3.2 for P-CNC, PS-CNC-44, PS-CNC-16, PS-CNC-8, S-CNC, and TEMPO-S-CNC, respectively) and (c) CNC surface charge density.

The individual sulfate, phosphate and carboxylate contents and the total surface charge group content (i.e., charge density) are shown in Table 6.1 and Figure 6.2c, respectively. The measurements were obtained by elemental analysis and conductometric titration for the six CNC types. P-CNCs have the lowest surface charge density (< 5 mmol/kg CNC), which is similar to values reported previously.[34,35] For the acid blend PS-CNCs, the total surface charge density, which is a combination of both phosphate and sulfate half-ester groups, is proportional to the amount of sulfuric acid added to the hydrolysis. This data correlates with the increased zeta potential magnitudes discussed in the paragraph above. (The discrepancy between zeta potential and charge density for TEMPO-S-CNCs is because zeta potential was measured close to the pK_a of the carboxylic acid groups.) The CNCs hydrolyzed with a phosphoric to sulfuric acid molar ratio of 8:1 have a surface charge density of ca. 30 mmol/kg CNC; over 6 times that of the CNCs hydrolyzed with phosphoric acid alone. The highest surface charge densities, however, were obtained by hydrolyzing

CNCs with only sulfuric acid. S-CNCs and TEMPO-S-CNCs have surface charge densities that are approximately one to two orders of magnitude higher (at 200 and 680 mmol/kg, respectively) than that of P-CNCs and PS-CNCs.

The lower charge density of P-CNCs and PS-CNCs implies a resistance of phosphoric acid to esterify surface hydroxyl groups on CNCs. P-CNCs are hydrolyzed with a phosphoric acid concentration of 10.9 M, which is significantly higher than the 5.4 M sulfuric acid solution normally used to obtain S-CNCs. A higher acid concentration should result in the esterification of more surface hydroxyl groups since less water is present.[75] Water is a product of esterification, as such, increased presence of water would push the reaction equilibrium towards the reactants.[72,75] Since the high acid concentration used in hydrolyzing P-CNCs does not result in a high surface charge density, we infer that the esterification of surface hydroxyl groups to phosphate esters is less favorable than sulfate esters. This mechanism, however, appears to be catalysed by small amounts of sulfuric acid since the phosphate content of PS-CNC-44 (i.e., with merely 5 mL of H_2SO_4 added to 256 mL of H_3PO_4) is significantly greater than that of P-CNCs (Table 6.1).[76] When even more sulfuric acid is added to the hydrolysis (and the H_3PO_4:H_2SO_4 molar ratio is further decreased), exponentially more sulfate than phosphate groups are grafted to the CNC surface (and phosphate content actually decreases). PS-CNC-8, for example, is hydrolyzed with 9.9 M phosphoric acid and 1.3 M sulfuric acid; however, it has over ten times more sulfate groups than phosphate groups. Thus, not only is the phosphoric acid hydrolysis a weaker hydrolysis due to acid molecules not being fully dissociated, it also does not encourage esterification of hydroxyl groups to the extent that a sulfuric acid hydrolysis does.

Table 6.1. Physico-chemical properties of CNCs produced from hydrolysis with single acids, acid blends and with an additional post-oxidation step.

	Sulphur Content (mmol S/kg CNC)	Phosphate Content (mmol P/kg CNC)	Carboxylate Content (mmol COOH/kg CNC)	Zeta Potential (mV)	Degree of Poly-merization (DP)	Polydispersity Index (PDI)	% Crystallinity (NMR)	% Crystallinity (XRD)
P-CNC	—	4.9 ± 0.1^a	—	-10.9 ± 0.5	179	3.72	63	93
PS-CNC-44	5.4 ± 0.2^a	6.8 ± 0.3^a	—	-11 ± 2	194	3.60	63	94
PS-CNC-16	14 ± 1^a	4.0 ± 0.1^a	—	-16 ± 2	196	3.67	64	95
PS-CNC-8	30 ± 2^a	2.3 ± 0.1^a	—	-23.2 ± 0.8	188	3.75	66	95
S-CNC	190 ± 10^a 200 ± 10^b	—	—	-40.8 ± 0.3	94	2.57	73	98
TEMPO-S-CNC	200 ± 30^b	—	480 ± 30^b	-40 ± 1	154	3.24	71	99

[a]elemental analysis
[b]conductometric titration

Table 6.1 also presents the weight average degree of polymerization for the six types of CNCs (determined by GPC of carbanilated cellulose), and the molecular weight distributions are shown in Figure 6.3. The CNCs have different DP values depending on their hydrolysis method; P-CNCs and PS-CNCs have similar DP values between 179 and 196, while those hydrolyzed with sulfuric acid have the lowest DP, around half, at 94. TEMPO-S-CNCs have a DP of 154. All DP values measured are lower than the reported LODP for cotton which we partly attribute to the measurement method and the unknown degree of carbanilation, which would underestimate DP (as discussed in the Experimental section). For comparison, some published DP values determined by intrinsic viscosity are 280,[4] 220[77] and 260.[78] DP values similar to ours (all under 200) have been reported for S-CNCs using the same carbanilation/GPC method[30,79] and as such, we are primarily interested in the relative values and trends in DP rather than the absolute values. It is also worth noting that the TEMPO-S-CNCs were made from post-treating S-CNCs and it is highly unlikely that TEMPO oxidation could *increase* DP (i.e., 154 vs. 94). We believe that the carbanilation reaction was not as efficient with these CNCs and omit TEMPO-S-CNCs from further DP discussion.
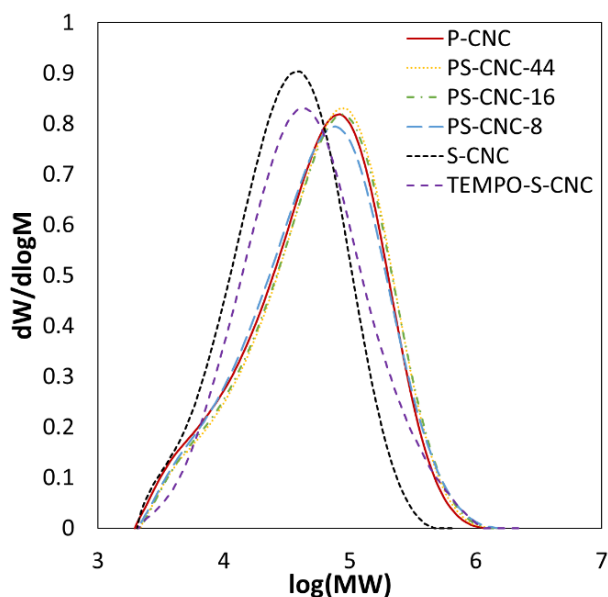
Figure 6.3. Molecular weight distribution of CNCs produced from different methods as measured by GPC of carbanilated cellulose in DMF.

The polydispersity index (PDI) values are also shown in Table 6.1; they vary between 2.57 and 3.75. P-CNCs and PS-CNCs have very similar PDI values, ranging from 3.60 to 3.75. S-CNCs have the lowest PDI (2.57) indicating a narrow spread of cellulose chain lengths due to a harsher and more uniform hydrolysis. This supports the AFM images in Figure 6.1, where the S-CNCs appear to have a more uniform size distribution, while the P-CNCs and PS-CNCs appear more polydisperse. The overlapping molecular weight distributions

for P-CNCs and PS-CNCs further confirm the similarity in polymer chain lengths in these samples (Figure 6.3). Furthermore, this similarity in DP suggests that P-CNCs are likely similar in length to PS-CNCs and the larger "size" seen from DLS and AFM is merely a result of CNC agglomeration (some end-to-end) due to low colloidal stability. The distribution of molecular weights in S-CNCs however, is shifted to the left, indicating the presence of significantly shorter polymer chains. All samples except the TEMPO-S-CNCs have a small low-molecular weight shoulder that is generally attributed to insoluble oligosaccharides precipitated onto the CNC surface.[30] The TEMPO oxidation likely transforms these oligosaccharides into soluble cellulose derivatives which are then removed during the purification steps. Upon analysis of Figure 6.3 and the calculated data in Table 6.1, the five esterified CNC samples appear to fall into two categories: (1) CNCs with higher DP cellulose and larger PDI, hydrolyzed with phosphoric acid or acid blends, and (2) CNCs with lower DP cellulose and smaller PDI, hydrolyzed with sulfuric acid alone.

It is interesting that there is no trend between the amount of sulfuric acid used to produce the PS-CNCs and the resulting cellulose DP. As the amount of sulfuric acid increases, the acid strength of the blend increases, which would be expected to further depolymerize the cellulose due to an increase in the rate of cellulose hydrolysis. Since all P-CNC and PS-CNC samples have the same reaction time (90 minutes), the similarity in their DP suggests that their hydrolysis rates are similar, regardless of the amount of sulfuric acid that has been added. The S-CNCs, however, have cellulose chains half the length of P-CNCs and PS-CNCs, despite their shorter reaction time of 45 minutes. The acid in larger proportions thus dictates the hydrolysis rate and resulting DP.

Additionally, it is noteworthy that P-CNCs appear to be significantly larger than PS-CNCs in both AFM and DLS measurements, despite having similar DP values and molecular weight distributions. This is exemplified by the apparent particle size by DLS where P-CNCs (296 ± 4 nm) are nearly three times larger than PS-CNC-8 (105 ± 3 nm) yet have a DP of 179 and 188, respectively. The larger particle size of P-CNCs is thus mostly attributed to agglomeration (as expected from zeta potential) and also similar end-to-end agglomeration of CNCs has been reported recently in systems where surface charge was highly screened or removed through thermal treatment.[43,80] In general, the weak trend in size and DP highlights the difficulties associated with characterizing naturally polydisperse materials.

Another key morphological property for CNCs is the degree of crystallinity; since CNCs are isolated by degrading disordered/defect regions in the cellulose structure they are generally highly crystalline, however, the exact value is known to depend on the measurement method and sample preparation.[81–84] All six types of CNCs prepared had high crystallinity as evidenced by XRD and solid state NMR (Table 6.1). This indicates that few disordered regions are present in the final nanocrystals, regardless of the hydrolysis conditions. According to XRD, the crystallinity values are all over 90%, with increasing crystallinity correlated with increasing harshness of hydrolysis. However, the values from XRD in Table 6.1 are within the experimental precision of the method estimated to be $\pm$

5%. As such, degree of crystallinity was also determined via NMR and the same trend was observed: crystallinity increased with increased harshness of hydrolysis, ranging from 63-73% (with precision taken to be ± 0.1%). The discrepancy in values between the two techniques is well known[82] and, simplistically stated, is a result of the fact that NMR does not "see" the CNC surfaces as crystalline but XRD does (XRD is therefore more dependent on how the sample is dried and packed). Despite the trend of crystallinity increasing with hydrolysis strength, the differences between P-CNCs and S-CNCs are much smaller than one would expect based on the large differences in DP values. This may imply that some of the "disordered" regions are in fact very small defects that, although they may be more susceptible to chemical attack, they are not significantly large enough or disordered enough to be detected as "non-crystalline" by XRD and NMR. This conclusion is similar to the neutron study of Nishiyama et al.[8] and a report by Usov et al. that demonstrates that along a given cellulose nanofibril (obtained via TEMPO-mediated oxidation of wood pulp), no variation in mechanical properties can be detected within a spatial resolution of a few nanometers, implying that disordered regions either do not exist or are exceptionally small.[85]

Thermal properties of CNCs. The thermal stability of each CNC type, in both the sodium and acid form (i.e., the surface sulfate or phosphate half-ester group has a Na^+ or proton counterion), was evaluated using TGA. In Figure 6.4, the degradation profiles of CNCs in sodium form are shown, as well as the mass loss rates with respect to temperature (dW/dT). The application of CNCs in sodium form is widespread and is the most industrially relevant since commercial CNCs are normally shipped as dried powders, spray dried or freeze dried from neutralized sodium form suspensions. This is done because only CNCs dried from the sodium form are re-dispersible in water and other media – acid form CNCs tend to aggregate irreversibly when dried.[86] According to Figure 6.4a, in sodium form, TEMPO-S-CNCs have the lowest onset of thermal degradation (226 °C) and are the only sample to have more than one degradation peak. Next, S-CNCs begin to degrade at 272 °C. Next, samples P-CNC, PS-CNC-44, PS-CNC-16 and PS-CNC-8 all begin to degrade at similar temperatures (281 °C, 284 °C, 297 °C and 292 °C, respectively) and show significantly higher resistance to *start* thermally degrading compared to TEMPO-S-CNCs and S-CNCs.

Table 6.2 shows the maximum degradation rate for each CNC type and the temperatures at which it occurs (i.e., the peaks in the derivative curves in Figure 6.4b). In sodium form, S-CNCs and TEMPO-S-CNCs experience their maximum degradation rate at the lowest temperatures: 309 °C and 318 °C, respectively. P-CNCs and PS-CNCs all experience their maximum degradation rate at very similar temperatures, between 359 °C and 362 °C. The rates themselves are also informative. The degradation of S-CNCs is fast; in fact, this sample reaches the highest rate of degradation (-2.14%/°C) of all samples analysed by TGA. P-CNCs and PS-CNCs all have similar maximum degradation rates (between -1.56%/°C and -1.43%/°C), while TEMPO-S-CNCs have the lowest maximum degradation rate of -1.04%/°C.

Figure 6.4. Thermogravimetric analysis of CNCs in neutralized sodium-salt form. (a) Sample mass as a function of increasing temperature and (b) sample mass loss rate with respect to temperature, as a function of increasing temperature.

The thermal degradation profiles for all sodium form CNCs hydrolyzed with phosphoric acid or acid blends are nearly identical. Despite their varying surface chemistries, surface charge densities, zeta potential values, particle sizes and degrees of crystallinity, they respond similarly to high temperatures. Once neutralized (i.e., converted to sodium form), surface phosphate and sulfate ester groups appear not to affect the thermal stability of the CNCs they are grafted to. Conversely, the thermal degradation behavior can be attributed to the single property that is consistent across all P-CNCs and PS-CNCs: the DP of cellulose chains. Likewise, S-CNCs, which degrade at lower temperatures, have lower DP. Since their cellulose chains are shorter, there are more reducing ends in a given mass of S-CNCs compared to higher DP celluloses. These reducing ends are the initiating sites for depolymerization and degradation.[46] The TEMPO-S-CNCs, however, do not demonstrate the same DP and thermal stability correlation and the effect of the carboxylate groups on the thermal stability appears significant, even in sodium form. (This phenomenon will be discussed further below with the results for acid form TEMPO-S-CNCs.) However, overall, for CNCs with phosphate and/or sulfate half-ester groups, the thermal stability in sodium form is shown for the first time to be primarily dictated by the DP of cellulose rather than by the surface charge density or the nature of the surface charge groups, as speculated previously.

Table 6.2. Onset of thermal degradation, maximum thermal degradation rates and maximum thermal degradation temperatures for CNCs in sodium and acid form.

	Onset of Thermal Degradation in Sodium Form (°C)	Max. Degradation Rate in Sodium Form (% mass/°C)	Temp. @ Max. Degradation Rate in Sodium Form (°C)	Onset of Thermal Degradation in Acid Form (°C)	Max. Degradation Rate in Acid Form (% mass/°C)	Temp. @ Max. Degradation Rate in Acid Form (°C)	Difference Between Acid and Sodium Form Temp. @ Max. Rate (°C)
	Sodium Form			**Acid Form**			
P-CNC	281	-1.52	362	299	-1.99	356	5.8
PS-CNC-44	284	-1.56	360	297	-1.81	361	-0.38
PS-CNC-16	297	-1.47	360	275	-1.41	339	21
PS-CNC-8	292	-1.43	359	249	-0.93	326	33
S-CNC	272	-2.14	309	166	-0.44	220	89
TEMPO-S-CNC	226	-1.04	318	168	-0.46	232	86

Figure 6.5a and 5b shows the TGA curves and mass loss rates with respect to temperature for the six CNC types in the acid form. Acid form CNCs generally appeared less thermally stable than sodium form, as demonstrated previously for S-CNCs,[24] and shown by the comparison of TGA curves in both acid and sodium form for S-CNCs and P-CNCs in Figure 6.5c. Rates and temperatures at the maximum degradation rate are listed in Table 6.2. S-CNCs and TEMPO-S-CNCs again begin to degrade at the lowest temperatures: 166 °C, and 168 °C, respectively. For P-CNC, PS-CNC-44, PS-CNC-16 and PS-CNC-8, the onset of thermal degradation occurs at 299 °C, 297 °C, 275 °C, and 249 °C, respectively. As such, P-CNC and PS-CNC-44 samples are the most thermally stable. These results demonstrate a correlation between thermal stability and surface chemistry/surface charge density (Table 6.1) for CNCs when they are in acid form. The lower the surface charge density, the higher the thermal stability. Conversely, as more sulfuric acid is used in the hydrolysis and more surface charge groups are formed on the CNC surface, thermal degradation occurs at lower temperatures. However, the effect of the carboxylic acid groups on thermal stability of TEMPO-S-CNCs (in acid form) appears negligible; the mass loss curve for this sample is identical to that of the S-CNCs.

Many studies have linked reduced thermal stability of CNCs to increased density of sulfate half-ester groups without making a distinction between the counterions or "form" of the CNCs.[24,75,87] Sulfate groups on CNC surfaces are known to undergo self-catalyzed desulfation, this process is faster at higher temperatures and is fastest for dried CNCs (as compared to CNCs in aqueous suspensions).[88] A similar process likely occurs for phosphated CNCs. Following these de-esterification reactions which eliminate surface groups, free sulfate and phosphate groups can recombine with bound water (since "dry" CNCs always have some residual moisture estimated at around 2-5 wt%) and with the water

released as a byproduct of the pyrolysis reactions, to produce localized and concentrated acid at the CNC surface. This acid then catalyses further de-esterification, acid hydrolysis, degradation and depolymerization of cellulose.[56,59] When CNCs are in the neutralized sodium form, acid-driven degradation pathways are not invoked to the same degree. Therefore, in acid form, the surface phosphate and sulfate half-ester groups appear to govern the thermal degradation behavior of CNCs.
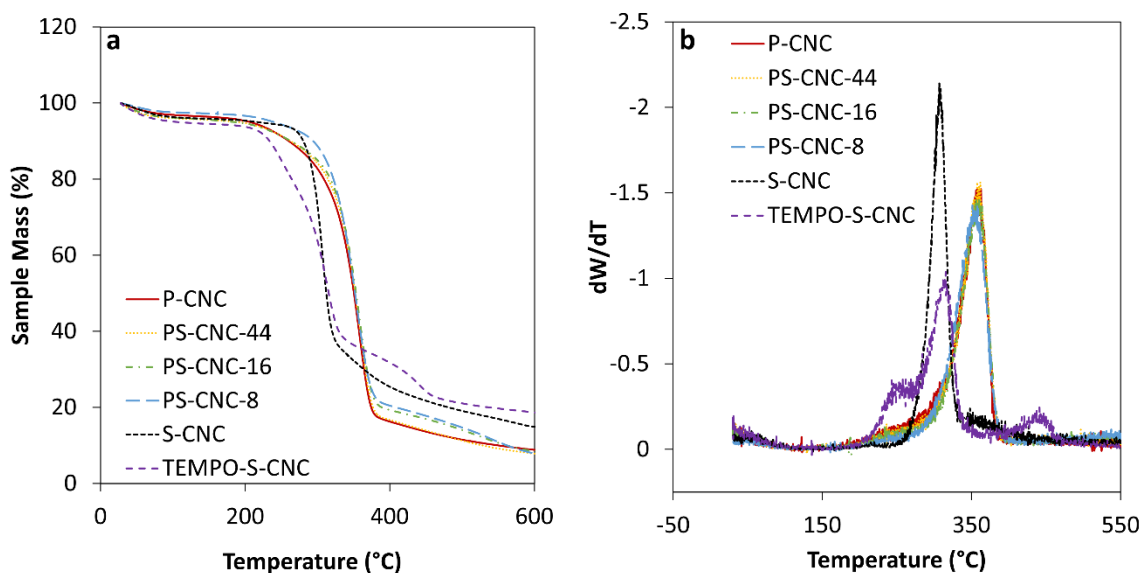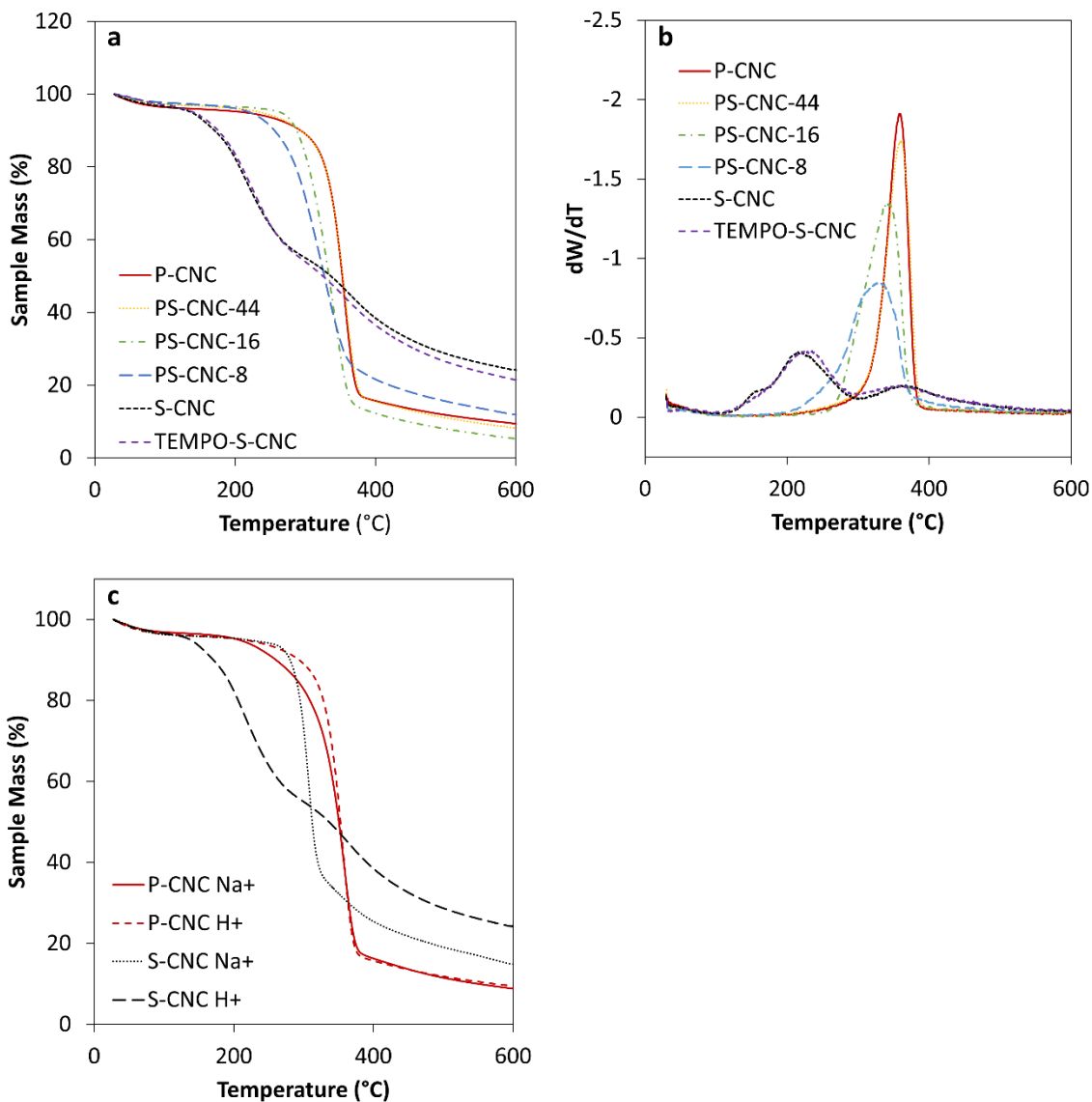

Figure 6.5. Thermogravimetric analysis of CNCs in acid form. (a) Sample mass as a function of increasing temperature, (b) sample mass loss rate with respect to temperature, as a function of increasing temperature and (c) comparison of P-CNC and S-CNC mass loss as a function of increasing temperature in both acid form and neutralized sodium form.

Other noticeable features from both Figure 6.5 and Table 6.2 are the maximum degradation rates of each sample and the temperatures at which they occur. Acid form CNCs with low surface charge density (P-CNC and PS-CNC-44) begin thermally degrading at the highest temperatures and have their maximum degradation rates at the highest temperatures (ca. 360 °C) but because of these high temperatures, also degrade the fastest (at nearly -2%/°C). As surface charge density increases, the maximum degradation rates and the temperatures at which they occur both decrease. For S-CNCs and TEMPO-S-CNCs, the sample mass never changes by more than -0.5%/°C and the maximum degradation rates occur at 220 °C and 232 °C, respectively. High degradation rates favor fast pyrolysis processes at high temperatures and produce more volatile pyrolysis products.[48,50] This can be seen from Figure 6.5a where CNCs with high thermal stability and fast degradation rates (i.e., P-CNCs and PS-CNCs) are primarily degraded into small, volatile molecules rather than forming char, leading to low remaining sample masses at the end of the TGA measurement (ca. 10% at 600 °C). Conversely, S-CNCs with lower thermal stability follow slow pyrolysis processes (at lower temperatures) and are converted to char, a stable solid material that is apparent as ca. 25% of the sample mass remaining at 600 °C.

TEMPO-S-CNCs standout amongst the CNC types with vastly different thermal behavior, both favorable and unfavorable properties are observed. This is somewhat surprising since they are derived from the same S-CNCs characterized here and have similar dimensions and crystallinity. They likely have similar DP as well; however, further optimization of the carbanilation/GPC protocol is needed. In sodium form, TEMPO-S-CNCs start degrading at the lowest temperature and the TGA profile has two major peaks that are characteristic of TEMPO-oxidized cellulose. The first peak corresponds to the degradation of the anhydroglucuronic acid units and as the sample is heated, the carboxylate groups also participate in decarbonation and decarboxylation reactions that degrade the cellulose chains.[60] The second peak corresponds to the degradation of the remaining un-functionalized cellulose.[60] These two decomposition pathways act to decrease the maximum thermal degradation rates by 50%. However, this is only the case for the sodium form; in acid form, TEMPO-S-CNCs and S-CNCs have the same decomposition profiles and the differences between sodium and acid form maximum degradation temperature are also similar, implying that the sulfate half ester groups strongly dominate the behavior. This also implies that the carboxyl groups have little to no effect on thermal stability in acid form (due to the low degradation temperature) and that the oxidizing effects of carboxyl groups are relevant only at the higher temperatures that sodium form CNCs can reach. We can thus conclude that the effect of neutralizing surface charge groups to improve thermal stability is only relevant for the sulfate and phosphate half ester groups and not for carboxylic acid groups. Additionally, these results only pertain to CNCs oxidized with TEMPO after a sulfuric acid hydrolysis (TEMPO-S-CNC), as CNCs with carboxylic acid groups obtained via hydrolysis with organic acids have been shown to have higher thermal stability than S-CNCs.[39] CNCs hydrolyzed with organic acids, however, can likely attribute their higher thermal stability to higher DP since the hydrolysis conditions are not as harsh as those of a sulfuric acid hydrolysis. This suggests that the hydrolysis process (and the

resulting CNC DP) likely dictates the thermal properties more than the final surface chemistry.

By directly comparing thermal stability of CNCs in sodium and acid form, new insight into thermal degradation behavior emerges. As shown in Table 6.2, neutralizing the CNCs generally increases the degradation onset (also shown in Figure 6.5c for P-CNCs and S-CNCs specifically), the maximum degradation temperature, and the degradation rate. The largest differences between the two forms are seen for CNCs with the highest surface charge densities. For example, for S-CNCs, the onset and maximum degradation temperatures are increased almost 100 °C by neutralizing but with the trade-off of increasing the decomposition rate, which may be an important consideration depending on the intended application and processing conditions for CNC-based materials. P-CNC and PS-CNC-44 samples are the opposite of S-CNCs and show very similar degradation profiles, regardless of counterion, because their surface charge densities are negligible. (PS-CNC-16 and PS-CNC-8 fall in between the two extremes.) Again, this supports the notion that the difference between thermal degradation profiles in sodium and acid form is the effect of neutralization of the surface ester groups. Once these groups have been neutralized and cannot create localized acid (or for CNCs with very low surface charge density), the thermal stability of CNCs is primarily dependent on the cellulose DP.

Figure 6.6 demonstrates the two main correlations elucidated in this study: the temperature at the maximum degradation rate for CNCs as a function of DP (Figure 6.6a), and the temperature difference at the maximum degradation rate between acid and sodium form CNCs as a function of surface charge density (Figure 6.6b). Both data sets in Figure 6.6a have positive correlations between DP and the temperature at which the maximum degradation rate occurs, though the correlation coefficient (R^2) for sodium form CNCs is higher. In acid form, there is still a correlation between DP and thermal stability (with a smaller R^2 but with a larger slope) because the surface charge density also plays a large role and cannot be decoupled in this plot. Figure 6.6b decouples the effect of DP from surface charge and clearly demonstrates the effect of neutralizing surface ester groups on thermal stability of CNCs; as discussed above and shown in Figure 6.5c, CNCs with higher surface charge density have larger differences between acid and sodium form thermal stability, while CNCs with lower surface charge densities have less significant differences. Although other physico-chemical properties vary between the six types of CNCs analyzed in this study, CNC surface charge density and cellulose DP appear to have the greatest effects on thermal stability. (Weak correlations and small slopes were found for plots of thermal stability versus the other CNC properties and furthermore, the temperature at maximum degradation rate was found to better show trends in thermal stability compared to the onset of thermal degradation.)

It is worth noting that, although higher degrees of crystallinity are known to result in higher thermal stability for macroscopic cellulosic samples,[51,52] this was not the case for the samples tested in this study. S-CNCs have a statistically significant higher degree of crystallinity (as measured by NMR) than P-CNCs or PS-CNCs, yet they degrade at the lowest temperatures. We hypothesize that for highly crystalline materials, the nuances in

degree of crystallinity are outweighed by the effects of surface charge density and cellulose DP.
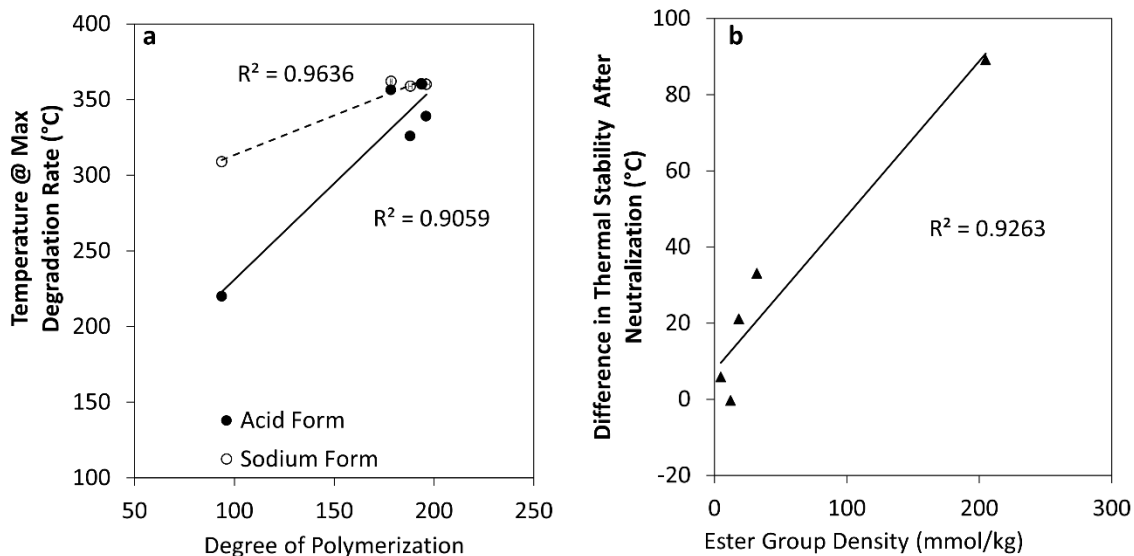
Figure 6.6. Temperature at which the maximum degradation rate is measured for acid (●) and sodium (○) form CNCs as a function of degree of polymerization (a) and difference between the temperature at which the maximum degradation rate occurs for acid form and neutralized sodium-salt form CNCs as a function of ester group density (b). TEMPO-S-CNCs were not included in this analysis.

6.5 Conclusions

This study has provided new insight into the thermal stability of CNCs and their degradation behavior in both sodium and acid form. We can now propose a number of routes to tailor CNC thermal stability depending on the desired behavior. The first route is to change the onset of thermal degradation and maximum degradation temperature (and rate) by changing the CNC hydrolysis conditions or using a post-oxidation modification step. Weaker hydrolyses and no oxidation step gave more thermally stable CNCs. The second route is to change the counterion on the CNC surface group through neutralization; sodium form CNCs were more thermally stable and the spread in thermal properties amongst the six CNC types was smaller (i.e., all materials behaved more consistently), compared to acid form CNCs.

The wide range of CNC properties obtained here through hydrolysis with single acids or acid blends provided the ideal platform to link specific physico-chemical properties to CNC thermal degradation behavior. For the first time is was shown that in sodium form, surface charge groups had minimal impact on thermal stability and it was the DP of cellulose that dominated the behavior. All CNCs isolated with phosphoric acid or acids blends had similar DP values and thermal degradation profiles. Sulfuric acid hydrolyzed CNCs had the lowest thermal stability because of their low DP (and higher number of reducing ends). Conversely, thermal stability of CNCs in acid form was highly dependent on surface charge

density of ester groups – carboxylic acid groups did not change the thermal behavior. This is because the localized acid that is produced when half-ester groups are eliminated from the CNC surfaces further accelerates acid hydrolysis and degradation of cellulose at high temperatures. Even higher temperatures are likely required for carboxylic acid groups to affect thermal stability via decarboxylation and decarbonation reactions. In acid form, CNCs with the highest surface charge densities (S-CNCs and TEMPO-S-CNCs) degraded at the lowest temperatures, whereas P-CNCs and PS-CNCs were more thermally stable.

Finally, producing CNCs with acid blends is a novel and adaptable method to control CNC properties. While the focus here was on thermal stability, it is noteworthy that the colloidal stability could also be tailored with charge densities spanning three orders of magnitude. Doping the phosphoric acid hydrolysis with sulfuric acid elucidated the catalytic effects of strong acids on cellulose hydrolysis and provided a straightforward way to tailor cellulose DP for a new "toolbox" of CNCs with unique properties.

6.6 References

1.   Leung, A. C. W. *et al.* Characteristics and properties of carboxylated cellulose nanocrystals prepared from a novel one-step procedure. *Small* **7**, 302–305 (2011).

2.   Nelson, K. *et al.* American process: Production of low cost nanocellulose for renewable, advanced materials applications. *Springer Ser. Mater. Sci.* **224**, 267–302 (2016).

3.   Habibi, Y., Lucia, L. A. & Rojas, O. J. Cellulose Nanocrystals : Chemistry , Self-Assembly , and Applications. **110**, 3479–3500 (2010).

4.   Nickerson, R. F. & Habrle, J. A. Cellulose intercrystalline structure. *Ind. Eng. Chem.* **39**, 1507–1512 (1947).

5.   Battista, O. A., Coppick, S., Howsmon, J. A., Morehead, F. F. & Sisson, W. A. Level-off degree of polymerization. *Ind. Eng. Chem.* **48**, 333–335 (1956).

6.   Rånby, B. G., Banderet, A. & Sillén, L. G. Aqueous colloidal solutions of cellulose micelles. *Acta Chem. Scand.,* **3**, 649–650 (1949).

7.   Mukherjee, S. M. & Woods, H. J. X-ray and electron microscope studies of the degradation of cellulose by sulphuric acid. *Biochim. Biophys. Acta* **10**, 499–511 (1953).

8.   Nishiyama, Y. *et al.* Periodic disorder along ramie cellulose microfibrils. *Biomacromolecules* **4**, 1013–1017 (2003).

9.   Reid, M. S., Villalobos, M. & Cranston, E. D. Benchmarking cellulose nanocrystals: from the laboratory to industrial production. *Langmuir* **33**, 1583–1598 (2017).

10.   Mariano, M., El Kissi, N. & Dufresne, A. Cellulose nanocrystals and related nanocomposites: Review of some properties and challenges. *J. Polym. Sci. Part B Polym. Phys.* **52**, 791–806 (2014).

11.   Cao, Y., Zavaterri, P., Youngblood, J., Moon, R. & Weiss, J. The influence of cellulose nanocrystal additions on the performance of cement paste. *Cem. Concr. Compos.* **56**, 73–83 (2015).

12.   Cao, Y. *et al.* The influence of cellulose nanocrystals on the microstructure of cement paste. *Cem. Concr. Compos.* **74**, 164–173 (2016).

13.   Moon, R. J., Martini, A., Nairn, J., Simonsen, J. & Youngblood, J. Cellulose nanomaterials review: structure, properties and nanocomposites. *Chem. Soc. Rev.* **40**, 3941–3994 (2011).

14.   Capron, I., Rojas, O. J. & Bordes, R. Behavior of nanocelluloses at interfaces. *Curr. Opin. Colloid Interface Sci.* **29**, 83–95 (2017).

15.   De France, K. J., Hoare, T. & Cranston, E. D. Review of Hydrogels and Aerogels

Containing Nanocellulose. *Chem. Mater.* **29**, 4609–4631 (2017).

16.   Giese, M., Blusch, L. K., Khan, M. K. & MacLachlan, M. J. Functional materials from cellulose-derived liquid-crystal templates. *Angew. Chemie - Int. Ed.* **54**, 2888–2910 (2015).

17.   Domingues, R. M. a R., Gomes, M. E. M. & Reis, R. R. L. The potential of cellulose nanocrystals in tissue engineering strategies. *Biomacromolecules* **15**, 2327–2346 (2014).

18.   Dastjerdi, Z., Cranston, E. D. & Dubé, M. A. Pressure sensitive adhesive property modification using cellulose nanocrystals. *Int. J. Adhes. Adhes.* **81**, (2018).

19.   Revol, J.-F., Bradford, H., Giasson, J., Marchessault, R. H. & Gray, D. G. Helicoidal self-ordering of cellulose microfibrils in aqueous suspension. *Int. J. Biol. Macromol.* **14**, 170–172 (1992).

20.   Dong, X. M., Revol, J.-F. & Gray, D. G. Effect of microcrystallite preparation conditions on the formation of colloid crystals of cellulose. *Cellulose* **5**, 19–32 (1998).

21.   Beck-Candanedo, S., Roman, M. & Gray, D. G. Effect of reaction conditions on the properties and behavior of wood cellulose nanocrystal suspensions. *Biomacromolecules* **6**, 1048–1054 (2005).

22.   Bondeson, D., Mathew, A. & Oksman, K. Optimization of the isolation of nanocrystals from microcrystalline cellulose by acid hydrolysis. *Cellulose* **13**, 171–180 (2006).

23.   Dong, S., Bortner, M. J. & Roman, M. Analysis of the sulfuric acid hydrolysis of wood pulp for cellulose nanocrystal production: A central composite design study. *Ind. Crops Prod.* **93**, 76–87 (2016).

24.   Kargarzadeh, H. *et al.* Effects of hydrolysis conditions on the morphology, crystallinity, and thermal stability of cellulose nanocrystals extracted from kenaf bast fibers. *Cellulose* **19**, 855–866 (2012).

25.   Chen, L. *et al.* Tailoring the yield and characteristics of wood cellulose nanocrystals (CNC) using concentrated acid hydrolysis. *Cellulose* **22**, 1753–1762 (2015).

26.   Habibi, Y. Key advances in the chemical modification of nanocelluloses. *Chem. Soc. Rev.* **43**, 1519–1542 (2014).

27.   Kedzior, S. A. *et al.* Incorporating cellulose nanocrystals into the core of polymer latex particles via polymer grafting. *ACS Macro Lett.* 990–996 (2018) doi:10.1021/acsmacrolett.8b00334.

28.   Roman, M. Toxicity of cellulose nanocrystals: a review. *Ind. Biotechnol.* **11**, 25–33

(2015).

29.   Araki, J., Wada, M. & Kuga, S. Steric stabilization of a cellulose microcrystal suspension by poly(ethylene glycol) grafting. *Langmuir* **17**, 21–27 (2001).

30.   Bouchard, J., Méthot, M., Fraschini, C. & Beck, S. Effect of oligosaccharide deposition on the surface of cellulose nanocrystals as a function of acid hydrolysis temperature. *Cellulose* **23**, 3555–3567 (2016).

31.   Eyley, S. S. & Thielemans, W. Surface modification of cellulose nanocrystals. *Nanoscale* **6**, 7764–79 (2014).

32.   Araki, J., Wada, M., Kuga, S. & Okano, T. Flow properties of microcrystalline cellulose suspension prepared by acid treatment of native cellulose. *Colloids Surfaces A Physicochem. Eng. Asp.* **142**, 75–82 (1998).

33.   Yu, H. *et al.* Facile extraction of thermally stable cellulose nanocrystals with a high yield of 93% through hydrochloric acid hydrolysis under hydrothermal conditions. *J. Mater. Chem. A* **1**, 3938–3944 (2013).

34.   Camarero Espinosa, S., Kuhnt, T., Foster, E. J. & Weder, C. Isolation of Thermally Stable Cellulose Nanocrystals by Phosphoric Acid Hydrolysis. *Biomacromolecules* **14**, 1223–1230 (2013).

35.   Vanderfleet, O. M., Osorio, D. A. & Cranston, E. D. Optimization of cellulose nanocrystal length and surface charge density through phosphoric acid hydrolysis. *Philos. Trans. R. Soc. London A Math. Phys. Eng. Sci.* **376**, 1–7 (2018).

36.   Sadeghifar, H., Filpponen, I., Clarke, S. P., Brougham, D. F. & Argyropoulos, D. S. Production of cellulose nanocrystals using hydrobromic acid and click reactions on their surface. *J. Mater. Sci.* **46**, 7344–7355 (2011).

37.   Yu, H. Y., Zhang, D. Z., Lu, F. F. & Yao, J. New Approach for Single-Step Extraction of Carboxylated Cellulose Nanocrystals for Their Use As Adsorbents and Flocculants. *ACS Sustain. Chem. Eng.* **4**, 2632–2643 (2016).

38.   Wang, R., Chen, L., Zhu, J. Y. & Yang, R. Tailored and integrated production of carboxylated cellulose nanocrystals (CNC) with nanofibrils (CNF) through maleic acid hydrolysis. *ChemNanoMat* **3**, 328–335 (2017).

39.   Chen, L., Y. Zhu, J., Baez, C., Kitin, P. & Elder, T. Highly thermal-stable and functional cellulose nanocrystals and nanofibrils produced using fully recyclable organic acids. *Green Chem.* **18**, 3835–3843 (2016).

40.   Heggset, E. B., Chinga-Carrasco, G. & Syverud, K. Temperature stability of nanocellulose dispersions. *Carbohydr. Polym.* **157**, 114–121 (2017).

41.   Molnes, S. N., Paso, K. G., Strand, S. & Syverud, K. The effects of pH, time and temperature on the stability and viscosity of cellulose nanocrystal (CNC)

dispersions: implications for use in enhanced oil recovery. *Cellulose* (2017) doi:10.1007/s10570-017-1437-0.

42.   Molnes, S. N., Torrijos, I. P., Strand, S., Paso, K. G. & Syverud, K. Sandstone injectivity and salt stability of cellulose nanocrystals (CNC) dispersions—Premises for use of CNC in enhanced oil recovery. *Ind. Crops Prod.* **93**, 152–160 (2016).

43.   Lewis, L., Derakhshandeh, M., Hatzikiriakos, S. G., Hamad, W. Y. & MacLachlan, M. J. Hydrothermal Gelation of Aqueous Cellulose Nanocrystal Suspensions. *Biomacromolecules* **17**, 2747–2754 (2016).

44.   Wang, Q., Zhao, X. & Zhu, J. Y. Kinetics of strong acid hydrolysis of a bleached kraft pulp for producing cellulose nanocrystals (CNCs). *Ind. Eng. Chem. Res.* **53**, 11007–11014 (2014).

45.   Lin, N. & Dufresne, A. Surface chemistry, morphological analysis and properties of cellulose nanocrystals with gradiented sulfation degrees. *Nanoscale* **6**, 5384–5393 (2014).

46.   Matsuoka, S., Kawamoto, H. & Saka, S. What is active cellulose in pyrolysis? An approach based on reactivity of cellulose reducing end. *J. Anal. Appl. Pyrolysis* **106**, 138–146 (2014).

47.   Agustin, M. B., Nakatsubo, F. & Yano, H. The thermal stability of nanocellulose and its acetates with different degree of polymerization. *Cellulose* **23**, 451–464 (2016).

48.   Bradbury, A. G. W., Sakai, Y. & Shafizadeh, F. A kinetic model for pyrolysis of cellulose. *J. Appl. Polym. Sci.* **23**, 3271–3280 (1979).

49.   Shafizadeh, F. & Bradbury, a G. W. Thermal-Degradation Of Cellulose In Air And Nitrogen At Low-Temperatures. *J. Appl. Polym. Sci.* **23**, 1431–1442 (1979).

50.   Lin, Y., Cho, J., Tompsett, G. a, Westmoreland, P. R. & Huber, G. W. Kinetics and Mechanism of Cellulose Pyrolysis Kinetics and Mechanism of Cellulose Pyrolysis. *Cellulose* 20097–20107 (2009) doi:10.1021/jp906702p.

51.   Kim, U. J., Eom, S. H. & Wada, M. Thermal decomposition of native cellulose: Influence on crystallite size. *Polym. Degrad. Stab.* **95**, 778–781 (2010).

52.   Poletto, M., Zattera, A. J., Forte, M. M. C. & Santana, R. M. C. Thermal decomposition of wood: Influence of wood components and cellulose crystallite size. *Bioresour. Technol.* **109**, 148–153 (2012).

53.   Zhao, Y., Zhang, Y., Lindström, M. E. & Li, J. Tunicate cellulose nanocrystals: Preparation, neat films and nanocomposite films with glucomannans. *Carbohydr. Polym.* **117**, 286–296 (2015).

54.   Ávila Ramírez, J. A., Suriano, C. J., Cerrutti, P. & Foresti, M. L. Surface

esterification of cellulose nanofibers by a simple organocatalytic methodology. *Carbohydr. Polym.* **114**, 416–423 (2014).

55.   Hu, W., Chen, S., Xu, Q. & Wang, H. Solvent-free acetylation of bacterial cellulose under moderate conditions. *Carbohydr. Polym.* **83**, 1575–1581 (2011).

56.   Kaur, B., Gur, I. S. & Bhatnagar, H. L. Thermal degradation studies of cellulose phosphates and cellulose thiophosphates. *Die Angew. Makromol. Chemie* **147**, 157–183 (1987).

57.   Jain, R., Lal, K. & Bhatnagar, H. Thermal degradation of cellulose and its esters in air. *Indian J. Text. Res.* **7**, 49–55 (1982).

58.   Ghanadpour, M., Carosio, F., Larsson, P. T., Wågberg, L. & W??gberg, L. Phosphorylated Cellulose Nanofibrils: A Renewable Nanomaterial for the Preparation of Intrinsically Flame-Retardant Materials. *Biomacromolecules* **16**, 3399–3410 (2015).

59.   Scherirs, J., Camino, G. & Tumiatti, W. Overview of water evolution during the thermal degradation of cellulose. *Eur. Polym. J.* **37**, 933–942 (2001).

60.   Fukuzumi, H., Saito, T., Okita, Y. & Isogai, A. Thermal stabilization of TEMPO-oxidized cellulose. *Polym. Degrad. Stab.* **95**, 1502–1508 (2010).

61.   de Britto, D. & Assis, O. B. G. Thermal degradation of carboxymethylcellulose in different salty forms. *Thermochim. Acta* **494**, 115–122 (2009).

62.   Isogai, A., Saito, T. & Fukuzumi, H. TEMPO-oxidized cellulose nanofibers. *Nanoscale* **3**, 71–85 (2011).

63.   Foster, E. J. *et al.* Current characterization methods for cellulose nanomaterials. *Chem. Soc. Rev.* **47**, 2609–2679 (2018).

64.   Bhattacharjee, S. DLS and zeta potential - What they are and what they are not? *J. Control. Release* **235**, 337–351 (2016).

65.   Stålbrand, H. *et al.* Analysis of molecular size distributions of cellulose molecules during hydrolysis of cellulose by recombinant Cellulomonas fimi beta-1,4-glucanases. *Appl. Environ. Microbiol.* **64**, 2374–2379 (1998).

66.   Conner, A. H. Size Exclusion Chromatography of Cellulose and Cellulose. *Handb. size exclusion Chromatogr.* 331–352 (1995).

67.   Grønli, M., Antal, M. J. & Várhegyi, G. A round-robin study of cellulose pyrolysis kinetics by thermogravimetry. *Ind. Eng. Chem. Res.* **38**, 2238–2244 (1999).

68.   Driemeier, C. & Calligaris, G. A. Theoretical and experimental developments for accurate determination of crystallinity of cellulose I materials. *J. Appl. Crystallogr.* **44**, 184–192 (2011).

69.   Ahvenainen, P., Kontro, I. & Svedström, K. Comparison of sample crystallinity determination methods by X-ray diffraction for challenging cellulose I materials. *Cellulose* **23**, 1073–1086 (2016).

70.   Noguchi, Y., Homma, I. & Matsubara, Y. Complete nanofibrillation of cellulose prepared by phosphorylation. *Cellulose* **24**, 1295–1305 (2017).

71.   Saito, N., Seki, K. & Aoyama, M. Super absorbent materials from lignocellulosic materials by phosphorylation. *Sen'i Gakkaishi* **47**, 255–258 (1991).

72.   Lu, P. & Hsieh, Y. Lo. Preparation and properties of cellulose nanocrystals: Rods, spheres, and network. *Carbohydr. Polym.* **82**, 329–336 (2010).

73.   Cherif, M., Mgaidi, A., Ammar, N., Vallée, G. & Fürst, W. A New Investigation of Aqueous Orthophosphoric Acid Speciation Using Raman Spectroscopy. *J. Solution Chem.* **29**, 255–269 (2000).

74.   Brinkmann, A. *et al.* Correlating cellulose nanocrystal particle size and surface zrea. *Langmuir* **32**, 6105–6114 (2016).

75.   Roman, M. & Winter, W. T. Effect of sulfate groups from sulfuric acid hydrolysis on the thermal degradation behavior of bacterial cellulose. *Biomacromolecules* **5**, 1671–1677 (2004).

76.   Mao, R. L. Van, Zhao, Q., Dima, G. & Petraccone, D. New Process for the Acid-Catalyzed Conversion of Cellulosic Biomass (AC3B) into Alkyl Levulinates and Other Esters Using a Unique One-Pot System of Reaction and Product Extraction. *Catal. Letters* **141**, 271–276 (2011).

77.   Nelson, M. L. & Tkipp, V. W. Determination of the leveling-off degree of polymerization of cotton and rayon. *J. Polym. Sci.* **X**, 577–586 (1949).

78.   Battista, O. A. Hydrolysis and Crystallization of Cellulose. *Ind. Eng. Chem.* **42**, 502–507 (1950).

79.   Criado, P. *et al.* Gamma-irradiation of cellulose nanocrystals (CNCs): investigation of physicochemical and antioxidant properties. *Cellulose* **24**, 2111–2124 (2017).

80.   Honorato-Rios, C. *et al.* Fractionation of cellulose nanocrystals: enhancing liquid crystal ordering without promoting gelation. *NPG Asia Mater.* **10**, 455–465 (2018).

81.   Nishiyama, Y., Sugiyama, J., Chanzy, H. & Langan, P. Crystal Structure and Hydrogen Bonding System in Cellulose Iα from Synchrotron X-ray and Neutron Fiber Diffraction. *J. Am. Chem. Soc.* **125**, 14300–14306 (2003).

82.   Park, S., Baker, J. O., Himmel, M. E., Parilla, P. A. & Johnson, D. K. Cellulose crystallinity index: Measurement techniques and their impact on interpreting cellulase performance. *Biotechnol. Biofuels* **3**, 1–10 (2010).

83.   French, A. D. & Santiago Cintrón, M. Cellulose polymorphy, crystallite size, and

the Segal Crystallinity Index. *Cellulose* **20**, 583–588 (2013).

84. Agarwal, U. P., Ralph, S. A., Reiner, R. S. & Baez, C. Probing crystallinity of never-dried wood cellulose with Raman spectroscopy. *Cellulose* **23**, 125–144 (2016).

85. Usov, I. *et al.* Understanding nanocellulose chirality and structure-properties relationship at the single fibril level. *Nat. Commun.* **6**, (2015).

86. Beck, S., Bouchard, J. & Berry, R. Dispersibility in water of dried nanocrystalline cellulose. *Biomacromolecules* **13**, 1486–1494 (2012).

87. Wang, N., Ding, E. & Cheng, R. Thermal degradation behaviors of spherical cellulose nanocrystals with sulfate groups. *Polymer (Guildf).* **48**, 3486–3493 (2007).

88. Beck, S. & Bouchard, J. Auto-Catalyzed acidic desulfation of cellulose nanocrystals. *Nord. Pulp Pap. Res. J.* **29**, 6–14 (2014).

Appendix 6
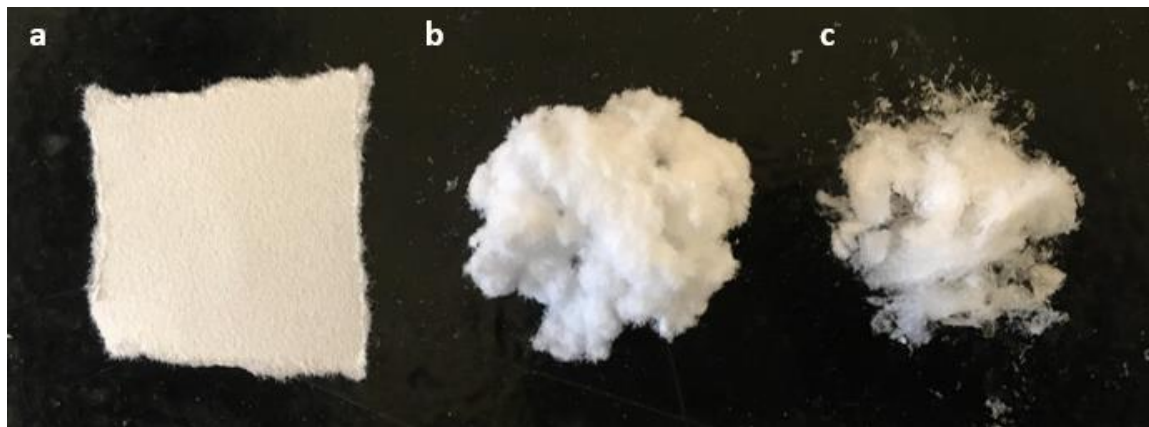
Figure A6.1: (a) Whatman filter aid before blending in magic bullet, (b) Whatman filter aid after blending in magic bullet to increase surface area and (c) freeze dried CNCs after hydrolysis of blended filter aid with sulfuric acid.
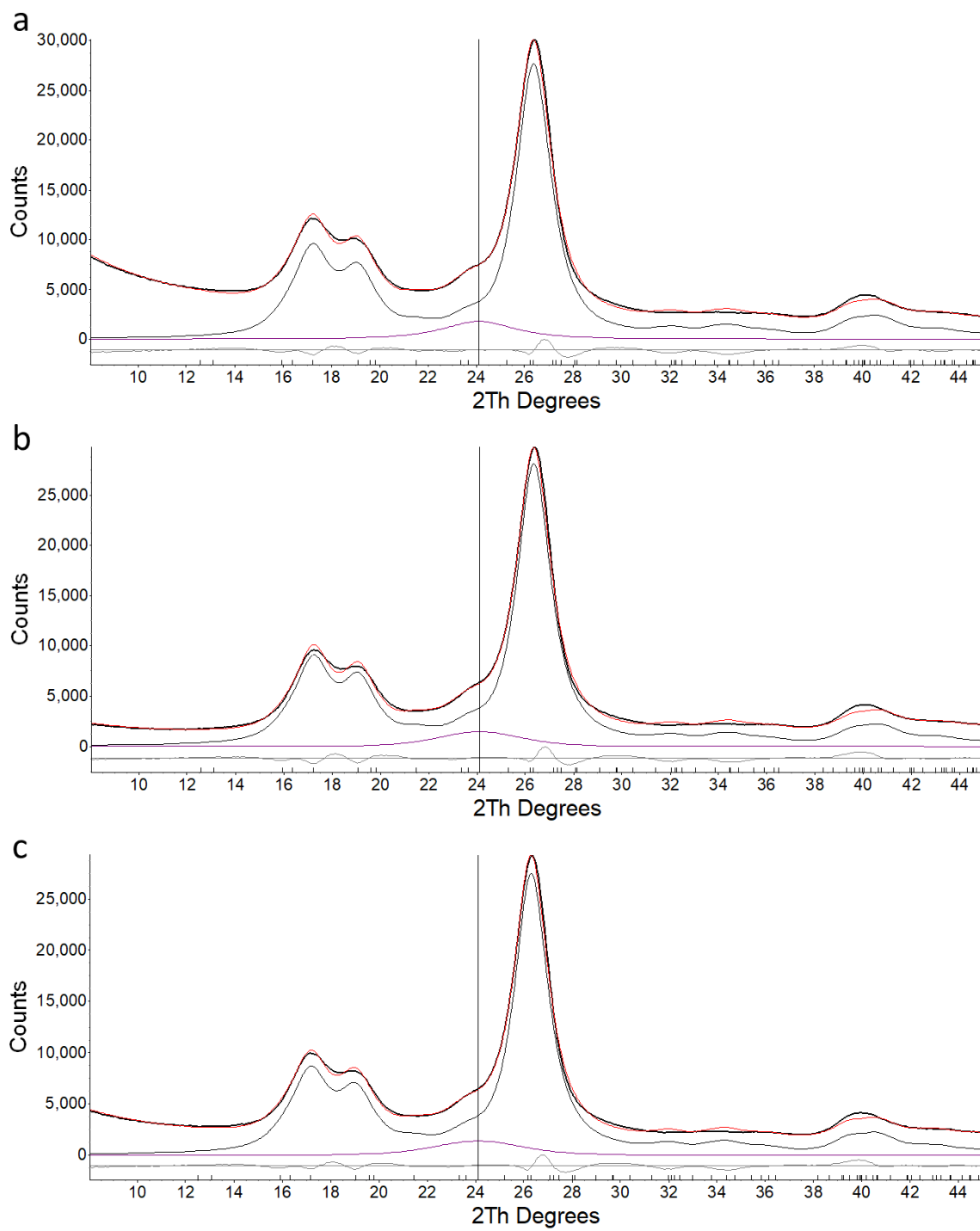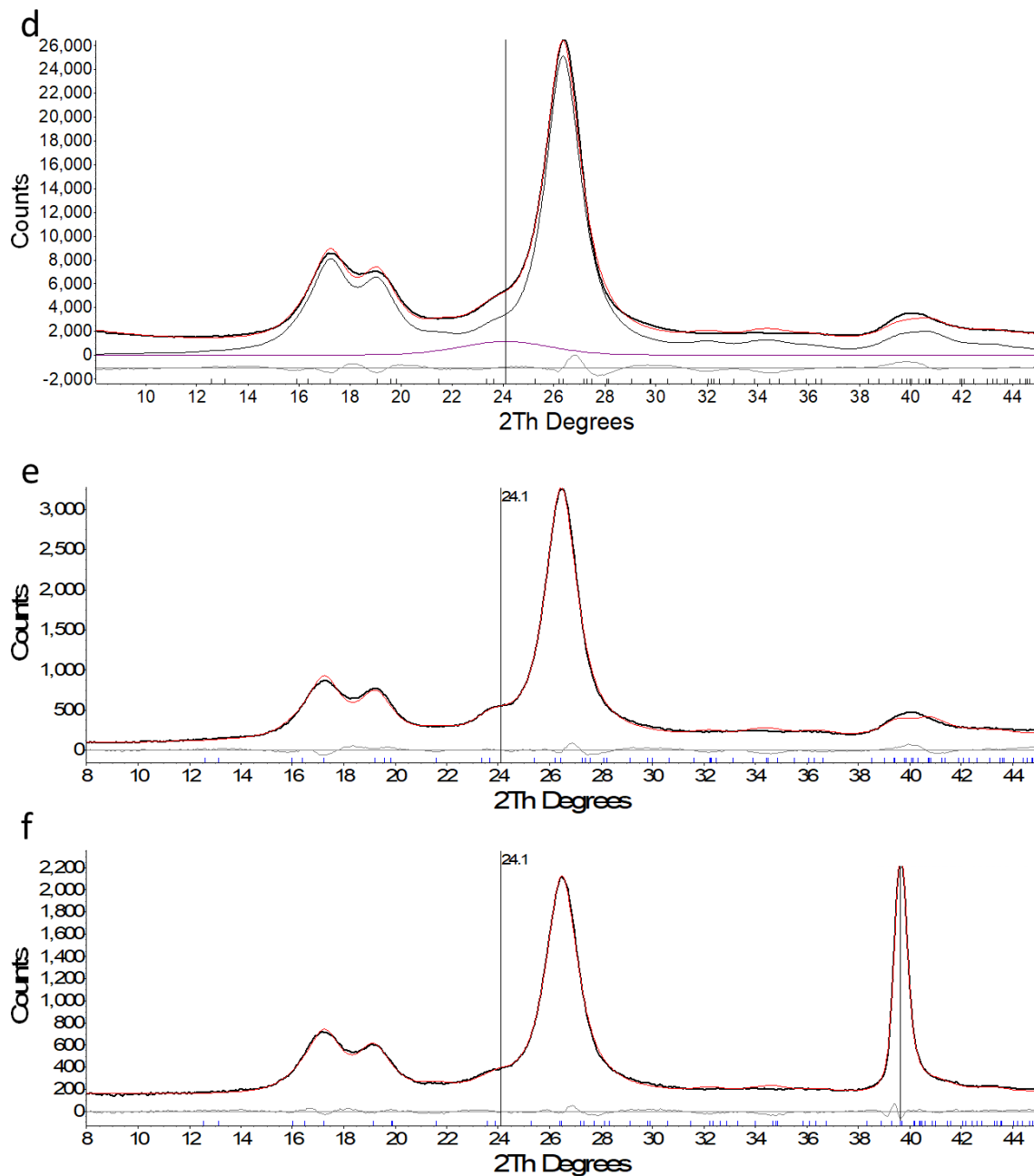
Figure A6.2. Intensity vs 2θ for (a) P-CNC, (b) PS-CNC-44, (c) PS-CNC-16, (d) PS-CNC-8, (e) S-CNC and (f) TEMPO-S-CNC. Red curves represent the calculated profiles, black curves represent the experimental data, and the grey curve represents the difference between the two. Samples (a)-(d) also demonstrate the amorphous profile as the purple curve. The TEMPO-S-CNC shows some interference from the aluminum sample mount; however, this crystalline peak was not used to calculate the crystallinity index.
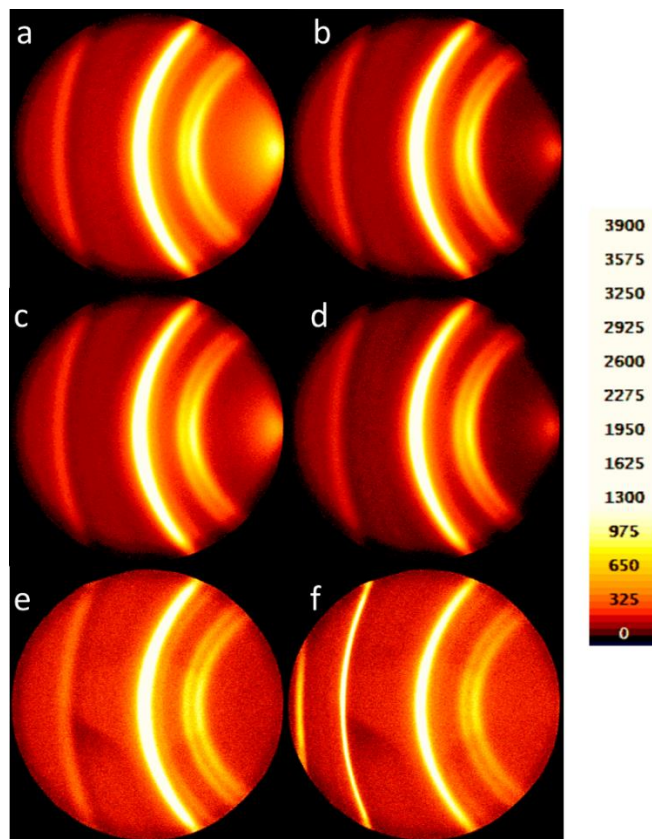
Figure A6.3. X-Ray diffraction patterns for (a) P-CNC, (b) PS-CNC-44, (c) PS-CNC-16, (d) PS-CNC-8, (e) S-CNC and (f) TEMPO-S-CNC.

Table A6.1. Results of the Rietveld refinement for all six CNC types as measured by XRD.

	Crystalline Area	Amorphous Area	% Crystallinity (XRD)
P-CNC	125,471.8	8,923.1	93
PS-CNC-44	121,980.9	7,107.6	94
PS-CNC-16	119,116.5	6,663.2	95
PS-CNC-8	109,256.9	5,500.7	95
S-CNC	11,904.9	193.1	98
TEMPO-S-CNC	7,802.9	73.0	99

Chapter 7

Effects of surface chemistry and counterion selection on the thermal behavior of carboxylated cellulose nanocrystals

_____

Chapter 6 elucidated the effects of phosphate and sulfate groups (as well as other CNC properties) on the thermal performance of dried CNCs. With a growing interest in carboxylated CNCs from both end users and industrial producers (see Chapter 3), however, there is a need to thoroughly understand the effects of carboxylate groups and sodium/proton counterions on CNC thermal performance. In this chapter, four carboxylated CNCs are subject to thermogravimetric analysis and their results are compared to those of typical sulfated CNCs.

In this work, I led the project conceptualization and experimental planning. I prepared all CNC samples, except for one sample which was provided by Dr. Akira Isogai at the University of Tokyo. I also characterized all CNC samples via dynamic light scattering and zeta potential measurements, conductometric titrations, atomic force microscopy, particle size analysis, and thermogravimetric analysis. The thermogravimetric analysis data was analysed jointly by myself and Francesco D'Acierno. X-Ray diffraction measurements were performed by a technician. I wrote the manuscript with assistance from Dr. Emily Cranston. This chapter is in preparation for publication and will be submitted to *Chemistry of Materials* once complete.

7.1 Abstract

Numerous research efforts have focused on improving the thermal stability of cellulose nanocrystals (CNCs) via new production routes, many of which use oxidative methods or organic acid hydrolyses to produce CNCs with carboxylate functional groups. The observed improvements in CNC thermal stability and the CNC properties which cause them, however, are not well understood. This study utilized new and existing methods to produce carboxylated CNCs with varying surface chemistries, surface charge contents, and morphological properties. The thermal performance of these materials was evaluated with two counterions and benchmarked against that of typical sulfated CNCs. The results confirmed that sulfated and carboxylated CNCs are more thermally stable in sodium form and acid form, respectively, and as such, should not be compared with a single counterion. Furthermore, the thermal degradation of carboxylated CNCs was generally found to occur in both the pre-pyrolysis and primary pyrolysis stages. In sodium form, a larger fraction of each sample degraded in the pre-pyrolysis stage, suggesting that the presence of sodium ions accelerates the degradation of carboxylated CNCs. Furthermore, higher carboxylate contents and specific surface areas were found to shift CNC degradation towards lower temperatures. Overall, a side-by-side comparison of five CNC types is provided to elucidate the effects of nanoparticle morphology and surface chemistry on the thermal degradation behavior of cellulose and cellulose derivatives.

7.2 Introduction

With the global prioritization of emissions reduction targets, researchers are looking for sustainable materials to replace plastics derived from non-renewable and emissions intensive petrochemical resources. Cellulose-based materials show great promise in replacing plastics or enhancing bio-derived plastics (e.g. polylactic acid, polyhydroxyalkanoates and thermoplastic starch) due to their highly ordered polymeric structure and the abundance and renewability of their feedstock. Additionally, cellulose can be manipulated at the nanoscale through the production of cellulose nanocrystals (CNCs), which are rod-shaped nanoparticles produced from cellulose sources such as wood or cotton.[1,2] In addition to their sustainability, CNCs have advantageous properties including impressive mechanical properties (e.g., high specific Young's modulus) and a high aspect ratio.[1] This makes them ideal reinforcing agents in polymer composites, where highly crystalline CNCs form strong percolated networks to increase the mechanical properties of a matrix material.[3,4] The usage of CNCs in such applications, however, is limited by their thermal performance since many composites are melt-processed and CNC degradation can occur if the polymer melting point is greater than the thermal stability of CNCs.[5] Typical CNCs produced through a sulfuric acid hydrolysis have a thermal stability of ca. 150°C in their native acid form; however, this can be extended to nearly 300°C through a counterion exchange with sodium ions.[6–8] While the latter value is impressive for an organic material, many researchers have focused on further improving CNC thermal stability to expand the potential suite of applications for this bio-based nanomaterial.

Researchers' motivation to improve CNC thermal stability has led to the consideration of new CNC production routes, many of which introduce new surface chemistries while simultaneously altering the structure and morphology of CNCs. CNCs produced with, for example, organic acids (e.g., citric, maleic, and oxalic acids) have exhibited higher thermal stabilities than those produced with sulfuric acid.[9,10] The reasons for these improvements in thermal stability, however, are often unclear since numerous CNC properties are altered by new production routes, including their surface chemistry, surface charge content, dimensions, crystallinity, and cellulose degree of polymerization.[2] Furthermore, CNCs produced using weaker hydrolyses typically have higher thermal stabilities than their harsh hydrolysis counterparts; this behavior is attributed to their lower surface charge content and higher cellulose degree of polymerization.[8] In fact, sulfuric acid hydrolyzed CNCs can achieve similar improvements in thermal stability by producing them following less harsh hydrolyses or by desulfating the nanoparticles, both of which reduce their surface charge content.[7,11] Therefore, this puts into question the necessity for new production routes motivated by thermal performance.

Nevertheless, many new production methods targeting thermally stable CNCs utilize organic acids which impart carboxylate groups on CNC surfaces.[9,10] As such, CNC surface chemistry likely plays a large role in their behavior at high temperatures, though the impact of citric or oxalic acid surface groups is not understood. While CNC sulfate groups undergo desulfation at high temperatures, nanocelluloses with carboxylate groups undergo decarboxylation reactions.[12,13] Furthermore, the counterion associated with each charge group significantly affects cellulose degradation. In contrast to sulfated CNCs, which are more thermally stable in sodium form, nanocelluloses (specifically cellulose nanofibrils) with carboxylate groups (obtained via a TEMPO (2,2,6,6-tetramethylpiperidine 1-oxyl)-mediated oxidation) exhibit superior thermal performance in acid form.[14] As such, comparing the thermal performance of sulfated and carboxylated CNCs in either acid or sodium form can lead researchers to attribute improvements in thermal stability to CNCs themselves rather than to interactions between surface groups and their counterions. This outlines the necessity for broader experimental matrices which directly compare the thermal stability of various CNC types with multiple counterions.

In considering the thermal behavior of CNCs, their overall performance in products and processes must also be evaluated. In polymer composites, for example, sacrificing thermal stability for colloidal stability is not advantageous, as highly aggregated CNCs lose their "nanoscale advantage". Herein, we present a systematic study in which the thermal degradation behavior of four carboxylated CNCs (including CNCs produced through organic acid hydrolyses and oxidation) are directly compared and benchmarked against the more typical sulfated CNCs. The CNCs are thoroughly characterized to assess their surface charge content, morphology, and the dispersibility of their aqueous suspensions. Ultimately, this study aims to elucidate the influence of various carboxylated CNC properties on their thermal stability and to emphasize the combined effects of surface chemistry and counterion.

194

7.3 Materials & methods

Materials. Hydrochloric acid (36 wt%), sodium hydroxide (96 wt%), and sodium chloride (salt) were purchased from Caledon Laboratories Ltd. (Georgetown, Canada). Dialysis tubing (14 kDa MWCO), citric acid (99.5%), oxalic acid (98%), hydrochloric acid (0.1N), sodium hydroxide (0.1N), and Dowex® Marathon[TM] C Hydrogen form strong acid cation exchange resin were purchased from Sigma-Aldrich (St. Louis, Missouri, USA). Whatman ashless filter aid (Catalog No. 1703-050) and Whatman glass microfiber filter paper (both GF/B and GF/D) were obtained from GE Healthcare Life Sciences Canada (Mississauga, Ontario, Canada). Poly(allylamine hydrochloride) (PAH, M_w 120,000–200,000 g/mol) was purchased from PolySciences (Warrington, USA). All water used (''purified water'') was MilliQ-grade and had a resistivity of 18.2 MΩ•cm.

Carboxylated cellulose nanocrystals. CNCs produced through extensive ultrasonication of TEMPO-oxidized wood pulp (U-TO-CNCs) were provided by Professor Isogai from the University of Tokyo.[15] Briefly, softwood bleached kraft pulp was oxidized using a TEMPO/NaBr/NaClO system followed by a reduction with $NaBH_4$. The oxidized pulp was purified via washing, filtration, and centrifugation. Next, CNCs were produced by ultrasonication of the oxidized pulp with a titanium tip for 60 min, followed by an additional centrifugation step. A more detailed description of this process can be found in the original publication.[15] The samples were received in sodium form (e.g. at a neutral pH with sodium counterions); acid-form CNCs were obtained by passing a dilute U-TO-CNC suspension (ca. 0.2 wt%) through a column with hydrogen form strong acid cation-exchange resin.

CNCs were also produced from a hydrochloric acid hydrolysis of TEMPO-oxidized wood pulp (H-TO-CNCs), using the same starting material as used to make U-TO-CNCs. Similar HCl hydrolyses have been performed by Araki et al.[16] and Salajková et al.;[17] the protocol used herein utilizes concepts from both publications. The TEMPO-oxidized wood pulp fiber/water slurry was obtained from the Professor Isogai at the University of Tokyo, where it was prepared from a commercial softwood bleached kraft pulp by TEMPO-mediated oxidation and successive post reduction with $NaBH_4$, followed by isolation and purification with water. Next, 102 g of TEMPO-oxidized wood pulp, which has a concentration of 2.4%, was diluted with purified water to a final volume of 140 mL. 69 mL of concentrated hydrochloric acid (12.1 M) was added to the wet pulp. The resulting acid slurry was placed in an oil bath heated to 80°C, where continuous mechanical mixing was provided. The reaction proceeded for 225 min, after which the acid slurry was quenched with 210 mL of purified water. The quenched slurry was divided equally among four 250 mL Nalgene bottles, which were then centrifuged in a Sorvall RC-5 superspeed refrigerated centrifuge from Dupont for 15 min at 6000 rpm. The supernatant was poured off and an additional 50 mL of purified water was added to each bottle before performing a second centrifugation cycle. After this cycle, the supernatant was turbid and could not be poured off. The acidic CNC suspension was placed in dialysis tubing and dialyzed against purified water until the pH of the dialysis water stabilized at a value of ca. 5.5. After dialysis, the CNC suspension was sonicated in an ice bath with a Sonifier SFX550 probe sonicator from Branson Ultrasonics for 24 min/L of suspension at 60% output. Finally, to remove any metal contaminants from the sonicator probe, the suspension was filtered through a glass

microfiber filter with a 1 µm pore size (GF/B). A portion of the CNC suspension was left in acid form and the remainder was converted to sodium form by adding dilute sodium hydroxide to achieve a pH of 7.

Citric acid hydrolysis of cotton was used to produce CA-CNCs following a modified version of the protocol by Yu et al.[9] To start, two acid solutions were prepared: 45 mL of 12 M hydrochloric acid and 405 mL of 3 M citric acid. Next, Whatman ashless filter aid was blended in a Magic Bullet® to increase its surface area and allow for a more homogeneous hydrolysis. The blended filter aid was then oven dried at 80°C for 1 h, after which 9 g was placed in an Erlenmeyer flask. The two acid solutions were combined, and the resulting citric/hydrochloric acid mixture was poured into the flask containing the blended filter aid. The acid/cellulose slurry was then placed in an oil bath which had been pre-heated to 80°C. The reaction proceeded for 4 h with continuous mixing from a mechanical mixer. After 4 h, the slurry was quenched in an ice bath until its temperature reached 40°C. To purify the cooled slurry, it was evenly divided into six 250 mL Nalgene bottles for centrifugation in a Sorvall RC-5 superspeed refrigerated centrifuge from Dupont. Next, 100 mL of purified water was added to each bottle, after which the diluted slurry was centrifuged for 10 min at 6000 rpm. The supernatant was poured off and an additional 50 mL of purified water was added to each bottle before performing a second centrifugation cycle. After this cycle, the supernatant was turbid and could not be poured off. The acidic CNC suspension was placed in dialysis tubing and dialyzed against purified water until the pH of the dialysis water stabilized at a value of ca. 5.5. After dialysis, the CNC suspension was sonicated in an ice bath with a Sonifier 450 probe sonicator from Branson Ultrasonics for 15 min/L of suspension at 60% output. Finally, to remove any metal contaminants from the sonicator probe, the suspension was filtered through a glass microfiber filter with a 2.7 µm pore size (GF/D). A portion of the CNC suspension was left in acid form and the remainder was converted to sodium form by adding dilute sodium hydroxide to achieve a pH of 7.

Oxalic acid hydrolysis of cotton was used to produce OA-CNCs following a modified version of the protocol by Chen et al.[10] To start, Whatman ashless filter aid was blended in a Magic Bullet® to increase its surface area and allow for a more homogeneous hydrolysis. The blended filter aid was then oven dried at 80°C for 1 h. To make the oxalic acid solution, 46 g of purified water was first heated to 80°C in an oil bath. Next, 64 g of solid oxalic acid was gradually added to the water while simultaneously increasing the temperature of the oil bath to 100°C. Once the acid was solubilized and its temperature reached 100°C, 4.3 g of dried filter aid was added to the acid solution. The reaction proceeded for 90 min while mixing with a magnetic stir bar. To end the reaction, 160 ml of purified water (heated to 80°C) was added to the acid slurry. The slurry was then filtered through a glass microfiber filter with a 2.7 µm pore size (GF/D) and the filter cake was retrieved. 900 mL of purified water was added to the filter cake to form a homogeneous suspension. This suspension was placed in dialysis tubing and was rinsed with purified water ca. 15 times. After dialysis, the CNC suspension was sonicated in an ice bath with a Sonifier 450 probe sonicator from Branson Ultrasonics for 15 min/L of suspension at 60% output. Finally, to remove any metal contaminants from the sonicator probe, the suspension was filtered through a glass

microfiber filter with a 2.7 µm pore size (GF/D). A portion of the CNC suspension was left in acid form and the remainder was converted to sodium form by adding dilute sodium hydroxide to achieve a pH of 7.

Sulfated cellulose nanocrystals. Sulfated cellulose nanocrystals (S-CNCs) were produced as described in a recent publication from our group.[18] Briefly, Whatman ashless filter aid was subjected to a 45 min hydrolysis at 45°C with 64 wt% sulfuric acid, followed by purification via quenching, centrifugation, and dialysis.

Conductometric titrations. The surface charge content of carboxylated CNCs was determined using conductometric titrations.[19] To start, a dilute CNC suspension (ca. 60 mL) was prepared with a known amount of CNCs (ca. 35 mg for OA-CNCs and CA-CNCs or ca. 10 mg for U-TO-CNCs and H-TO-CNCs). Next, a known amount of 0.1 M HCl was added to the suspension to reduce its pH to ca. 3.4. Once a stable pH was reached, a known amount of NaCl was added to the suspension to increase its conductivity to ca. 170 µS/cm. Lastly, the titration was performed through the incremental addition of a 10 mM NaOH solution. The carboxylate content of each sample was calculated through the determination of two equivalence points, as described by Foster et al. for weak acid titrations.[19] The carboxylate contents and error values reported in this manuscript represent the average and standard deviation of three measurements, respectively.

Atomic force microscopy (AFM). CNC morphology and particle dimensions were observed using AFM. Prior to imaging, silicon wafers were cleaned using a piranha solution of 3:1 concentrated sulfuric acid to hydrogen peroxide.[19] Dilute CNC suspensions (0.001% to 0.01%) were deposited onto clean silicon wafers with 0.1 wt% PAH as an anchoring layer. Each layer was deposited via spin-coating at 4000 rpm for 30 s and a rinsing step was performed with purified water between the PAH and CNC layers. Two microscopes were used to image the four CNC samples: an MFP-3D AFM (Asylum Research an Oxford Instruments Company, Santa Barbara, USA) was used to image U-TO-CNCs, CA-CNCs, and OA-CNCs, while H-TO-CNCs were imaged with a Bruker Multimode 8 AFM (Bruker, Santa Barbara, CA, USA). The U-TO-CNC, CA-CNC, and OA-CNC images were obtained in tapping mode using FMR cantilevers with a nominal force constant of 2.8 N/m and a resonance frequency of 75 15 Hz (NanoWorld, Neuchâtel, Switzerland) and were flattened using Asylum Research 13.17 and Igor Pro 6.37 software. The H-TO-CNC images were obtained in tapping mode using NCHR cantilevers with a nominal force constant of 42 N/m and a resonance frequency of 330 Hz (NanoWorld, Neuchâtel, Switzerland) and were flattened using Nanoscope Analysis 1.8. Particle sizing efforts were performed with Gwyddion 2.56 following methodology from a recent interlaboratory comparison.[20] Approximately 100 particles (between 97 and 105) were measured for each sample. All individualized and fully visible CNCs were measured; any aggregates or CNCs touching the edge of the image were omitted.

X-Ray diffraction (XRD). XRD was used to determine the crystallinity index of each carboxylated CNC sample. Samples were prepared by weighing out ca. 10 mg of freeze-dried CNCs and compressing the sample between two rubber stoppers in a 1 mL syringe, as described previously for thermogravimetric analysis measurements.[21] The samples were

mounted on a silicon wafer and oriented with a vertical D8 h-h goniometer. An electron beam with a wavelength of 1.79026 Å, an acceleration voltage of 35 kV, and a probe current of 45 mA was emitted from a cobalt sealed tube and aligned with a 0.5 mm short collimator and 0.5 mm micro slit. A Bruker D8 Discover diffractometer with Davinci Design was used to collect two-dimensional frames at a detector distance of 14 cm. These two-dimensional frames were integrated with Diffrac.eva 4.0 and the blank frames from empty silicon wafer measurements were subtracted. Rietveld refinement was used to process the resulting diffraction patterns.[22,23] The cellulose I single crystal information file was used to determine the crystalline peak position, while the March Dollase preferred orientation model determined the peak intensity. The amorphous phase was determined with a Pseudo-Voigt function and a fixed peak at 24.1°. The crystallinity index was calculated by comparing the contribution of both crystalline and amorphous peaks to the measured diffraction patterns. The measurement/fitting error is taken to be ca. ± 5%.

Electrophoretic mobility and dynamic light scattering (DLS). A Malvern Panalytical Zetasizer Nano-ZS (Malvern, United Kingdom) was used to measure CNC zeta potential and apparent size by DLS, respectively. Electrophoretic mobility measurements were performed on 0.1 wt% CNC suspensions with 5 mM sodium chloride. The corresponding zeta potentials were calculated using the Smoluchowski's equation. DLS measurements were performed on dilute CNC suspensions (0.25 wt%) to determine the diffusion coefficients of CNCs in suspension, which were then converted to hydrodynamic radii using the Stokes-Einstein equation. Both zeta potentials and hydrodynamic radii are reported as the average of three measurements, and the reported confidence intervals represent the standard deviation.

Thermogravimetric analysis (TGA). TGA was performed using a TA Instruments Q500 (New Castle, USA). Samples were prepared by weighing out ca. 10 mg of freeze-dried CNCs and compressing the sample between two rubber stoppers in a 1 mL syringe, as described previously.[21] The samples were heated from ambient temperature to 600°C at a rate of 10°C/min in a sealed chamber with a nitrogen flow rate of 60 mL/min.

7.4 Results & discussion

CNC characterization. The carboxylated CNC samples in this study can be divided into two categories: those produced via organic acid hydrolyses and those produced via regioselective oxidative reactions. The first category includes CNCs made from citric acid (CA-CNCs) and oxalic acid (OA-CNCs), both of which esterify hydroxy groups on the CNC surface. As such, while these CNCs possess carboxylic acid functional groups, they are connected to cellulose via ester bonds (Table 7.1). Furthermore, citric and oxalic acids are weak acids and CNCs produced with weak acids generally have lower surface charge contents/densities and larger sizes than those produced with strong acids (e.g. sulfuric acid).[2] Conversely, CNCs with carboxylate groups obtained via TEMPO-mediated reactions, which make up our second category, generally have much higher surface charge contents than sulfated CNCs.[15] Their morphology, however, is highly dependent on their production method since the TEMPO-mediated oxidation is merely a functionalization and cannot concurrently cleave cellulose chains. In this study, oxidation reactions were

combined with ultrasonication (U-TO-CNC) and a hydrochloric acid hydrolysis (H-TO-CNC) to produce typical rod-shaped CNCs. Altogether, these four CNC types possess various surface chemistries, surface charge contents/densities, and morphological and structural features (Table 7.1) which have enabled us to elucidate property-thermal behavior relationships.

Table 7.1. Physicochemical properties comparing typical sulfated CNCs (ref. 18) to carboxylated CNCs made via citric acid hydrolysis or oxalic acid hydrolysis of cotton, and sonication or hydrochloric acid hydrolysis of TEMPO-oxidized wood pulp.

	S-CNC (from ref.[18])	H-TO-CNC	U-TO-CNC	CA-CNC	OA-CNC
Suggested surface chemistry[a]					
Carboxylate content (mmol COO$^-$/kg CNC)	-	1530±90	1520±40	140±10	120±10
Sulfate group content (mmol S/kg CNC)	269±3	-	-	-	-
Surface charge density (e$^-$/nm^2)[b]	0.52	1.4	1.0	0.21	0.17
CNC length by AFM (nm)	190±40	130±50	140±60	120±60	120±50
CNC height by AFM (nm)	8±2	4±1	3±1	6±3	6±3
Aspect ratio	27	32	51	20	20
Surface area of 10 mg CNCs (m^2)[c]	3.1	6.4	9.2	4.0	4.2
Crystallinity index (%)	91	94	93	87	88
Zeta potential (mV)	-33±1	-34±2	-34±1	-23±1	-21±1
Apparent size by DLS (nm)	81±1	154±3	121±2	409±8	268±5

[a]Suface chemistries for CA-CNCs and OA-CNCs are as suggested in refs. 9 and 10, respectively.
[b]Surface charge density was calculated by assigning one elementary charge to each functional group (e.g., carboxylate or sulfate) and dividing the total charge content by CNC specific surface area (calculated with a CNC density of $1.61*10^{-23}$ g/nm^3 and AFM measurements with a rectangular cuboid shape).
[c]Similarly, surface area of 10 mg was calculated using a CNC density of $1.61*10^{-23}$ g/nm^3 and AFM measurements with a rectangular cuboid shape.

Surface chemistry and total charge content
CNC surface chemistry and surface charge density are determined by the chemical reagents used to produce CNCs as well as reaction parameters, which can generally be tuned to increase or decrease functionalization of surface hydroxy groups.[7,21,24] CA-CNCs were produced with a combination of citric acid and hydrochloric acid;[9] the latter was added to increase the concentration of hydronium ions and further hydrolyse cellulose chains. Citric acid is a tricarboxylic acid; as such, upon esterification of one carboxylate group, each bonded citric acid moiety could have two exposed carboxylate groups (Table 7.1).[9] Citric acid is also a known cellulose cross-linking agent;[25,26] however, the temperature used in the

CA-CNC hydrolysis (80°C) is likely insufficient to promote this mechanism. Although the pioneering study of this production route reported surface charge contents over 1000 mmol/kg,[9] our CNCs possess surface charge contents of ca. 140 mmol/kg, which are also lower than those reported for typical S-CNCs.[27] Furthermore, CA-CNCs were produced with relatively harsh hydrolysis parameters: 80°C for 4 h, versus 45°C for 45 min for typical S-CNCs.[27] As such, these harsher conditions and the resulting low surface charge content suggest that citric acid does not esterify cellulose hydroxy groups to the same extent as sulfuric acid. This result is in line with the general theory that weaker acids produce larger and less charged CNCs than those produced via strong acid hydrolyses.[2]

Oxalic acid is a stronger acid than citric acid and is in fact stronger than certain mineral acids including phosphoric acid, which has been used to produce phosphated CNCs.[21,28] As such, OA-CNCs were produced in a single acid hydrolysis, where oxalic acid both esterified and hydrolyzed cellulose. Oxalic acid is a dicarboxylic acid, meaning only one carboxylic acid group remains exposed for each functionalized hydroxy group (Table 7.1).[10] The carboxylate charge content observed in this study (Table 7.1) is in line with previous reports on OA-CNCs, which were found to possess 110-390 mmol COO-/kg CNC (the latter values occurring as a result of higher acid concentrations or longer hydrolysis times).[10] Despite oxalic acid being a stronger acid than citric acid, OA-CNCs have less carboxylate groups present on CA-CNC surfaces. This could be attributed to the shorter oxalic acid hydrolysis time or the fact that citric acid CNCs gain two carboxylate groups for each functionalized surface moiety. Regardless, these differences are advantageous as obtaining a larger range of surface charge contents provides more clarity in connecting CNC properties to thermal performance.

CNCs functionalized through a TEMPO-mediated oxidation possess carboxylate groups which are directly bonded to CNC surfaces via carbon-carbon bonds. Furthermore, this oxidation is regioselective and as such only targets the C6 primary hydroxy group (Table 7.1).[29] Unlike cellulose esterification with organic acids, TEMPO-mediated oxidation has been extensively studied and optimized.[29,30] It is commonly used as a post-production surface modification on sulfated CNCs to increase their surface charge content or impart carboxylate groups for further functionalization or grafting reactions.[31–33] The TEMPO-mediated oxidation yields higher surface charge contents than acid hydrolyses; U-TO-CNC and H-TO-CNC both possess ca. 1500 mmol COO$^-$/kg CNC. Both U-TO-CNCs and H-TO-CNCs are produced from TEMPO-oxidized softwood bleached kraft pulp; as such, their surface charge contents were expected to be similar. Furthermore, the similarity in COO$^-$ contents across these two CNCs demonstrate that neither the ultrasonication nor the HCl hydrolysis significantly affect the COO$^-$ moieties on CNCs, which is in line with previous reports.[15,17]

Morphology and structure
CNCs were characterized via AFM and XRD to determine their dimensions and crystallinity indices, respectively. AFM images of dilute CNC suspensions demonstrate key differences in CNC size as well as in the uniformity of the observed nanoparticles (Figure 7.1). While nanoparticles (i.e., particles with at least one dimension in the nanometer range)

were observed amongst all samples, CNCs produced via oxidative methods appeared more uniform in shape and size. Conversely, CA-CNCs and OA-CNCs included many small particles with low aspect ratios, "typical" individualized and rod-shaped CNCs, as well as larger agglomerates or unhydrolyzed cellulose particles. Upon measuring ca. 100 particles for each sample, average particle lengths were found to be similar amongst all samples (Table 7.1). The particle heights, however, varied significantly, with the oxidized CNCs having smaller average cross-sections than the CNCs produced with organic acids. The oxidized CNCs also demonstrated a narrower distribution of cross-sections in comparison to the CA-CNCs and OA-CNCs. Among all samples, the U-TO-CNCs had the smallest cross-sections and the narrowest distribution of dimensions: over 60% of the measured particles had heights between 2 and 3 nm. These results support previous nanocellulose characterization efforts, where wood pulp was subjected to a TEMPO-mediated oxidation, resulting in individualized microfibrils with similar widths (measured by transmission electron microscopy) to cellulose crystallites measured by small-angle X-ray scattering.[34] Conversely, CNCs produced using acid hydrolysis methods often display ribbon-like morphologies, whereby CNCs are made up of multiple laterally aggregated fibrils.[35,36]
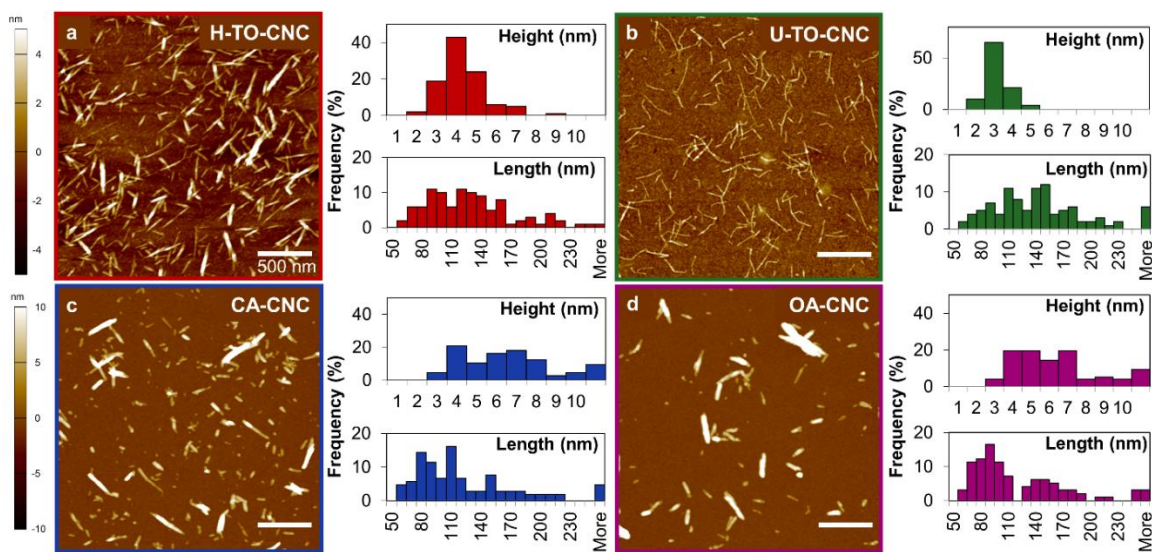
Figure 7.1. AFM images and particle size distributions of (a) H-TO-CNC, (b) U-TO-CNC, (c) CA-CNC, and (d) OA-CNC.

In combining the length and height measurements of each sample, CNC aspect ratios were calculated (Table 7.1). These values further highlight the different particle morphologies which are observed in the AFM images. U-TO-CNCs appear longer and thinner than other CNC types and have an aspect ratio of 51, which is significantly higher than that of typical S-CNCs.[20,27] Next, the H-TO-CNCs have a lower aspect ratio than U-TO-CNCs; furthermore, this value is comparable to that of our recently benchmarked and lab-made S-CNCs, as well as those of industrially produced S-CNCs reported in the literature.[20,27] Lastly, both the CA-CNCs and OA-CNCs have lower aspect ratios than both the oxidized samples and the S-CNC control material.

CNC particle dimensions are relevant when evaluating their thermal performance as a higher specific surface area correlates to lower thermal stability for cellulosic materials.[6,37] For this reason, the approximate surface area (based on particle lengths and heights) of 10 mg of each CNC type was calculated. This mass was selected because pellets made up of ca. 10 mg CNCs were used to perform TGA measurements. Unsurprisingly, U-TO-CNCs had the highest surface area (9.2 m^2), followed by H-TO-CNCs (6.4 m^2), OA-CNCs (4.2 m^2), CA-CNCs (4.0 m^2), and S-CNCs (3.1 m^2). These calculated CNC surface areas can also be used to determine CNC surface charge density, measured in elementary charges per nm^2. This determination unveils a key difference between the TEMPO-oxidized CNCs: despite their similar surface charge contents, H-TO-CNCs have a higher surface charge density due to their lower specific surface area.

Cellulose crystallinity has also been linked to thermal performance: cellulosic materials with higher crystallinity indices or larger crystallite size can better resist thermal degradation.[38] Herein, we probed the crystallinity index of each CNC sample using XRD. While all samples in this study demonstrate the high crystallinity indices which are expected of CNCs,[2] subtle differences can be observed (Table 7.1). The acid-free CNCs (U-TO-CNCs) are similarly crystalline to those produced with strong acids such as hydrochloric acid (H-TO-CNCs) or sulfuric acid (S-CNCs). The CNCs produced with oxalic and citric acid, however, have lower crystallinity indices; this was expected as CNCs produced with organic acids are typically less crystalline than those produced with mineral acids.[2] Similarly, increased acid concentration has been correlated to increased crystallinity for S-CNCs (to an extent).[7] Reduced crystallinity indices are likely a result of the overall proton concentration in a hydrolysis system, which is lower for less concentrated or weaker acids. Nevertheless, the differences observed are so subtle that their effects on CNC thermal performance are likely overshadowed by differences in particle morphology and/or surface chemistry.[8,37]

Suspension properties

While aqueous suspension properties are not generally linked to CNC thermal performance, they can be used to obtain a more thorough understanding of bulk sample properties. This is especially true because particle sizing efforts (including those available in the literature and those completed in this study) only include individualized CNCs and exclude aggregates.[20] As such, zeta potential and light scattering measurements can be used to evaluate CNC colloidal stability and apparent size, respectively. While both techniques have inherent assumptions that are not met for CNCs due to their non-spherical nature, we believe the relative comparison between samples is insightful and recognize reports that aim to make these measurements more quantitative for CNCs.[39–41] CNCs produced using a TEMPO-mediated oxidation (in combination with sonication or hydrochloric acid) have similar zeta potential values (-34 mV) to S-CNCs (-33 mV) and are classified as highly colloidally stable.[40] Furthermore, the apparent sizes of both U-TO-CNCs and H-TO-CNCs line up with average CNC sizes measure by AFM, suggesting that these samples are largely made up of individualized CNCs and that the particle dimensions (and the resulting specific surface areas) are representative of the bulk samples.

Conversely, CA-CNCs and OA-CNCs have zeta potential values of -23 and -21 mV, respectively, meaning they are only moderately colloidally stable. Furthermore, despite having the shortest CNC lengths measured from AFM images (ca. 120 nm), CA-CNCs and OA-CNCs have apparent DLS sizes of 409 nm and 268 nm, respectively. This suggest that large unhydrolyzed particles or CNC aggregates are present in these samples; these particles/aggregates are included in the DLS measurements yet are excluded from the AFM particle sizing efforts. As such, the specific surface area of these CNC samples is likely overestimated. It is also worth noting that the CA-CNCs have the highest apparent size of all samples, despite having more surface charge than OA-CNCs. This indicates that citric acid, while able to efficiently esterify CNC hydroxy groups, does not uniformly hydrolyse cellulose chains (which concurs with CA-CNCs having the lowest crystallinity index as well). The CA-CNC sample contains the largest cellulose particles or CNC aggregates, which could impact its thermal performance. Overall, the four carboxylated CNC samples in this study have varying morphologies, surface chemistries, and surface charge densities, all of which are likely to impact their behavior at high temperatures.

Thermal behavior. In acid form, all carboxylated CNCs appeared more thermally stable than S-CNCs, which have the earliest onset of degradation (Figure 7.2a). This trend, however, is reversed in sodium form, where S-CNCs began to degrade at a higher temperature than their carboxylated counterparts (Figure 7.2b). The difference in thermal stability between acid and sodium-form S-CNCs is well documented.[6,8,37] In acid form, desulfation of surface sulfate groups occurs; the resulting free sulfate ions combine with chemically bound water to form sulfuric acid, which further catalyzes the degradation of cellulose. In sodium form, however, CNCs have sodium sulfate surface groups which prevent the formation of acid and increase their thermal stability.[6,37]
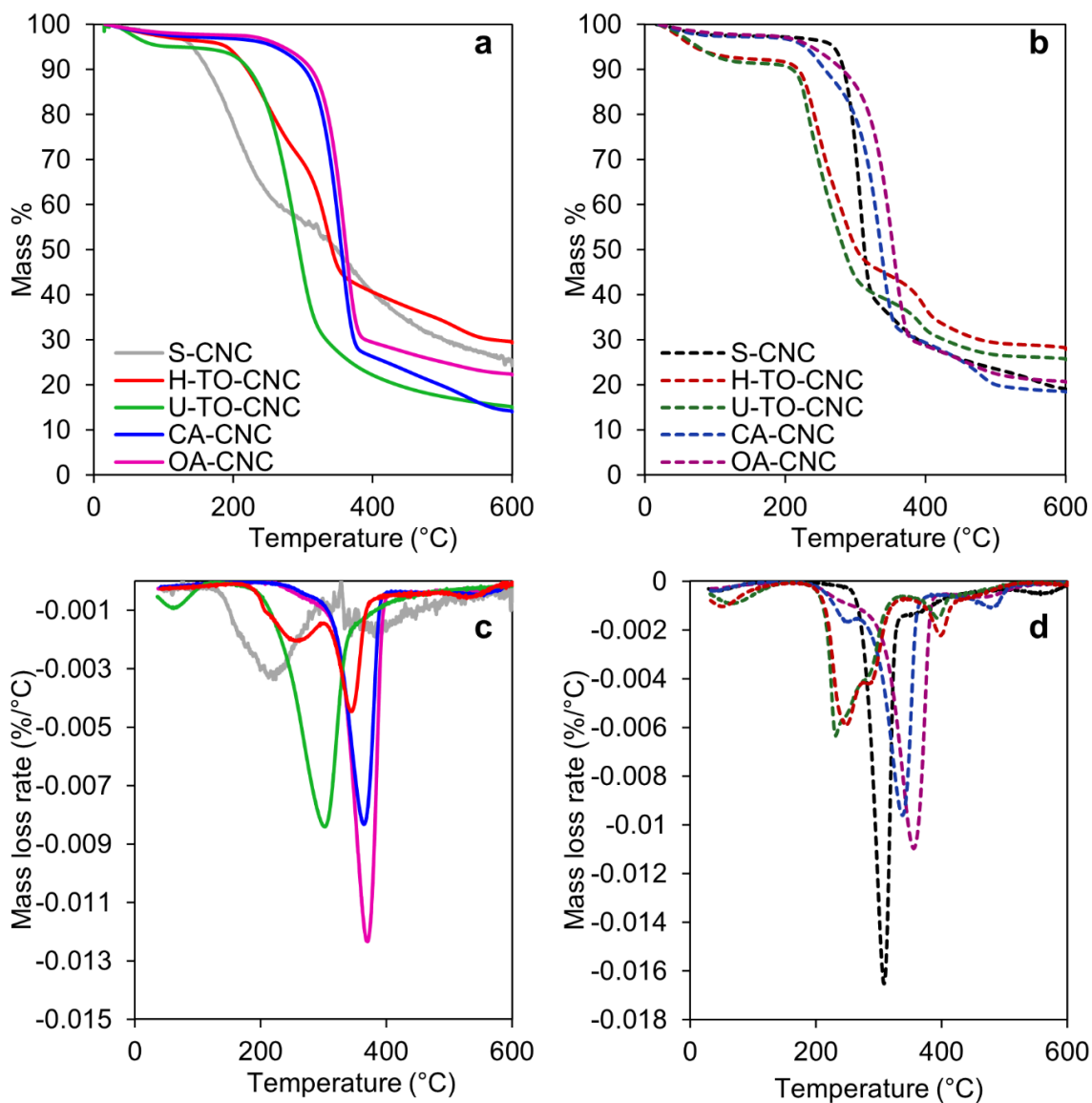
Figure 7.2. Thermogravimetric analysis curves for S-CNCs, H-TO-CNCs, U-TO-CNCs, CA-CNCs, and OA-CNCs in (a) acid form and (b) sodium form as well as their derivatives in (c) acid form and (d) sodium form. Panels (a) and (b) demonstrate the onsets of thermal degradation (T_{onset}) and char values, while panels (c) and (d) demonstrate the rates of degradation and the temperature at which the maximum degradation rate occurs (T_{max}).

Carboxylated CNCs do not follow the same trend as S-CNCs (Table 7.2); in fact, the carboxylated CNCs in this study underwent a reduction in thermal stability when the samples were heated in sodium form (except for H-TO-CNCs, which had a similar thermal stability in both acid and sodium form). This agrees with previous findings from the literature whereby cellulose nanofibrils (CNFs) with sodium carboxylate groups (COONa) degrade at lower temperatures than those with carboxylic acid groups (COOH).[13] The

introduction of carboxylate groups on cellulose surfaces (regardless of counterion) is known to reduce thermal stability because decarboxylation occurs at high temperatures and accelerates aromatization and the formation of carbonyl groups.[13,42] In the presence of COONa, however, sodium carbonate is formed as a by-product of decarboxylation and dehydration reactions.[13] Nevertheless, while the formation of sodium carbonate clearly influences the thermal stability of carboxylated CNCs, their onset of degradation (T_{onset}) only occurred at temperatures 15°C to 24°C lower in sodium form than in acid form (except for H-TO-CNC, which has a T_{onset} 8°C higher in sodium form). Conversely, the T_{onset} of S-CNCs increased by 136°C from acid to sodium form (Table 7.2). As such, while the presence of acidic sulfate groups drastically changes S-CNC thermal stability, COONa groups have a less severe effect on the onset of thermal degradation of cellulose substrates. This is further emphasized by the fact that acid-form S-CNCs exhibited the lowest thermal stability of all CNCs in this study despite having surface charge densities one third to half as high as the H-TO-CNCs and U-TO-CNCs.

Table 7.2. Thermal properties of carboxylated and sulfated CNCs.

	S-CNC		H-TO-CNC		U-TO-CNC		CA-CNC		OA-CNC	
Counterion	H^+	Na^+	H^+	Na^+	H^+	Na^+	H^+	Na^+	H^+	Na^+
Onset of degradation (°C)	148	283	204	212	236	198	246	222	250	226
Char content at 600 °C (%)	25	19	30	28	16	26	14	18	22	21
Temperature at maximum degradation rate (°C)	214[b]	306[b]	333[b]	251[a]	275[b]	242[a]	353[b]	333[b]	359[b]	351[b]

[a]Maximum degradation rate occurs at pre-pyrolysis peak
[b]Maximum degradation rate occurs at primary pyrolysis peak

While the onset of degradation is the parameter most often discussed from TGA results, additional information can be obtained by studying other parameters, such as the char content of the sample at the end of the thermal sweep (Table 7.2). The char content is indicative of whether the chemical reactions which have occurred throughout the thermal sweep produce volatile components or char. Typically, cellulose degradation occurring at lower temperatures favors the formation of char and gases (e.g., carbon monoxide and carbon dioxide), whereas reactions at higher temperatures produce volatile components (e.g., anhydrosugars such as levoglucosan).[43,44] The CNCs included in this study generally followed this trend: S-CNCs degraded at lower temperatures and produced more char in acid form because the low-temperature pyrolysis process produces a flame-retardant material. Conversely, in sodium form, S-CNCs possess a low char value because the

cellulosic structure collapses and releases gases within a narrow temperature window.[37] Carboxylated CNCs typically demonstrate the opposite behavior and produce more char in sodium form, due to the formation of sodium carbonate.[13] While the U-TO-CNCs and CA-CNCs followed this trend, the H-TO-CNCs and OA-CNCs had similar char contents in acid and sodium form (albeit slightly higher in acid form). In the case of OA-CNCs, this is likely due to their low charge densities, which minimize the amount of sodium carbonate produced throughout the degradation reactions. In the case of H-TO-CNCs, however, this result is quite surprising and requires further analysis.

The effects of different surface charge groups and counterions on CNC thermal performance can be further understood by examining the stages of pyrolysis occurring in each sample. To start, each sample underwent a dehydration stage at ca. 60°C, where residual moisture (which was previously adsorbed on highly hygroscopic CNC surfaces) evaporated. At this stage, clear differences between acid and sodium-form CNC samples appeared. In acid form, the sample weight loss at the dehydration stage increased with increasing specific surface area (Figure 7.3a); as such, U-TO-CNCs, which have the highest surface area, underwent the greatest weight loss. CNCs with higher surface area possess more bound water, which is ultimately released in the first stage of the thermogravimetric analysis. In sodium form, however, this trend was not observed. CNCs with moderate surface charge contents (S-CNCs, CA-CNCs, OA-CNCs) underwent similar dehydration weight losses in both acid and sodium form. Conversely, CNCs with high surface charge contents (H-TO-CNCs and U-TO-CNCs) underwent increased dehydration weight losses in sodium form. Furthermore, the dehydration weight losses of these two sodium-form TO-CNC samples were the same, suggesting that the presence of large numbers of sodium ions (proportional to the number of surface charge groups) overshadows the effect of specific surface area (Figure 7.3b). This could be explained by the kosmotropic nature of sodium ions, which are known to increase the packing of water molecules at interfaces (e.g., CNC surfaces).[45,46] As such, even at early pyrolysis stages, sodium ions affect the thermal behavior of carboxylated and sulfated CNCs.
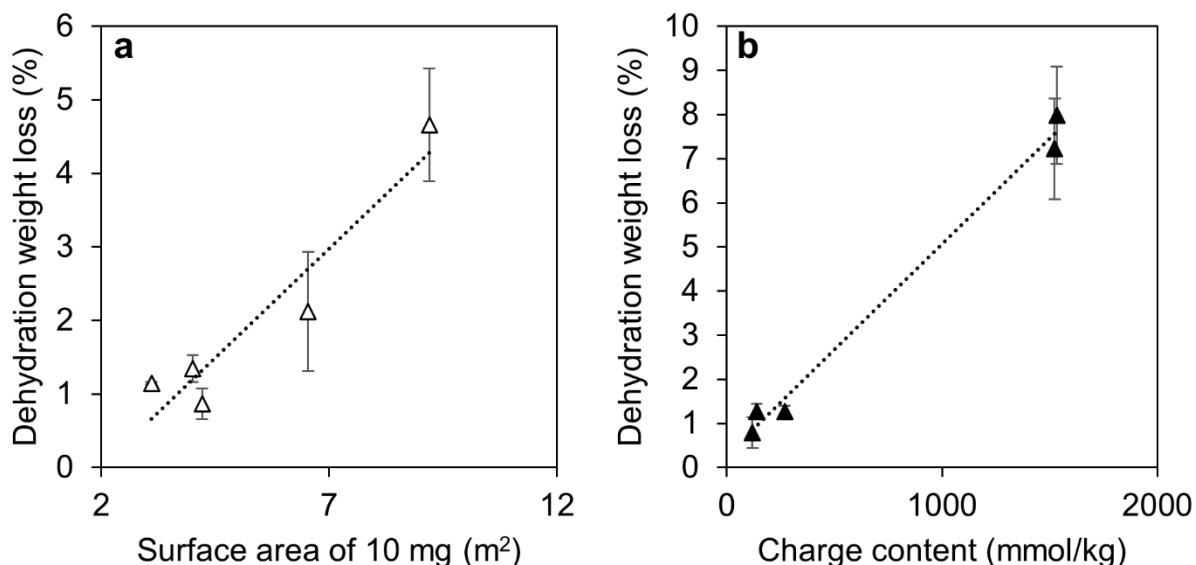
Figure 7.3. Dehydration weight loss at ca. 60°C of (a) acid-form CNCs as a function of surface area and (b) sodium-form CNCs as a function of charge content.

Following dehydration, CNCs undergo a primary pyrolysis stage, which, in some cases, is preceded by a pre-pyrolysis stage. In this study, all acid-form CNCs (both sulfated and carboxylated) except for U-TO-CNCs underwent a pre-pyrolysis degradation stage. (Additionally, acid-form H-TO-CNCs had a small shoulder on their pre-pyrolysis peak, which, for the purpose of this analysis, will be included in the pre-pyrolysis peak.) S-CNCs had a 5% weight loss at the pre-pyrolysis stage, where desulfation is known to occur. At this stage, sulfuric acid swells on the surface, yet it does not volatilize until the secondary pyrolysis stage.[37] For CA-CNCs and OA-CNCs, the pre-pyrolysis stage accounted for 2% and 1% of the sample's weight loss, respectively. Conversely, for H-TO-CNCs, the pre-pyrolysis stage accounted for 26% of the sample's weight loss (Figure 7.4a). This suggests that the weight loss associated with the pre-pyrolysis stage of acid-form carboxylated CNCs is dependent on the number of carboxylate groups (or surface charge content) and is likely representative of degradation occurring from surface decarboxylation reactions.[13,42] Overall, this demonstrates the significant role of sulfate and carboxylate groups on CNC surfaces; they initiate low-temperature thermochemical reactions.
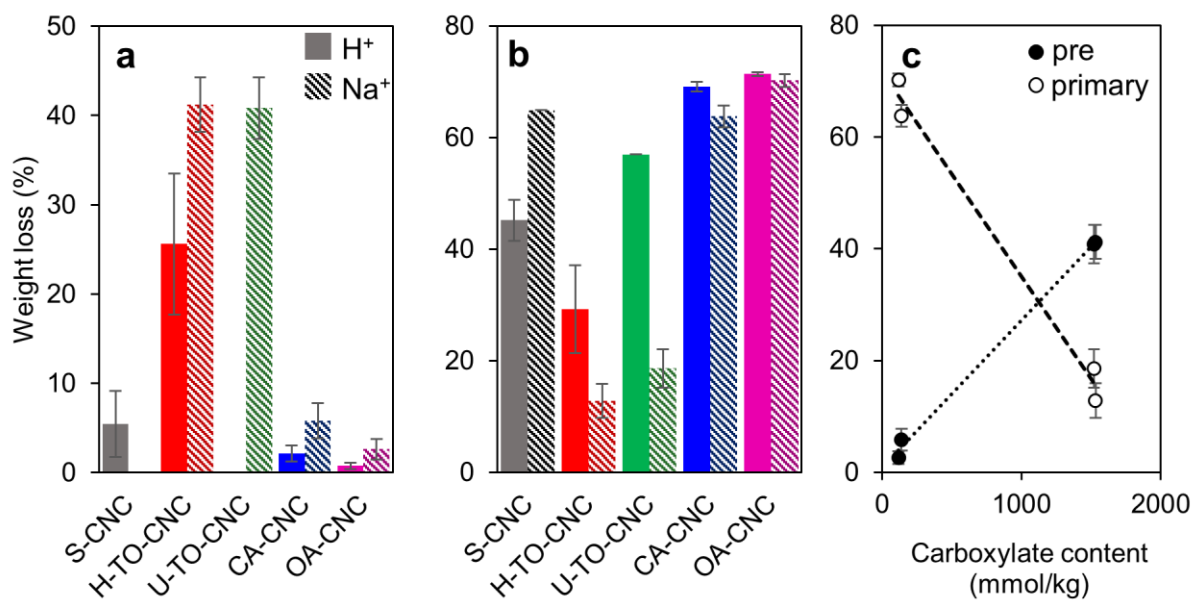
Figure 7.4. Weight loss of acid-form (solid bars) and sodium-form (dashed bars) CNCs at (a) pre-pyrolysis and (b) primary pyrolysis stages. (c) Weight loss of sodium-form carboxylated CNCs at the pre-pyrolysis (black markers) and primary pyrolysis stages (white markers).

Interestingly, the acid-form U-TO-CNC sample did not undergo a pre-pyrolysis stage (Figure 7.4a); rather, this sample predominantly degraded at the primary pyrolysis stage (Figure 7.4b). The peak of the U-TO-CNC primary pyrolysis stage, however, occurred at a similar temperature to the peaks of the pre-pyrolysis stages for the remaining carboxylated CNCs (275°C for U-TO-CNC, versus 252-292°C for CA, OA, and H-TO-CNCs, Figure 7.2c). As such, the primary pyrolysis stage of the U-TO-CNC sample can likely be attributed to the same degradation mechanism (e.g., decarboxylation) as the pre-pyrolysis stages of the remaining carboxylated CNCs. Since the U-TO-CNC sample possesses the highest specific surface area, it is made up of a larger fraction of surface cellulose chains (which are vulnerable to decarboxylation) versus "inner" bulk cellulose chains. As a result, this sample degrades homogeneously at 275°C, while the other acid-form carboxylated CNCs degrade in two distinct stages (e.g., surface degradation at 252-292°C, followed by degradation of the inner CNC core at a later stage).

In sodium form, all carboxylated CNCs underwent both pre-pyrolysis and primary pyrolysis stages (Figures 4a and b). The fractions of these samples degrading in each stage, however, drastically changed in comparison to the acid-form CNCs, whereby larger fractions of the carboxylated CNC samples were degrading at the pre-pyrolysis stage in sodium form (i.e., 1.6 to 3.5 times more weight loss than in acid form) (Figure 7.4a). To compensate, a lower proportion of these samples degraded at the primary pyrolysis stage (i.e., up to 2/3 less weight loss than in acid form) (Figure 7.4b). As such, while the onsets of thermal degradation were generally similar for COOH and COONa CNCs, the pyrolysis

stages (and therefore the temperatures) at which the bulk of the cellulosic material degrades are vastly different. Moreover, the weight loss of the sodium-form carboxylated CNCs occurring at the pre-pyrolysis stage increased as a function of carboxylate content, whereas the opposite is true at the primary pyrolysis stage (Figure 7.4c). Conversely, sodium-form S-CNCs did not exhibit a pre-pyrolysis stage in sodium form; the primary pyrolysis stage occurred rapidly and over a narrow temperature range. Similarly to the degradation of U-TO-CNCs in acid form, sodium-form S-CNCs degrade homogeneously.

The effects of functional groups and their associated counterions on thermal degradation are further understood by assessing the temperature at which the maximum degradation rate occurs (T_{max}), its associated pyrolysis stage, and the influence of both counterions on this measure (Figure 7.2a, 7.2b, and Table 7.2). While the T_{max} for S-CNCs occurred at the primary pyrolysis stage in both acid and sodium form, the latter occurred at a temperature 92°C higher than the former. This represents the largest change in T_{max} observed amongst all the studied CNCs and therefore highlights the extreme instability of acidic-form CNC sulfate groups at high temperatures. All carboxylated CNCs exhibited a higher T_{max} in acid form versus sodium form. For CNCs with low charge contents (CA-CNC and OA-CNC), both T_{max} occurred at the primary pyrolysis peak. Moreover, the differences in T_{max} in acid and sodium form were 20°C and 8°C for CA-CNCs and OA-CNCs, respectively. As such, due to their low carboxylate contents, these CNCs demonstrated similar performance in acid and sodium form. For H-TO-CNCs and U-TO-CNCs, the T_{max} shifted from the primary pyrolysis peak in acid form to the pre-pyrolysis peak in sodium form. This was accompanied by decreases in T_{max} of 82°C and 32°C for H-TO-CNCs and U-TO-CNCs, respectively. These highly charged CNCs therefore heavily degrade at the pre-pyrolysis stage (and therefore at significantly lower temperatures) when sodium counterions are present.

While the difference in thermal performance between highly charged (U-TO-CNC and H-TO-CNC) and moderately charged (CA-CNC and OA-CNC) CNCs is largely attributed to their carboxylate contents, surface chemistry likely plays a role as well. As discussed above, the TEMPO-mediated oxidation grafts carboxyl groups at the C6 position, whereas both citric and oxalic acids esterify CNC hydroxy groups with larger functional groups possessing carboxylic acid end group(s). The thermal performance of CA-CNCs and OA-CNCs, however, more closely follows that of the TEMPO-oxidized CNCs than that of esterified CNCs including S-CNCs. Despite being attached to CNCs via ester linkages, the citric and oxalic acid functional groups decrease CNC thermal stability in sodium form, suggesting that decarboxylation reactions in sodium form (and the supposed formation of sodium carbonate) are more influential than de-esterification reactions in acid form (and the formation of citric or oxalic acid).

Nevertheless, CA-CNCs and OA-CNCs differ from their TEMPO-oxidized counterparts, as both possess a "spacer" group which separates the carboxyl end group from the cellulose backbone. The proximity of the carboxyl functional group to the cellulose surface has been shown to impact thermal stability: cellulosic materials with carboxyl groups directly bound to the ring structure (e.g., at the C6 position) are less thermally stable than those with side

chain carboxyl groups (e.g. carboxymethylcellulose).[47] Herein, the proximity of COOH or COONa groups to the cellulose backbone likely affects the onset of thermal degradation, whereby carboxyl groups further from the chain could delay thermal degradation (Table 7.2). Once degradation did occur, however, the extent of this degradation appeared proportional to the density of carboxyl groups on CNC surfaces: CNCs with more COONa groups experienced greater weight loss at the pre-pyrolysis stage (Figure 7.4). Conversely, CNCs with fewer COONa groups (e.g., CA-CNCs and OA-CNCs) experienced the most significant weight loss during the primary pyrolysis stage.

This study emphasizes the differences in the thermal performance of sulfated and carboxylated CNCs and can act as a guide for researchers looking to optimize the performance of CNC-based materials at high temperatures. Overall, sodium-form S-CNCs had the highest onset of thermal degradation and are therefore ideal additives, in, for example, polymer composites with melting temperatures below 280°C. Conversely, at temperatures above this threshold, sodium-form S-CNCs degrade rapidly; researchers may therefore prefer to use acid form CA-CNCs or OA-CNCs, which do not undergo widespread degradation (i.e. reach their maximum degradation rate) until temperatures of 353°C and 359°C, respectively. Lastly, if flame-retardancy and high-char values (i.e., material retention) are a priority, highly-charged CNCs with "unstable" counterions would be preferable (e.g., acid form S-CNCs or sodium form H-TO-CNCs and U-TO-CNCs). As such, in comparing various CNC types for high temperature applications, there generally is not one CNC type which is undeniably superior. Rather, decisions on which CNCs to use must consider the specific needs of the application in question and must rely on a thorough understanding of the effects of CNC properties (e.g., surface chemistry, morphology, charge density, and counterion) on their thermal performance.

7.5 Conclusions

Overall, this study outlines key differences between the thermal performance of sulfated and carboxylated CNCs. Acid-form S-CNCs had the lowest onset of degradation of all the tested CNCs, suggesting that acid-form sulfate groups induce more thermal instability than carboxylate groups with either tested counterion. Furthermore, their differences in both the onset of degradation and T_{max} (upon changing the counterion) were the largest of all the tested CNCs. Conversely, carboxylated CNCs exhibited similar onsets of degradation regardless of counterion. Additionally, their differences in acid and sodium-form T_{max} varied across the four carboxylated CNCs: those with moderate charge densities (produced from citric and oxalic acid hydrolyses) exhibited similar T_{max} regardless of counterion, whereas those with high charge densities (produced from oxidation reactions) exhibited larger differences.

Carboxylated CNCs were generally found to degrade in two stages at low temperatures: pre-pyrolysis and primary pyrolysis stages (though secondary pyrolysis stages were exhibited at 400°C or higher). The sample weight loss occurring in the pre-pyrolysis stage was attributed to decarboxylation reactions. In sodium form, larger fractions of carboxylated CNC samples degraded at the pre-pyrolysis stage; furthermore, the sample weight loss at this stage increased with increasing carboxylate contents. The specific

surface area was also found to play a role in the thermal degradation behavior of carboxylated CNCs: U-TO-CNCs had the highest specific surface area and degraded homogeneously at the primary pyrolysis stage in acid form (at a similar temperature to the pre-pyrolysis peaks for the other acid form samples). While CNCs with larger cross-sections may degrade in two stages (surface degradation reactions followed by degradation of the CNC core), thin CNCs (e.g., U-TO-CNCs in this study) can degrade in a single stage if their carboxylate content and surface area are sufficiently high. Ultimately, this study presents key insights on the thermal performance of CNCs and highlights the effects of surface chemistry, morphology, and counterion selection on their behavior at high temperatures. While new CNC production methods can produce CNCs with increased thermal performance, systematic comparisons with multiple counterions are required to link physicochemical properties to thermal behavior.

7.6 References

1. Habibi, Y., Lucia, L. A. & Rojas, O. J. Cellulose Nanocrystals : Chemistry , Self-Assembly , and Applications. **110**, 3479–3500 (2010).

2. Vanderfleet, O. M. & Cranston, E. D. Production routes to tailor the performance of cellulose nanocrystals. *Nat. Rev. Mater.* (2020) doi:10.1038/s41578-020-00239-y.

3. Favier, V., Chanzy, H. & Cavaillé, J. Y. Polymer nanocomposites reinforced by cellulose whiskers. *Macromolecules* **28**, 6365–6367 (1995).

4. Favier, V., Cavaille, G. R. C. J. Y., Chanzy, H. & D, A. Nanocomposite Materials from Latex and Cellulose Whiskers. **6**, 351–355 (1995).

5. Zheng, T. & Pilla, S. Melt Processing of Cellulose Nanocrystal-Filled Composites : Toward Reinforcement and Foam Nucleation. (2020) doi:10.1021/acs.iecr.0c00170.

6. Wang, N., Ding, E. & Cheng, R. Thermal degradation behaviors of spherical cellulose nanocrystals with sulfate groups. *Polymer (Guildf).* **48**, 3486–3493 (2007).

7. Kargarzadeh, H. *et al.* Effects of hydrolysis conditions on the morphology, crystallinity, and thermal stability of cellulose nanocrystals extracted from kenaf bast fibers. *Cellulose* **19**, 855–866 (2012).

8. Vanderfleet, O. M. *et al.* Insight into thermal stability of cellulose nanocrystals from new hydrolysis methods with acid blends. *Cellulose* **26**, 507–528 (2019).

9. Yu, H.-Y., Zhang, D.-Z., Lu, F.-F. & Yao, J. New approach for single-step extraction of carboxylated cellulose nanocrystals for their use as adsorbents and flocculants. *ACS Sustain. Chem. Eng.* **4**, 2632–2643 (2016).

10. Chen, L. *et al.* Highly thermal-stable and functional cellulose nanocrystals and nanofibrils produced using fully recyclable organic acids. *Green Chem.* **18**, 3835–3843 (2016).

11. Lin, N. & Dufresne, A. Surface chemistry, morphological analysis and properties of cellulose nanocrystals with gradiented sulfation degrees. *Nanoscale* **6**, 5384–5393 (2014).

12. Fukuzumi, H., Fujisawa, S., Saito, T. & Isogai, A. Selective permeation of hydrogen gas using cellulose nanofibril film. *Biomacromolecules* **14**, 1705–1709 (2013).

13. Lichtenstein, K. & Lavoine, N. Toward a deeper understanding of the thermal degradation mechanism of nanocellulose. *Polym. Degrad. Stab.* **146**, 53–60 (2017).

14. Lavoine, N., Bras, J., Saito, T. & Isogai, A. Improvement of the Thermal Stability

of TEMPO-Oxidized Cellulose Nanofibrils by Heat-Induced Conversion of Ionic Bonds to Amide Bonds. *Macromol. Rapid Commun.* **37**, 1033–1039 (2016).

15.   Zhou, Y., Saito, T., Bergström, L. & Isogai, A. Acid-free preparation of cellulose nanocrystals by TEMPO oxidation and subsequent cavitation. *Biomacromolecules* **19**, 633–639 (2018).

16.   Araki, J., Wada, M., Kuga, S. & Okano, T. Flow properties of microcrystalline cellulose suspension prepared by acid treatment of native cellulose. *Colloids Surfaces A Physicochem. Eng. Asp.* **142**, 75–82 (1998).

17.   Salajková, M., Berglund, L. A. & Zhou, Q. Hydrophobic cellulose nanocrystals modified with quaternary ammonium salts. *J. Mater. Chem.* **22**, 19798–19805 (2012).

18.   Delepierre, G., Vanderfleet, O. M., Niinivaara, E., Zakani, B. & Cranston, E. D. Benchmarking Cellulose Nanocrystals Part II: New Industrially Produced Materials. *Langmuir,* la-2021-00550w (2021).

19.   Foster, E. J. *et al.* Current characterization methods for cellulose nanomaterials. *Chem. Soc. Rev.* **47**, 2609–2679 (2018).

20.   Bushell, M. *et al.* Particle size distributions for cellulose nanocrystals measured by atomic force microscopy: an interlaboratory comparison. *Cellulose* **4**, (2021).

21.   Vanderfleet, O. M., Osorio, D. A. & Cranston, E. D. Optimization of cellulose nanocrystal length and surface charge density through phosphoric acid hydrolysis. *Philos. Trans. R. Soc. London A Math. Phys. Eng. Sci.* **376**, 1–7 (2018).

22.   Driemeier, C. & Calligaris, G. A. Theoretical and experimental developments for accurate determination of crystallinity of cellulose I materials. *J. Appl. Crystallogr.* **44**, 184–192 (2011).

23.   Ahvenainen, P., Kontro, I. & Svedström, K. Comparison of sample crystallinity determination methods by X-ray diffraction for challenging cellulose I materials. *Cellulose* **23**, 1073–1086 (2016).

24.   Dong, X. M., Revol, J.-F. & Gray, D. G. Effect of microcrystallite preparation conditions on the formation of colloid crystals of cellulose. *Cellulose* **5**, 19–32 (1998).

25.   Ferreira, E. S., Cranston, E. D. & Rezende, C. A. Naturally Hydrophobic Foams from Lignocellulosic Fibers Prepared by Oven-Drying. *ACS Sustain. Chem. Eng.* **8**, 8267–8278 (2020).

26.   Meftahi, A., Khajavi, R., Rashidi, A., Rahimi, M. K. & Bahador, A. Preventing the collapse of 3D bacterial cellulose network via citric acid. *J. Nanostructure Chem.* **8**, 311–320 (2018).

27. Reid, M. S., Villalobos, M. & Cranston, E. D. Benchmarking cellulose nanocrystals: from the laboratory to industrial production. *Langmuir* **33**, 1583–1598 (2017).

28. Camarero Espinosa, S. *et al.* Isolation of thermally stable cellulose nanocrystals by phosphoric acid hydrolysis. *Biomacromolecules* **14**, 1223–1230 (2013).

29. Isogai, A. & Kato, Y. Preparation of polyuronic acid from cellulose by TEMPO-mediated oxidation AKIRA. *Cellulose* **5**, 153–164 (1998).

30. Saito, T. & Isogai, A. TEMPO-mediated oxidation of native cellulose. The effect of oxidation conditions on chemical and crystal structures of the water-insoluble fractions. *Biomacromolecules* **5**, 1983–1989 (2004).

31. Montanari, S., Roumani, M., Heux, L. & Vignon, M. R. Topochemistry of carboxylated cellulose nanocrystals resulting from TEMPO-mediated oxidation. *Macromolecules* **38**, 1665–1671 (2005).

32. Habibi, Y., Chanzy, H. & Vignon, M. R. TEMPO-mediated surface oxidation of cellulose whiskers. *Cellulose* **13**, 679–687 (2006).

33. Araki, J., Wada, M. & Kuga, S. Steric stabilization of a cellulose microcrystal suspension by poly(ethylene glycol) grafting. *Langmuir* **17**, 21–27 (2001).

34. Saito, T., Nishiyama, Y., Putaux, J. L., Vignon, M. & Isogai, A. Homogeneous suspensions of individualized microfibrils from TEMPO-catalyzed oxidation of native cellulose. *Biomacromolecules* **7**, 1687–1691 (2006).

35. Elazzouzi-Hafraoui, S. *et al.* The shape and size distribution of crystalline nanoparticles prepared by acid hydrolysis of native cellulose. *Biomacromolecules* **9**, 57–65 (2008).

36. Chen, M., Parot, J., Hackley, V. A., Zou, S. & Johnston, L. J. AFM characterization of cellulose nanocrystal height and width using internal calibration standards. *Cellulose* **0**, (2021).

37. D'Acierno, F., Hamad, W. Y., Michal, C. A. & Maclachlan, M. J. Thermal Degradation of Cellulose Filaments and Nanocrystals. *Biomacromolecules* **21**, 3374–3386 (2020).

38. Poletto, M., Zattera, A. J., Forte, M. M. C. & Santana, R. M. C. Thermal decomposition of wood: Influence of wood components and cellulose crystallite size. *Bioresour. Technol.* **109**, 148–153 (2012).

39. Boluk, Y. & Danumah, C. Analysis of cellulose nanocrystal rod lengths by dynamic light scattering and electron microscopy. *J. Nanoparticle Res.* **16**, (2014).

40. Bhattacharjee, S. DLS and zeta potential - What they are and what they are not? *J. Control. Release* **235**, 337–351 (2016).

41.   Lin, K.-H. *et al.* An analysis on the electrophoretic mobility of cellulose nanocrystals as thin cylinders: relaxation and end effect. *RSC Adv.* **9**, 34032–34038 (2019).

42.   Fukuzumi, H., Saito, T., Okita, Y. & Isogai, A. Thermal stabilization of TEMPO-oxidized cellulose. *Polym. Degrad. Stab.* **95**, 1502–1508 (2010).

43.   Lin, Y., Cho, J., Tompsett, G. a, Westmoreland, P. R. & Huber, G. W. Kinetics and Mechanism of Cellulose Pyrolysis Kinetics and Mechanism of Cellulose Pyrolysis. *Cellulose* 20097–20107 (2009) doi:10.1021/jp906702p.

44.   Bradbury, A. G. W., Sakai, Y. & Shafizadeh, F. A kinetic model for pyrolysis of cellulose. *J. Appl. Polym. Sci.* **23**, 3271–3280 (1979).

45.   Collins, K. D. & Washabaugh, M. W. The Hofmeister effect and the behaviour of water at interfaces. *Q. Rev. Biophys.* **18**, 323–422 (1985).

46.   Liu, Z., Zhang, C., Liu, R., Zhang, W. & Kang, H. Dissolution of cellobiose in the aqueous solutions of chloride salts : Hofmeister series consideration. *Cellulose* **23**, 295–305 (2016).

47.   Sharma, P. R. & Varma, A. J. Thermal stability of cellulose and their nanoparticles: Effect of incremental increases in carboxyl and aldehyde groups. *Carbohydr. Polym.* **114**, 339–343 (2014).

Chapter 8

Hydrothermal treatments of aqueous cellulose nanocrystals suspensions: Effects on structure and surface charge content

_____

Chapters 6 and 7 investigated the thermal performance of dried CNCs; however, for applications using aqueous CNC suspensions (e.g., oil and gas extraction fluids), these results are not particularly relevant. Herein, the thermal performance of various CNC suspensions is examined through hydrothermal treatments at temperatures up to 180°C for up to 7 days.

In this work, I led the project conceptualization and experimental planning. I prepared and characterized the samples with assistance from my undergraduate research assistant, Jaclyn Winitsky. X-Ray diffraction measurements were performed by a technician. I analysed the resulting data, again with assistance from Jaclyn Winitsky, and wrote the manuscript with assistance from Dr. Emily Cranston and Dr. Julien Bras. My industrial collaborators at Schlumberger (Drs. Jazmin Godoy-Vargas and Valerie Lafitte) provided experimental discussion and guidance throughout the duration of this project. This chapter has been submitted to *Cellulose* for publication.

Vanderfleet, O.M., Winitsky, J., Bras, J., Godoy-Vargas, J., Lafitte V., Cranston, E.D., "Hydrothermal treatments of cellulose nanocrystal suspensions: Effects on structure and surface charge content", *Cellulose*, submitted.

8.1 Abstract

Cellulose nanocrystals (CNCs) are ideal rheological modifiers for aqueous oil and gas extraction fluids. CNCs are typically produced with sulfuric acid and their aqueous suspensions have uniform and predictable properties under ambient conditions; however, drastic changes occur at elevated temperatures. Herein, the effects of high temperature treatments (ranging from 80°C to 180°C for 1 hour to 7 days) on the properties (including uniformity, colloidal stability, and color) of sulfated, phosphated, and carboxylated CNC suspensions were studied. Additionally, cellulose molecular weight, and CNC surface charge content and crystallinity index were quantified before and after heating. CNCs underwent few morphological changes; their molecular weight and crystallinity index were largely unchanged under the conditions tested. Their surface charge content, however, was significantly decreased after heat treatments; this resulted in a loss of colloidal stability and aggregation of CNCs. The largest change in suspension properties was observed for sulfated CNCs whereas CNCs with a combination of sulfate and phosphate esters, or carboxylate groups, were less affected and maintained colloidal stability at higher temperatures. In fact, desulfation was found to occur rapidly at 80°C, while many carboxylate groups persisted at temperatures up to 180°C; calculated rate constants (based on second order kinetics) suggested that desulfation is 20 times faster than decarboxylation but with a similar activation energy. Overall, this study elucidates CNC suspension behavior after heat exposure and demonstrates routes to produce CNCs with improved high temperature performance.

8.2 Introduction

Cellulose nanocrystals (CNCs) are highly crystalline, rod-shaped nanoparticles that form stable suspensions in water and other polar solvents.[1–3] They are industrially produced in tonne per day quantities, most commonly by subjecting cellulose sources (e.g. wood or cotton) to a sulfuric acid hydrolysis.[4] This procedure is bifunctional: hydrolysis of glycosidic linkages within cellulose chains and esterification of surface hydroxy groups occur simultaneously.[5] The amorphous regions of cellulose are most susceptible to hydrolysis and degrade rapidly, while crystalline cellulose chains remain intact.[6] Additionally, surface cellulose chains are functionalized with anionic sulfate half ester groups.[7] The resulting CNCs form stable aqueous suspensions due to the electrostatic repulsion of negative surface charge groups.[1,2] Moreover, CNCs have high aspect ratios and uniform particle size distributions; each nanoparticle is made up of highly ordered cellulose chains with approximately 280 repeat units.[6] Due to their numerous functional attributes, CNCs can be incorporated into a variety of products and processes to replace petrochemically-derived components with bio-based alternatives. In many applications, however, there is a desire for consistent or predictable rheological behavior over a large range of temperatures. For example, CNCs show promise as rheological modifiers in oil and gas extraction fluids, however, these can be subject to temperatures up to 180°C and pressures up to 135 MPa. Unfortunately, studies have shown that CNC properties, as well

as the behavior of their aqueous suspensions, can undergo drastic changes as a function of heating.[8–10] If these changes are not well understood, CNCs and their suspensions may be excluded from high temperature applications.

The surface sulfate half ester groups which allow CNCs to maintain colloidal stability are particularly vulnerable to high temperatures. While desulfation has been reported to occur at temperatures as low as 4°C,[8] its impact is not significant until ca. 40-50°C,[11] and further increases with temperature. CNCs with reduced surface charge contents have higher viscosities, which can be attributed to two phenomena: increased effective volume of CNCs and/or the formation of aggregates or network structures.[12–14] The extent of desulfation, as well as the initial concentration of the CNC suspensions, should ultimately determine the extent of the rheological changes. Abitbol et al. demonstrated that the rheological behavior of CNCs with moderate surface charge contents (>0.3% sulfur) was governed by the effective volume occupied by CNCs.[13] Conversely, the viscosity of CNCs with low surface charge contents (<0.3% sulfur) was primarily affected by the formation of aggregates.[13] As such, if sufficient desulfation occurs, CNCs lose colloidal stability and succumb to attractive van der Waals forces,[9] ultimately forming aggregates, or, if heated at high concentrations, thixotropic gels.[14]

In addition to desulfation, CNCs can undergo thermally induced morphological changes due to degradation of the cellulose chains. This phenomenon has been suggested by recent studies in which discoloration was observed upon heating CNC suspensions.[9,14] The extent of discoloration varied depending on the concentration of the initial suspension as well as the temperature and length of the treatment. Molnes et al. observed discoloration in a 2% (w/w) suspension heated at just 120°C for 48 h,[9] while Lewis et al. did not observe discoloration until a 4% suspension was heated to 150°C for 20 h.[14] The discoloration was attributed to the degradation of cellulose chains and the production of furfural and hydroxymethylfurfural.[9] Surprisingly, Molnes et al. reported an increase in viscosity for the heavily discolored CNC suspensions, suggesting the bulk of the CNC particle structure was still intact.[9] These few studies imply that the effects of high temperatures on CNC suspensions are not well understood, and the relationship between discoloration and cellulose degradation remains unclear.

The aforementioned CNC desulfation and degradation that occur at high temperatures can affect the performance of aqueous formulations. For some applications (e.g. consumer facing products such as paints, cosmetics and foods), changes in formulation appearance or rheological profile are unacceptable. To expand the usage of CNCs in such products, additives such as sodium chloride[9] or sodium formate[10] have been used to reduce discoloration. Alternatively, less thermally labile surface chemistries (e.g. sulfonate groups) or steric stabilization (e.g. CNCs with amorphous cellulose dialdehyde chains[15,16] or grafted polymers like polyethylene glycol)[17,18] could be implemented to avoid the formation of aggregates. Nevertheless, while some applications may require CNCs to

maintain consistent properties over a specific temperature range, others may benefit from thermally induced changes in colloidal stability or particle size. Enhanced oil recovery, for example, could benefit from heat-triggered CNC aggregation as the aggregates would block larger pores and direct fluids towards low-permeability and oil-rich regions.[19–21]

Herein, we investigate the fundamental CNC properties that lead to changes in their suspension performance at high temperatures. CNC properties are evaluated over a range of temperatures and time points to deepen our understanding of the effects of high temperatures on aqueous CNC suspension properties including colloidal stability, color, and turbidity. Furthermore, we evaluate the effects of CNC surface chemistry and overall charge content on thermal performance through the examination of carboxylated, phosphated, and sulfated CNCs. Changes in CNC morphology were probed through size exclusion chromatography and X-ray diffraction. These results will provide CNC users with a deeper understanding of aqueous CNC suspension behavior over their intended range of operating temperatures. Furthermore, this work contributes to a greater understanding of bio-based materials which may expand CNC usage into a wider range of commercial products and processes.

8.3 Materials and methods

Materials. Sulfuric acid (98 wt%), phosphoric acid (85 wt%), hydrochloric acid (36 wt%), and methanol, were purchased from Caledon Laboratories Ltd. (Georgetown, Canada). Dialysis tubing (14 kDa molecular weight cut-off), 2,2,6,6-(tetramethylpiperidin-1-yl)oxyl (TEMPO, 99%), sodium chloride, sodium hydroxide (1 M), sodium bromide (NaBr, Reagent Plus® > 99%), sodium hypochlorite (NaClO, 10–15%), dimethylsulfoxide (DMSO) and phenyl isocyanate (> 98%) were purchased from Sigma-Aldrich (St. Louis, Missouri, USA). Anhydrous ethanol was purchased from University of British Columbia Chemistry Stores. Whatman ashless filter aid (Catalog No. 1703-050) and Whatman glass microfiber filter paper (both GF/B and GF/D) were obtained from GE Healthcare Life Sciences Canada (Mississauga, Ontario, Canada). Poly(allylamine hydrochloride) (PAH, M_w 120,000–200,000 g/mol) was purchased from PolySciences (Warrington, USA). Purified water with a resistivity of 18.2 MΩ cm, was obtained through a Barnstead GenPure Pro water purification system from Thermo Fisher Scientific (Waltham, USA).

Acid hydrolysis method. Five types of CNCs were produced from Whatman ashless filter aid: CNCs with sulfate groups (S-CNCS), CNCs with phosphate groups (P-CNCs) and mixed-acid CNCs with three different ratios of sulfate and phosphate groups (PS-CNCs). S-CNCs were produced following a procedure from Cranston et al.[22] Briefly, 40 g of filter aid was blended in a Magic Bullet® and dried overnight at 80°C. Next, 700 mL of 64 wt% sulfuric acid (which was previously heated to 45°C) was added to the dried filter aid. The acid slurry was then placed in a 45°C water bath with a mechanical mixer. After 45 min, the hot acid slurry was quenched with 7 L of ice-cold water and allowed to settle for 30 min, after which the supernatant was decanted. The remaining slurry was evenly split

among 12 bottles, which were centrifuged for 10 min at 6000 rpm in a Sorvall RC-5 superspeed refrigerated centrifuge from Dupont. Following centrifugation, the supernatant was decanted and purified water was added to the precipitate. The centrifugation was repeated until a clear supernatant could no longer be decanted.

P-CNCs and PS-CNCs were produced following procedures from Camarero-Espinosa et al.[23] and Vanderfleet et al.,[24] respectively. To form a pulp, 2 g of filter aid was blended with 100 mL of purified water in a Magic Bullet®. A 261 mL acid solution was prepared with varying molar ratios of phosphoric acid to sulfuric acid. For P-CNCs, the acid solution consisted of 85 wt% phosphoric acid, while for PS-CNCs, solutions with phosphoric acid to sulfuric acid molar ratios of 44:1 (PS-CNC-44), 16:1 (PS-CNC-16) and 8:1 (PS-CNC-8) were prepared. The pulp was placed into an ice bath and the acid solution was added dropwise, ensuring the temperature of the acid slurry stayed below 30°C. Next, the acid slurry was poured into a round bottom flask and placed in a pre-heated oil bath at 100°C with magnetic stirring. The reaction proceeded for 90 min, after which it was quenched by placing the round bottom flask into an ice bath for ca. 15 min. Next, the CNC suspensions were split amongst six Nalgene bottles and purified via two centrifugation cycles: each adding 600 mL purified water to the suspension and centrifuging at 3600 rpm for 15 min.

After centrifugation, all CNC types (S-CNC, P-CNCs and PS-CNCs) were dialyzed against purified water until its pH stabilized (ca. 15 rinses). The CNC suspensions were then sonicated with a Sonifier 450 probe sonicator from Branson Ultrasonics at 60% amplitude for 15 min/L to break up any loose aggregates. Finally, to remove any unhydrolyzed cellulose and/or contaminants, the suspensions were filtered through a glass microfiber filter with 1 µm (for S-CNCs) or 2.7 µm (for P-CNCs and PS-CNCs) pores.

TEMPO-mediated oxidation. A TEMPO-mediated oxidation was performed on S-CNCs to impart surface carboxylate groups, as outlined by Isogai et al.[25] A 200 mL solution containing 0.15 g TEMPO and 1.6 g NaBr was added dropwise to 500 mL of a 1 wt% CNC suspension in acid form (at room temperature). Next, 30 g of sodium hypochlorite was added dropwise, maintaining a consistent pH. The reaction proceeded for 3 hours while monitoring the pH of the suspension and adding 1 M NaOH if the pH fell below 9.8, being careful not to let it exceed 10.2. To end the reaction, 14.2 g of ethanol was added, followed by enough 1 M HCl to reach a pH of 2 (~ 20 mL). To purify the TEMPO-oxidized CNCs, the resulting suspension was centrifuged at 4500 rpm for 15 min, followed by dialysis against purified water.

Heat treatments. Heat treatments of aqueous CNC suspensions were divided in two categories: short heat treatments with stirring, and long heat treatments without stirring. The former was performed using a 4842 PARR reactor (400 mL volume) with a glass liner and mechanical stirring. The reactor was pressurized with compressed air and brought up to the desired temperature (100°C, 120°C, 150°C or 180°C), after which the heat treatment was allowed to proceed for one hour (unless otherwise noted). For longer heat treatments,

a 500 mL, 303 stainless steel OFITE aging cell with a glass liner was used. The aging cell was placed in an oven set to the desired temperature and left undisturbed for up to 7 days. Unless otherwise noted, all heat treatments were performed on never-dried, acid-form aqueous CNC suspensions at a concentration of 0.1 wt%.

Zeta potential and dynamic light scattering. The colloidal stability of CNC suspensions and the apparent size of CNCs in suspension were determined using a Malvern Zetasizer Nano ZS. The colloidal stability of CNC suspensions was assessed by measuring the electrophoretic mobility of 0.1 wt% suspensions with 5 mM NaCl and subsequently calculating the zeta potential following Smoluchowski's theory. The apparent size of CNCs was measured using dynamic light scattering on dilute CNC suspensions (0.025 wt%) with no added salt. "Apparent" is used in recognition of the assumptions in DLS that particles are spherical, which is not valid for rod-shaped CNCs, but gives relative sizes for comparison and a reasonable measure of dispersion/aggregation in suspension. For both techniques, triplicate measurements were performed and average values along with their standard deviation are presented.

Atomic force microscopy. Atomic force microscopy (AFM) was used to infer the degree of aggregation of CNCs in suspension as well as the morphology of aggregates in dried samples. The samples were prepared by first cleaning silicon wafers using a piranha solution composed of 3:1 sulfuric acid to hydrogen peroxide. Next, a cationic anchoring layer was deposited on the silicon wafer by spin-coating 0.1 wt% PAH at 4000 rpm for 30 s, followed by a rinse with purified water. Lastly, the CNCs were deposited onto the wafers by spin-coating dilute CNC suspensions (0.005% or 0.01%), again at 4000 rpm for 30 s. The CNC-coated wafers were then imaged using an Asylum Research and Oxford Instruments MFP-3D atomic force microscope in tapping mode, equipped with Nanoworld FMR cantilevers (nominal force constant: 2.8±0.7 N/m, resonance frequency: 75±15 Hz). Images were flattened using the "magic mask" feature in Asylum Research 3.17 and Igor Pro 6.37. Larger surface areas were analyzed on each coated wafer and a representative AFM image were selected for discussion.

Conductometric titration. Conductometric titrations were performed to determine the number of accessible, i.e., surface, charge groups on CNCs. Titrations were not performed on P-CNCs or PS-CNCs as these CNCs have low surface charge contents which, in our experience, cannot be precisely detected. Prior to titrating, CNC suspensions were dialyzed to remove any impurities and ions which may have been released during heat treatments. For each titration, ~15-30 mg of CNCs in ~60 mL of purified water was used. For S-CNCs, which have only strong acid groups, a small amount of sodium chloride (~0.3 g of 200 mM) was added to stabilize the conductivity. For TEMPO-S-CNCs, which have both strong and weak acid groups, ~0.3 g of 1 M HCl was added to the suspension to reduce its pH to 3.2. Afterwards, the CNC suspensions were titrated against small increments of 10 mM sodium hydroxide while monitoring both pH and conductivity. For each sample, two to three

titrations were performed, depending on the amount of available material. Following conductometric titrations, reaction rate constants were determined by plotting the inverse concentration of sulfate or carboxylate groups (in mol/L) vs. time and calculating the slope of the linear trendline. The concentration of sulfate or carboxylate groups was converted to mol/L units via multiplication of the titration results (in mmol/kg CNC) with the suspension concentration (0.1 g CNC/100 g suspension) with appropriate unit conversions.

Determination of cellulose molecular weight. The molecular weight distributions of the cellulose chains in each CNC sample were determined using size exclusion chromatography. To do so, the cellulose chains were first solubilized in DMSO via a carbanilation reaction.[26,27] To start, 25 mg of freeze-dried CNCs were placed in a vial and dried at 80°C overnight. Next, 10 mL of DMSO and 1 mL of phenyl isocyanate were added to the vials, which were heated in an oil bath at 70°C. The reaction proceeded for 40 h with intermittent agitation of the vials. To end the reaction, 2 mL of methanol was added to each vial; afterwards, the excess methanol was evaporated. The resulting tricarbanilated cellulose solutions were analyzed with an Agilent 1100 gel permeation chromatography (GPC) instrument equipped with an Agilent 1260 ISO pump and Styragel HR 4, HR 3 and HR 1 columns. The columns were eluted with 0.5% LiBr in DMSO, at a rate of 0.5 mL/min. After filtering the cellulose solutions with a 0.45 µm polytetrafluoroethylene (PTFE) syringe filter, 100 µL of each sample was injected sequentially. The refractive index intensity was measured at 785 nm by a WYATT 477-TREX optilab T-rex detector. To determine the molecular weight of the cellulose chains, polystyrene sulfonate standards were used to calibrate the signal of the refractive index. From here, the degree of polymerization could be determined by assuming complete carbanilation of cellulose chains and a resulting repeat unit molecular weight of 519 g/mol.[28,29]

X-Ray diffraction. The crystallinity index of each sample was obtained through X-ray diffraction. Freeze-dried CNCs were compressed into a firm pellet using a 1 mL syringe and rubber plunger. The pellet was placed on a silicon wafer, using a vertical D8 θ-θ goniometer to ensure proper positioning. The X-ray source (an electron beam with a wavelength of 1.79026 Å, an acceleration voltage of 35 kV and a probe current of 45 mA) was emitted from a sealed cobalt tube and adjusted with 0.5 mm micro slits and collimators. The diffraction signal was detected by a Bruker D8 Discover diffractometer with Davinci Design, which was positioned 14 cm away from the sample. To obtain suitable data for analysis, the signal from the empty silicon wafer was subtracted and the resulting two-dimensional frames were integrated with Davinci Design to obtain one-dimensional frames. Lastly, Rietveld refinement was used to associate the diffraction spectra with models for crystalline and amorphous cellulose, the latter of which was modelled with a Pseudo-Voigt function and a fixed peak at 24.1°. The overall crystallinity index for each sample was determined by calculating the contribution of both crystalline and amorphous peaks to the overall diffraction spectra. The precision in the fitted values is assumed to be ca. 5% based on past experience.

8.4 Results and discussion

Short heat treatments. Upon heating various CNC suspensions for one hour at five different temperatures between 100°C and 180°C, significant changes in colloidal stability were observed. The extent of these changes, along with the rate at which they occurred, were dependent on CNC properties. In acid-form, typical sulfated CNCs (S-CNCs) exhibited slight reductions in colloidal stability (i.e., increasing negative zeta potential) after heat treatments of one hour at 100°C and 120°C (Figure 8.1a). Nevertheless, the increased zeta potential values of ca. -30 mV still classified the suspensions as "moderately to highly colloidally stable".[30] Upon increasing the temperature of the heat treatments, further (and more extensive) reductions in colloidal stability occurred: zeta potentials of -13 mV and -1 mV were observed after heating S-CNCs for one hour at 150°C and 180°C, respectively. These zeta potential values classify the S-CNC suspensions as "colloidally unstable".[30] The observed loss of colloidal stability can be attributed to auto-catalyzed desulfation, by which ester bonds linking sulfate groups to the CNC surfaces are hydrolyzed.[8] The resulting CNCs (referred to as desulfated) have fewer anionic surface groups; as a result, their colloidal stability decreases.
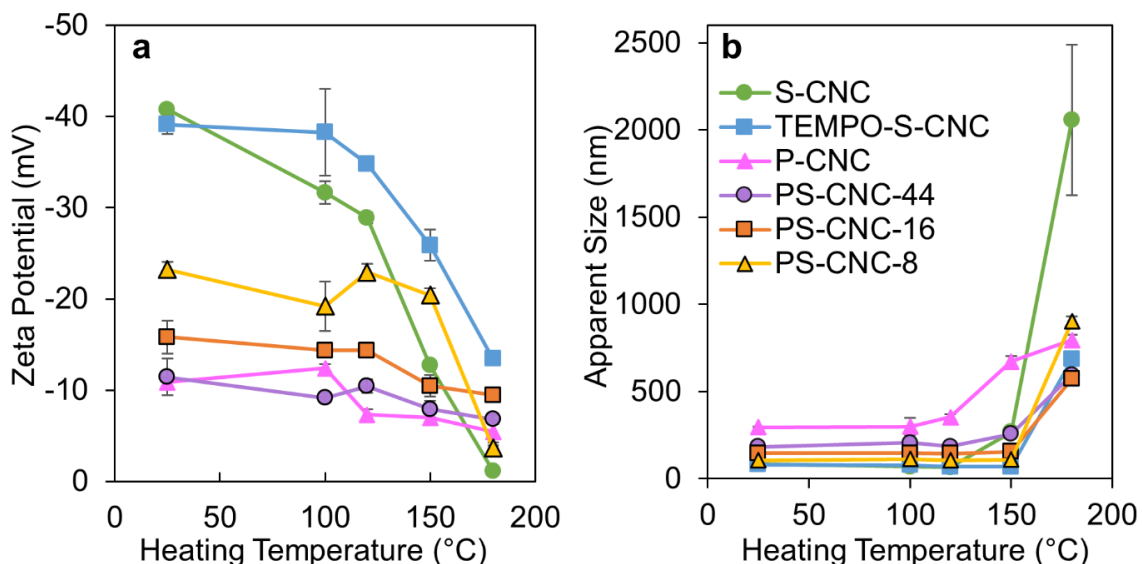
Figure 8.1. (a) Zeta potential and (b) apparent size by dynamic light scattering of acid-form CNC suspensions heated for 1 hour at various temperatures.

In addition to reduced electrostatic repulsion, the released free sulfate groups increase the ionic strength of the CNC suspension, further screening the remaining S-CNC charge groups. As such, the electrical double layer thickness decreases, allowing CNCs to come closer together without double layers overlapping. At low interparticle distances, van der Waals forces dominate (i.e., the net interaction is attractive) and CNC aggregates are formed. Furthermore, at high temperatures, CNC aggregation is also favored due to the

disruption of CNC hydration shells, which, in turn, reduces their repulsive hydration forces.[31]

The extent of CNC aggregation was measured using dynamic light scattering (Figure 8.1b) and AFM (Figure 8.2). S-CNCs did not aggregate when heated for one hour at 100°C or 120°C; however, aggregates began to form at 150°C. At this temperature, the apparent size of the S-CNCs in suspension increased from <100 nm to 266 nm. Additionally, loosely hinged aggregates were visible via AFM (Figure 8.2iia) Both lateral and end-to-end aggregates were observed; though the formation of lateral aggregates is thermodynamically favorable.[32] Upon further increasing the temperature to 180 °C, the apparent size of S-CNC aggregates increased exponentially up to ca. ~2000 nm (Figure 8.1b). AFM suggests that these aggregates are more densely packed than those observed after heating up to 150 °C (Figure 8.2iia and vs. 8.2iiia). This is in line with observations on the fractal aggregation of CNCs in salt solutions, whereby neutral CNCs formed denser aggregates than charged CNCs.[33] In this case, exposing S-CNC suspensions to higher temperatures essentially produces uncharged CNCs, increasing interparticle interactions and allowing them to come into closer proximity and form denser aggregates. The presence and size of aggregates in CNC suspensions play an important role in suspension rheology;[34,35] large aggregates, particularly those fractal in nature, can form interconnected networks which increase the viscosity of CNC suspensions.[35]

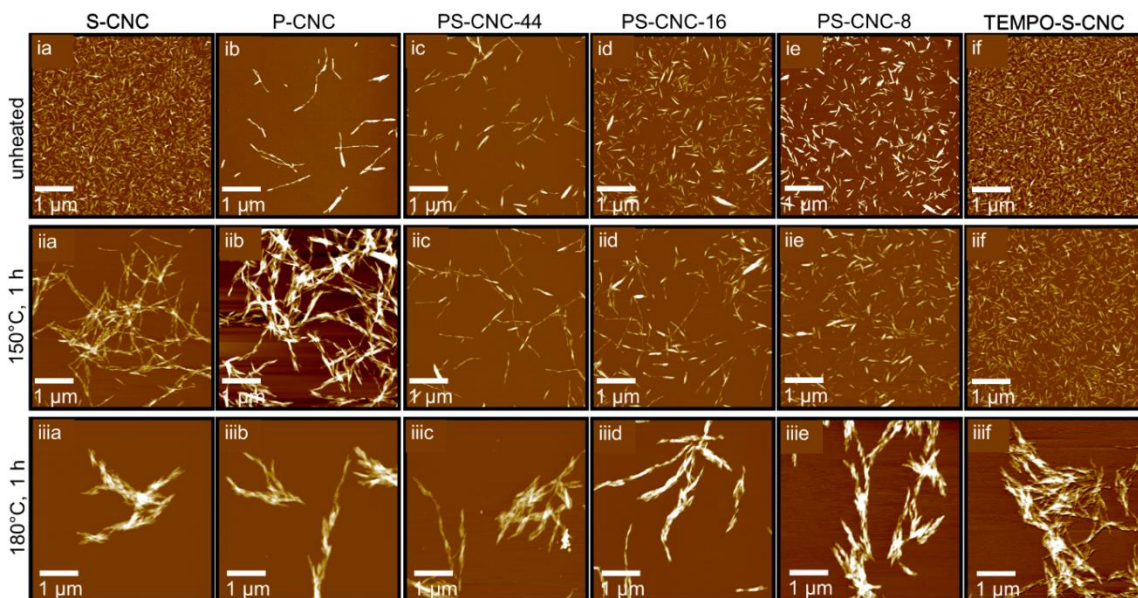Figure 8.2. AFM height images of (i) unheated CNC suspensions and CNC suspensions heated for 1 hour at (ii) 150°C and (iii) 180°C. CNC types are (a) S-CNC, (b) P-CNC, (c) PS-CNC-44, (d) PS-CNC-16, (e) PS-CNC-8, and (f) TEMPO-S-CNC.

To further elucidate the behavior of CNC suspensions at high temperatures, additional experiments were performed with different CNC types, which varied in surface chemistry, surface charge content, and morphology. In comparison to S-CNCs, CNCs produced with phosphoric acid (P-CNCs) have phosphate surface groups, and are comprised of cellulose with a higher degree of polymerization and a lower overall surface charge content.[24] As a result of their weak acid hydrolysis, P-CNCs have high zeta potential values (i.e., closer to zero) (Figure 8.1a) and are loosely aggregated at room temperature (Figure 8.2ib). Upon exposure to high temperatures, they form larger and denser-looking aggregates (Figures 8.1b, 8.2iib and 8.2iiib). In dried form, P-CNCs have a higher thermal stability than S-CNCs;[23] however, this is largely attributed to their lower surface charge content.[24] In suspension, this lower charge content is a hindrance: while P-CNCs undergo less significant changes than those of S-CNCs, they do not perform better at any tested temperature due to their initial lack of colloidal stability.

We have previously shown that CNCs can be hydrolyzed with a blend of sulfuric and phosphoric acids to improve their performance as compared to P-CNCs.[24] These acid blend CNCs (PS-CNCs) have both phosphate and sulfate surface groups. Furthermore, their total surface charge contents and their subsequent colloidal stability and suspension uniformity, depend on the ratio of phosphoric to sulfuric acid used in the hydrolysis production process. As this molar ratio decreases from 44 to 8 (i.e., as more sulfuric acid is used), the zeta potential of the CNCs decreases from -11 mV to -23 mV (Figure 8.1a). Likewise, the apparent size of the CNCs decreases from 184 nm to 105 nm and they form more uniform dispersions with fewer visible aggregates (Figures 8.1b, 8.2ic, 8.2id, and 8.2ie).

Upon heating the acid blend CNC suspensions to 150°C, they demonstrated an improvement in performance over both S-CNCs and P-CNCs. The PS-CNC-8 sample, for example, only underwent a minor reduction in colloidal stability. Furthermore, the apparent size of the CNCs in suspension, which represents dispersion "quality", remained unchanged (Figure 8.1b). AFM further confirmed this high thermal performance: the CNCs remained well-dispersed and did not form any aggregates (Figure 8.2iie). The ability of PS-CNCs to maintain colloidal stability appears unrelated to surface group type since CNCs with either phosphate or sulfate groups undergo significant aggregation when heated at 150°C. As such, their behavior may be attributed to the low total surface charge content and the proximity of neighboring phosphate or sulfate ester groups on the CNC surface. Beck et al. demonstrated that upon heating S-CNCs in varying concentrations, more concentrated CNC suspensions underwent more extensive desulfation.[8] It was stipulated that local proton concentrations within a CNC's bound water layer governed desulfation.[8] As such, desulfation is an "intra-CNC" reaction by which the proton from one sulfate group catalyzes the desulfation of a neighboring sulfate group (on the same CNC or on a nearby CNC).[8] In the case of PS-CNCs, their overall surface charge content is low (30 mmol S or P/kg CNC vs. 200 mmol S/kg CNC for S-CNCs),[24] meaning sulfate or phosphate groups are spaced further apart along the cellulose chain, and are less likely to undergo auto-

catalyzed de-esterification. Despite this benefit, all PS-CNCs form large aggregates when heated to 180°C, suggesting that most or all ester groups are removed at this temperature.

To further probe the effects of CNC characteristics on their thermal performance, S-CNCs were subject to a TEMPO-mediated oxidation to introduce surface carboxylate groups. The TEMPO-S-CNCs are similar to S-CNCs: they form well-dispersed (Figure 8.2if) and colloidally stable CNC suspensions with apparent particle sizes of 80 nm (Figure 8.1). They do, however, possess additional surface charge groups; as such, TEMPO-S-CNCs have a different surface chemistry and a significantly greater surface charge content than their unmodified counterparts. Upon heating, the added carboxylate groups improved the thermal performance of CNC suspensions. While the colloidal stability of the TEMPO-S-CNCs decreased with increasing heating temperature, the effects are less severe than those observed with S-CNCs. After heating at 150°C for 1 h, the TEMPO-S-CNCs are still colloidally stable and in fact have a *reduced* apparent size (69 nm vs. 83 nm unheated). This reduction, which was also observed for S-CNCs heated at 100 and 120°C, could be attributed to DLVO theory, by which repulsive forces increase with increasing temperature, therefore breaking up some previously "loosely hinged" CNCs. Regardless, the presence of the carboxylate groups allows the CNCs to maintain colloidal stability at 150°C. Unfortunately though, upon increasing the temperature to 180°C, the TEMPO-S-CNCs perform similarly to the various CNCs discussed above: large, dense aggregates form (Figure 8.2iiif). Nevertheless, at short heat treatments, the carboxylated TEMPO-S-CNCs remained the most colloidally stable (with PS-CNCs, particularly PS-CNC-8, in a close second), while the S-CNCs were the most destabilized by thermal processing.

Long heat treatments. To further elucidate the effects of surface chemistry and surface charge content on thermal performance, longer heat treatments were performed in an aging cell. Unlike the PARR reactor, the aging cell did not utilize mechanical stirring, however, it eliminated operating time constraints, thus allowing CNC suspensions to be heated for up to seven days. The P-CNCs and PS-CNCs were not included in this experimental matrix because their decreased performance after heating was attributed to similar destabilization mechanisms as S-CNCs (with less severe aggregation due to their lower charge densities). Conversely, the carboxylate groups significantly altered the thermal behavior of the TEMPO-S-CNCs; as such, these were selected for further experiments alongside typical S-CNCs. The longer heat treatments were performed at 150°C because S-CNCs and TEMPO-S-CNCs displayed drastically different behaviors at this temperature: S-CNCs lost colloidal stability and aggregated, while those with additional carboxylate groups did not.

After two and six-hour heat treatments, the CNC suspensions appeared similar; aggregation was not visible to the naked eye (Figure 8.3). After heating suspensions for 24 hours or more, however, S-CNC suspensions were turbid, which is indicative of severe aggregation. Unsurprisingly, the TEMPO-S-CNC suspensions did not appear turbid, even after enduring seven days of exposure to 150°C. The TEMPO-S-CNC suspensions did, however, show

discoloration, which began to appear at the 24-hour mark. This result is in line with work by Heggset et al., in which oxidized cellulose nanofibril (CNF) suspensions underwent severe heat-induced color changes.[10] Similar color changes have also been observed upon heating dried TEMPO-oxidized nanocelluloses or celluloses and are generally attributed to the degradation of ketones and aldehyde groups which are formed as side reactions during TEMPO-mediated oxidations.[25,36]
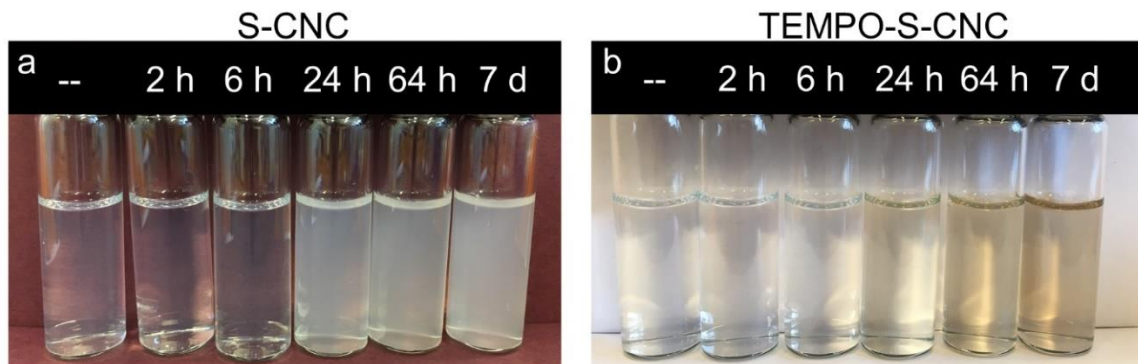

Figure 8.3. Visual appearance of acid-form, 0.1 wt% (a) S-CNC as well as (b) TEMPO-S-CNC suspensions after heating at 150°C for up to 7 days.

The lack of observable color changes in the S-CNC suspensions can be attributed to CNC concentration. Molnes et al. discovered severe discoloration of concentrated S-CNC suspensions (2 wt%) heated to only 120°C for 48-168 h.[9] As such, while desulfation is largely attributed to "intra-CNC" reactions and local proton concentration at CNC surfaces,[8] cellulose degradation and discoloration can be attributed to an acid hydrolysis mechanism which is a function of acid concentration/suspension pH. Due to desulfation, highly concentrated S-CNC suspensions produce more free sulfuric acid, thus catalyzing the hydrolysis of cellulose chains to produce oligosaccharides and sugars, which can further degrade to form furanic compounds.[37] While degradation can occur at dilute sulfuric acid concentrations,[38] the low S-CNC concentration used in this study (0.1 wt%) likely did not produce enough sulfuric acid to cause significant hydrolysis of cellulose chains. CNC structural changes (or lack thereof) will be further discussed below.

The zeta potential and apparent size of the heated S-CNC and TEMPO-S-CNC suspensions were further evaluated to understand the effects of prolonged exposure at 150°C (Figures 8.4a and 8.4b, respectively). Furthermore, sodium hydroxide was used to neutralize CNC suspensions and evaluate charge group counterion effects on thermal performance. The S-CNCs in acid-form demonstrated a dramatic reduction in colloidal stability after just 2 h at 150°C (i.e., zeta potential increased from -35 ± 1 to -23 ± 1 mV), and an even more dramatic reduction after 6 h at 150°C (i.e., zeta potential went up to -9 ± 1mV). These results are in line with the those discussed above for the shorter heat treatments, whereby S-CNC suspensions underwent significant changes in colloidal stability upon heating at 150°C (Figure 8.1).

This drop in colloidal stability, could, however, be mitigated through a counterion exchange (i.e., switching from acid form to sodium form); S-CNC suspensions heated in sodium form for 2 h and 6h had zeta potentials of -33 ± 2 and -19 ± 1 mV. As such, while acid-form S-CNCs reached "highly unstable" zeta potential values (<|10 mV|) after heating for 6 h, sodium-form S-CNCs did not reach this point until they had been heated for 24 h. After 24 h or more at 150°C, both acid and sodium-form S-CNC suspensions were colloidally unstable, with measured zeta potentials at or near 0 mV. Overall, however, the difference in thermal performance between acid and sodium-form S-CNC suspensions is not as drastic as the differences observed for dried S-CNCs, where thermal stability measured via thermogravimetric analysis ranges from ca. 150°C in acid form to ca. 300°C in sodium form.[24,39,40] Essentially, while desulfation is catalyzed by higher local proton concentrations, it appears to occur to nearly the same extent in sodium form at the tested temperatures. This is contrary to Beck et al.'s observations at lower temperatures (ca. 70-85°C), where sodium-form S-CNCs underwent negligible desulfation.[8] As such, these results suggest that counterion choice for S-CNCs does not drastically change the thermal performance of their aqueous suspensions (within the conditions tested in this study).
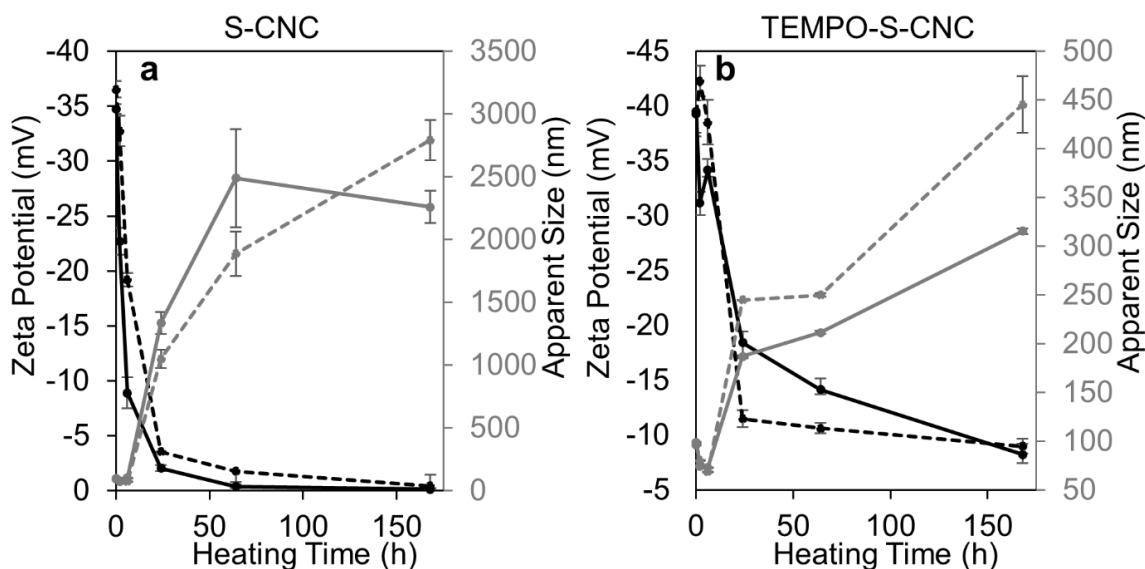
Figure 8.4. Zeta potential (black) and apparent size (grey) of both acid-form (solid line) and sodium-form (dashed line) (a) S-CNCs and (b) TEMPO-S-CNCs after heating at 150°C for up to 7 days.

The TEMPO-S-CNC suspensions behaved differently than S-CNCs upon exposure to 150°C over long time periods (Figure 8.4b). As discussed above, the changes in colloidal stability and apparent size were less severe (Figure 8.1), which suggests carboxylate groups are more thermally stable than sulfate groups. This was confirmed via conductometric titrations: prior to heating, TEMPO-S-CNCs possessed 764±35 mmol COO⁻/kg CNC and 137±44 mmol OSO₃⁻/kg CNC. After exposure to 150°C for 6 hours, 399±80 mmol COO⁻

/kg CNC remained, while no traces of sulfate half ester groups were detected. Since carboxylic acids are weak acids, desulfation of surface sulfate groups could reduce the suspension pH enough to protonate the carboxylate groups, which have a pK_a of 3.6-3.7.[41–43] In fact, after heating a 0.1 wt% TEMPO-S-CNC suspension at 150°C for 6 hours, the suspension pH decreased from 3.81 to 3.25, the latter of which is below this pK_a. To further probe the effect of reducing the pH on the colloidal stability of TEMPO-S-CNCs, the heated suspension was dialyzed following its 6 h heat treatment and its pH and zeta potential were determined after dialysis. Surprisingly, while the pH increased to 4.23 after dialysis, the measured zeta potential of the heated TEMPO-S-CNC suspensions did not change; their measured values were -34±1 mV and -31±2 mV before and after dialysis, respectively. As such, the reduction in pH occurring as a result of desulfation does not impact the colloidal stability of the TEMPO-S-CNCs. This suggests CNC carboxylate groups remained sufficiently charged in the presence of free sulfate groups (which both lower suspension pH and increase ionic strength). Nevertheless, if higher concentrations of sulfate groups were present on CNC surfaces, their desulfation could sufficiently decrease suspension pH to result in protonation of carboxylate groups. As such, carboxylated CNCs would likely demonstrate more predictable thermal performance if no sulfate groups were present, for example, in the case of TEMPO-CNCs produced directly by oxidation,[44] i.e., without a sulfuric acid hydrolysis step, or carboxylated CNCs produced following alternative methods.[45–49]

While the exchange of protons with sodium counterions resulted in improvements for S-CNC thermal performance, the opposite was true for TEMPO-S-CNCs. After heat treatments of 2 h and 6 h, both acid and sodium-form TEMPO-S-CNCs maintained high colloidal stabilities (i.e., zeta potentials between -42 and -34 mV). After longer heat treatments (24 h and 64 h), however, TEMPO-S-CNCs demonstrated less colloidal stability and larger apparent sizes in sodium form than in acid form (Figure 8.4b). These results align with studies on the thermal performance of dried oxidized celluloses and nanocelluloses, which are less stable with sodium counterions than in acid form.[50,51] In the dried state, sodium-form oxidized celluloses produce sodium carbonate as a result of dehydration and decarboxylation reactions; this ultimately reduces their thermal stability.[51] While the exact mechanism is unclear, it appears that the presence of sodium ions also destabilizes carboxylate groups in heated CNC suspensions, perhaps resulting in further decarboxylation.

To further understand the effects of surface chemistry on CNC suspension thermal performance, a series of conductometric titrations were performed to determine rate constants for the removal of surface charge groups via desulfation or decarboxylation (Figure 8.5). These results ascertain all previous observations whereby S-CNCs undergo significant changes at earlier temperatures than TEMPO-S-CNCs. Sulfate contents (and desulfation) were probed at 80°C and 100°C (Figure 8.5a), while carboxylate contents (and decarboxylation) were probed at 150°C and 180°C (Figure 8.5b). Desulfation is known to

occur rapidly in its initial phase[8] and later plateau as the spacing of remaining sulfate groups on CNC surfaces increases and fewer intra-particle interactions occur. Our S-CNCs underwent similar changes: at 80 and 100°C, sulfate content rapidly decreased from 190 mmol OSO_3^-/kg CNC to 79 and 46 mmol OSO_3^-/kg CNC, respectively. These changes are characteristic of second-order reactions, where rate constants are proportional to the square of the reactant concentration. As such, the inverse sulfate concentration (in mol/L) was plotted vs. time, and a strong correlation (confirmed via high R^2 values) was observed at both temperatures (Figure 8.5c). Furthermore, for S-CNCs, the reaction rate constants, which represent the slopes of the aforementioned correlations, were found to be 0.106 $L·mol^{-1}s^{-1}$ and 0.162 $L·mol^{-1}s^{-1}$ for desulfation at 80°C and 100°C, respectively. Unsurprisingly, the rate constant increased as a function of temperature, which aligns with our previous observations of more severe S-CNC aggregation at higher temperatures.
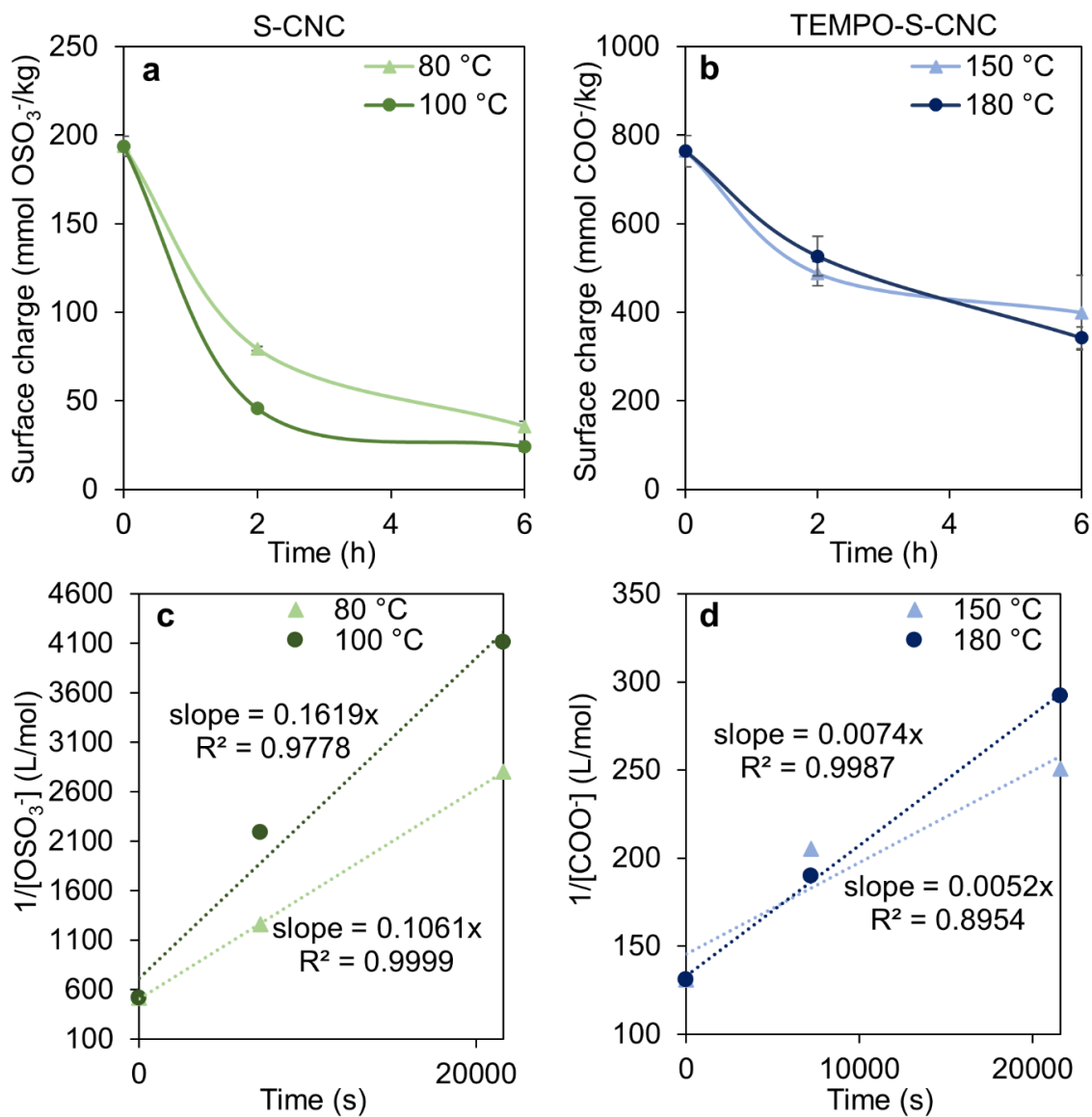
Figure 8.5. Surface charge groups per unit mass of CNCs obtained via conductometric titrations of heated acid-form (a) S-CNCs and (b) TEMPO-S-CNCs at 0.1 wt%. Rate constants (assuming 2nd order kinetic reactions) are shown for the loss of (c) sulfate groups from S-CNCs and (d) carboxylate groups from TEMPO-S-CNCs.

The effect of temperature on the decarboxylation of TEMPO-S-CNCs in suspension was less clear (Figure 8.5b). At the tested temperatures (150 and 180°C), similar charge contents were reported after heating TEMPO-S-CNCs (760 mmol COO-/kg CNC) for two hours (500 mmol COO-/kg CNC) and six hours (350-400 mmol COO-/kg CNC). Overall, the stability of the carboxylate groups on CNCs significantly outperforms that of sulfate groups. In addition to withstanding higher temperatures than sulfate groups, decarboxylation did not occur as rapidly. After two hours of heating at each tested

temperature, over half of the initial carboxylate groups remained on CNC surfaces. Conversely, sulfate contents on CNC surfaces were reduced to 24-42% of their initial concentration after two-hour heat treatments.

To evaluate the reaction kinetics of the decarboxylation of TEMPO-S-CNCs, a second order reaction was once again assumed. While this was the best fit for the loss of carboxylate groups at 180°C (R^2=0.9987), the correlation between reaction time and the inverse concentration of carboxylate groups was not as strong at 150°C (R^2=0.8954). As such, it is unclear whether decarboxylation of CNC carboxylate groups is a second-order reaction; further experiments (e.g., additional temperatures and time points) are likely needed to determine precise kinetics. Furthermore, the presence of sulfate groups on TEMPO-S-CNCs and/or sulfate ions within the suspension cannot be ignored; these could affect the reaction kinetics of decarboxylation (by altering pH and/or participating in competitive or cooperative reactions). Nevertheless, insights can be gained by comparing the observed kinetics to those of CNC desulfation. Overall, the rate constants for decarboxylation are significantly lower than those for desulfation (e.g., 0.0052-0.0074 vs. 0.1061-0.1619 L·mol^{-1}s^{-1}), indicating that reaction rates for desulfation are more concentration dependent than those for decarboxylation. Additionally, the rate constants for desulfation are more temperature dependant than those for decarboxylation: despite using a narrower temperature range (Δ=20°C for sulfated CNCs vs. 30°C for carboxylated CNCs), larger differences were observed among the desulfation rate constants.

The rate constants determined above were used to calculate activation energies *via* the Arrhenius equation: S-CNCs and TEMPO-S-CNCs were found to have activation energies of 26 and 21 kJ/mol, respectively. While the rate constants imply that desulfation occurs ca. 20 times faster than decarboxylation, their activation energies indicated similar energetic barriers for both endothermic reactions. Nevertheless, the slightly higher activation energy for S-CNCs suggests that desulfation is more temperature sensitive than decarboxylation. We note that a direct comparison of these activation energy values may be misleading since the rate constants were calculated over different temperature ranges, the number of transition states/steps are unknown, and there is a larger uncertainty in the rate constant for TEMPO-S-CNCs because decarboxylation does not follow 2nd order kinetics as directly. Overall, the activation energies are lower than those calculated for the thermal degradation of dried S-CNCs, i.e., 71-123 kJ/mol (where higher activation energies were observed for CNCs with fewer sulfate groups),[52] supporting that CNC desulfation/decarboxylation occur with less energy input (i.e., at lower temperatures) than true thermal degradation, which would include cellulose depolymerization and destruction of the nanoparticle morphology.

As discussed above, discoloration in heated CNC suspensions can be indicative of degradation.[9,10] Based on the appearance of both CNC types (Figure 8.3), we hypothesized that S-CNCs had not undergone any appreciable degradation, whereas CNCs with carboxylate groups discolored, implying cellulose degradation at high temperatures. As such, X-ray diffraction was used to evaluate changes in S-CNC and TEMPO-S-CNC morphology as a function of heating time at 150°C. It is worth noting that the observed

crystallinity indices are all above 90% and that one value is listed as 100%. We recognize that our CNC samples are not 100% crystalline and that this high value encompasses experimental error of ca. 5%. The crystallinity indices calculated from X-ray diffraction using a Rietveld refinement showed no changes to the crystal structure of either CNC type over the seven-day heating period (Table 8.1). If the CNCs had undergone significant degradation, lower crystallinity indices would have been observed. D'Acierno et al., for example, observed a total loss of crystallinity (from ca. 80% to ~0) for *dried* acid-form S-CNCs heated between 160 and 250°C (calculated by NMR).[53] Likewise, exposure to high temperature and acidic conditions could result in further cellulose hydrolysis since harsh sulfuric acid conditions are known to reduce the crystallinity of CNCs.[39]

Table 8.1. Crystallinity indices and weight-average molecular weights (M_w) for CNCs heated in acid form at 150°C. All CNC suspensions have been dialyzed and sonicated after heating. Instrumental and fitting error for crystallinity indices is normally taken to be ca. 5%; however, triplicates were completed for both unheated and 7-day TEMPO-S-CNC samples, which revealed errors of 0.4% and 0.3%, respectively.

Heating time (at 150°C)	S-CNC		TEMPO-S-CNC	
	Crystallinity Index (%)	M_w (kDa)	Crystallinity Index (%)	M_w (kDa)
unheated	92	221	100	221
2 hours	99	292	98	228
6 hours	98	274	96	208
24 hours	97	266	96	211
64 hours	98	274	98	217
7 days	98	275	98	224

To further confirm that heat treatments at 150°C did not significantly alter the morphology of sulfated and carboxylated CNCs, size exclusion chromatography (on tricarbanilated and solubilized cellulose) was used to probe the molecular weight distributions of the cellulose chains which make up CNCs (Table 8.1 and Figure 8.6). Overall, thermally induced end-wise degradation was not observed upon heating S-CNC and TEMPO-S-CNC suspensions for up to 7 days; however, surface cellulose degradation of TEMPO-S-CNCs (likely resulting from decarboxylation reactions) was detected. Unheated S-CNCs were used as the control for both S-CNCs and TEMPO-S-CNCs since the latter are simply a surface-modified S-CNC (i.e., we assume that the internal particle cellulose structure does not change). It is worth noting that the control sample exhibited a lower M_w than the heated S-CNC samples (Table 8.1), however, if thermally induced end-wise degradation had occurred, the opposite shift would have been observed (i.e., degradation produces lower molecular weight cellulose chains). As such, the difference between the control and heated samples was attributed to the influence of surface charge groups on the effectiveness of the tricarbanilation reaction which was used to solubilize cellulose chains. Nevertheless, the

molecular weight distributions (and M_w) of the cellulose chains within S-CNCs underwent no significant changes upon exposure to longer heat treatments (e.g., 2 h vs. 7 d) as shown in Table 8.1 and Figure 8.6a.
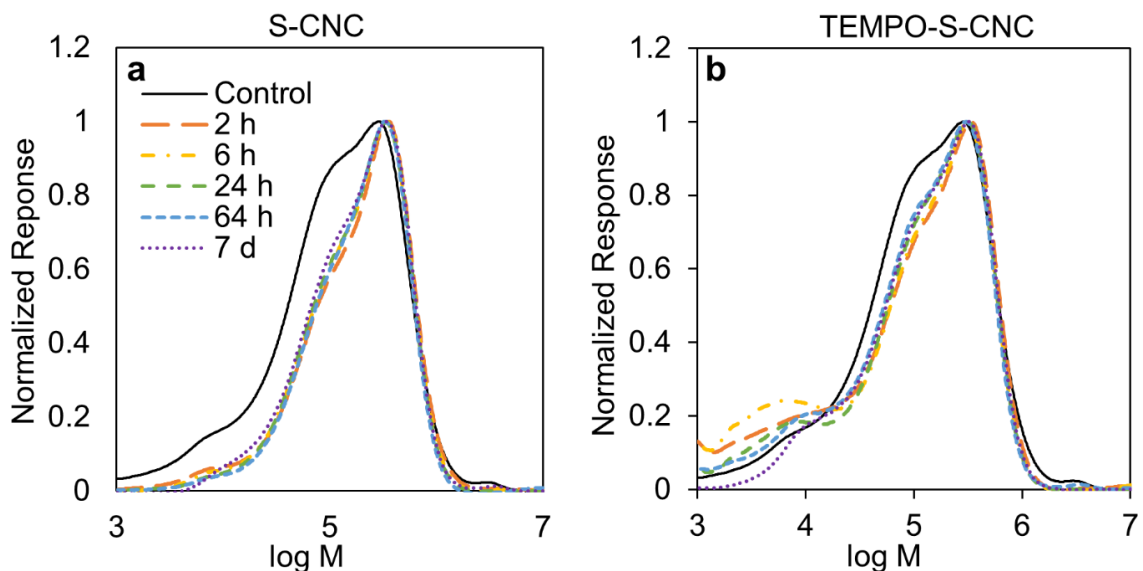

Figure 8.6. Molecular weight distributions of (a) S-CNCs and (b) TEMPO-S-CNCs heated at 150°C in acid-form. All CNC suspensions were dialyzed after heating.

Conversely, the molecular weight distributions of the TEMPO-S-CNCs demonstrated small changes in the intensity of low molecular weight cellulose chains (e.g., in the $\log(M) = 4$ range, Figure 8.6b). Assuming full substitution of the surface hydroxy groups during the tricarbanilation derivatization reaction,[26] these low molecular weight cellulose chains possess 5-20 repeat anhydroglucose units, which suggests the presence of oligosaccharides. The fluctuating response in this molecular weight region could be attributed to degradation of aldehyde and ketone groups on TEMPO-S-CNCs (as discussed above) or some surface cellulose degradation induced by decarboxylation reactions. Nevertheless, these changes are minor and can likely be attributed to small-scale surface reactions rather than widespread degradation of the CNC structure. The consistent molecular weight distributions agree with the unchanging X-ray diffraction results discussed above, supporting that no significant changes occurred to the morphology of S-CNCs or TEMPO-S-CNCs heated at 150°C for up to seven days. This is significant because it implies that even after long-term exposure to heat and pressure, the CNCs remain intact and their structural and mechanical properties remain constant – this is crucial for both reinforcement potential and rheological modification.

Although our results above suggest that hydrothermal treatments do not induce cellulose degradation, previous studies on more concentrated suspensions have demonstrated severe discoloration and presumed degradation.[9,14] These differences suggest that an acid

hydrolysis mechanism is responsible for cellulose degradation within high temperature aqueous suspensions, whereby suspensions with higher CNC concentrations are subject to "harsher" hydrolysis conditions and are therefore more susceptible to degradation. Herein, we discussed thermally induced desulfation and subsequent reductions in suspension pH, both of which would be exacerbated if more CNCs (and therefore more sulfate ions) were present in an aqueous suspension. Moreover, Heggset et al., who quantified the production of furfural and hydroxymethylfurfural in heated CNF and CNC suspensions, determined that CNCs produced negligible amounts of these degradation by-products due to their highly crystalline structure.[10] Conversely, mechanically fibrillated CNFs produced more degradation by-products and also demonstrated greater color changes after hydrothermal treatments. This is in line with the acid hydrolysis mechanism which produces CNCs: heat and acidic conditions preferentially degrade disordered regions until a level-off degree of polymerization (LODP) is reached.[6,54] CNCs are highly crystalline and are typically at or near their LODP, while CNFs are more susceptible to acid hydrolyses. This behavior is opposite to the thermal degradation of dried nanocelluloses, whereby thermally induced depolymerization is initiated at reducing ends,[55,56] meaning CNFs are typically more thermally stable than CNCs because they possess higher molecular weight cellulose. As such, unlike dried CNCs which consistently degrade at similar temperatures, the thermal performance of CNC suspensions is highly dependent on formulation characteristics including CNC concentration and the presence of other chemical components (e.g., buffers to stabilise pH, surfactants, other polymers, etc.).

8.5 Conclusions

This work investigated the effects of high temperature treatments on aqueous CNC suspension properties for sulfated, carboxylated, and phosphated CNCs. Suspensions were exposed to temperatures ranging from 80°C to 180°C for up to seven days. Sulfated CNCs were most susceptible to decreases in colloidal stability and the formation of CNC aggregates, while CNCs with carboxylate groups maintained more consistent suspension properties. This is attributed to the stability of carboxylate groups at high temperatures; desulfation occurred rapidly at temperatures as low as 80°C, while ca. 50% of carboxylate groups remained on CNC surfaces after exposure to 180°C. Rate constants were determined for the loss of surface sulfate half ester and carboxylate groups, implying second order kinetics and revealing that reaction rates for desulfation are faster and more temperature dependent. The starting surface charge content was also revealed to affect the thermal performance of CNC suspensions; PS-CNCs, which possess lower charge densities, maintained colloidal stability at higher temperatures than S-CNCs.

Furthermore, changes in cellulose molecular weight and cellulose crystallinity were probed to determine whether the tested conditions caused CNCs to degrade. Ultimately, although carboxylated CNCs underwent color changes, no significant particle or cellulose degradation was detected. As such, in heating dilute CNC suspensions for up to 7 days, loss of surface charge groups was found to be the dominant factor affecting the performance of

these aqueous suspensions. Researchers looking to utilize CNCs at high temperatures should therefore select carboxylated CNCs or sulfated/phosphated CNCs with lower charge densities (e.g., PS-CNCs or partially desulfated S-CNCs) to maximize the performance (and consistency) of CNCs within their targeted application.

8.6 References

1. Rånby, B. G. The Colloidal Properties of Cellulose Micelles. *Discuss. Faraday Soc.* **11**, 158–164 (1951).

2. Marchessault, R. H., Morehead, F. F. & Koch, M. J. Some Hydrodynamic Properties of Neutral As Related To Size and Shape 1. *J. Colloid Sci.* **344**, 327–344 (1961).

3. Viet, D., Beck-Candanedo, S. & Gray, D. G. Dispersion of cellulose nanocrystals in polar organic solvents. *Cellulose* **14**, 109–113 (2007).

4. Reid, M. S., Villalobos, M. & Cranston, E. D. Benchmarking cellulose nanocrystals: from the laboratory to industrial production. *Langmuir* **33**, 1583–1598 (2017).

5. Lu, P. & Hsieh, Y. Lo. Preparation and characterization of cellulose nanocrystals from rice straw. *Carbohydr. Polym.* **87**, 564–573 (2012).

6. Nickerson, R. F. & Habrle, J. A. Cellulose intercrystalline structure. *Ind. Eng. Chem.* **39**, 1507–1512 (1947).

7. Revol, J.-F., Bradford, H., Giasson, J., Marchessault, R. H. & Gray, D. G. Helicoidal self-ordering of cellulose microfibrils in aqueous suspension. *Int. J. Biol. Macromol.* **14**, 170–172 (1992).

8. Beck, S. & Bouchard, J. Auto-Catalyzed acidic desulfation of cellulose nanocrystals. *Nord. Pulp Pap. Res. J.* **29**, 6–14 (2014).

9. Molnes, S. N., Paso, K. G., Strand, S. & Syverud, K. The effects of pH, time and temperature on the stability and viscosity of cellulose nanocrystal (CNC) dispersions: implications for use in enhanced oil recovery. *Cellulose* (2017) doi:10.1007/s10570-017-1437-0.

10. Heggset, E. B., Chinga-Carrasco, G. & Syverud, K. Temperature stability of nanocellulose dispersions. *Carbohydr. Polym.* **157**, 114–121 (2017).

11. Dong, X. M. & Gray, D. G. Effect of counterions on ordered phase formation in suspensions of charged rodlike cellulose crystallites. *Langmuir* **13**, 2404–2409 (1997).

12. Araki, J., Wada, M., Kuga, S. & Okano, T. Flow properties of microcrystalline cellulose suspension prepared by acid treatment of native cellulose. *Colloids Surfaces A Physicochem. Eng. Asp.* **142**, 75–82 (1998).

13.   Abitbol, T., Kam, D., Levi-Kalisman, Y., Gray, D. G. & Shoseyov, O. Surface Charge Influence on the Phase Separation and Viscosity of Cellulose Nanocrystals. *Langmuir* **34**, 3925–3933 (2018).

14.   Lewis, L., Derakhshandeh, M., Hatzikiriakos, S. G., Hamad, W. Y. & MacLachlan, M. J. Hydrothermal Gelation of Aqueous Cellulose Nanocrystal Suspensions. *Biomacromolecules* **17**, 2747–2754 (2016).

15.   Yang, H., Chen, D. & van de Ven, T. G. M. Preparation and characterization of sterically stabilized nanocrystalline cellulose obtained by periodate oxidation of cellulose fibers. *Cellulose* **22**, 1743–1752 (2015).

16.   Van De Ven, T. G. M. & Sheikhi, A. Hairy cellulose nanocrystalloids: A novel class of nanocellulose. *Nanoscale* **8**, 15101–15114 (2016).

17.   Araki, J., Wada, M. & Kuga, S. Steric stabilization of a cellulose microcrystal suspension by poly(ethylene glycol) grafting. *Langmuir* **17**, 21–27 (2001).

18.   Kloser, E. & Gray, D. G. Surface grafting of cellulose nanocrystals with poly(ethylene oxide) in aqueous media. *Langmuir* **26**, 13450–13456 (2010).

19.   Molnes, S. N., Mamonov, A., Paso, K. G., Strand, S. & Syverud, K. Investigation of a new application for cellulose nanocrystals: a study of the enhanced oil recovery potential by use of a green additive. *Cellulose* **25**, 2289–2301 (2018).

20.   Aadland, R. C. *et al.* High-temperature core flood investigation of nanocellulose as a green additive for enhanced oil recovery. *Nanomaterials* **9**, (2019).

21.   Bashir Wani, O., Shoaib, M., Al Sumaiti, A., Bobicki, E. R. & Alhassan, S. M. Application of Green additives for enhanced oil recovery: Cellulosic nanocrystals as fluid diversion agents in carbonate reservoirs. *Colloids Surfaces A Physicochem. Eng. Asp.* **589**, (2020).

22.   Cranston, E. D. & Gray, D. G. Morphological and optical characterization of polyelectrolyte multilayers incorporating nanocrystalline cellulose. *Biomacromolecules* **7**, 2522–2530 (2006).

23.   Camarero Espinosa, S. *et al.* Isolation of thermally stable cellulose nanocrystals by phosphoric acid hydrolysis. *Biomacromolecules* **14**, 1223–1230 (2013).

24.   Vanderfleet, O. M. *et al.* Insight into thermal stability of cellulose nanocrystals from new hydrolysis methods with acid blends. *Cellulose* **26**, 507–528 (2019).

25.   Isogai, A., Saito, T. & Fukuzumi, H. TEMPO-oxidized cellulose nanofibers. *Nanoscale* **3**, 71–85 (2011).

26.   Evans, R., Wearne, R. H. & Adrian, F. A. Molecular Weight Distribution of Cellulose as Its Tricarbanilate by High Performance Size Exclusion Chromatography. **37**, 3291–3303 (1989).

27.   Bouchard, J., Méthot, M., Fraschini, C. & Beck, S. Effect of oligosaccharide deposition on the surface of cellulose nanocrystals as a function of acid hydrolysis temperature. *Cellulose* **23**, 3555–3567 (2016).

28.   Conner, A. H. Size Exclusion Chromatography of Cellulose and Cellulose. *Handb. size exclusion Chromatogr.* 331–352 (1995).

29.   Stålbrand, H. *et al.* Analysis of molecular size distributions of cellulose molecules during hydrolysis of cellulose by recombinant Cellulomonas fimi beta-1,4-glucanases. *Appl. Environ. Microbiol.* **64**, 2374–2379 (1998).

30.   Bhattacharjee, S. DLS and zeta potential - What they are and what they are not? *J. Control. Release* **235**, 337–351 (2016).

31.   Silveira, R. L., Stoyanov, S. R., Kovalenko, A. & Skaf, M. S. Cellulose Aggregation under Hydrothermal Pretreatment Conditions. *Biomacromolecules* **17**, 2582–2590 (2016).

32.   Uhlig, M. *et al.* Two-Dimensional Aggregation and Semidilute Ordering in Cellulose Nanocrystals. *Langmuir* **32**, 442–450 (2016).

33.   Cherhal, F., Cousin, F. & Capron, I. Influence of charge density and ionic strength on the aggregation process of cellulose nanocrystals in aqueous suspension, as revealed by small-angle neutron scattering. *Langmuir* **31**, 5596–5602 (2015).

34.   Shafiei-Sabet, S., Hamad, W. Y. & Hatzikiriakos, S. G. Ionic strength effects on the microstructure and shear rheology of cellulose nanocrystal suspensions. *Cellulose* **21**, 3347–3359 (2014).

35.   Xu, Y., Atrens, A. D. & Stokes, J. R. Rheology and microstructure of aqueous suspensions of nanocrystalline cellulose rods. *J. Colloid Interface Sci.* **496**, 130–140 (2017).

36.   Takaichi, S., Saito, T., Tanaka, R. & Isogai, A. Improvement of nanodispersibility of oven-dried TEMPO-oxidized celluloses in water. *Cellulose* **21**, 4093–4103 (2014).

37.   Wang Q, Zhao X, Zhu JY, . Kinetics of strong acid hydrolysis of a bleached kraft pulp for producing cellulose nanocrystals (CNCs). *Ind Eng Chem Res* **53**, 11007–11014 (2014).

38.   Gurgel, L. V. A., Marabezi, K., Zanbom, M. D. & Curvelo, A. A. D. S. Dilute acid hydrolysis of sugar cane bagasse at high temperatures: A Kinetic study of cellulose saccharification and glucose decomposition. Part I: Sulfuric acid as the catalyst. *Ind. Eng. Chem. Res.* **51**, 1173–1185 (2012).

39.   Kargarzadeh, H. *et al.* Effects of hydrolysis conditions on the morphology, crystallinity, and thermal stability of cellulose nanocrystals extracted from kenaf bast fibers. *Cellulose* **19**, 855–866 (2012).

40.   Lin, N. & Dufresne, A. Surface chemistry, morphological analysis and properties of cellulose nanocrystals with gradiented sulfation degrees. *Nanoscale* **6**, 5384–5393 (2014).

41.   Fujisawa, S., Okita, Y., Fukuzumi, H., Saito, T. & Isogai, A. Preparation and characterization of TEMPO-oxidized cellulose nanofibril films with free carboxyl groups. *Carbohydr. Polym.* **84**, 579–583 (2011).

42.   Fukuzumi, H., Fujisawa, S., Saito, T. & Isogai, A. Selective permeation of hydrogen gas using cellulose nanofibril film. *Biomacromolecules* **14**, 1705–1709 (2013).

43.   Jiang, F. & Hsieh, Y. Lo. Self-assembling of TEMPO Oxidized Cellulose Nanofibrils As Affected by Protonation of Surface Carboxyls and Drying Methods. *ACS Sustain. Chem. Eng.* **4**, 1041–1049 (2016).

44.   Zhou, Y., Saito, T., Bergström, L. & Isogai, A. Acid-free preparation of cellulose nanocrystals by TEMPO oxidation and subsequent cavitation. *Biomacromolecules* **19**, 633–639 (2018).

45.   Leung, A. C. W. *et al.* Characteristics and properties of carboxylated cellulose nanocrystals prepared from a novel one-step procedure. *Small* **7**, 302–305 (2011).

46.   Yu, H. Y., Zhang, D. Z., Lu, F. F. & Yao, J. New Approach for Single-Step Extraction of Carboxylated Cellulose Nanocrystals for Their Use As Adsorbents and Flocculants. *ACS Sustain. Chem. Eng.* **4**, 2632–2643 (2016).

47.   Chen, L., Y. Zhu, J., Baez, C., Kitin, P. & Elder, T. Highly thermal-stable and functional cellulose nanocrystals and nanofibrils produced using fully recyclable organic acids. *Green Chem.* **18**, 3835–3843 (2016).

48.   Andrews, M. P. & Morse, T. Method for producing functionalized nanocrystalline cellulose and functionalized nanocrystalline cellulose thereby produced. (2017).

49.   McAlpine, S. & Nakoneshny, J. Production of crystalline cellulose. (2019).

50.   Fukuzumi, H., Saito, T., Okita, Y. & Isogai, A. Thermal stabilization of TEMPO-oxidized cellulose. *Polym. Degrad. Stab.* **95**, 1502–1508 (2010).

51.   Lichtenstein, K. & Lavoine, N. Toward a deeper understanding of the thermal degradation mechanism of nanocellulose. *Polym. Degrad. Stab.* **146**, 53–60 (2017).

52.   Roman, M. & Winter, W. T. Effect of sulfate groups from sulfuric acid hydrolysis on the thermal degradation behavior of bacterial cellulose. *Biomacromolecules* **5**, 1671–1677 (2004).

53.   D'Acierno, F., Hamad, W. Y., Michal, C. A. & Maclachlan, M. J. Thermal Degradation of Cellulose Filaments and Nanocrystals. *Biomacromolecules* **21**, 3374–3386 (2020).

54.   Battista, O. A., Coppick, S., Howsmon, J. A., Morehead, F. F. & Sisson, W. A. Level-off degree of polymerization. *Ind. Eng. Chem.* **48**, 333–335 (1956).

55.   Matsuoka, S., Kawamoto, H. & Saka, S. What is active cellulose in pyrolysis? An approach based on reactivity of cellulose reducing end. *J. Anal. Appl. Pyrolysis* **106**, 138–146 (2014).

56.   Agustin, M. B., Nakatsubo, F. & Yano, H. The thermal stability of nanocellulose and its acetates with different degree of polymerization. *Cellulose* **23**, 451–464 (2016).

Chapter 9

Conclusions and outlook

_____

9.1 Conclusions

This thesis explores new and existing cellulose nanocrystal (CNC) production methods and evaluates their effects on CNC properties, with an emphasis on their thermal performance. CNCs from known production methods, including large-scale and laboratory scale processes, were thoroughly characterized. Additionally, new methods to produce CNCs, including hydrolyses with acid blends and an *in-situ* oligosaccharide modification, were introduced. The effects of these production methods on CNC properties (including surface charge content, morphology, and structure) and performance (including rheological and self-assembly behavior, and thermal performance) were evaluated. Lastly, by studying the behavior of dried CNCs and aqueous CNC suspensions at high temperatures, a thorough understanding of the properties which govern CNC thermal performance was gained. Overall, these contributions satisfy the goals outlined in *Chapter 1*, which set out to:

1. **Explore new and existing production methods and their influence on CNC properties and performance**. In *Chapter 3*, industrially produced sulfated and carboxylated CNCs were characterized and benchmarked against lab-made sulfated CNCs. Their variations in particle morphology, surface chemistry, and surface charge content led to significant differences in CNC rheological and self-assembly behaviors as well as thermal performance. Most notably, carboxylated CNCs were more thermally stable than sulfated CNCs, yet only sulfated CNCs underwent a liquid crystalline phase separation which is a prerequisite for some applications (but not all).

   To further expand the usage of CNCs in commercial products, numerous modified production routes (beyond those which are currently operating at industrial scales) have been proposed to improve CNC properties. *Chapter 4* outlined an optimization study on phosphoric acid hydrolysis parameters to produce thermally stable and colloidally stable phosphated CNCs. Under optimal hydrolysis conditions, the colloidal stability of the phosphated CNCs was marginally improved while maintaining their characteristically high thermal stability. More interestingly, however, was the observed tunability of CNC length: the length of phosphated CNCs could be controlled over a larger range than what is typically attainable for sulfated CNCs. While this control over CNC length is promising in polymer

composite applications, the low dispersibility/colloidal stability of phosphated CNCs is likely a barrier to their widespread usage.

In *Chapter 5,* a novel surface modification method was proposed which utilized the selective solubility of cellulose phosphate oligosaccharides to control their deposition onto CNC surfaces. CNCs modified with oligosaccharides possessed higher surface charge contents, lower water adsorption capacities, and lower suspension viscosities than their unmodified counterparts. Moreover, the proposed surface modification method could easily be implemented in existing large-scale CNC production facilities and could be extended to include oligosaccharides with various functionalities.

2. **Investigate the effects of CNC properties on thermal performance.** While *Chapters 4 and 5* demonstrated new production routes to improve CNC properties, the observed differences in their dried thermal performance were minute. Conversely, *Chapters 6 and 7* utilized CNCs with significantly different thermal performances to deepen our understanding of CNC degradation at high temperatures. CNCs with varying surface chemistries (including phosphate, sulfate, and carboxylate groups, or mixtures thereof), surface charge contents, and structural properties were subject to thermogravimetric analysis. Sulfated and phosphated CNCs behaved similarly upon exposure to heat; however, the temperatures at which degradation occurred were heavily dependent on their surface charge contents and the degree of polymerization of their cellulose chains. Furthermore, these CNCs demonstrated superior thermal performance in sodium form because their acidic functional groups were neutralized. Conversely, carboxylated CNCs produced with organic acids or via oxidation reactions demonstrated superior thermal performance in acid form. The thermal performance of carboxylated CNCs was also highly dependent on CNC specific surface area, surface charge content, and surface chemistry. Namely, CNCs with carboxylate groups separated from the cellulose backbone via "spacers", as well as lower charge contents and specific surface areas were found to be more thermally stable.

Despite the relevance of dried thermal performance for the incorporation of CNCs into, for example, polymer composites, many applications utilize CNCs in liquid formulations. As such, *Chapter 8* investigated the effects of hydrothermal treatments on CNC suspensions. Surprisingly, little to no degradation of cellulose chains or crystallinity occurred at the tested conditions (up to 180 °C). Nevertheless, suspension properties changed drastically due to the loss of their surface charge groups. Carboxylate groups were more resistant than sulfate groups to high temperatures and as such, carboxylated CNCs were found to be more suitable for high temperature applications such as oil and gas extraction fluids.

In achieving the goals outlined above (and in *Chapter 1*), several fundamental contributions were made to the field of nanocellulose research, namely:

- Demonstration of the effects of CNC production routes on cellulose degree of polymerization and the significant influence of this property on CNC thermal stability
- Elucidation of the confounding effects of surface charge content and CNC structure (including cellulose chain length and specific surface area) on the thermal performance of all dried CNCs, regardless of surface chemistry and confirmation that less harsh production routes result in more thermally stable CNCs
- Illustration of key interactions between CNC surface groups and their counterions and the necessity to understand and control these interactions when heating both dried CNCs and aqueous CNC suspensions
- Elucidation of key differences between the stability of CNC sulfate and carboxylate groups throughout hydrothermal treatments, whereby the loss of carboxylate groups from cellulose surfaces was found to occur more slowly and to be less temperature dependent and less concentration dependent than the loss of sulfate groups

Overall, the results presented in this thesis highlight the importance of thoroughly characterizing CNC properties to better understand how they will react in various formulations and processes. As the variety of available CNC types continues to grow, researchers and commercial CNC users must understand the impacts of CNC morphology, structure, surface chemistry, and surface charge content on the performance of CNC-based materials. Furthermore, it is essential that researchers recognize the CNC properties which challenge their incorporation into, for example, hydrophobic matrices, high ionic strength liquid formulations, and high temperature applications. Ultimately, expanding the usage of CNCs into commercial products will require targeted production routes and/or modifications which directly address these challenges. This can only be achieved by thoroughly understanding the links between various production methods, CNC properties, and their performance in products and processes. This thesis has greatly contributed to this area of research by providing researchers and commercial CNC users with the appropriate knowledge to select (or design) the right CNCs for their desired application.

9.2 Outlook and future work

Several opportunities exist to build on the contributions of this thesis and further expand the usage of CNCs in commercial applications. Simple surface modification routes are of particular interest; for example, tailored oligosaccharides or other short chain polymers (e.g., mixed linkage glucans) could be used to modify CNC surfaces for improved compatibility and/or stability. Ultimately, modifications capable of sterically stabilizing CNCs at high temperatures (e.g., once desulfation has occurred) or in high ionic strength environments would greatly impact their suitability and performance in liquid

formulations. This could be achieved by further tuning the oligosaccharide surface modification method proposed in *Chapter 5* to coat CNCs with short chain polymers whose tails or ends extend into the aqueous suspension, thereby acting as steric stabilizers. These short chain polymers could, for example, consist of more highly charged oligosaccharides which would, due to electrostatic repulsion, precipitate onto CNCs with fewer contact points.

Similarly, the introduction of more stable surface chemistries (e.g., sulfonate functional groups) on CNC surfaces would likely improve their thermal performance as de-esterification occurs at relatively low temperatures. Additionally, aqueous suspensions of CNCs exclusively functionalized with carboxylate groups would likely exhibit superior thermal performance to those of CNCs possessing both sulfate and carboxylate groups. For example, aqueous suspensions of industrially produced carboxylated CNCs (i.e., Anomera and BGB CNCs), CNCs hydrozlyzed with organic acids, and those produced using TEMPO-oxidations could be exposed to hydrothermal treatments to further elucidate the effects of surface chemistry and charge content on the colloidal stability of CNCs at high temperatures. As the commercial production of carboxylated CNCs becomes more widespread, these experiments are becoming increasingly relevant to the CNC community.